THE ELECTROCHEMICAL SOCIETY

ELECTRONICS DIVISION ABSTRACTS

Volume 9 Number 1

Spring Meeting — Chicago

May 1 - 5, 1960

THE ELECTROCHEMICAL SOCIETY, INC.

Spring Meeting, May 1 - 5, 1960

Chicago, Illinois

ELECTRONICS DIVISION ABSTRACTS

Volume 9 Number 1

Subjects:

General Electronics

Luminescence

Semiconductors

The Electrochemical Society, Inc.
1860 Broadway
New York 23, N.Y.

CONTENTS

Abstract Number		Page
	GENERAL ELECTRONICS	
36	"Micromodular Solid Tantalum Capacitors" by A. W. H. Smith	1
37	"Digital Programming Unit for Automatic Temperature Control" by N. L. Hozak, J. S. Cook, and D. R. Mason	3
38	"An Economical Automatic Differential Thermal Analysis System" by C. E. Barnes and D. R. Mason.	8
39	"Electroluminescent-Piezoelectric Flat Panel Displays" by S. Nudelman, J. Lambe, J. Mudar, and G. Trytten	12
	LUMINESCENCE	
40	"Phenomenological Theory of Luminescence of Nonphotoconducting Phosphors" by Yasuo Uehara	19
41	"Irreversible Thermodynamics of Solid-State Luminescence" by F. E. Williams	22
42	"Shape of Absorption Bands in Solids" by J. J. Markham	25
43	"Atomic Wave Functions of Activators" by K. H. Butler	26
44	"The Significance of Measurements of the Temperature Dependence of Luminescence Intensity" by C. H. Haake	27
45	"Absolute Spectral Reflectance of Phosphors" by J. E. Eby	30
46	"Infrared Spectroscopy in Phosphor Research" by M. J. B. Thomas and C. W. Jerome	31
47	"Factors Influencing the Luminescent Emission States of the Rare Earth Ions" by L. G. Van Uitert.	32
48	"Some Optical Properties of Powder and Crystal Halophosphate Phosphors" by P. D. Johnson	36

Abstract Number		Page
	LUMINESCENCE (contd.)	
49	"Energy Levels of the Antimony Center in Halophosphates" by F. E. Williams	40
50	"Lead- and Manganese-Activated Calcium-Cadmium Silicate Phosphors" by Yasuo Uehara, Yoshimasa Kobuke, Isoo Masuda, and Takashi Kushida	43
51	"Luminescence vs. Composition Studies of Complex Zinc and Cadmium Orthophosphates Containing Sodium and Lithium" by A. L. Smith	46
52	"Cadmium Phosphate Phosphors" by R. C. Ropp	52
53	"Luminescence of AlN" by I. Adams, J. W. Mellichamp, and G. A. Wolff	55
54	"Crystal Structure and Spectra of Alkali Halide Phosphors" by F. D. Klement	58
55	"On the Hydrogen-Like Model for Traps in Zinc Sulfide" by G. Curie, N. Arpiarian, P. Gueret, and D. Curie	61
56	"A Numerical Table for the Computation of Trap Depths from Thermoluminescence Experiments" by G. Curie and D. Curie	67
57	"Gold Activated (Zn,Cd)S Phosphors" by M. Avinor	71
58	"Low-Temperature Luminescence of ZnSCdS Phosphors" by R. W. A. Gill and S. Rothschild	72
59	"Infrared Stimulation and Quench of Zinc Sulfide Phosphors" by C. C. Klick	73
60	"Synthesis and Crystallography of Structurally Pure Cubic and Hexagonal Crystals of ZnS" by Harold Samelson and V. A. Brophy	77
61	"Infrared Absorption of n-Type (Zn,Cd)S" by R. M. Potter	79
62	"Formation of Phosphor Films by Evaporation" by L. R. Koller	83
63	"Continuous Films of II-VI Phosphors and Photoconductors Made by Vapor Reaction" by D. A. Cusano	84
64	"Transparent and Powder Phosphor Screens under High Ambient Illumination" by A. E. Hardy	85
65	"Mechanism of Depreciation of Electroluminescent Phosphors" by I. L. Smith, R. M. Potter, and M. Aven	89

Abstract Number		Page
	LUMINESCENCE (contd.)	
66	"Electroluminescent Maintenance" by W. A. Thornton	92
67	"Effects of Interaction among Particles in Electroluminescent Layers" by A. T. Halpin and Paul Goldberg	95
68	"On the Physical Characteristics and Chemical Composition of Electroluminescent Phosphors" by Paul Goldberg and Sicdeniel Faria	98
68A	"Detection of Ionization of Eu^{++} in the Phosphor SrS-Eu, Sm by Paramagnetic Resonance Absorption" by V. V. Antonov-Romanovsky, V. G. Dubinin, A. M. Prokhorov, Z. A. Trapeznikova, and M. V. Fock	101
69	"Copper-Chloride Relationships in Photoluminescent and Electroluminescent Zinc Sulfide Phosphors" by A. L. Solomon and P. Goldberg	105
70	"Effect of CdS on the Electroluminescence of ZnS:Cu Halid Phosphors" by Arthur Dreeben	111
71	"ZnS:Cu,Cl and (Zn,Cd)S:Cu,Cl Electroluminescent Phosphors" by A. Wachtel	113
72	"(Zn,Hg)S and (Zn,Cd,Hg)S Electroluminescent Phosphors" by A. Wachtel	119
73	"Influence of Mg and Cd on the Electroluminescence of ZnS:Cu Phosphors" by P. M. Jaffe	124
74	"Influence of Halogen-Coactivator on the Electroluminescence of ZnS:Cu Phosphors, I. Green Emission" by P. M. Jaffe	126
75	"Electroluminescent Time Average Light Output of a ZnS:Se Phosphor" by J. Mudar, S. Nudelman, and K. Kamyszek	128
76	"Temperature-Induced Color Shifts in Electroluminescence" by L. W. Strock	129
77	"On the Role of a Stimulating Action of Exciting Lights in the Luminescence Kinetics of the Crystalline Phosphor ZnS:Cu" by L. A. Vinokurov and M. V. Fock	130
77A	"On the Valency States of Manganese in Phosphor Systems" by V. V. Osiko	137
77B	"Physical Processes in Alkali Halide Phosphors Activated by Mercury-Like Ions" by Ch. B. Lushchik, I. W. Jaek, G. G. Ludja, N. E. Lushchik and K. K. Schwarz	141

Abstract Number		Page
	SEMICONDUCTORS	
78	"An Apparatus for the Preparation of Semiconductor Grade Silicon" by R. C. Ellis, Jr.	144
79	"Twin Generation and Seeding Mechanism in Dendritic Growth" by J. W. Faust, Jr., and H. F. John	145
80	"Propagation of Germanium Dendrites" by R. G. Seidensticker and D. R. Hamilton	152
81	"Some Aspects of Lateral Growth in Dendrites" by H. F. John and J. W. Faust, Jr.	156
82	"Dendritic Growth Studies by Pulse Plating Techniques" by R. C. Smith	159
83	"Growth of Atomically Flat Surfaces on Germanium Dendrites" by A. I. Bennett, R. L. Longini, and W. J. Smith	163
84	"Dendritic Growth of Indium Antimonide" by J. W. Faust, Jr., H. Nicholson, and R. Moss	165
85	"Preparation of Highly Arsenic-Doped Germanium" by P. L. Moody and A. J. Strauss	167
86	"Crystal Model Studies of Growth Phenomena in III-V Compounds" by R. C. Sangster	172
87	"Orientation Dependent Distribution Coefficients of Tellurium in Indium Antimonide Crystals" by J. B. Mullin	176
88	"Anisotropic Segregation in InSb" by W. P. Allred and R. K. Willardson	178
89	"Study of Copper Precipitation in Silicon Single Crystals" by G. H. Schwuttke	184
90	"Reactions of Oxygen in Ge" by C. S. Fuller, C. D. Thurmond, and W. Kaiser	186
91	"Preparation and Properties of Pseudo-Binary System GaAs-AlAs" by E. P. Stambaugh, J. I. Genco, and R. C. Himes	187
92	"Preparation and Properties of the Pseudo-Binary System GaSb-AlSb" by J. F. Miller, H. L. Goering, and R. C. Himes	189
93	"Phase Diagram for the Binary System Cadmium-Tellurium" by D. R. Mason and B. M. Kulwicki	192
94	"Effect of Inhomogeneities on the Hall Coefficient in InSb" by R. T. Bate	198

Abstract Number		Page
	SEMICONDUCTORS (contd.)	
95	"Properties of P-Type GaAs Prepared by Copper Diffusion" by F. D. Rosi, D. Meyerhofer, and R. V. Jensen	205
96	"Preparation and Properties of ZnSb" by R. C. Bourke, R. Simon, and M. H. Lougher	206
97	"Preparation and Properties of Gallium Phosphide" by C. J. Frosch, M. Gershenzon, and D. F. Gibbs.	212
98	"Preparation and Characteristics of P-N Junctions in Gallium Phosphide" by M. Gershenzon and R. M. Mikulyak	215
99	"Preparation and Properties of Grown P-N Junctions of InSb" by H. C. Gorton, A. R. Zacaroli and F. J. Reid	218
100	"Influence of Crystal Size on the Spectral Response Limit of Evaporated PbTe and PbSe Photoconductive Cells" by W. D. Lawson, A. S. Young, and F. A. Smith	220
101	"On the Mechanism of Chemically Etching Germanium and Silicon" by D. R. Turner	222
102	"Experimental Micro-Etch Techniques on Millimeter Wave-length Diodes" by D. G. Langlais	226
103	"Non-Diffusion of Boron Thru Solid Quartz" by Frank Keywell and Marshall Nechtow	229
104	"Oxidation-Induced Diffusion in Silicon" by H. W. Cooper, E. I. Doucette, and R. A. Mehnert	231
105	"Gaseous Diffusion of Arsenic in Germanium" by Carl Pihl and Kurt Lehovec	235
106	"Open Tube Diffusion of Antimony into Germanium" by A. E. Blakeslee	236
107	"Surface Concentration of Indium in Germanium from Gaseous Diffusion, II" by Karl Busen and Earl Meeks	238
108	"A Diffusion Mask for Germanium" by E. L. Jordan and D. J. Donahue	239
109	"Diffusion of Phosphorus in Silicon" by I. M. Mackintosh	241
110	"Experimental Evidence of Surface Damage and Precipitation in Diffused Silicon" by L. Gerlach and R. Haberecht	242

Abstract Number		Page
	SEMICONDUCTORS (contd.)	
111	"Precision Lapping, Damage, and Diffusion" by C. J. Spector and T. E. McGahan	244
112	"A New Solution to New Diffusion Equation and a New Application of Analog Solutions" by R. Moore and J. Colburn	245
113	"Localized Breakdown in Diffused Silicon Junctions" by B. D. James and P. S. Flint	246
115	"Production of a Germanium PNPN Switching Transistor by Post-Alloy Diffusion" by Fred Barson and John Gow	249
116	"A High-Frequency PNP Diffused Silicon Transistor Produced by the Oxide Masking Technique" by O. Stavik	254
118	"Physical Metallurgy in Semiconductor Device Fabrication, I. Gold Electrode Attachments to Silicon and Germanium" by L. Bernstein, B. G. Bender, and W. B. Warren	257
119	"Physical Metallurgy in Semiconductor Device Fabrication, II. Studies of Gold-Aluminum and Gold-Tin in Electrode Attachment" by L. Bernstein, W. B. Warren, and B. G. Bender	259
120	"Effects of High Aluminum Concentration in Emitters of Germanium Alloyed Power Transistors" by H. K. Becherer and Ernest Paskell	261

Abstract Number 36

MICRO MODULAR SOLID TANTALUM CAPACITORS

A. W. H. Smith

P. R. Mallory & Co. Inc.
3029 E. Washington St., Indianapolis, Indiana

Solid tantalum capacitors have been made for the R.C.A.-Signal Corps Micromodule Program in the following ratings:

2.2μf	6v DC
1 μf	12v DC
4.7μf	5v DC
3.0μf	10v DC=
1.0μf	20v DC
30.0μf	5v DC

The capacitors were made in the conventional way by depositing manganese dioxide onto an anodized tantalum slug by pyrolysis of manganous nitrate. A silver-filled epoxy resin was used to make a cathode termination and the capacitor was fixed to a ceramic wafer by a silver-filled epoxy resin cement. This cement made a cathode connection to the appropriate notch on the edge of the wafer via a screen printed gold/platinum track. The anode connection was made by welding the tantalum lead from the anode to a piece of pre-tinned nickel which was soldered to the appropriate notch on the wafer. A thin coat of silicone resin was applied to the capacitor for protection in transit and during "plotting." The maximum overall thickness of finished units was 0.031" for capacitors of up to 15 μ f.v and 0.038" for up to 30 μ f.v.

The finished units were tested in specially made holders and electrical connection made by gold plated spring wires to the solder in the anode and cathode notches on the ceramic wafer. Signal Corps Technical Requirement SCL-6402-A was used to determine passing limits, except for leakage current values which were held to 0.04 μ a $\cdot$ μ f^{-1} $\cdot$ v^{-1} at 25°C and 0.2 μ a $\cdot$ μ f^{-1} $\cdot$ v^{-1} at 85°C in accord with R.C.A. requirements. Measurements of capacitance and power factor were made with 1000 cps and 120 cps A.C. at -55°C, 25°C and 85°C. For capacitances of 5.0 μ f or less control of capacitance and power factor was good. However there were some rejections for a temperature coefficient of capacitance greater than 10% at 1000 cps between 25°C and -55°C.

Life Tests for selected ratings of these capacitors have been carried out at elevated temperature with rated voltage applied. The results are summarized graphically. The results are not strictly additive, as some units which had been found to be out of specified D.C. leakage limits

(120% of initial requirements) at some time interval were back within limits when tested 500 or 1000 hours later. There appears to be little correlation between the initial leakage current of a given capacitor and its time to failure. The capacitance and power factor changes found during life testing are well within the SCL-6402-A requirements, and, as would be expected, changes in capacitance, if any, are downwards.

Abstract Number 37

DIGITAL PROGRAMMING UNIT FOR AUTOMATIC TEMPERATURE CONTROL*

Norman L. Hozak, J. Stanley Cook and Donald R. Mason

Department of Chemical and Metallurgical Engineering
The University of Michigan
Ann Arbor, Michigan

Introduction

In studying the electronic properties of inorganic compounds the preparation of satisfactory high purity materials remains as a factor of major importance.[1] It is not surprising, therefore, to find much effort directed to this area alone.

One of the more obvious methods of compound preparation, that of precipitation from solution, must be rejected at once due to the introduction of contaminants from the solution, containers, filters, etc. Many investigators[2,3] have found that the direct fusion of stoichiometric amounts of highly purified elements in clean and non-reactive containers, either in vacuum or in an inert atmosphere, remains as one of the simplest and best preparational procedures. This latter method has been successfully used only after overcoming a major fusion problem.

In practice the non-reactive container is a fused silica tube sealed off under vacuum after loading of the elemental constituents. The degree of difficulty encountered in fusion of this sample is, among other things, a function of the heat of formation of the compound from the elements. The furnace fusion cycle must be adjusted in such a way as to allow adequate dissipation of such heat, otherwise a great pressure build-up will result followed by an explosion. Our experience indicates that by using samples of constant geometry, charge composition, and charge mass, the explosion point in a given temperature cycle is reasonably reproducible. The explosion can usually be avoided in subsequent samples of the same type by heating at the usual rate of 100°C. to 400°C. per hour from room temperature to a point 25°C. to 50°C. below

*Contribution No. 3 from The Semiconductor Materials Research Laboratory, College of Engineering, The University of Michigan, Ann Arbor, Michigan. This work was supported in part by grant NSF-G4127 from the National Science Foundation, and in part by Project MICHIGAN, under Department of the Army Contract (DA-36-039-SC-78801), administered by the U. S. Army Signal Corps.

the previously determined explosion point and holding there for one to four hours before resuming heating. Normal completion of the cycle would involve increasing the temperature from the hold temperature to a point about 50°C. above the liquidus temperature of the system, and then cooling.

During cooling the principal problems that arise are generally associated with wettability of the fused silica container and/or the differential in the coefficients of thermal expansion between the fused silica and the contents. The container may crack because of differential stresses but this too can often be mitigated by cooling slowly and allowing the compound to anneal and relieve the stresses which give rise to cracking.

From the foregoing discussion it should be evident that a means of automatically adjusting and controlling fusion cycles becomes not only desirable but necessary if one is to operate with any degree of efficiency. A device which has successfully met these needs[4] is described in detail in the following paragraphs.

Programmed Automatic Temperature Control

Although there are several different types of control units available for providing variable temperature cycles, none so successfully met the requirements of simplicity, low cost, compactness, and flexibility as well as the digital programmer designed and built for this laboratory. The programmer and its operation as an integrated part of the fusion furnace circuit can best be visualized and understood by referring to Figure 1. The emf output from the controller thermocouple is not introduced directly into the controller, but is modified by having an additional emf from the emf generator added in series with it. The temperature controller will control when the sum of the thermocouple emf and the additional emf are equivalent to the set point on the controller. By using a stepping switch selector circuit, the magnitude of the additional emf can be changed as a function of time. As a result the furnace temperature will also vary with time in the manner prescribed by the patchboard between the emf generator and the selector circuit.

The emf generator utilizes a 1.5 volt dry cell and a series resistance circuit drawing about 20 microamperes. The voltage drop across each 51 ohm precision resistor then is equivalent to about 25°C. for a chromel-alumel thermocouple. The forty precision resistors then provide a maximum emf equivalent to 1000°C., which can be reduced by any multiple of 25°C.

The selector circuit is designed so that it steps successively through 87 different positions, remaining in each position for 15 minutes. Hence it takes 21-3/4 hours for the selector circuit to complete one cycle. The selector circuit can be wired to select any equivalent emf between 0°C. and 1000°C. at each 15 minute interval, which will be added to the thermocouple emf to produce the control signal. Hence each 15 minutes a new control signal can be established which is entirely independent of either the previous signal or the following signal. Wide fluctuations in

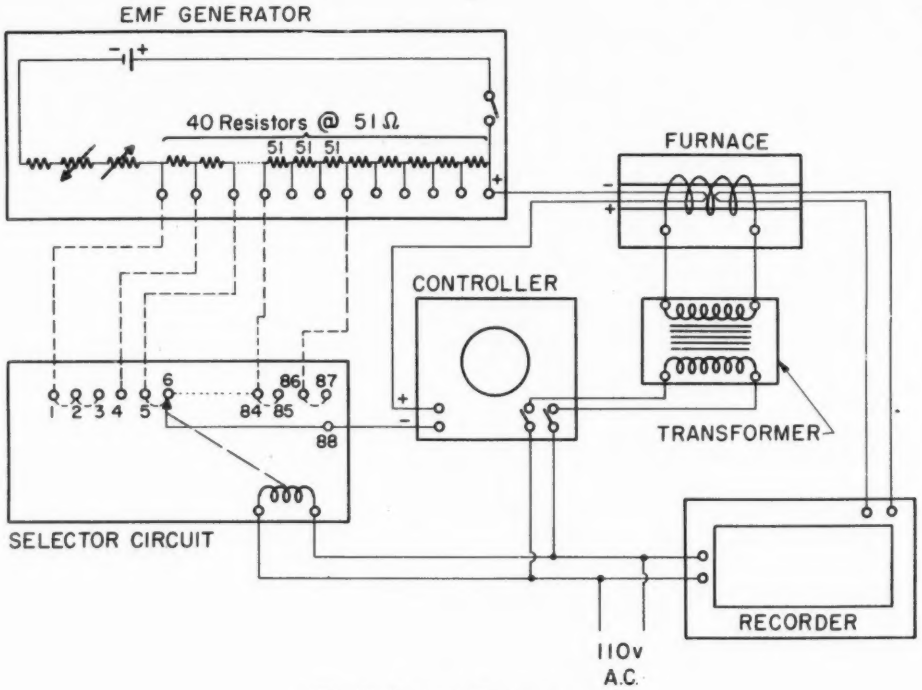

Fig. 1—Furnace Programmer

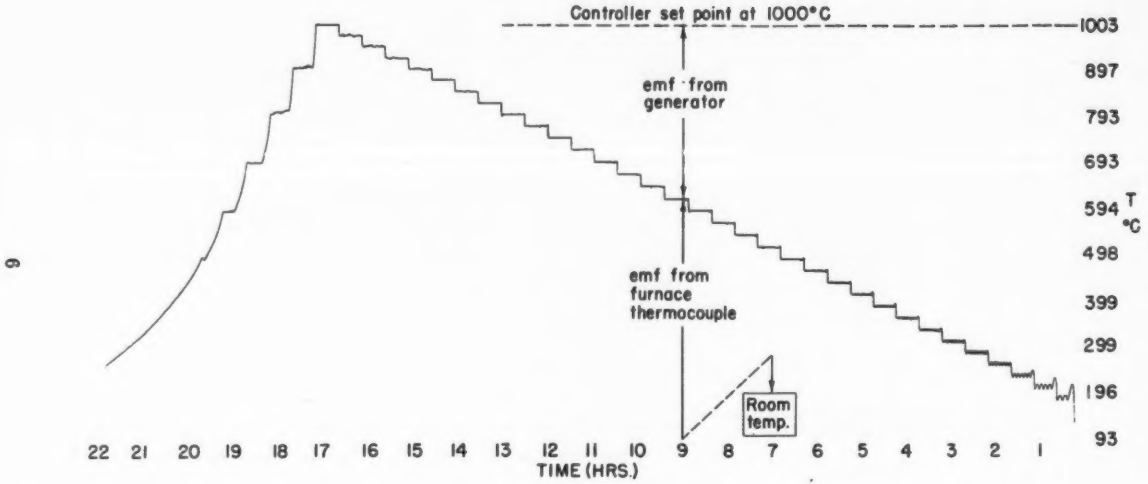

Fig. 2—Temperature Profile

control point can be obtained if desired, limited only by the time constant of the furnace. Heating rates, cooling rates, and holding times and levels can be selected easily, readily, and reproductibly. The actual furnace cycle is recorded from the recorder thermocouple on the recorder. The temperature profile for an actual furnace run is shown graphically in Figure 2 where the relationship between the emf generator output and the furnace thermocouple emf is indicated.

Because of the variable resistance in the control thermocouple circuit, it is necessary to use a potentiometric controller which is relatively insensitive to the input resistance. A Leeds & Northrup Speedomax Model H recorder-controller as well as a Micromax recorder-controller have been both used quite satisfactorily.

References

1. J. A. Kafalas, P. H. Robinson, "Purification of Semiconductor Materials by Chemical Means," presented before the Electrochemical Society, Ottawa meeting, Sept. 29, 1958, Abstract in Journal of the Electrochemical Society, 105, 164c (Aug. 1958).

2. G. Busch, U. Winkler, "Elektrische Leitfahigkeit und Hall-effekt intermetallischer Verbindungen," Helv. Phys. Acta, 26: 395 (1953).

3. H. J. Hrostowski, M. Tanenbaum, "Recent Work on Group III Antimonides and Arsenides," Physica, 20: 1065 (1954).

4. Thomassen, L., and Mason, D. R., "Phase Diagram for the Binary System CdTe-In_2Te_3," Abstract in J. Electrochem., 106, 206c (1959), Electrochemical Society, Fall Meeting, Columbus, Ohio, Oct. 21, 1959.

Abstract Number 38

AN ECONOMICAL, AUTOMATIC, DIFFERENTIAL THERMAL ANALYSIS SYSTEM*

Charles E. Barnes and Donald R. Mason

Department of Chemical and Metallurgical Engineering
The University of Michigan
Ann Arbor, Michigan

In order to prepare pure, homogeneous test samples for measuring the electrical and optical properties of semiconductor materials, it is necessary to know something of the phase transformation relationships of the materials. Often this amounts only to a characterization of the material itself, determining its transition temperature, melting point if congruently melting, or peritectic temperature. Satisfactory test samples can be prepared only after the phase behavior is known.

The important phase transitions, such as fusions, usually occur in conjunction with relatively large latent heat effects. Hence the differential thermal analysis technique is a valuable method for determining the magnitudes and the positions of the latent heat effects, or transitions.

Whenever completely new materials are studied, their characteristics over a large temperature range must be analyzed. In searching for the transition points at a new material one must often cover ranges as large as 200°C to 1250°C. If any accuracy is to be obtained in finding these transitions, one must come as close as possible, within practical limits, to equilibrium conditions. This requires slow, uniform heating and cooling rates. Therefore, the complete analysis of a material over this maximum temperature range may often take 16-22 hours. Since the transition points are not known, readings must be taken during most of the run at least once every minute.

It is now obvious that DTA is most time-consuming and tedious if done manually. It would be desirable, therefore, to find a method of automating the DTA apparatus as much as possible. The problem of automation then consists of finding an automatic system which will

*Contribution No. 4 from The Semiconductor Materials Research Laboratory, College of Engineering, The University of Michigan, Ann Arbor, Michigan. This work was supported in part by Grant NSF-G4127 from the National Science Foundation, and in part by Project MICHIGAN, under Department of the Army Contract (DA-36-039-SC-78801), administered by the U. S. Army Signal Corps.

provide a substantially linear heating rate which can be varied from approximately 1°C/min. to 6°C/min, and a system which will record the sample temperatures and the temperature differentials every 15 to 30 seconds.

An automatic DTA system has been designed and constructed which can measure two samples simultaneously. A block diagram showing the operation of the system is shown in Figure 1. All the operations in the system are actuated by a pulse generator. A short 110 volt, 60 cycle, AC pulse, about 1/4 to 1/3 second in duration is generated each 20 seconds by a microswitch which rides against a cam on a clock motor which makes one revolution every 20 seconds.

The pulses are used to generate a linear heating rate in a Kanthal furnace, and to switch the thermocouple circuits and recorder ranges. The power to the furnace is provided from a motor-driven autotransformer. Each pulse can drive the autotransformer through about 1/200 of its full range. If all the pulses were used to drive the autotransformer motor the heating rate would be too rapid, and hence it was necessary to devise a pulse selector circuit. With such a circuit it is possible to establish a heating rate of from 1°C/min to 6°C/min by varying the time between the successive pulses which are used to drive the autotransformer. This circuit is designed around an auxiliary stepping switch which comprises a stepping circuit and a reset circuit. As the stepping coil is triggered by the pulse generator the contact arm advances along the various contacts from #1 to #21. Whenever the reset coil is triggered, the contact arm is returned by a detent spring to contact #1. The short AC pulses are used not only to trigger the stepping coil but are also fed through the contacts of the auxiliary stepping switch. Hence, by connecting the autotransformer motor to the appropriate contact on the auxiliary stepping switch, the time interval between each selected pulse can be varied in 20 second steps from 60 sec to 420 sec. This is accomplished by providing 20 two-terminal outlets on the front panel with one terminal (A) of each outlet being connected sequentially from contact #2 to contact #21 on the auxiliary stepping switch. The autotransformer motor is activated when the auxiliary stepping switch advances to feed the pulse through the outlet into a plug leading to the autotransformer motor.

The second terminal (B) on each outlet is connected to the subsequent contact on the stepping switch, and leads to the reset coil. The next pulse then triggers the reset coil and returns the contact arm to contact #1 for another cycle. For example, in order to select a pulse each 60 seconds, the plug would be inserted into the second outlet. As the contact arm advances to contact #3, the pulse is fed through terminal (A) of outlet #3 and activates the autotransformer motor. The next pulse advances the contact arm to contact #4 which feeds the pulse to terminal (B) of the third outlet. At this point the reset coil is triggered and the contact arm is returned to contact #1 to start the cycle over again.

The automatic recording of sample temperatures and temperature differentials is carried out on a Wheelco dual range, single point

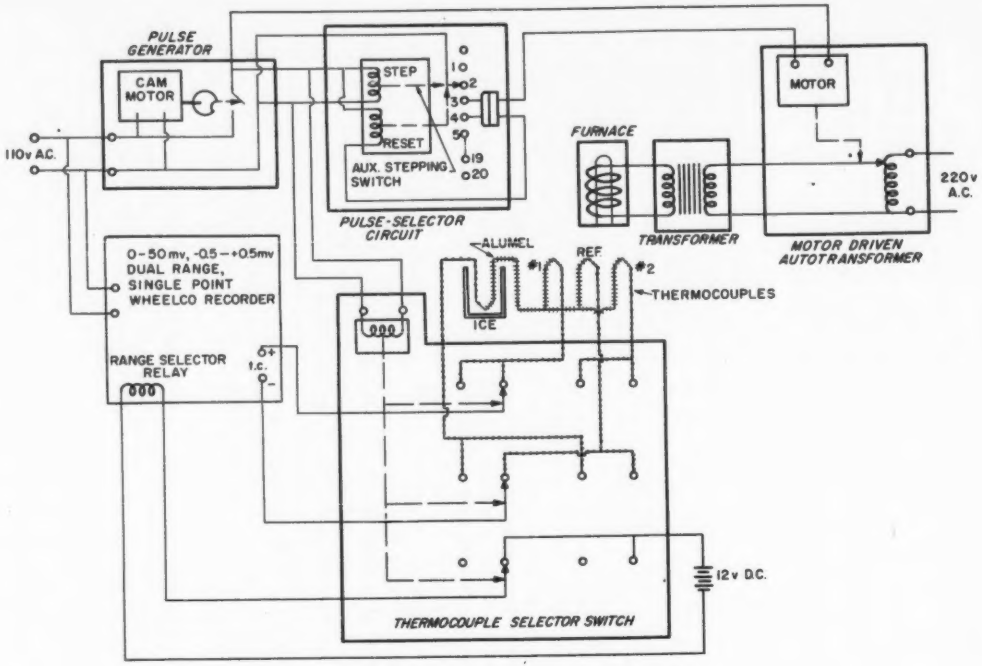

Fig. 1—Differential Thermal Analysis System

recorder. The switching circuit for the thermocouple input to the recorder uses another stepping switch, which is also pulsed every 20 sec by the pulse generator, and is also shown on the block diagram. Since only four different readings are taken only the first four rows of contacts on the stepping switch are shown, although the switch has 30 rows of contacts and the same thermocouple is measured 7 times in one revolution of the stepping switch. Two of the thirty contacts are by-passed on each revolution. A relay on the recorder is used to switch from the high scale (0 to 50mv) to the low scale (-.5 to +0.5mv). This relay is activated by a 12 volt source through the stepping switch so that the recorder is on the low scale whenever a temperature differential is being measured. Additional manual switches are provided in the thermocouple circuit which lend some flexibility to the recording system. For example, the switches can be arranged for simultaneous measurement of the temperature differential by the recorder and sample temperature measurement with an auxiliary potentiometer. This allows extremely accurate measurements to be made if desired. The operation of the recording system can also be modified by switching for special uses, such as the determination of temperature vs. autotransformer position for a certain heating rate. This case would imply continuous temperature measurement.

Since the temperature of a sample and its differential with respect to the standard are not measured simultaneously, this delay will affect the accuracy of the measurements. However, the differential is measured immediately after the temperature. Although the pen can traverse the entire chart in less than 4 sec, it will hardly ever have to traverse more than half the chart during a normal transition, the time interval which occurs between temperature measurement and temperature differential measurement is, on the average, considerably less. For an average heating rate of 2.5°C/min this would mean a change in temperature of 0.08°C between the recorded temperature and the actual temperature at the time the temperature differential is measured. This is entirely within the experimental error of the apparatus.

The cost of the automated portion of the DTA apparatus is low compared to other equipment of similar nature that has been described. The only expensive items are the Wheelco recorder and the motor-driven autotransformer. The rest of the system, being built from small, standard components, is rather inexpensive.

This equipment is currently in use in our laboratory and the results from these operations will undoubtedly be reported at some future time.

In conclusion, the authors would like to express their appreciation for discussions and assistance tendered by their colleagues in the design and construction of this system.

Abstract Number 39

ELECTROLUMINESCENT-PIEZOELECTRIC FLAT PANEL DISPLAYS*

S. Nudelman, J. Lambe,** J. Mudar and G. Trytten

The University of Michigan,
Willow Run Laboratories

The success of any electroluminescent image display using a raster-type writing program depends on the design of an electric field sweep and the ability to modulate the sweep with video information. The display panel proposed here will use the electric field generated at the surface of piezoelectric materials when operated in their resonant condition to excite electroluminescent phosphors and to provide the electric field sweep by sweeping the applied frequency.†

Electric Field Sweep Design

The device operation can be demonstrated with reference to Figure 1. A group of five barium titanate piezoelectric cylinders are placed electrically in parallel across a variable frequency generator. Each of the cylinders has its own resonant frequency, different from the others. When the generator is tuned to one of the resonant frequencies, a cylinder will respond in its vibrational mode and a strong polarization (electric) field is generated across its end surfaces. The intensity of the field is dependent on the voltage output of the generator, and an electroluminescent phosphor deposited on an end surface lights up accordingly. The different cylinders can be made to respond one at a time by changing the generator frequency, with the light output following the tuned cylinder and the light intensity modulation being achieved by modulation of the generator voltage. By miniaturizing compounds a fine resolution panel display composed of a matrix of cylinders is readily conceivable.

It is also possible to provide continuous light movement by using shaped bodies such as the quartz wedge shown in Figure 2. Localized

*This work was conducted by Project MICHIGAN under the Department of the Army contract DA 36-039 SC-78801, administered by the United States Army Signal Corp.

**Present Address: J. Lambe, Scientific Laboratories, Ford Motor Company, Dearborn, Michigan.

†An application of electroluminescent phosphors for detecting piezoelectric material stress patterns is described by C. A. ROSEN, U. S. Pat. 2,816,236.

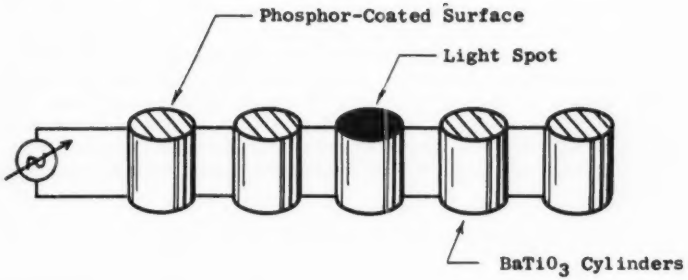

Figure 1

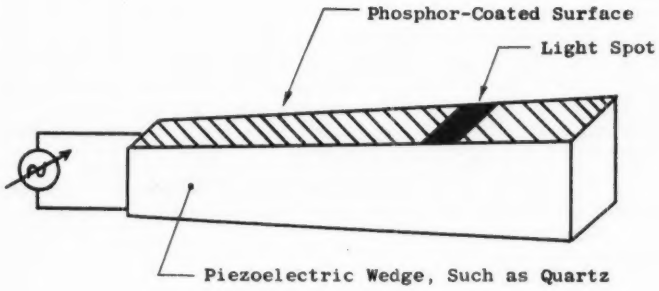

Figure 2

resonance is obtained in a wedge, since the resonant frequency is a sharp function of geometry. A light spot can then be made to move along the wedge simply by varying the generator frequency.

The important feature in device applications that derive from this type of sweep is that a localized field spot is generated without any need for electrodes placed in close proximity to it. The field is generated by polarization charges appearing at the crystal surface. These charges can be made to appear at surfaces to which no electrical connections are made. If the piezoelectric crystal is shaped properly, the vibrational polarization field can be induced with electrodes placed a significant distance along the crystal away from the surface of interest. This has been demonstrated with the configuration of Figure 3. The transparent grounded electrode placed across the phosphor layer provides the minimum path length for the field and therefore the maximum field intensity.

Flat Panel Display

When the electric field spot sweep is coupled with an electroluminescent phosphor for a flat panel display, essentially performing as a TV-type display, the construction of the panel may look like Figures 4. In Figure 4, a mosaic of spots appears at the panel surface sufficient for good resolution and spaced to comply with some scan pattern. Each spot represents the surface of a piezoelectric cylinder. The length of the cylinder and the material of which it is made determines the resonant frequency of the cylinder. All cylinders may be placed electrically in parallel and tuned to oscillate independently of one another so that only one spot lights up at a time. By frequency modulation of the generator, the light spot then moves in any desired scan pattern. By amplitude modulation video information is displayed. If the state-of-the-art of electroluminescent phosphors or piezoelectric materials places restrictions on the electrical bandwidth of operation, the mosaic of spots can be arranged in lines, so that one line at a time may be scanned by frequency modulation. Then by simple switching techniques, all lines can be scanned in any desired sequence.

A block diagram of the electronics system needed to drive the piezoelectric-electroluminescent flat panel display is shown in Figure 5.

Additional Devices

Dials for instrument panels might be developed in a relatively simple manner. For example, if a luminescent circle designating some particular area were needed, a dial could be formed from a piezoelectric disc. The disc would be flat on one surface, have a conical hole bored in the other, and be coated on the flat surface with an electroluminescent phosphor. The application of a single driving frequency would cause a luminescent circle to appear. Changing the driving frequency would cause the circle to get larger or smaller, thereby delineating perhaps a varying target area.

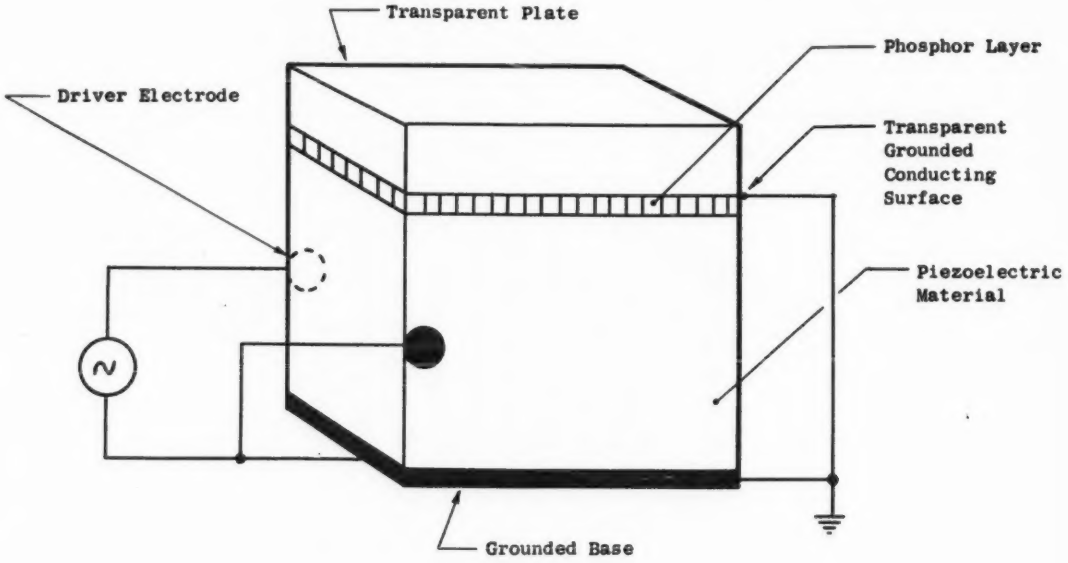

Fig. 3—A Useful Electrode Arrangement

resonance is obtained in a wedge, since the resonant frequency is a sharp function of geometry. A light spot can then be made to move along the wedge simply by varying the generator frequency.

The important feature in device applications that derive from this type of sweep is that a localized field spot is generated without any need for electrodes placed in close proximity to it. The field is generated by polarization charges appearing at the crystal surface. These charges can be made to appear at surfaces to which no electrical connections are made. If the piezoelectric crystal is shaped properly, the vibrational polarization field can be induced with electrodes placed a significant distance along the crystal away from the surface of interest. This has been demonstrated with the configuration of Figure 3. The transparent grounded electrode placed across the phosphor layer provides the minimum path length for the field and therefore the maximum field intensity.

Flat Panel Display

When the electric field spot sweep is coupled with an electroluminescent phosphor for a flat panel display, essentially performing as a TV-type display, the construction of the panel may look like Figures 4. In Figure 4, a mosaic of spots appears at the panel surface sufficient for good resolution and spaced to comply with some scan pattern. Each spot represents the surface of a piezoelectric cylinder. The length of the cylinder and the material of which it is made determines the resonant frequency of the cylinder. All cylinders may be placed electrically in parallel and tuned to oscillate independently of one another so that only one spot lights up at a time. By frequency modulation of the generator, the light spot then moves in any desired scan pattern. By amplitude modulation video information is displayed. If the state-of-the-art of electroluminescent phosphors or piezoelectric materials places restrictions on the electrical bandwidth of operation, the mosaic of spots can be arranged in lines, so that one line at a time may be scanned by frequency modulation. Then by simple switching techniques, all lines can be scanned in any desired sequence.

A block diagram of the electronics system needed to drive the piezoelectric-electroluminescent flat panel display is shown in Figure 5.

Additional Devices

Dials for instrument panels might be developed in a relatively simple manner. For example, if a luminescent circle designating some particular area were needed, a dial could be formed from a piezoelectric disc. The disc would be flat on one surface, have a conical hole bored in the other, and be coated on the flat surface with an electroluminescent phosphor. The application of a single driving frequency would cause a luminescent circle to appear. Changing the driving frequency would cause the circle to get larger or smaller, thereby delineating perhaps a varying target area.

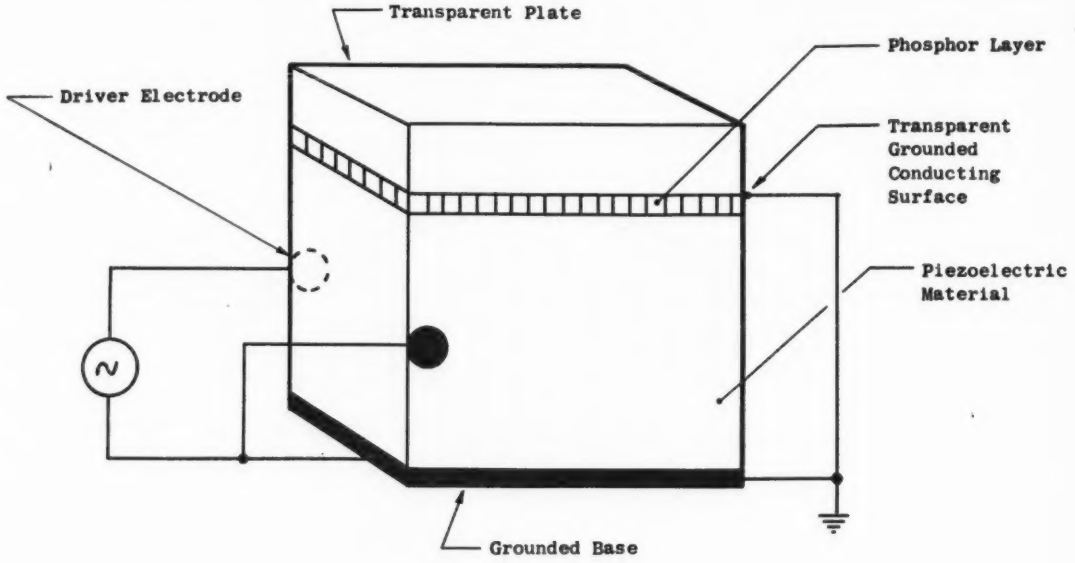

Fig. 3—A Useful Electrode Arrangement

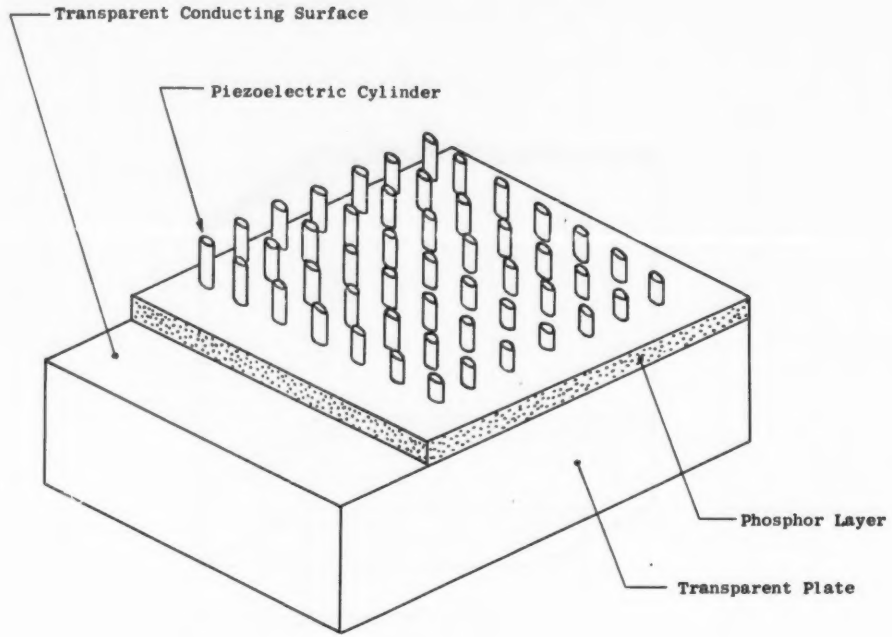

Fig. 4—Electroluminescent Panel with Piezoelectric Cylinders

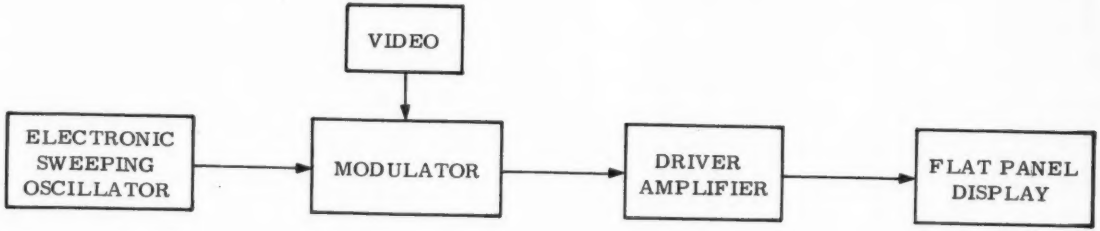

Fig. 5—Block Diagram for Electronic System Needed to Drive Piezoelectric-Electroluminescent Materials Flat Panel Display

One- and two-dimensional switches can be obtained from simple display panels such as those described above. The speed with which a light spot moves along the surface is determined by the speed with which the electrical generator frequency is changed. When a panel is coupled to an array of photodetectors, any desired sequence of events can be triggered, with complete and independent control of the timing of these events. Since the panel is a fabricated solid state device requiring no internal electronics or gadgetry for its operation, and photodetectors such as CdS meet the same description, panels and photodetectors can be fabricated in a unit package. These can be shaped and positioned to fit unusual compartment requirements. It follows from these applications that computer circuitry may well be simplified and expanded.

Display panels such as we have described can also serve admirably as frequency spectrum analyzers. Any signal fed into the display can have its frequency components examined by the luminescent pattern on the panel. Another useful device naturally evolves from this kind of application. One can readily conceive of a character display, where a signal consisting of a mixture of frequencies is fed to the panel so that a number, letter, or a figure will appear and be sustained as long as the signal is applied. Therefore, keyed characters, or automated character sequences are well within reach.

Abstract Number 40

PHENOMENOLOGICAL THEORY OF LUMINESCENCE OF NONPHOTOCONDUCTING PHOSPHORS

Yasuo Uehara

Matsuda Research Laboratory
Tokyo Shibaura Electric Co., Ltd.,
Kawasaki, Japan

A fundamental equation of luminescence which can explain various luminescent properties of nonphotoconducting phosphors under excitation by ultraviolet radiation of constant intensity at thermal equilibrium is formulated. In order to check its validity, various characteristics of copper-activated β-calcium orthophosphate phosphor reported in a previous paper[1] is calculated as an example. Furthermore, it is expanded to the interpretation of properties of cathodoluminescence or scintillators.

From the theory of adiabatic approximation concerning a system consisting of a number of nuclei and electrons, it is well known that the electronic energy states in the system are represented by the potential surfaces of multidimensions in a configuration space. Optically allowed transitions between these states are responsible for the adsorption and emission of light, that is, the luminescence of phosphors. Perturbation of the system represents the order of magnitude of the approximation. This perturbation is responsible for the so-called radiationless transition in the phosphor. At high temperatures, the main part of the radiationless transition will be given by the absolute rate theory of thermal reaction[2], but at low temperatures, the transition arising from the quantum mechanical resonance effect will be predominant. The following expression for the radiationless transition, therefore, will be assumed as an approximation:

$$\mathcal{A}'_{ji} = A'_{ji} + k'_{ji}, \tag{1}$$

where A'_{ji} is the probability of radiationless transition due to resonance from state i to j and is assumed to be independent of temperature, k'_{ji} is the absolute rate constant of thermal reaction for the transition from state i to j.

Let the probability of spontaneous emission for the transition from state i to j be A_{ji} and that of induced adsorption be $J_{ij}B_{ji}$ in which J_{ij} denotes the energy density of the exciting radiation, then the total probability of possible transitions from state i to j is given by

$$\mathcal{A}_{ji} = J_{ij}B_{ji} + A_{ji} + A'_{ji} + k'_{ji}. \tag{2}$$

The transition probability of induced adsorption can be expressed by

use of the flux density of exciting photons $N_{E,ij}$ (photons · cm^{-2} sec^{-1}) and of the adsorption cross-section $\sigma_{ji}(cm^2)$ as follows:

$$J_{ij}B_{ji} = \mathcal{N}_{E,ij} \cdot \sigma_{ji}. \tag{3}$$

It will be possible to extend the above relations to the case of charged particle excitation by considering $\mathcal{N}_{E,ij}$ as the flux density of secondary electrons generated by the collision of primary particles and σ_{ji} as the collision cross-section for secondary electrons, neglecting the effect of the recombination process between positive holes and electrons as an approximation.

Let us now consider the nonphotoconducting phosphor under excitation by ultraviolet radiation of constant flux density at thermal equilibrium. Let the number of activator centers per unit volume be n_0 and that of energy states in the activator center be m, then the rate of change of the state density at any time t after the beginning of excitation can be given by a set of homogeneous linear differential equations of the first order, that is

$$-\frac{d\mathcal{N}_i}{dt} = \mathcal{A}_{ii}\mathcal{N}_i - \sum_j{}' \mathcal{A}_{ij}\mathcal{N}_j, \quad (i = 1,2,\cdots,m) \tag{4}$$

with

$$\mathcal{A}_{ii} = \sum_j{}' \mathcal{A}_{ji} \tag{5}$$

where n_i and N_j are the state density of state i and j, respectively. Substituting the change of variables

$$N_i = l_i e^{-\lambda t} \tag{6}$$

into eq. (4), we obtain the secular equation

$$[A]\mathcal{N} - \lambda\mathcal{N} = 0, \tag{7}$$

where the matrix (A) is given by

$$[A] = [\delta_{ij}\mathcal{A}_{ij}] \tag{8}$$

with

$$\delta_{ij} = 1, \text{ if } j=i \text{ or } \delta_{ij} = -1, \text{ if } j \neq i$$

and n is the vector of the m-th order having the explicit form of $(n_1, n_2, \cdots\cdots, n_m)$.

Eq. (7) is the fundamental equation of luminescence for nonphotoconducting phosphors under excitation by ultraviolet radiation. By solving eq. 7 under given boundary conditions, we can exactly calculate almost all the characteristics of luminescence of nonphotoconducting phosphors under excitation by ultraviolet of constant intensity at thermal equilibrium, if the configuration of phosphor involving all energy states and all values of transition probabilities are proposed beforehand. As as example, this method was applied to copper-activated calcium orthophosphate phosphor and then expanded to the calculation of the characteristics of nonphotoconducting phosphors under excitation by charged particles. The calculated results were in a reasonable agreement with those observed.

References

1. Y. Uehara, Y. Kobuke, and I. Masuda, J. Electroch. Soc., 106, 200 (1959).
2. S. Glastone, K. J. Laidler, and H. Eyring, "Theory of Rate Processes", McGraw Hill Book Co., Inc., New York and London (1941); F. E. Williams and H. Eyring, J. Chem. Phys., 15, 289 (1947).
3. R. Kubo and Y. Toyosawa, Proc. Theor. Phys., 13, 160 (1955).

Abstract Number 41

THE IRREVERSIBLE THERMODYNAMICS OF SOLID-STATE LUMINESCENCE

Ferd E. Williams

General Electric Research Laboratory

Equilibrium thermodynamics has been applied to luminescence. Landau[1] considered the isolated system consisting of the luminescent body plus radiation, and calculated the entropy of the radiation. He was apparently concerned with the photoluminescence of gases since he considered the effective temperature of the radiation to be several tens of thousands of degrees. For such a system Landau concluded that the intensity of anti-Stokes radiation must become insignificant compared with the exciting radiation for appreciable anti-Stokes shift in spectra. More recently, Weinstein[2] has considered the equilibrium thermodynamic limitations on the conversion of heat into light, particularly as applied to carrier injection electroluminescence. It had been suggested earlier that electroluminescent emission exceeding the electrical input might be achieved by this mechanism.[3,4] The additional energy would be taken as heat from the lattice and the system would thereby cool. Weinstein showed that for typical luminescent spectra of phosphors and for practical light intensities the effective temperature of the radiation is approximately a thousand degrees Kelvin; therefore, electroluminescent efficiencies as great as 140 per cent are not forbidden by equilbrium thermodynamics.

The luminescence of solids is, however, an irreversible phenomenon. For impurity-activated phosphors, the irreversibility is evident from the fact that emission at the wavelengths for absorption is not observed when the photoluminescent material is exposed to radiation of the wavelength for ordinary emission. More generally, the effective temperature of the luminescent emission is large compared to the lattice temperature and the phosphor is interacting with a power source, therefore, the phenomenon is irreversible. For photoluminescence the power source is the exciting radiation; for electroluminescence the power source is the voltage source.

Irreversible thermodynamics is concerned with precisely such phenomena, that is, with open systems which interact with their environment in a stationary way.[5] Irreversible thermodynamics places more severe limitations on irreversible phenomena than does equilibrium thermodynamics. In particular, irreversible thermodynamics requires that the entropy production due to irreversible processes be positive in every macroscopic region of the system, that is, in every region sufficiently large for microscopic fluctuations to be negligible.[6]

For luminescence involving energy transport between different macroscopic regions not in equilibrium with each other this "local" formulation of the second law is more restrictive than the "global" formulation of equilibrium thermodynamics. Such energy transport is involved in sensitized photoluminescence, in some mechanisms of multiple-excited anti-Stokes photoluminescence, and in both impact excitation and carrier injection electroluminescence. We shall consider in some detail carrier injection electroluminescence.

Let us consider the electroluminescent system as consisting of p- and n-type materials separated by an intrinsic material capable of efficient radiative recombination. With a constant voltage $V > \frac{kT}{e}$ applied to the electroluminescent system which is in contact with a thermostat at temperature T and which emits radiation characterized by the temperature $T_R > T$, we are clearly concerned with a steady-state phenomenon amenable to irreversible thermodynamics. Electrons are injected from the n-type region; holes, from the p-type region into the intrinsic region where radiative recombination occurs. In this process the electron-hole pairs are annihilated and photons are created. In the steady-state the annihilation of pairs in the intrinsic region is just balanced by the creation of pairs elsewhere in the system. The creation of the charge carriers can be considered as occurring at the appropriate electrodes. Irreversible thermodynamics requires that the rates of entropy production involved in the electron and hole creation processes at their respective electrodes be positive:

$$\frac{dS_e{}^c}{dt} > 0, \quad \frac{dS_h{}^c}{dt} > 0 \tag{1}$$

and also that the rate of entropy production in the intrinsic material be positive. If no other dissipative processes occur in the junction, then:

$$\frac{dS_R}{dt} + \frac{dS_e{}^a}{dt} + \frac{dS_h{}^a}{dt} > 0 \tag{2}$$

where the first term is the rate of entropy production associated with the radiation, and the second and third terms are the rates of entropy production associated with the annihilation of electron and hole. Both terms in Eq. (1) and the first term of Eq. (2) are positive; the second and third terms of Eq. (2), negative. Equilibrium thermodynamics permits the interference of the creation terms of Eq. (1) with the annihilation terms of Eq. (2); irreversible thermodynamics does not. The production of radiation entropy $\frac{dS_R}{dt}$ can be evaluated from the Bose-Einstein statistics; the other terms of Eq. (1) and (2), from the Sachur-Tetrode equation. The limitations imposed by irreversible thermodynamics on the efficiency of injection electroluminescence can then be determined for different values of the applied voltage V compared to the band gap E_G. It is found that Eq. (2) precludes for this injection mechanism practical electroluminescent emission intensities in excess of the electrical input.

The irreversible thermodynamics of other injection electroluminescent systems and of other solid-state luminescent phenomena will be considered.

References

1. L. D. Landau, Journ. of Physics (USSR) 10, 503 (1946).
2. M. A. Weinstein (to be published).
3. J. Tauc, Czech. J. Phys. 7, 275 (1957).
4. R. N. Hall (private communication)
5. R. De Groot, "Ther Thermodynamics of Irreversible Processes," Interscience, N. Y. (1951).
6. I. Prigogine, "Introduction to Thermodynamics of Irreversible Processes," C. C. Thomas, Springfield, Illinois (1955).

Abstract Number 42*

SHAPE OF ABSORPTION BANDS IN SOLIDS

J. J. Markham

Zenith Radio Corp.,
Chicago, Ill.

The theories of the shape of an optical absorption band in solid are reviewed. The shape is related to the emission and the absorption of phonons. It depends on the temperature of the crystal. The theories are related to the measured absorption bands associated with F centers in KCl and NaCl.

*Enlarged Abstract not available.

Abstract Number 43*

ATOMIC WAVE FUNCTIONS OF ACTIVATORS

K. H. Butler

Sylvania Lighting Products
60 Boston St., Salem, Mass.

The sp configuration is characteristic of the excited states of many primary activator ions, i.e., Sb^{3+}, Sn^{2+}, Tl^{+}. Quantum mechanical formulas show that the electron density distribution of this configuration depends strongly on the coupling of the electron spins and the magnetic quantum number of the combined electrons. The marked difference in the shapes of an ion in the $^1P_1^0$ and $^3P_1^0$ states, combined with variations in the coordinator number of the surrounding anions in different crystal structures, explains such phenomena as the polarization of luminescence in KCl:Tl and the appearance of two emission bands in many tin-activated phosphors as contrasted to the single emission band for most materials activated by lead or antimony.

*Enlarged Abstract not Available.

Abstract Number 44

THE SIGNIFICANCE OF MEASUREMENTS OF THE TEMPERATURE DEPENDENCE OF LUMINESCENCE INTENSITY

C. H. Haake

Research Dept.,
Westinghouse Electric Corporation,
Bloomfield, N. J.

In various applications it is required that phosphors show a stability of luminescence at relatively high temperatures. In a preliminary search for suitable "high-temperature" phosphors one, therefore, measures the temperature dependence of luminescence intensity in addition to measuring spectra of emission and absorption. If care has been taken that the luminescence readings are not influenced by a possible shift in the emission spectrum with changing temperature, one expects the shape of such a curve to be a true reflection of internal phosphor properties. It is, therefore, of importance to know whether or not these curves really convey undistorted information of these phosphor properties.

With increasing temperature phosphors sometimes exhibit an initial rise and a subsequent drop of luminescence intensity. This is due to a competition of thermal quenching and an increasing absorptance of the phosphor for the exciting radiation.

The number of quanta $L(\lambda,T)$ emitted at a temperature T from a phosphor layer when excited by radiation in the wavelength range between λ and $\lambda+d\lambda$ is approximately given by

$$L(\lambda, T) = N(\lambda)\, \eta\, (\lambda,T) A(\lambda,T) \qquad (1)$$

(N, number of exciting quanta; η, quantum efficiency; A, absorptance). The thermal behavior of the quantum efficiency can be expressed in the simplified form

$$\eta = [1 + \text{const. } \exp(-E/kT)]^{-1} \qquad (2)$$

where E is the quenching energy and k is the Boltzmann constant. The energy E and, the constant η for a given N, are internal phosphor properties. The absorptance A, on the other hand, is a rather complex function of internal and external parameters: the thickness, s, of the phosphor layer; the size, d, of the individual phosphor crystals; the refractive index, n, and the extinction coefficient, ϵ, of the bulk material. An expression for the absorptance, A, of a radiation scattering layer has been derived by Schuster[1] and applied to phosphors by several workers.[2,3,4]

$$A(\alpha,r,s) = \frac{\left(\sqrt{\left(\frac{\alpha}{r}\right)^2 + 2\frac{\alpha}{r}} + \frac{\alpha}{r}\right)\left(e^{rs\sqrt{\left(\frac{\alpha}{r}\right)^2 + 2\frac{\alpha}{r}}} - 1\right)}{\left(\sqrt{\left(\frac{\alpha}{r}\right)^2 + 2\frac{\alpha}{r}} + \frac{\alpha}{r} + 1\right)\left(e^{rs\sqrt{\left(\frac{\alpha}{r}\right)^2 + 2\frac{\alpha}{r}}} + 1\right)} \qquad (3)$$

where α and r are generalized coefficients of absorption and scattering, respectively. If Eq. (3) is applied to phosphor layers, α is approximately proportional to the extinction coefficient, ϵ, of the bulk material whereas r is a function of n and d. Generally, a thermal increase of n is negligibly small so that the temperature dependence of A lies mainly in the absorption coefficient.

It is obvious from Eq. (3) that the thermal rate of increase of the absorptance depends not only on the thermal rate of increase of α but also on the thickness, s, of the phosphor layer. As long as the exponential terms in A are small compared to unity, their effect on A is strong, i.e., A can increase rapidly with increasing temperature. If, however, the exponential terms are much larger than unity, the increase of A is largely determined by the expressions in the first brackets of the numerator and the denominator of Eq. (3), i.e., A increases more slowly. For a given absorption coefficient the numerical value of the exponential terms can be changed considerably by choosing different layer thicknesses s. The quantum efficiency, on the other hand, is independent of s. Thus the position of the peak in a plot of luminescence versus temperature can be varied over a wide range. Fig. 1 represents two plots of emitted quanta versus temperature measured on a magnesium fluorogermanate phosphor activated with Mn. The wavelength of excitation was 365mμ. The curve obtained with the thin layer peaks at 360° C. with a height of 180% above the value observed at room temperature. The thick layer, on the other hand, produces a peak already at 240° C. with a height of only 17% above the room temperature value.

Therefore, if the thermal behavior of phosphors is to be compared on the basis of measurements of luminescence versus temperature, valid conclusions can be drawn only if the thickness of the phosphor samples considered is the same.

References

1. A. Schuster, Astrophys. j. 21, 1, (1905).
2. J. W. Coltman, E. G. Ebbighausen and W. Altar, J. Appl. Phys. 18, 530 (1947).
3. I. Broser, Ann. Phys. 5, 401 (1950).
4. C. H. Haake, J. Electrochem. Soc. 106, 866 (1959).

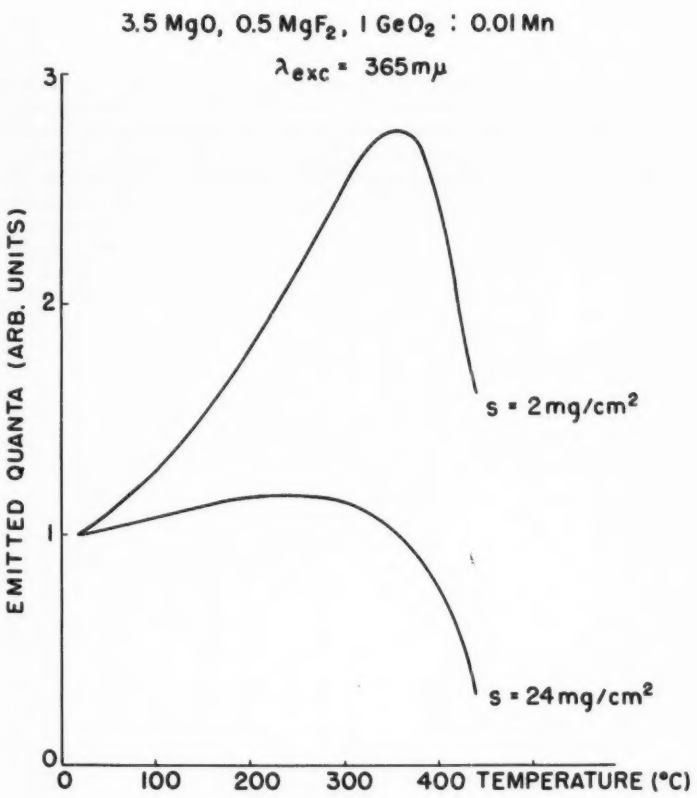

Fig. 1—Emitted Quanta versus Temperature

Abstract Number 45*

ABSOLUTE SPECTRAL REFLECTANCE OF PHOSPHORS

J. E. Eby

Sylvania Lighting Products
60 Boston St., Salem, Mass.

Absolute measurements of the spectral reflectivity were made on a number of phosphor samples using a modified Beckman DK-1 Spectrophotometer. The method of making these measurements, which covered the range from 240 μ to 750 μ, is described and data given. These data were then used in conjunction with determinations of particle size distribution to compute the absorption coefficient of the luminescent materials.

*Enlarged Abstract not Available.

Abstract Number 46*

INFRARED SPECTROSCOPY IN PHOSPHOR RESEARCH

M. J. B. Thomas and C. W. Jerome

Sylvania Lighting Products
60 Boston St., Salem, Mass.

Use of infrared spectrophotometry as a technique for the identification of compounds has become extremely important with respect to organic compounds and to a somewhat lesser extent with respect to inorganic compounds. There has been, however, no application of this technique to luminescent materials. Infrared studies of the various commercial phosphors and the starting materials used in their manufacture have been made in the 3-15 μ region. The absorption structures of many of the materials are characteristic and may be used in the study of mechanism of phosphor formation.

*Enlarged Abstract not Available.

Abstract Number 47

FACTORS INFLUENCING THE LUMINESCENT EMISSION STATES OF THE RARE EARTH IONS

L. G. Van Uitert

Bell Telephone Laboratories, Inc.
Murray Hill, New Jersey

The number of electronic states from which luminescent emission by rare earth ions can be observed is dependent upon the extent to which the host lattice perturbs their f-orbital electrons. The number of emitting states observed does not appear to be as critically dependent upon geometric considerations as are the crystal field splitting or the relative strengths of the emission lines.

Amongst others the perturbing influences under consideration may stem from the following sources:

1. The coulombic affinities of the entities surrounding the rare earth ions for the electrons they share with the latter.
2. Concentration effects - exchange coupling.
3. Thermal effects - vibronic interactions.

Coulombic Affinity

There is considerable evidence that bond strength increases with an increase in the affinity of one or both of the bonded atoms for the electrons they share.[1,2] As a first approximation one may consider the electron affinities or ionization potentials of the entities surrounding the rare earth ions in the several host lattices to provide a measure of the extent to which these surroundings may perturb the f-orbital electrons of the rare earths.

Process	Ionization Potential	Reference
$La \rightarrow La^{+}$	5.61 e.v.	Ref. 3, p. 156
$La^{+} \rightarrow La^{2+}$	11.4 e.v.	Ref. 3, p. 156
$La^{2+} \rightarrow La^{3+}$	19.2 e.v.	Ref. 4, p. 139
$H_2O \rightarrow H_2O^{+}$	12.6 e.v.	Ref. 5, p. 265
Organic-0 $\rightarrow$ Organic-0+	>10.0 e.v.	Ref. 5, p. 265

Process	Electron Affinity	Reference
$F \rightarrow F^{-}$	4.27 e.v.	Ref. 3, p. 161
$O \rightarrow O^{-}$	3.1 e.v.	Ref. 5, p. 40
$O \rightarrow O^{=}$	-7.28 e.v.	Ref. 3, p. 161

It is evident that one cannot ascribe full possession of the electrons about the above anions, water, or the organic oxygen atoms to these entities when they are bonded to the trivalent rare earth ions. Electron diffraction work carried out on beryl ($Be_3Al_2Si_3O_{18}$) by Bragg and West[6] has shown that in the silicates the silicon and oxygen atoms are closer to the Si^+ and O^- ionic states than to the Si^{4+} and $O^=$ states. Hence, one may expect the ionization potential of oxygen to depend upon the central cation when it is part of an anionic group such as $WO_4^=$.

By analogy with the work of Coulsen[2] on the relation between bond order and bond length in organic molecules, one can expect a stronger bonding of ketonic oxygen (double bonded to carbon) to the rare earth ions than occurs with ethers or alcohols. Further one might expect an additional increase in bonding strength to the rare earth through oxygen in the chelates, such as the acetylacetonates, due to the development of resonance structures.

The above considerations, in conjunction with the observations given below, suggest that the following environments diminished in perturbing influence in the order: O-O chelates, ketones and hydrates, fluorides, high central charge anionic groups ($WO_4^=$), less covalent oxides. In the case of europium, one emission state (17,300 cm^{-1}) is active in the chelate,[7,8] and an additional state (19,000 cm^{-1}) is observed in the hydrate[7]; a third (21,500 cm^{-1}) is apparent in the fluoride[9] and a fourth (24,200 cm^{-1}) in the tungstate[10] and calcium oxide.[11]

In a like manner, one emission state (20,700 cm^{-1}) is observed for terbium in the chelate, hydrate[7] and fluoride[9]; a second (26,500 cm^{-1}) is found in the tungstate[12]; and there are possibly three or more when terbium is combined with aluminum oxide.[11,13] Erbium does not luminesce in the chelate or hydrate but exhibits two main emission states (15,300 and 18,400 cm^{-1}) in the fluoride[9] and a third (24,500 cm^{-1}) in the tungstates and calcium oxides.[11] Parallel patterns are observed for a number of the other rare earths.

Concentration Effects

It appears that exchange coupling between paramagnetic rare earth ions can produce effects quite comparable to the results observed by changing the host environments in the above series. This is deomonstrated by changing the concentrations of rare earth ions in the series $Ca_{1-2x}Na_xRE_xWO_4$, all of which have the scheelite structure. In the case of Tb^{3+}, emission from the 26,500 cm^{-1} state is dominant at low concentrations (blue to the eye), and emission from 20,700 cm^{-1} is dominant at high concentrations (green to the eye). In $Na_{0.5}Tb_{0.5}WO_4$, the blue spectrum is essentially quenched, and the green spectrum is very bright (comparable to ZnS phosphors).

In the same manner, the high frequency spectrum of europium is quenched by increasing the concentration. It appears that the 24,000 cm^{-1} emission is quenched by pairs of Eu^{3+} ions occurring in neighboring Ca^{2+} sites, and emission from 19,000 and 21,500 cm^{-1} is

quenched by the association of three or more europium ions. $Na_{0.5}Eu_{0.5}WO_4$, dominated by emission from 17,000 cm^{-1}, also luminesces very brightly. In contrast, dysprosium luminesces brightly at 1% concentration but is completely quenched in $Na_{0.5}Dy_{0.5}WO_4$.

Thermal Effects

Thermal effects play an important role in the emission spectra of erbium in the scheelite structure.[14] Items to be considered are:

(a) At room temperature there are three strong emission peaks just on the high frequency side of the peaks due to emission from 18,400 cm^{-1}. The ratios of the intensities of the several peaks to each other are markedly concentration dependent, and the three high frequency peaks disappear at liquid nitrogen temperatures.

(b) Emission from the three main excited levels at room temperature increases and then quenches uniformly with concentration instead of sequentially as occurred for increasing exchange coupling in Tb^{3+} and Eu^{3+}.

(c) Cooling those samples which were nearly quenched at room temperature to liquid nitrogen temperatures greatly increased their luminescent intensities.

At liquid nitrogen temperature, the luminescence of $Na_{0.5}Er_{0.5}WO_4$ is as bright as that of the materials containing optimum erbium concentrations at room temperature. These results indicate that vibronic interactions lead to populated thermal emission states at low erbium concentrations and provide a means for the dissipation of energy from the normal excited states by radiationless transitions at room temperatures. $Na_{0.5}Er_{0.5}WO_4$ is an example of a concentrated rare earth salt that luminesces brightly (albeit at low temperatures) although it is not a close neighbor to gadolinium in the periodic table.

Acknowledgements

The author is indebted to D. Wood, C. G. B. Garrett, and A. Liehr of these Laboratories for their helpful discussions.

References

1. Gordy, J. Chem. Phys., 14, 305 (1946).
2. A. D. Walsh, J. Chem. Soc., London, 398 (1948).
3. T. Moeller, "Inorganic Chemistry," J. Wiley & Sons, New York (1955).
4. C. E. Moore, "Atomic Energy Levels" National Bureau of Standards V3 (1958).

5. Y. K. Syrkin and M. E. Dyatkina, "Structure of Molecules in the Chemical Bond," Interscience Publishers, New York (1950).

6. W. L. Bragg and J. West, Proc. Roy. Soc., A111, 691 (1926) and Ref. 4, p. 335.

7. O. Deutschbein and R. Tomaschek, Ann. d. Phys. (5) 29.S, 311 (1937).

8. V. V. Kuznetsoua, A. N. Sevchenko, Akad. Nauk. Izv., 23, No. 1, 2 (1959).

9. N. Chatterjee, Z. Phys., 113, 96 (1939).

10. L. G. Van Uitert and R. R. Soden, submitted for publication.

11. G. Urb in, Ann. d. Chim. et Phys. [8] 18, 222 (1902).

12. L. G. Van Uitert and R. R. Soden, J. Chem. Phys (1960).

13. M. Ch. de Rohden, Ann. de Chemie, 3, 338 (1915).

14. L. G. Van Uitert and R. R. Soden, to be published.

Abstract Number 48

SOME OPTICAL PROPERTIES OF POWDER AND CRYSTAL HALOPHOSPHATE PHOSPHORS

Peter D. Johnson

General Electric Research Laboratory
Schenectady, New York

Optical absorption, diffuse reflectivity and excitation spectra of some halophosphate phosphors have been determined in the spectral region 1100 to 3000Å. Transitions characteristic of the host lattice, manganese and antimony respectively, have been found.

Powder phosphors containing manganese and antimony separately and together and unac ivated halophosphates were made by usual commercial procedures. The host lattice materials were $3[Ca_3(PO_4)_2]\cdot CaF_2$, $3[Ca_3(PO_4)_2]\cdot CaCl_2$ and $3[Ca_3(PO_4)_2]\cdot 0.3\ CaCl_2\cdot 0.7\ CaF_2$, all with the structure of the mineral apatite. Small single crystals and clear polycrystalline pieces, up to 3 x 5 x 8 mm in dimensions, of some of the phosphors were made by melting in rf-heated iridium crucibles in an atmosphere of CO_2.

The diffuse reflectivities of the halophosphate powders with no deliberately added impurities show an abrupt decrease with decreasing wavelength at about 1500A for the fluorophosphate and 1570Å for the chlorophosphate. The reflectivities do not change appreciably in the wavelength region 1100 to 1500Å. It can be calculated[1] that the absorption in the region of low reflectivity is greater than 2000 cm^{-1}. Since this absorption cannot be accounted for by impurities, we conclude that intrinsic optical absorption begins at 7.9 ev in chlorophosphate and at 8.25 ev in fluorophosphate. There are strong absorption bands at 2000Å in the chlorophosphate and 1900Å in the fluorophosphate. Optical absorption of clear polished polycrystalline pieces of fluorophosphate, Fig. 1, shows the absorption band at 1900Å to reach a value of 200 cm^{-1}. Work is in progress to determine what electronic processes are responsible for the absorption edge at 1500Å and the band at 1900Å in the flurophosphate.

The introduction of manganese alone into the flurophosphate depresses the reflectivity in three unresolved bands at 1600, 1750 and 2150Å. It is possible to excite luminescence in manganese directly by irradiation in these bands in the absence of a sensitizer. Three peaks in the excitation spectrum for manganese emission are found at the same wavelengths as the reflectivity minima.

The diffuse reflectivity of fluorophosphate containing antimony indicates a broad absorption extending from the intrinsic absorption at

1500Å to about 2900Å. The 2537Å mercury line is not at a position of minimum reflectivity. Powders with both antimony and manganese have reflectivity spectra essentially the same as samples with antimony alone. The absorption due to antimony is very strong, reaching at least 2000 cm^{-1} in samples with approximately one per cent antimony. The reflectivities of the activated chlorophosphates are similar to the fluorophosphates.

There appears to be very little structure in the reflectivity due to antimony. However, the excitation spectra given in Fig. 2 show five unresolved peaks at 1600, 1750, 2050, 2200 and 2450Å. The 2537Å mercury line is appreciably removed from the longest wavelength excitation peak. Excitation in the 1600A band, which is common to both activators, results in more effective excitation of manganese emission relative to antimony emission than excitation in the other bands. Excitation in the fundamental absorption region below 1500Å is inefficient. Chlorophosphate has excitation spectra similar to the fluorophosphate with only minor shifts in peak positions and relative intensities.

Further work to elucidate the relationships among the energy levels and transitions discovered in this work is in progress.

References

1. P. D. Johnson, J. Opt. Soc. Am. 42, 978 [1952].

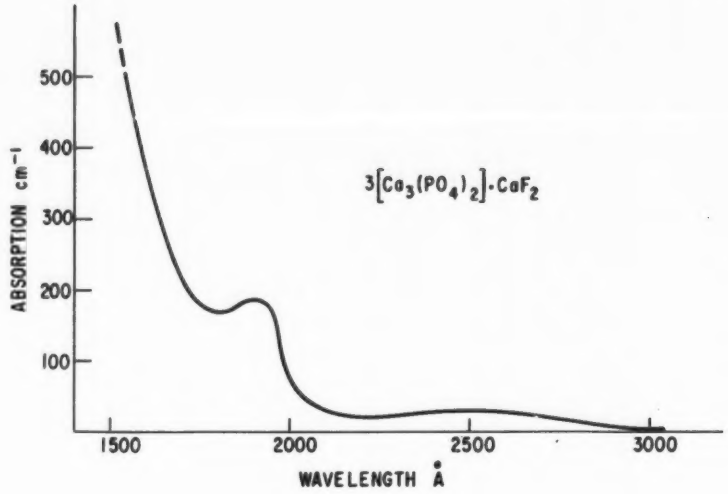

Fig. 1—Optical absorption of crystalline fluorophosphate.

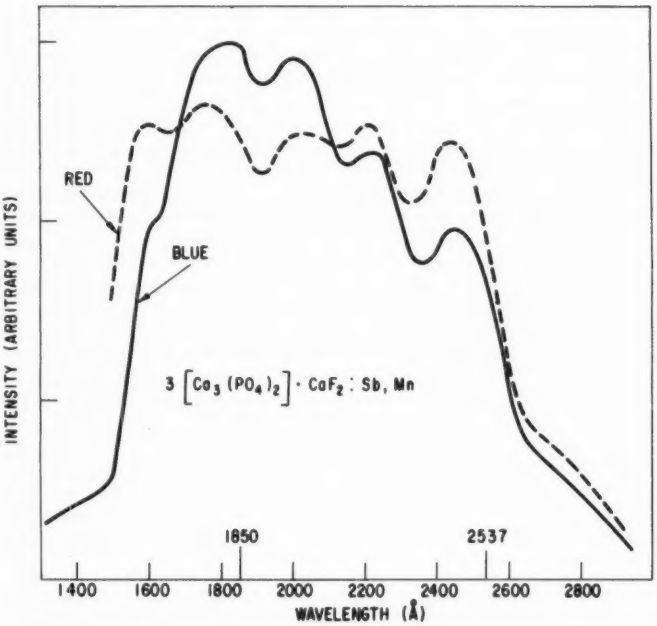

Fig. 2—Excitation spectra of fluorophosphate phosphor, dashed line for manganese emission band, solid line for antimony emission band.

Abstract Number 49

THE ENERGY LEVELS OF THE ANTIMONY CENTER IN HALOPHOSPHATES

Ferd E. Williams

General Electric Research Laboratory

The calcium halophosphate phosphors have the crystal structure of the mineral apatite. There exist two structurally different Ca^{++} ion sites. Each of the four type I Ca^{++} sites in the unit cell have six $O^{=}$ nearest-neighbors, whereas each of the six type II Ca^{++} sites have as nearest-neighbors five $O^{=}$ and one F^{-}. The manganese responsible for the orange emission has been at ributed to Mn^{++} at the type II Ca^{++} sites.[2,3] The orange emission spectrum is, therefore, dependent on the F/Cl composition of the ha ophosphate. It was first suggested that the antimony responsible for the blue emission involved Sb^{+++} at type I Ca^{++} sites with charge compensation by an associated interstitial $O^{=}$.[2] More recently, the blue emission has been attributed to Sb^{+++} at the type II Ca^{++} sites with concurrent substitution of $O^{=}$ at nearest-neighbor X^{-} sites.[3,4] The latter identification is consistent with the chemistry of the halophosphate phosphors, including a lower X^{-} content than corresponds to the stoichiometry of the pure halophosphate.[5,6] Except very near the pure chlorophosphate composition where structural changes are expected,[7] the blue emission has a negligible dependence on F/Cl since the nearest-neighbors of the Sb^{+++} are six $O^{=}$. With either identification, the antimony is a substitutional impurity with an excess positive charge and is charge compensated by a negatively charged impurity. The antimony and the compensating impurity will be associated into ion pairs because of the coulombic interaction between them.

Since Sb^{+++} has an electronic structure similar to Tl^{+}, the extensive theoretical work on KCl:Tl[8] can be applied qualitatively to Sb^{+++} in the halophosphates. In both ions the ground state is the ^1S state with the s^2 configuration and the excited states involved in the luminescence are the $^3P_1°$ and $^1P_1°$ states with the sp configuration. The KCl:In[9,10] and the halophosphate phosphors are even more closely related since In^{+} and Sb^{+++} are precisely isoelectronic. For example, the mixing by spin-orbit interaction of the $^3P°$ and $^1P°$ states are more nearly the same for In^{+} and Sb^{+++} than for Tl^{+} and Sb^{+++}.

There is, however, one way in which the electronic structure of the antimony center in halophosphates differs from the indium and thallium centers in alkali halides. This difference arises from the difference in charge of the Sb^{+++} and the Ca^{++} it replaces and from the excess charge of the compensating impurity. In KCl:In and KCl:Tl the activator ions

have the same charge as the ions they replace and there are no associated compensating impurities.

For example, let us consider the most probable diatomic impurity system in the halophosphates; namely, Sb^{+++} substituted at type II Ca^{++} sites with concurrent substitution of $O^{=}$ at the nearest-neighbor X^{-} site. Electron transfer transitions can quite evidently occur in the Sb^{+++}-$O^{=}$ ion pair. This pair and those characterized by larger inter-impurity distances have features similar to the donor-acceptor pairs in zinc sulfide phosphors. The energy levels of donor-acceptor pairs have been examined theoretically in the effective mass approximation for both polar and nonpolar media.[11] In general, the energy levels of the donor and acceptor are perturbed towards their respective band edges as a consequence of association into pairs. Optical transitions involving the creation or annihilation of an exciton bound to the ion pair are to be expected. These transitions correspond, of course, to classical electron transfer processes. The Sb^{+++}-$O^{=}$ pairs can be described as donor-acceptor pairs within the limits of applicability to halophosphates of the effective mass approximation. From recent optical measurements on single crystals[12] it can be inferred that the band gap of halophosphates is approximately 8 ev. If the effects of the polar character and the central cell correction are included, isolated Sb^{+++} at Ca^{++} sites and isolated $O^{=}$ at X^{-} sites are expected to introduce electron and hole states several electron volts from the conduction and valence band edges, respectively. Electron transfer states of Sb^{+++}-$O^{=}$ pairs are, therefore, expected in the same energy range as the excited $^3P_1^\circ$ and $^1P_1^\circ$ atomic states of Sb^{+++}. The electron transfer states, in contrast to the atomic states, are coupled to the valence and conduction band edges.

The atomic and electron transfer models are not in conflict with each other. The correct crystal states will have some of the characteristics of each. In other words, configuration interaction between atomic and transfer states which have approximately the same energy will occur. The localized atomic rearrangements responsible for the Stokes shift of the absorption and emission spectra of the antimony center are probably determined by the atomic-like part of the impurity wavefunction, whereas sensitization of the orange manganese emission is probably determined by the diffuse electron transfer part of the wavefunction for the excited antimony center. Additional sensitization mechanisms are made possible by the transfer states. Quantitative calculation and additional optical and electrical measurements should reveal the relative importance of the atomic and electron transfer states of the antimony center in halophosphate phosphors.

References

1. St. Naray-Szabo, Z. Krist. 75, 387 (1930).
2. K. H. Butler and C. W. Jerome, J. Electrochem. Soc. 97, 265 (1950).

3. J. L. Ouweltjes, Phil. Tech. Rev. 13, 344 (1951).

4. J. S. Prener and F. E. Williams, Symposium Electrochem. Soc. May 1-5, 1955, Cincinnati.

5. W. L. Wanmaker, J. Physique Rad. 17, 636 (1956).

6. J. F. Ross, U. S. Patent 2,904,516, Sept. 15, 1959.

7. S. B. Hendricks, M. E. Jefferson and V. M. Moseley, Z. Krist. 81, 352 (1932).

8. e.g. F. E. Williams, J. Chem. Phys. 19, 457 (1951); J. Opt. Soc. Am. 47, 869 (1957).

9. F. E. Williams, B. Segall and P. D. Johnson, Phys. Rev. 108, 46 (1957).

10. N. E. Lushchik, Inst. Fig. i. Astron., Akad. Nauk, Eston SSR 6, 149 (1957).

11. F. E. Williams, J. Phys. Chem. Solids (in press).

12. P. D. Johnson, this meeting.

Abstract Number 50

LEAD-AND MANGANESE-ACTIVATED CALCIUM·CADMIUM SILICATE PHOSPHORS

Yasuo Uehara, Yoshima Kobuke, Isoo Masuda,
and Takashi Kushida

Matsuda Research Laboratory,
Tokyo Shibaura Electric Co., Ltd.,
Kawasaki, Japan

The characteristics of lead-and manganese-activated calcium·cadmium silicate phosphors with various mole ratios of cadmium to calcium were investigated. Two series of phosphors were prepared by firing the mixtures of (1-x) mole calcium carbonate, x mole cadmium compounds and 1.2 mole silica with 8 mole percent lead fluoride and 10 mole percent manganese chloride for two 2-hour periods at 1180°C, with intimate grinding between firings. The first and second group of phosphors were prepared with cadmium sulfate and carbonate as cadmium compounds, respectively.

The emission spectra of phosphors under excitation by 2537Å were measured with the Automatic Recording Spectroradiometer which was constructed by Uehara and coworkers by using a Zeiss Three Glass-Prism Monochromator reported in a previous paper[1]. The wavelength dependence of the quantum efficiency of the typical phosphor was measured by the direct optical method, as reported in a previous paper[2].

The lattice spacing of all the phosphors were measured by the powder photographic method.

The emission spectra of all the phosphors showed a broad band with three line like bands peaking always at about 6880, 6950 and 7050Å. As the cadmium content is increased up to about 0.5 - 0.7 or 0.9 mole percent in the first and second group of phosphors, respectively, the peak position of the broad band shifts gradually from about 6100 to 6430Å. Further increase of cadmium content shifts it toward shorter wave-lengths down to about 6200Å. On the other hand, the peak positions of three sharp bands were independent of the composition of phosphors. The concentration dependence curve of fluorescent intensity for the first group of phosphors showed a maximum at the concentration of 10-20 mole percent cadmium, while that for the second group of phosphors gave two maxima at the concentrations of about 30 and 60 mole percent cadmium and one minimum at the concentration of about 50 mole percent cadmium. The fluorescent intensity of these phosphors containing 30 and 60 mole percent cadmium was nearly equal to that of the most efficient phosphor in the first group. The

output of fluorescent lamps made with the phosphors of the second group containing 20 and 60 mole percent cadmium were about 550 and 260 lm/W at 100 hours, respectively. The quantum efficiency of the former phosphor was 0.71 at 2537Å and its maximum value was 0.73 at 2650Å.

The measured result of the lattice spacing of cadmium silicate phosphor was in reasonable agreement with the data reported for β-metacalcium silicate. The diffraction patterns for cadmium silicate phosphor were quite similar to that for calcium silicate. Furthermore, the diffraction patterns of calcium·cadmium silicate phosphors belonging to the two groups and having the same compositions were similar to each other. The relation between the lattice spacing and cadmium concentration was linear.

The broad band of the emission spectrum will be ascribed to Mn^{2+} ions, while the sharp bands, whose positions are independent of the composition of phosphors, may be attributable to Mn^{4+} ions for the same reason as reported for titanate, germanate or arsenate phosphors by several workers[3]. The shift of the position of the broad band will be caused by the variation of the lattice spacing, i.e. by that of interactions between Mn^{2+} and lattice ions. The characteristics of the sharp bands will be explained by the consideration of the shielding effect in Mn^{4+} ions.

The measured linear relation between the lattice spacing and concentration of cadmium suggests the formation of solid solution between calcium and cadmium silicate. According to the reported literatures[4], the crystal structure of β-calcium and cadmium silicate are monoclinic and orthorhombic, respectively. However, their lattice constants, in addition to the ionic radii of calcium and cadmium ion, are rather similar to each other. This is the reason for the formation of a solid solution.

The irregular shift of peak positions of emission spectra of both groups of phosphors will be explained by assuming the existence of monoclinic and orthorhombic crystal structure of solid solutions below and above the concentrations at which the concentration dependence curves of peak wave-length showed the maximum values, respectively. The difference of the characteristics between the two groups of phosphors may be explained by assuming the formation of a sulfosilicate in the first group of phosphors.

References

1. Y. Uehara, Y. Kobuke, and I. Masuda, J. Electrochem. Soc., 106, 200 (1959).
2. Y. Uehara, I. Masuda, and Y. Kobuke, to be published in the J. Electrochem. Soc., January (1960).
3. F. A. Kröger, Some Aspects of the Luminescence of Solids, Elsevier Publishing Co., Inc., New York, (1948); F. A. Kröger, and J. van den

Boomgaard, J. Electrochem. Soc., 97, 377 (1950); L. Thorington, J. Opt. Soc. Amer., 40, 579 (1950); M. Travnicek, F. A. Kröger, T. H. P. J. Botden, and P. Izalm, Physica, 18, 33 (1952).

4. E. Voos. Z. Anorg, Allgem. Chemie, 222, 201 (1935); J. D. Hanawalt, H. W. Rinn, and L. K. Frevel, Ind. Eng. Chem., Anal. Ed., 10 457 (1938); H. Ehrenberg, Z. Physik. Chem., B14, 425 (1931); G. R. Fonda and H. C. Froelich, Trans. Electrochem. Soc., 93, 114 (1948); ASTM X-Ray Diffraction Data Cards (1955).

Abstract Number 51

LUMINESCENCE-VERSUS-COMPOSITION STUDIES OF COMPLEX ZINC AND CADMIUM ORTHOPHOSPHATES CONTAINING SODIUM AND LITHIUM

Arthur L. Smith

Electron Tube Division, Radio Corporation of America
Lancaster, Pa.

Introduction

The existence of compounds of the type $M^{I}M^{II}PO_4$, formed by solid-state reactions, has been known for some time.[1] The manganese-activated luminescence of a few of these compounds has been reported.[2,3] Certain unusual features prompted a survey of a few of the many combinations which are possible in the generic system $M^{I}_3PO_4 + M^{II}_3(PO_4)_2$. The compounds studied were:

$Zn_3(PO_4)_2 + Li_3PO_4:Mn$
$Zn_3(PO_4)_2 + Na_3PO_4:Mn$
$Cd_3(PO_4)_2 + Li_3PO_4:Mn$
$Cd_3(PO_4)_2 + Na_3PO_4:Mn$

The end-member compounds were precipitated from solution by conventional means. The amounts of each component needed to produce 10-mole-per cent variations were ball-milled in water, the pebbles were removed, and the entire charge was then dried. Firing was conducted in open boats, in air, at temperature dictated by the particular combination, to prevent fusion.

The cathodoluminescence and X-ray diffraction patterns were obtained by conventional techniques.

A complexity not hitherto suspected was found in these systems. In addition to the $M^{I}M^{II}PO_4$ types previously reported, there are definitely other compounds of less simple stoichiometry which sometimes form solid solutions between themselves and the end members. The survey approach has left many problems unresolved, particularly the inexact correlation between the luminescence and X-ray data. Much more work will be necessary before valid conclusions can be drawn. In the zinc systems, for example, no attempt was made to obtain a pure phase as starting material.[3,4] There is evidence to indicate that the α and γ phases react through independent mechanisms, although the final product is the same for both forms.

Results and Conclusions

The results of the work are summarized in Figures 1-4. In these figures the product of reaction as determined by X-ray diffraction is shown by symbol for each composition fired. The peak wavelength of emission and the peak intensity of emission with $(Zn_3(PO_4)_2$:Mn used as standard are also noted for each composition.

As Hummel et al have pointed out, the addition of manganese introduces a new phase; hence the systems studied are in reality three-phase systems, with alkali phosphate, zinc or cadmium phosphate, and manganese phosphate comprising the three phases. In the Zn-Li systems the amount of manganese added and the firing temperature have been found to influence the intermediate X-ray patterns obtained, although they do not alter the formation of $ZnLiPO_4$ or the compound whose formula is assumed to be $3Cd0.3Li_20.2P_2O_5$. Check samples have definitely shown an analogous complexity in the Li_3PO_4 - $Mn_3(PO_4)_2$ system itself.

Of considerable interest is the formation of cubic compounds with the probable type formula $MO{\cdot}5Na_2O{\cdot}2P_2O_5$, where M is Zn or Cd. Although these compounds are non-luminescent, they are of importance in structural chemistry.

Because of the survey type of investigation, the formula of some of the new compounds must be taken with caution. Although there is no doubt of their existence, in some cases not enough work was done to establish with certainty the exact stoichiometry.

On the basis of this work, and a few check samples, it is predicted that potassium orthophosphate with zinc and cadmium orthophosphate will also form definite compounds not yet reported; also it is certain that the alkaline earth orthophosphates will similarly react with alkali orthophosphates to give as-yet-unknown compounds. It is also hypothesized that metaphosphates and pyrophosphates containing both Group I and II elements also exist.

References

1. E. Thilo, Naturwiss 16, 239 (1941). See also "Text-Book of Inorganic Chemistry," Vol. III, Part II, J. N. Friend, Editor; Griffin & Co. Ltd, (1926), P. 145.
2. F. A. Kroger, "Some Aspects of the Luminescence of Solids; Elsevier Publishing Co., Inc. (1948).
3. A. L. Smith, J. Elect. Soc. 98, 363 (1951).
4. F. A. Hummell and F. L. Katnack, J. Elect. Soc. 105, 528 (1958).

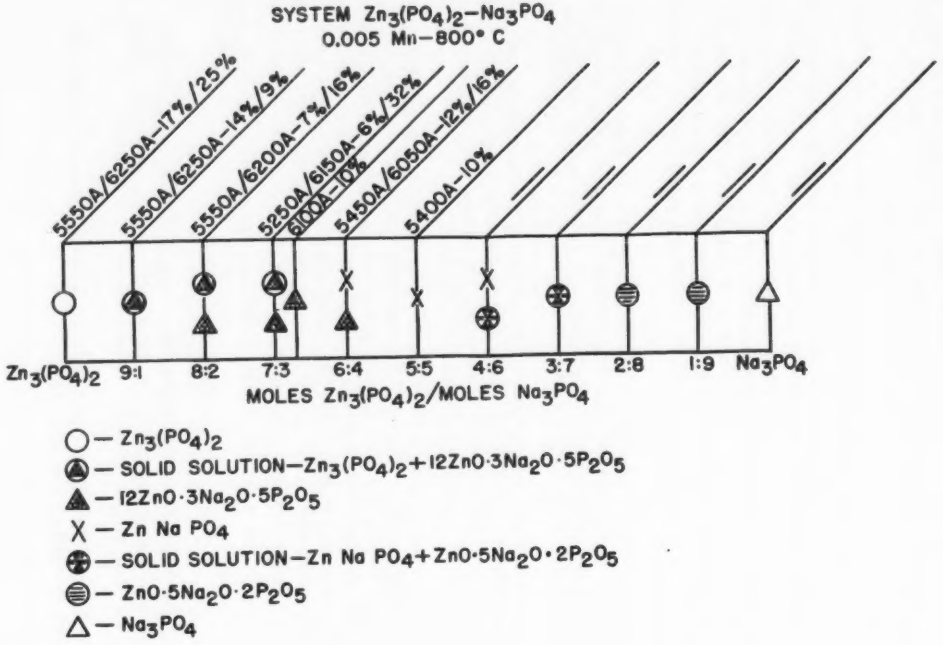
SYSTEM $Zn_3(PO_4)_2$–Na_3PO_4
0.005 Mn–800° C
5550A/6250A–17%/25%
5550A/6250A–14%/9%
5550A/6200A–7%/16%
5250A/6150A–6%/32%
6100A–10%
5450A/6050A–12%/16%
5400A–10%
$Zn_3(PO_4)_2$
9:1
8:2
7:3
6:4
5:5
4:6
3:7
2:8
1:9
Na_3PO_4
MOLES $Zn_3(PO_4)_2$/MOLES Na_3PO_4
— $Zn_3(PO_4)_2$
— SOLID SOLUTION—$Zn_3(PO_4)_2$+12ZnO·3Na_2O·5P_2O_5
— 12ZnO·3Na_2O·5P_2O_5
— Zn Na PO_4
— SOLID SOLUTION—Zn Na PO_4+ZnO·5Na_2O·2P_2O_5
— ZnO·5Na_2O·2P_2O_5
— Na_3PO_4

Figure 1

Figure 1

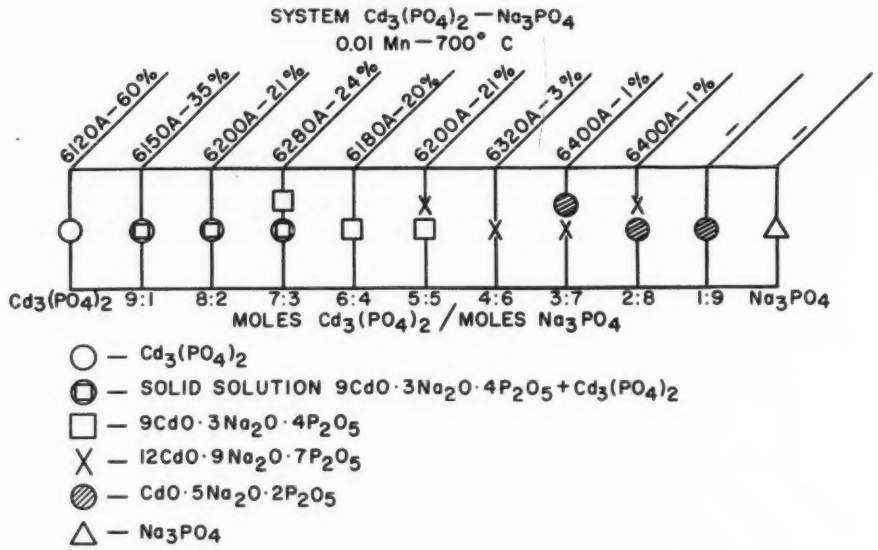
SYSTEM $Cd_3(PO_4)_2 - Na_3PO_4$
0.01 Mn — 700° C
6120A – 60%
6150A – 35%
6200A – 21%
6280A – 24%
6180A – 20%
6200A – 21%
6320A – 3%
6400A – 1%
6400A – 1%
$Cd_3(PO_4)_2$ 9:1 8:2 7:3 6:4 5:5 4:6 3:7 2:8 1:9 Na_3PO_4
MOLES $Cd_3(PO_4)_2$ / MOLES Na_3PO_4
— $Cd_3(PO_4)_2$
— SOLID SOLUTION $9CdO \cdot 3Na_2O \cdot 4P_2O_5 + Cd_3(PO_4)_2$
— $9CdO \cdot 3Na_2O \cdot 4P_2O_5$
— $12CdO \cdot 9Na_2O \cdot 7P_2O_5$
— $CdO \cdot 5Na_2O \cdot 2P_2O_5$
— Na_3PO_4

Figure 2

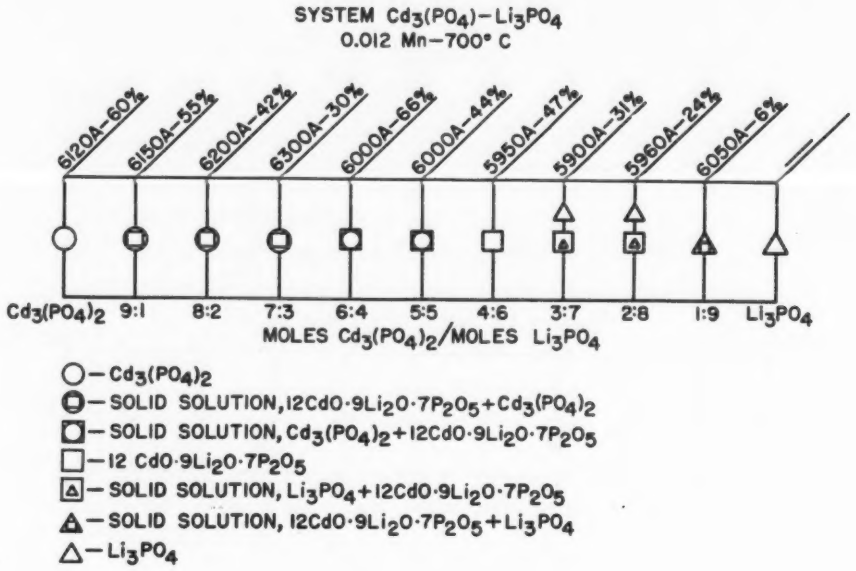
SYSTEM $Cd_3(PO_4)-Li_3PO_4$
0.012 Mn—700° C
6120A—60%
6150A—55%
6200A—42%
6300A—30%
6000A—66%
6000A—44%
5950A—47%
5900A—31%
5960A—24%
6050A—6%
$Cd_3(PO_4)_2$ 9:1 8:2 7:3 6:4 5:5 4:6 3:7 2:8 1:9 Li_3PO_4
MOLES $Cd_3(PO_4)_2$/MOLES Li_3PO_4
— $Cd_3(PO_4)_2$
— SOLID SOLUTION, $12CdO \cdot 9Li_2O \cdot 7P_2O_5 + Cd_3(PO_4)_2$
— SOLID SOLUTION, $Cd_3(PO_4)_2 + 12CdO \cdot 9Li_2O \cdot 7P_2O_5$
— $12\ CdO \cdot 9Li_2O \cdot 7P_2O_5$
— SOLID SOLUTION, $Li_3PO_4 + 12CdO \cdot 9Li_2O \cdot 7P_2O_5$
— SOLID SOLUTION, $12CdO \cdot 9Li_2O \cdot 7P_2O_5 + Li_3PO_4$
— Li_3PO_4

Figure 3

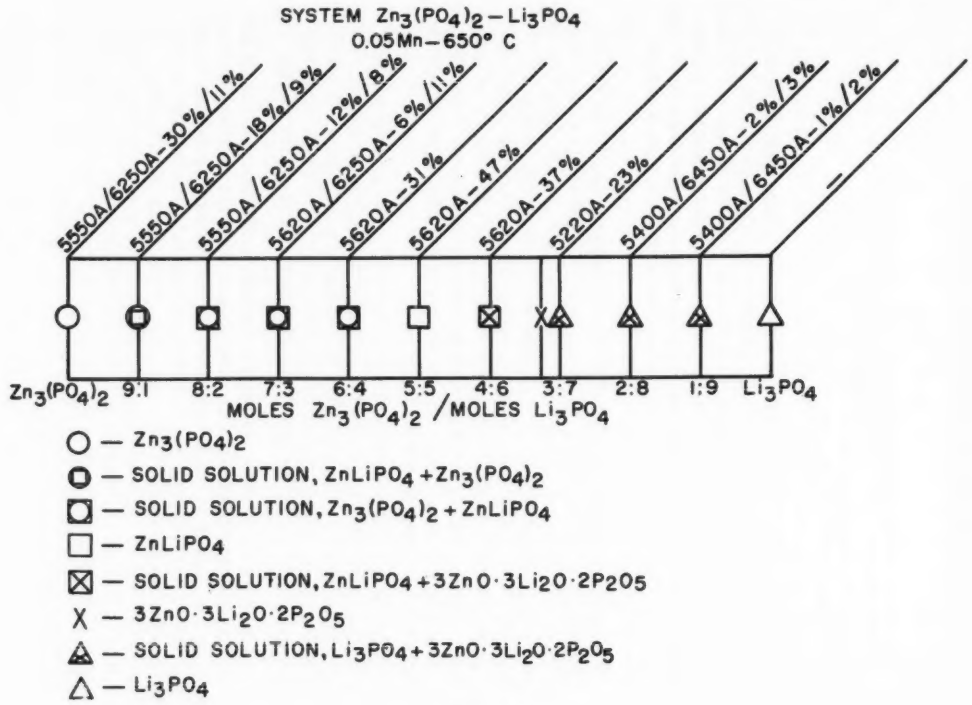
SYSTEM $Zn_3(PO_4)_2 - Li_3PO_4$
0.05Mn—650° C
5550A/6250A-30%/11%
5550A/6250A-18%/9%
5550A/6250A-12%/8%
5620A/6250A-6%/11%
5620A-31%
5620A-47%
5620A-37%
5220A-23%
5400A/6450A-2%/3%
5400A/6450A-1%/2%
$Zn_3(PO_4)_2$ 9:1 8:2 7:3 6:4 5:5 4:6 3:7 2:8 1:9 Li_3PO_4
MOLES $Zn_3(PO_4)_2$ / MOLES Li_3PO_4
○ — $Zn_3(PO_4)_2$
◎ — SOLID SOLUTION, $ZnLiPO_4 + Zn_3(PO_4)_2$
◎ — SOLID SOLUTION, $Zn_3(PO_4)_2 + ZnLiPO_4$
□ — $ZnLiPO_4$
⊠ — SOLID SOLUTION, $ZnLiPO_4 + 3ZnO \cdot 3Li_2O \cdot 2P_2O_5$
X — $3ZnO \cdot 3Li_2O \cdot 2P_2O_5$
△ — SOLID SOLUTION, $Li_3PO_4 + 3ZnO \cdot 3Li_2O \cdot 2P_2O_5$
△ — Li_3PO_4

Figure 4

Abstract Number 52

CADMIUM PHOSPHATE PHOSPHORS

R. C. Ropp

Sylvania Electric Products Inc.,
Towanda, Penna.

The phosphors, $Cd_2P_2O_7$:Mn and $Cd_3(PO_4)_2$:Mn have been described previously[1,2] as orange-emitting cathode-ray phosphors. Double activation by both lead and manganese is said to produce phosphors[3,4] which are ultraviolet sensitive as well. The present work describes a phenomenon by which the response of these cathode-ray phosphors to 254 mu ultra-violet radiation is increased several times following a second-step firing in a reducing atmosphere.

Cadmium pyrophosphate phosphors are easily prepared by solid-state reaction of $CdNH_4PO_4 \cdot H_2O$ and $MnNH_4PO_4 \cdot H_2O$ in suitable proportions at temperatures above 700°C. The addition of CdO, CdO_2, $Cd(OH)_2$ or $CdCO_3$ in proper quantity to the above raw materials will produce $Cd_3(PO_4)_2$:Mn. The presence of chlorides during prefiring in air or nitrogen must be avoided to prevent formation of cadmium chlorophosphate. Purity of the phosphors was excellent and no more than 100 ppm of impurities [excluding Cd, P, Mn and Ca (500 ppm)] were found to be present (spectrographic analysis).

$Cd_2P_2O_7$:Mn emits at 618 mu while $Cd_3(PO_4)_2$:Mn emits at 604 mu when excited by 254 mu radiation. Change in manganese content or firing atmosphere does not affect the emission band. Data are given to show that the pyrophosphates are by far the more efficient of the two systems and most of the data presented deal with the pyrophosphates.

A study of the excitation spectra of $Cd_2P_2O_7$:Mn as a function of firing atmosphere showed that the phosphor fired in air or nitrogen has an excitation peak in the far ultraviolet. Refiring in N_2 did not change the peak, but refiring in N_2-H_2 shifted the peak to 246 mu with a consequent large gain in 254 mu response. Weak absorption bands in the near-ultraviolet and blue spectral regions were observed corresponding to those found in Zn_2SiO_4:Mn and ZnS:Mn and attributed to the Mn^{+2} ion in the phosphors[5]. These were present irrespective of firing atmosphere. In addition, there was the broad excitation band, mentioned above, at the higher energies.

In contrast, $Mg_2P_2O_7$:Mn, $Zn_2P_2O_7$:Mn, $Sr_2P_2O_7$:Mn or $Ca_2P_2O_7$:Mn did not show this effect upon reduction. However, $Ca_2P_2O_7$:Mn and $Sr_2P_2O_7$:Mn did possess weak absorption bands in the near ultraviolet and blue regions of the spectrum, but did not have the broad excitation band at the higher energies characteristic of $Cd_2P_2O_7$:Mn. $Cd_2P_2O_7$

forms mixed phosphors with Mg, Zn, Sr and Ca pyrophosphates over a rather narrow concentration range, the plaque brightness decreasing to 40% of the original at 75 mol % Cd. The cadmium-calcium phosphors became greener with Ca content, whereas the cadmium-zinc or cadmium-magnesium pyrophosphates became redder as the Zn or Mg ratio increased.

The reduction reaction is a function of hydrogen content in the ambient atmosphere, firing temperature and firing time. Data are given showing changes in plaque response (254 mu) as a function of firing. The effect is reversible, to a degree, as long as the melting point is not too closely approached. The beneficial effect of reduction may be reversed by reheating in air and the phosphors so treated lose brightness. Conversely, inefficient phosphors may be made more responsive to 254 mu by a repeated heating in a reducing atmosphere.

For an unactivated phosphor, $Cd_2P_2O_7$ (Mn $<$ 1 ppm), the excitation peak is found at high energies (225 mu) and the emission peak is barely detectable at 592 mu. The introduction of Mn shifts the emission to 618 mu and the emission intensity increases many fold. The plaque brightness increases from 32% of cadmium borate phosphor at .01 mol Mn per mol pyrophosphate to 92% at .08 mol Mn, remains essentially the same to 0.20 mol Mn, and decreases to 50% at 0.30 mol Mn. The extremely wide activator concentration range is attributed to the marked similarity in the chemistry of the Cd and Mn phosphates and to the fact that these compounds easily form mutually soluble systems.

The excitation spectra also show a shift with Mn content and at 0.08 mol Mn, the peak appears at 252 mu, which explains the maximum in 254 mu response observed. A comparison of the spectral reflectance revealed that, at 1 ppm Mn content, no change in absorption could be detected, whereas for activator concentrations (30,000 ppm Mn) a definite increase in ultraviolet absorption was measured for the reduced phase as compared to the oxidized phase. This indicates that it is the reduction of manganese which causes the increase in response to 254 mu. A further comparison of excitation spectra as a function of Mn concentration for both the air-fired and reduced forms, showed a shift in excitation peak position due both to Mn content and the effect of reduction. Thus, for the air-fired phosphors - 0.01 Mn peaks at 229 mu and 0.08 Mn peaks at 240 mu, whereas upon reduction, 0.01 Mn peaks at 235 mu and 0.08 Mn at 252 mu.

The effect of reduction does not appear to be a simple reduction of the Mn in the phosphor, but a complex combination of reduction of both Mn and the host crystal to produce increased response to 254 mu ultraviolet radiation. The manganese is in the manganous state as indicated by the presence of the low energy absorption bands in the near-ultraviolet region, but the absorption band found at higher energies occurs only in the combination of $Cd_2P_2O_7$ and manganese. Reduction then increases the 254 mu response markedly.

Lamp brightnesses up to 30.0 LPW at 100 hrs. show that these phosphors are comparable in efficiency to the cadmium borate phosphor.

References

1. F. E. Williams, USP 2,463,449 (1949).
2. A. L. Smith and A. D. Power, J. Electrochem. Soc. 101, 244 (1954).
3. N. A. Gorbacheva, P. N. Lebedev, Phys. Fiz. 21, 305 (1951).
4. V. V. Zelinskii, F. M. Pekerman, T. V. Timofeeva and B. I. Vainberg, Zhur. Eksptl. Teoret. Fiz. 20, 395 (1950).
5. C. C. Klick, Brit. J. Appl. Phys. Suppl. No. 4, S74 (1955).

Abstract Number 53

LUMINESCENCE OF AIN

I. Adams, J. W. Mellichamp, and G. A. Wolff

U. S. Army Signal Research and Development Laboratory,
Fort Monmouth, New Jersey

An investigation of the electroluminescence (EL), phosphorescence (Ph), and cathodoluminescence (CL) of AlN has been made. As reported previously[1] the EL spectra show narrow bands in the 400-500 mμ region, identified as the second positive system of N_2, and broad bands in the 500-700 mμ region; the Ph and CL spectra show broad bands in both the 500-630 and the 300-500 mμ region. The following types of emission are observed:

1. Red emission in EL and PH is found in AlN samples that have been doped with small amounts of Mn(10 ppm) in the presence of Cl_2; the spectra show a broad band in the 580-650 mμ region with the maximum near 610 mμ. The same band has been observed in CL together with the blue emission which will be mentioned later. Possible activator is Mn^{4+}. A red emission is also observed in EL and Ph when Be^{++} is present.

2. Green emission is observed in El, CL and fluorescence of AlN with relatively high concentrations of Mn (1.%) possibly present as Mn^{++}. No Ph is found. In EL the corresponding broad band appears in the 490-570 mμ region with the maximum near 520 mμ. This luminescence has always been obtained in EL together with the red and blue bands cited under 1. and 3., respectively.

3. Blue emission in EL, Ph and CL is seen in AlN crystals with Si as possible activator or in samples of high purity (99.99%). This may also be caused by Al excess[2]. The latter sometimes do not show emission. In Ph and CL the corresponding broad band is found to extend from about 470 mμ into the UV with the peak at varying values. The Ph is excited by Hg 254 mμ or by shorter wave-length radiation. So far in EL it was not possible to detect this band. In its place narrow bands were observed which were identified as the second positive system of N_2. It also was found that in EL this system was always accompanied by what appears to be a broad band in the 630-730 mμ region, but which after a closer inspection reveals fine-structure. A comparison of these bands with the corresponding bands observed in the spectrum of N_2 of low pressure (1 mm Hg) which was excited by microwaves indicates the possible presence of the first positive system of N_2.

4. Yellow-greenish EL and Ph was also observed which was not

further investigated. In contrast to the blue Ph mentioned under 3. it was possible to excite this Ph by Hg 365 mμ radiation and from microwave excited N_2 inside a pyrex tube.

As has been mentioned under 3., it seems that the narrow bands observed in EL replace the broad Ph band in the same region. Since similarly the triboluminescence spectra of various materials were found to consist of the second and possibly of the first positive system of N_2, a similar excitation mechanism may be inferred. A possible mechanism is an energy transfer between the surface of AlN and the N_2 molecules. The influence of various ambients (CO, dry and humid N_2, a.o.) on the EL spectrum has been studied. EL was not obtained in vacuum, and was greatly reduced in gases other than N_2. The EL of AlN was studied in great detail by the application of voltages of varying square-wave characteristics and other parameters. Ph decay and glow-curve measurements indicate the existence at least two deep traps below the conduction band. The possibility exists that the energy gap is as high as 5.5 eV.

The AlN samples were prepared as follows. About 50 gms of high purity Al powder (99.999%) was placed in a high purity Al_2O_3 crucible ("Morganite"). The crucible was placed inside of a tungsten heating coil in a pressure reactor (figure). "Prepurified" N_2 gas was passed into the reactor until the pressure reached about 700 psi. A current of about 100 amps. heated the tungsten coil. At a pressure of about 1500 psi. and a temperature of about 1600°C the formation of AlN takes place as noticed by a sudden decrease in pressure. After five minutes the reaction is completed. After cooling, the hard solid mass is removed from the crucible, pulverized and treated with Cl_2 gas at about 600°C. In this way unreacted Al and other impurities are removed. The resultant crystalline powder is of a purity of 99.99-99.999%. It is doped in an N_2 atmosphere at elevated temperature followed by another treatment with Cl_2 gas to remove excess doping material. The conditions of preparation and doping may be varied for optimum results.

References

1. G. A. Wolff, I. Adams, and J. W. Mellichamp, Phys. Rev. 114, 1262 (1959).

2. C. Buhrer & E. Banks, Electrochem. Soc., Abstracts, Spring Mtg, 1958, p. 22.

AUTOCLAVE PRESSURE REACTOR

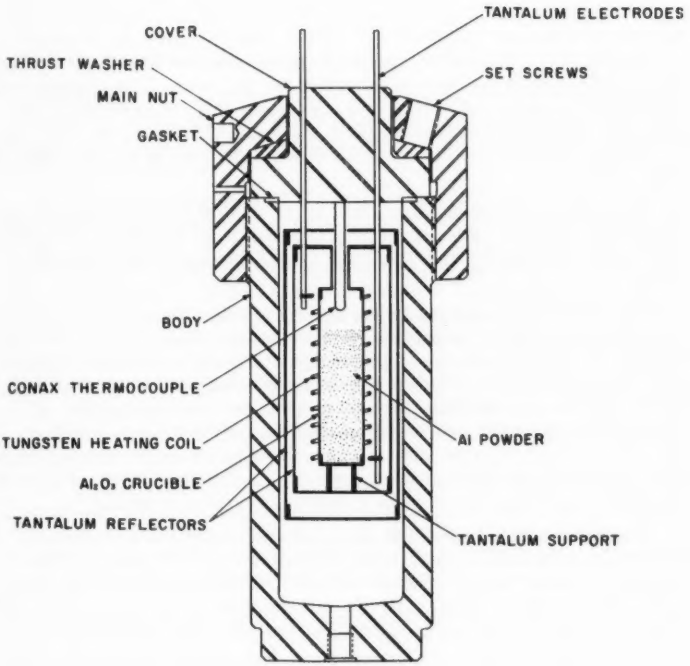

Figure 1

Abstract Number 54

CRYSTAL STRUCTURE AND SPECTRA OF ALKALI HALIDE PHOSPHORS

F. D. Klement

Physics and Astronomy Institute,
Academy of Sciences of the Estonian S.S.R.
Tartu, U.S.S.R.

Emission and absorption spectra in phosphors are usually determined by the activator in the field of the surrounding atoms. The character of this field (intensity and symmetry) affects not only the position of the spectral bands of the activator, their width and structure, but also the transition probabilities between different energy levels, i.e. the ratio of band intensities.

The present communication gives an account of relevant experimental results obtained under the author's guidance at the laboratories of Tartu State University and the Academy of Sciences of the Estonian S.S.R.

The influence of structure upon spectra (in those cases where the chemical composition of phosphors remains constant) is revealed by the changes of spectra that attend polymorphic transitions of the host crystal. N. Ivanova and A. Pae have investigated ammonium halide phosphors activated by thallium, tin and copper. As the temperature is gradually altered, the spectrum changes sharply at the polymorphic transition point. Similar spectra correspond to the same crystal structure of chemically different host crystals. In some cases the change of emission color may serve as an indicator of change in structure.

Investigations (J. Kirs) of polymorphic transitions in phosphors caused by hydrostatic compression showed changes of spectra when pressures producing polymorphic transitions were reached. This phenomenon provides a simpler way of determining the pressures required to produce polymorphic transitions than that of x-ray diffraction.

J. Kirs and A. Laisaar investigated spectral shifts when a decrease in atomic distances was caused by hydrostatic compression. The direction and magnitude of such shifts make it possible to draw conclusions concerning some energy characteristics of luminescence centers. The magnitude of the spectral shift is closely related to the compressibility of the crystals. This may be accounted for by the fact that both the elastic as well as optical properties of the crystals depend on the ability of the electronic shells to deform.

Investigations were devoted to the influence of lattice defects on the spectra of phosphors (T. Abdusadykov, A. Malysheva). In agreement

with the ideas of other authors, a lattice defect, e.g. a vacancy near the activator ion, changes its spectrum considerably. It was found that there are two different types of luminescence centers (activator ions at a substitutional site of the lattice and near the defect) and two corresponding groups of spectral bands. Monovalent activators give only one group of spectral bands in alkaline earth halides. The need for charge compensation in such systems indicates the activator is located only near an anion-vacancy.

The questions of lattice defects and activator location are related to the sizes of small crystals and the methods of activator introduction. Investigations by the author and A. Malysheva of phosphor synthesis by means of vacuum evaporation has shown that in the evaporated phosphors (as is always the case with activator diffusion in fine-grained host crystals) the long-wave bands corresponding to centers in the defect region predominate.

The author and A. Malysheva have shown the influence of a gaseous atmosphere on the crystallization processes of evaporated phosphor layers. This has also been investigated by means of the electronographic method (A. Haav).

In phosphors that are unstable solid solutions of an activator and base substances, grinding of the crystal leads to the decomposition of the solution (e.g. NaCl-Tl or KCl-Ag). In these phosphors the spectra depend largely on the activator concentration, and it is possible to observe the decomposition by means of spectral changes. The thermal quenching of emission that occurs when crystals are ground to powder in phosphors of these types can be explained, at least partly, by the decomposition of the solid solution (the author and R. Gindina). The spectral method also enables us to determine whether the activator is in a precipitated phase or whether it has been included in the activator centers. Chemical and x-ray methods of analysis are not sensitive enough for phosphors with low activator concentrations.

R. Gindina studied the decomposition of the solid solutions (e.g. NaCl-$PbCl_2$) with a microscope. The activator which precipitates during the heating of the crystal and the subsequent slow cooling is concentrated at the dislocation lines. The latter are decorated since chains of colloidal particles formed at dislocation lines diffuse light strongly.

The author and L. Teiss, studied the structure of the luminescence centers in phosphors of mixed host crystals. In these systems centers with different structures are formed. Such centers are distinguished by the ratio of the numbers of different ions of the components of the mixed crystals (different micro structures). The spectra of the activator in centers with different micro structures differ and the spectrum of the crystal as a whole will have structure which should be the easier to detect, the more the activator spectra are displaced in relation to one another in the corresponding host crystals. The character of this spectral structure or the general band form and its maximum position (when the structure is not resolved) depends on the energy advantage of the activator being in centers with one or another micro structure. Spectral

methods made it possible to detect such micro structures in KCl - KBr and NH_4Cl - NH_4Br activated by thallium. Thallium is located chiefly in the centers that contain the larger fraction of heavier anions.

By way of a discussion with L. Shamovsky, who maintains the idea of the surface nature of luminescence centers in phosphors, it has been shown on the basis of an analysis of spectral and other data that there are not only volume centers but also surface luminescence centers.

The present survey as well as data obtained by other authors on the dependence of spectra upon crystal structure illustrate the feasibility of developing a solid state spectroscopy. As regards the practical aspect these data may be employed to devise luminescent methods (as well as spectral methods in general) of physico-chemical and structure analysis. They may also be used for the intentional regulation of the spectral properties of phosphors.

ON THE HYDROGEN-LIKE MODEL FOR TRAPS IN ZINC SULFIDE

G. Curie, N. Arpiarian, P. Guéret, and D. Curie

Laboratoire de Luminescence
Faculté des Sciences, Paris, France.

In the Discussion section of the Paris Colloquium on Luminescence[1], one of us has proposed for traps in ZnS the following model, which draws its inspiration from Williams and Prener's model of "associated donor-acceptor centers":

a) the shallow traps may be ascribed to a substitutional charge +e (S-vacancy of effective charge unity if the percentage of ionic binding in ZnS is assumed to be 75%), which has trapped the electron upon an hydrogen atom-like orbit. The thermal and optical depths are respectively:

$$(1) \qquad E = \frac{R}{K^2_{eff}} \qquad h\nu = \frac{R}{K_{eff}K_0}$$

R = 13.5 eV the Rydberg constant, K_{eff} an "effective" dielectric constant, which may be calculated from K static and K_0 high frequency dielectric constant.

Table I. Trap depths according to the hydrogen atom-like model.

	K	K_0	K_{eff}	E (eV)	$h\nu$(eV)
ZnS	8.3	5.07	6.93	0.28	0.38
CdS	11.6	5.87	8.88	0.17	0.26
ZnO	12	3.88	7.25	0.26	0.47

b) the deep traps are ascribed to the preceeding trapping charge +e, A (in a Sulfur lattice site A) perturbed by the field due to the ionized Copper center in ZnS(Cu), acting as an other charge +e (in a Zinc lattice site B). The trapped electron moves upon an hydrogen molecule-ion like orbit, whose thermal and optical depths are approximately:

$$(2) \qquad E = \frac{R}{K^2_{eff}} + \frac{e^2}{Kr_{AB}} \qquad h\nu = \frac{R}{K_{eff}K_0} + \frac{e^2}{Kr_{AB}}$$

The distances r_{AB} between both charges +e are the successive distances of the neighboring S-sites A to the Zn-site B substituted at the origin. (See Fig. 1)

The formulas (2) are not accurate. A rigorous treatment has been given in (2), using the LCAO method for describing the trapped electron:

$$(3) \qquad \psi \text{ (trapped electron)} = \frac{1}{\sqrt{\pi a^3}} \left(e^{-r_A/a} + e^{-r_B/a}\right)$$

a is a parameter to be calculated by a variation method. In Fig. 2 are given the thermal (E) and optical ($h\nu$) ionization energies of an electron trapped according to the hydrogen molecule-ion like model in ZnS.

The next step is now to compute the successive distances r_{AB} in Blende and Wurtzite lattices. Then one can immediately read E and $h\nu$ for the successive groups of traps on Fig. 2. The results are given in Table II.

In the curves of Fig. 2 are given the results of the treatment "with binding", using the ψ described by (3), and the results of the treatment "without binding", using:

$$(3') \qquad \psi = \frac{1}{\sqrt{\pi a^3}} \; e^{-r_A/a}$$

When r_{AB} is small, the orbit of the trapped electron is around both charges A and B, and (3) is valid; when r_{AB} is large, the orbit is around A only and (3') is valid. The intersection of both curves gives the value of r_{AB} for which the hydrogen molecule-ion like model becomes meaningless. In ZnS, the occurs at $E \sim 0.46$ eV.

The same lattice distances—and thus the same traps—are found in Blende and Wurtzite. But in Wurtzite some supplementary groups occur. For instance, the distance between first neighbors ($r_0 = 2.35$Å) is the same in both lattices: it gives a trap $E = 0.815$ eV; this is quite a large depth and this trap hardly contributes to the phosphorescence decay at room temperature (on the other hand, it may be seen on the glow curve). The next S-site is in Wurtzite at the distance $r_{AB} = \frac{5}{3} r_0$ and leads to a trap $E = 0.715$ eV, which does not exist in Blende: as it is well known, Wurtzite has a longer visible persistance than Blende[3,4].

We have now succeeded in looking for almost all the computed trap depths upon the glow curve. Such a resolution of the glow peaks needs a convenient choice of the rate of heating β; this rate must be constrained to a constant value during the glow experiment with a great accuracy. We have chosen $\beta = 0.06$ °/second, whence:

$$(4) \qquad E_{eV} = \frac{T^{x(^\circ K)} - 7}{433}$$

It may be seen on Fig. 3 which gives glow curves of CnS(Cu), 1150°C firing, and trap depths computed from (4), that the traps corresponding to the 6 nearest neighbors, and for larger distances all the weighty

Table II: Trap Depths according to Hydrogen Molecule-Ion like Model

Blende		Wurtzite		ZnS		CdS	
Number of sites	r_{AB}	Number of sites	r_{AB}	E(eV)	hν(eV)	E(eV)	hν(eV)
4	1	4	1	0.815	0.96	0.475	0.60
		1	$\frac{5}{3}$	0.715	0.84	0.425	0.53
12	$\sqrt{\frac{11}{3}}$	9	$\sqrt{\frac{11}{3}}$	0.68	0.80	0.41	0.51
		6	$\frac{7}{3}$	0.63	0.75	0.39	0.48
12	$\sqrt{\frac{19}{3}}$	9	$\sqrt{\frac{19}{3}}$	0.61	0.72	0.38	0.46
16	3	9	3	0.565	0.67	0.36	0.45
		3	$\frac{1}{3}\sqrt{89}$	0.55	0.65	0.355	0.445
		6	$\frac{1}{3}\sqrt{97}$	0.54	0.63	0.35	0.44
24	$\sqrt{\frac{35}{3}}$	18	$\sqrt{\frac{35}{3}}$	0.53	0.62	0.34	0.43
		3	$\frac{1}{3}\sqrt{113}$	0.52	0.605	0.34	0.425
		7	$\frac{11}{3}$	0.51	0.595	0.335	0.42
12	$\sqrt{\frac{43}{3}}$	3	$\sqrt{\frac{43}{3}}$	0.50	0.585	0.33	0.41
		6	$\frac{1}{3}\sqrt{137}$	0.49	0.575	0.32	0.40
24	$\sqrt{17}$	12	$\sqrt{17}$	0.48	0.56	0.315	0.395

The distances r_{AB} are given in units $r_0 = 2.35$ Å for ZnS, $r_0 = 2.52$ Å for CdS; r_0 is the distance between nearest neighbors.

groups (those common to Blende and Wurtzite) have been effectively found on the thermoluminescence curve*.

Results for CdS. The traps are shallower than in ZnS, and even less separated, because of the higher value of K. It seems only possible to resolve the following groups:

E = 0.475 eV E ~ 0.42 eV E ~ 0.35 - 0.39 eV E ~ 0.17 eV

This seems to be in agreement with Bube[5], Broser-Warminsky[6], and de Boer's[7] experiments. In order to obtain the best agreement between calculated and experimental values, one must accept a lower value of the attempt-to-escape parameter s in CdS than in ZnS:

*In her Thesis, Mrs. G. Curie has studied an infra-red sensitive ZnS (Cu, Pb) and she finds the same trap depths as in ZnS (Cu) without Pb.

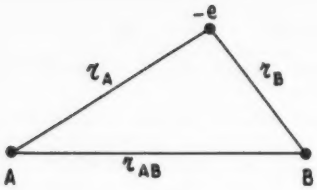

Fig. 1—The Hydrogen Molecule-ion Like Model for Traps

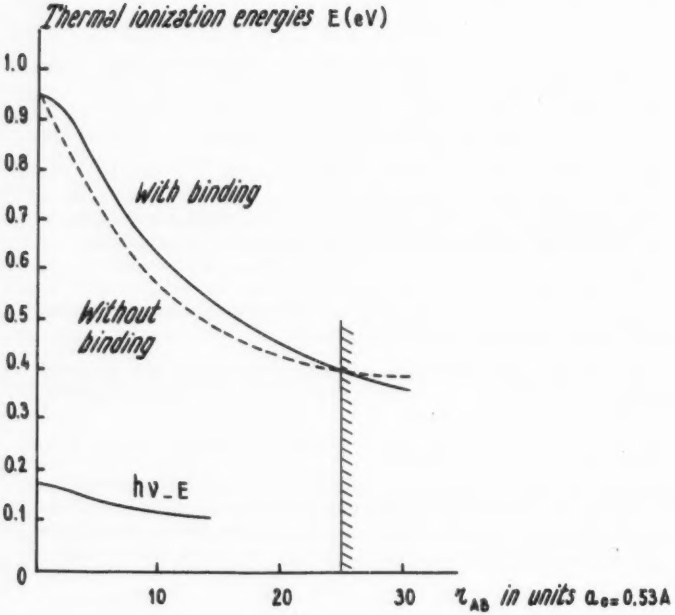

Fig. 2—Thermal and Optical Ionization Energies of an Electron Trapped According to the Hydrogen Molecule -ion Like Model in ZnS

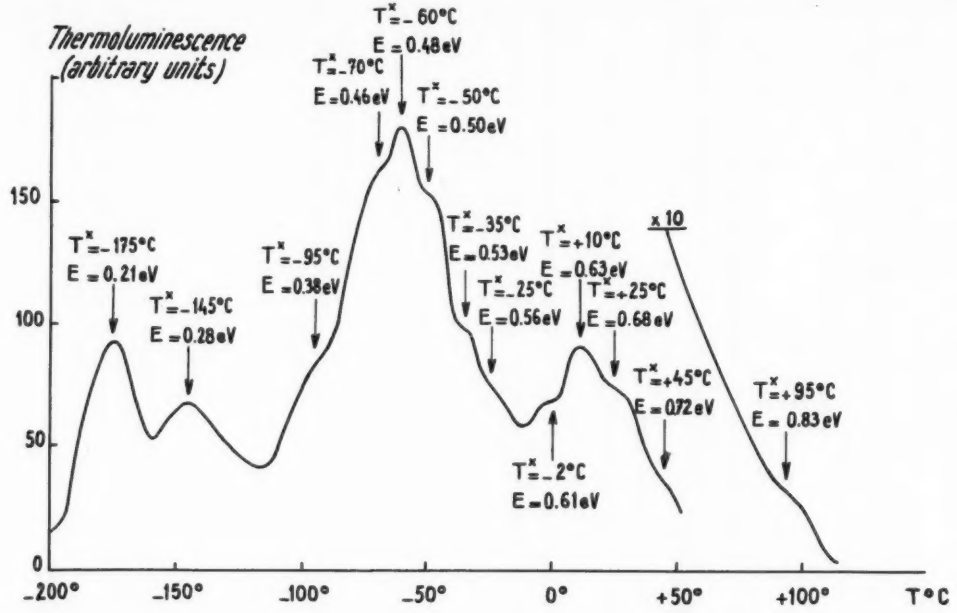

Fig. 3—Glow Curve at a ZnS(Cu), Fired at 1150°C.
Trap Depths Computed by Formula (4).

$s \sim 10^8$ sec^{-1} in CdS $s \sim 10^9$ sec^{-1} in ZnS

This agrees qualitatively with the conclusion of Bube[5].

References

1. F. E. Williams, D. Curie, Discussion Section on the paper "Propriétés des pièges à électrons et des centres luminogènes dans les sulfures", International Colloquium on the Luminescence of Anorganic Crystal Phosphors, Paris, May 1956. J. de Phys., 17, 703, 1956.
2. D. Curie, J. de Phys., 18, 214, 1957.
3. A. Guntz, Ann. de Chimie, 1926; Thèse Paris, 26 (Masson, Paris, 1925). D. Curie, Thèse Paris, 31 (Masson, Paris, 1952).
4. G. F. J. Garlick, Cornell Symposium, 107-111 (John Wiley and Sons, Inc., New-York, 1948).
5. R. H. Bube, J. Chem. Phys., 23, 18, 1955.
6. I. Broser and R. Broser-Warminsky, Zeits. für Phys., 133, 356, 1952.
7. K. W. Boer, S. Oberlander and J. Voigt, Ann. der Phys., VII, 2, 138, 1958.

A NUMERICAL TABLE FOR THE COMPUTATION OF TRAP DEPTHS FROM THERMOLUMINESCENCE EXPERIMENTS

Mrs. Germaine Curie and Daniel Curie

Laboratoire de Luminescence
Faculté des Sciences, Paris, France.

The purpose of this paper is to give precise formulas for the computation of "trap depths" E (thermal activation energies for the electrons escaping the traps) starting from the measured temperatures of the "glow peaks" T^X. Urbach's formula:

(1) $$E^{eV} \simeq \frac{T^{x\,°}K}{500}$$

gives rather good results in many cases, but one often needs more precise expressions.

1. Formulas using the monomolecular theory by Randall and Wilkins[1].

It is now well known that Randall and Wilkin's assumptions are somewhat oversimplified, but:

a) Evidence has been given that the monomolecular mechanism is a good approximation in ZnS(Cu) with usual excitation conditions, for the traps are localized in the neighborhood of the activator centers[2].

b) Even if the monomolecular assumption is not valid, the glow temperatures calculated by other theories are only little different from Randall and Wilkins's results (see below).

Let τ be the mean life of electrons in the traps at the temperature T:

$$\frac{1}{\tau} = s \exp(-E/kT)$$

and β the rate of heating. Randall and Wilkins[1], T. Louchtchik[3], F. E. Williams[4] and others have computed numerically the whole glow curve. But such computations are tedious and generally one prefers to characterize the glow peak only by its maximum, the glow temperature T^X. Booth[5], Bohun[6], Parfianovitch[7] have shown that T^X satisfies the implicit equation:

(2) $$\beta \frac{E}{kT^{X2}} = s \exp(-E/kT^X)$$

G. and D. Curie have derived from (2) explicit formulas[8] such as:

(3) $$E = \frac{T^X - T_0(\beta/s)}{K(\beta/s)}$$

It may be seen from (2) that the coefficients K and T_0 depend only on $\theta = \beta/s$ (dimensionally, θ is a temperature).

Formulas (3) must be accompanied by a table giving these coefficients. A partial table had been given in[8], but for recent purposes we need an extension of this table; the results are collected here:

Coefficients of the formula (3)
according to the value of $\theta = \beta/s$.

β/s (°K)	K(°/eV)	T_0(°K)
10^{-4}	833	35
10^{-5}	725	28
10^{-6}	642	22
10^{-7}	577 (577)	17 (17)
10^{-8}	524	13
10^{-9}	480	10
10^{-10}	441	7
10^{-11}	408	6
10^{-12}	379	6
10^{-13}	353	5
10^{-14}	331	5
10^{-15}	312	4

2. Examples of use.

a) In another paper, presented to this Meeting, are described the results of experiments performed on ZnS(Cu):

$$s = 10^9 \ s^{-1} \qquad \beta = 0.06 \ ^\circ/\text{second}$$

The table gives:

(4) $$E^{eV} = \frac{T^X - 7}{433}$$

b) Urbach's formula (1) - which has been derived by its author from experiments on KCl - gives also good results on ZnS for a rate of heating $\beta \sim 1°/s$. On the other hand, the formula (4) is appreciably different from (1) because the rate of heating 0.06°/s is rather low.

c) In ZnS, Randall and Wilkins have shown that the mean life τ is approximately 1 second at the glow temperature T^X:

(5) $$E \simeq kT^X \log s$$

But for unusual values of s this interesting result is not valid: for

$\beta/s = 10^{-5}$ °K, E = 0.4 eV, the glow temperature is 45°C and the mean life $\tau \simeq 2000$ s: the use of the formula (5) would lead to considerable errors.

3. Formulas using a simple bimolecular theory, with equal cross-sections for centers and traps (Garlick[9], Louchtchik[3], K. W. Boer and al.[10]).

Let n_0 the total number of traps, and n^x the number of filled traps at the maximum of the glow curve. After excitation to saturation (all the traps filled for $t=0$), the glow temperature is given by:

$$\beta \frac{E}{kT^{x2}} \frac{n_0}{2n^x} = s \exp(-E/kT^x) \tag{6}$$

The glow curve is not quite symmetrical, but in spite of this $n^x \simeq n_0/2$. Thus the glow temperature is practically the same as in Randall and Wilkins's theory (A. Wrzesinska[11]).

If the initial number of filled traps is pn_0, equation (6) must be replaced by:

$$\beta \frac{E}{kT^{x2}} \frac{n_0}{2n^x} = ps \exp(-E/kT^x) \tag{7}$$

The above table may also be used, but one must take care of replacing $\theta = \beta/s$ by $\theta = \beta/sp$.

Example of use. Let us consider the trap E = 0.61 eV, $s = 10^9$ s^{-1} in ZnS. For $\beta = 0.114$ °/s, the glow temperature is:

$T^x = 278$ °K for p = 1 (bimolecular mechanism) and for all values of p in a monomolecular mechanism;

$T^x = 305$ °K for p = 1/10 (bimolecular mechanism).

$T^x = 337$ °K for p = 1/100 (-id-).

Changes are effectively observed on the position of the glow peaks, when the glow experiment is performed after different decay times of the phosphor (G.F.J. Garlick[12], G. Curie[13]). But it seems that we must accept exaggeratedly low values of p, in order to explain these differences by the assumption of a bimolecular mechanism: one is led to assume the existence of distributions of trap depths in groups around the discrete E- values (G.F.J. Garlick[12], D. Curie[14]).

Thermostimulated current curves. With a monomolecular theory, the occurrence of some photoconductivity is not forbidden, and the photocurrent peak appears in the same time as the glow peak. With the simple bimolecular theory, it is found that the photocurrent maximum occurs for T^x satisfying to:

$$\beta \frac{E}{kT^{x2}} \frac{n_0}{n^x} = ps \exp(-E/kT^x) \tag{8}$$

Thus the table may also be used, but in this case one must put $\theta = 2\beta/sp$.

References

1. J. T. Randall and M. H. F. Wilkins, Proc. Royal Soc., A184, 372 (1945).
2. D. Curie, J. de Phys., 17, 699 (1956).
3. T. B. Louchtchik, Crystalphosphors, 17-73 (Eesti NSV Akademia Füüsika ja Astroonomia instituudi, Tartu, 1955).
4. F. E. Williams and H. Eyring, J. Chem. Phys., 15, 289 (1947). Cornell Symposium, 344 (John Wiley and Sons, Inc., New-York, 1948).
5. A. H. Booth, Canad. J. of Chem., 32, 214 (1954).
6. A. Bohun, Czeschosl. J. Phys., 4, 91 (1954).
7. I. Parfianovitch, J. Exp. and Theor. Phys. URSS, 26, 697 (1954).
8. G. Curie and D. Curie, J. de Phys., 16, 199 (1955).
9. G. F. J. Garlick, Cornell Symposium, 91 (John Wiley and Sons, Inc., New-York, 1948).
10. K. W. Boer, S. Oberländer, J. Voigt, Ann. der Phys., 2, 130 (1958).
11. A. Wrzesinska, Acta Phys. Polonica, 15, 151 (1956).
12. G. F. J. Garlick and A. F. Gibson, Proc. Phys. Soc., A 160, 574 (1948).
13. G. Curie, Thesis (Masson, Paris, 1959).
14. D. Curie, Thesis (Masson, Paris, 1952). Comptes-Rendus Acad. Sc., 229, 193 and 1321 (1949).

Abstract Number 57

GOLD ACTIVATED (Zn, Cd) S PHOSPHORS

M. Avinor

Philips Research Laboratories
Eindhoven, Netherlands

Gold activated CdS and (Cd,Zn)S phosphors were prepared. When using aluminum as coactivator a single emission band was found in CdS at 1.15μ . This band showed a regular shift towards shorter wavelengths, as part of the cadmium was replaced by zinc, and was shown to correspond to the 530 mμ gold band in ZnS.

Activation of CdS by gold alone produced two other emission bands at 640 and 800 mμ. The 640 mμ band predominates at low temperatures and moves to shorter wavelengths on substituting part of the cadmium by zinc. This band could not be followed up to ZnS because its intensity falls and also because of interference from other bands, but extrapolation shows that it should correspond to a violet emission in ZnS. The 800 mμ band appears at room temperature but is rather weak and could not be followed into the zinc rich region. If normal shift of the band with host lattice composition is assumed this band should correspond to the 470 mμ band of gold activated ZnS.

Abstract Number 58

LOW TEMPERATURE LUMINESCENCE OF ZnS CdS PHOSPHORS

Ronald W. A. Gill and S. Rothschild

Mullard Research Laboratories
Salfords, nr. Redhill, Surrey, England.

Self activated ZnS phosphors prepared in presence of NaCl under certain conditions show during excitation at low temperatures a band between the edge emission and the self activated emission (Kröger[1]). It was assumed that this band was due to sodium. During the present investigations a band in a corresponding position was found with ZnS CdS phosphors prepared with additions other than NaCl. The following table shows the peak of the band in mμ during excitation with 365 mμ at liquid N_2 temperature and the effect of the atmosphere present during firing on the appearance of the band with ZnS CdS phosphors containing 25 mol % CdS.

Additions	Position of Peak	Atmosphere	
		N_2	H_2S
NaCl	440	+	+
KCl	435	-	+
Cs Cl	435	-	+
NH_4Cl	440	+	+
Al	445	-	+

The peak of the room temperature emission band was found at 523 mμ in all cases. This band is, according to Prener and Weil[2], due to associated pairs of $(V_{Zn} - Al)^{-1}$ or $(V_{Zn} - Cl)^{-1}$. It is suggested that the low temperature band observed during the present investigations is due to V_{Zn}, centers.

References

1. F. A. Kröger, J. Opt. Soc. Am. 39, 670, 1949.

2. J. S. Prener and D. J. Weil, J. Electrochem. Soc., 106, 409, 1959.

Abstract Number 59

INFRA-RED STIMULATION AND QUENCHING OF ZINC SULPHIDE PHOSPHORS

Clifford C. Klick

United States Naval Research Laboratory
Washington 25, D. C.

Kroger and Dikhoff[1] first found that zinc sulphide phosphors co-activated with Sc, Ga, and In gave rise to two emission bands. One of these was characteristic of the activator and the other, at longer wavelengths, was characteristic only of the coactivator. Building on this information, Klasens[2] proposed the model of Figure 1A for the emission bands.

Recently Apple and Williams[3] have reexamined the emission spectra of these materials at both room temperature and liquid nitrogen temperatures. They find that the long wavelength emission depends strongly on the activator. The most pronounced difference occurs for ZnS:Cu, Ga, and ZnS:Ag, Ga for which the emission spectra peak at 6650A and 5900A respectively. A smaller effect occurs on varying coactivators. ZnS:Ag, In and ZnS:Ag, Ga emit at 6150A and 5900Å respectively. These authors propose that activators and coactivators form pairs at various spacings and that two transitions can occur as illustrated in Figure 1B depending on the pair spacing. The dashed level of that figure represents an excited state of T which is presumed to extend over a larger volume than the ground state. The temperature dependence of the emission spectra and the variation with concentration have been measured by Apple and Williams who find agreement with the medel of Figure 1B. Williams[4] has recently looked into the mutual effects on energy levels of bringing an activator and coactivator into close proximity.

Both the model of Klasens and that of Apple and Williams have the common feature that the level from which the long wavelength emission occurs is also the ground state of the coactivator. It seemed possible to check this feature of the models experimentally by shining infra-red light on the phosphors and noting the effect on the long wavelength emission maintained by steady ultra-violet excitation. In both cases the infra-red light should reduce this emission and the reduction should be not a transient effect, but approach a steady state change.

ZnS:Ag, Ga and ZnS:Ag, In have been investigated at room temperature and at liquid nitrogen temperatures. At room temperatures the effects are small-of the order of 5%-and show quenching and stimulation in both emission bands. A large transient increase-100% or more-is observed at 77°K in the long wavelength emission of both phosphors.

There is no measurable steady state quenching of the long wavelength emission. Only ZnS:Ag, Ga has a separately measurable blue emission at 77°K. It shows a 7% transient stimulation of the blue emission followed by a steady state quench of about 5%. The wavelength dependence of the infra-red light to cause stimulation in the long wavelength band is different in the two phosphors indicating that the trap for the electrons is associated with the In and Ga ions. Furthermore, visual observations show that infra-red irradiation at 77°K of previously excited phosphors gives stimulated emission and reduced the amount of thermoluminescence.

These results would seem to show that the normal traps introduced by In and Ga can be emptied by infra-red light and that these traps are not at the same time excited states for either the long or short wavelength emissions. One would conclude that an appreciable fraction of the coactivator is not an integral part of an emitting center. Since the number of activator and coactivator ions are equal to achieve charge compensation, an appreciable fraction of the activator ions must likewise be isolated from coactivators unless the possibility of larger clusters than pairs is invoked.

The model shown in Figure 1C may tentatively be proposed as being a simple model in agreement with presently known facts. Some coactivators are isolated in the lattice and these lead to the traps T. Some activators are isolated and these lead to levels C which give rise to the short wavelength emission. Other centers are formed of pairs of activator and coactivator and these lead to levels C, T which give rise to the long wavelength emission. While the detailed nature of the C, T center is not known, it seems likely from the results of the second paragraph above that it can be thought of as an activator perturbed by a nearby coactivator.

The temperature dependence of the emission spectra may have several interpretations some of which are compatible with the present model. Also, the variation of the emission spectrum with concentration follows quantitatively from this model if the number of C, T pairs arises merely from a random distribution of activator and coactivator.

The main differences between the present model and that of Figure 1B are (1) isolated coactivators are believed to give rise to trapping states, (2) isolated activators are believed to be the centers responsible for the short wavelength emission spectra, and (3) the number of paired activator-coactivator centers (which give rise to the long wavelength emission spectra) may arise only from random distributions of activator and coactivator.

References

1. F. A. Kroger and J. Dikhoff, Physica 16, 297 (1950).
2. H. A. Klasens, J. Electrochem. Soc. 100, 72 (1953).

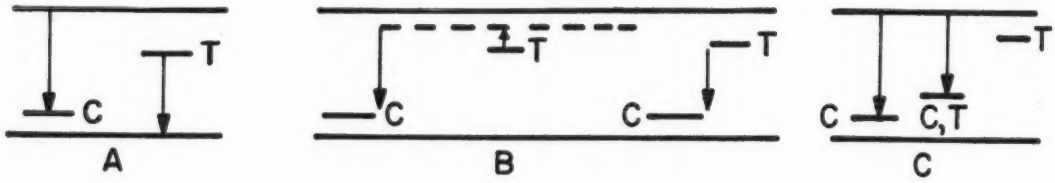

Fig. 1

3. E. F. Apple and F. E. Williams, J. Electrochem. Soc. 106, 224 (1959).

4. F. E. Williams, to be published.

Abstract Number 60

SYNTHESIS AND CRYSTALLOGRAPHY OF STRUCTURALLY PURE CUBIC AND HEXAGONAL SINGLE CRYSTALS OF ZnS

Harold Samelson and Vincent A. Brophy

Sylvania Electric Products Inc.
Bayside, N. Y.

Crystals of ZnS with pure zincblende and wurtzite structures have been reported to occur naturally.[1] ZnS crystals grown synthetically usually show deviations from these structures. These deviations usually result from the appearance of faulting in hexagonal close-packed planes perpendicular to the unique axes ([00.1] in hexagonal or [111] in cubic) of these structures; the faulting can be periodic or non-periodic in its occurrence. The periodic interruption of the layer sequence leads to the formation of polytypes[2] which have been observed with repeat patterns along [00.1] or [111] up to 36-layers. The non-periodic or random faulting leads to the formation of 'disordered' crystals and is evidenced as broading of spots or twinning in the X-ray diffraction films.[3]

The synthetic crystals discussed in this work have been made by a vapor phase method in a sealed tube. A previously outgassed sample of zinc sulfide powder is heated to an evaporation temperature between 1100°C and 1230°C. The condensation temperature will vary between 650°C and 1050°C depending on the condition of the experiment. The lower condensation temperatures are obtained by using large gradients (up to 70°C per inch) in the furnace, and either performing the experiment in vacuum or with a ZnS powder to which KCl has been added in an amount between 011 and 1.0 mole %. The higher condensation temperatures are obtained by performing the experiments in the presence of a gaseous ambient (usually H_2S) at a pressure greater than 300mm at the experimental temperatures.

Predominantly three layer or cubic crystals are obtained by this method only when the condensation temperatures are below 1020°C, which is the transition temperature found by Allen and Crenshaw.[4] The structurally pure cubic crystals were found only in those experiments where condensation occurred below 900°C, that is in those experiments where KCl was used.

The crystals found in runs made in an ambient where growth temperatures are greater than 1020°C, but less than 1200°C, are dominantly hexagonal but faulted. The structurally pure hexagonal crystals were

grown from pure ZnS powder in an ambient of 500mm pressure and a growth temperature of 1050°C. These experimental conditions are apparently very critical and have not been reproduced, but there were a very large number of crystals of this type grown in the one experiment.

The habits resulting from these growths were quite different. The hexagonal crystals were acicular or rod-like and the cubic crystals were thin plates. In the former, the unique or 'c' axis is along the length of the rod and in the plates this axis is perpendicular to the plates.

The structure identifications have been made by means of X-ray single crystal photographs and by optical microscopy using polarized light. Crystals which are pure hexagonal structurally show a single birefringent color throughout their length when viewed perpendicular to the unique axis between crossed nicols. Pure cubic shows extinction at all angles. Crystals which are crossed by many bands of birefringent color usually show the presence of disorder when X-rayed.

The single crystal films were made by precession camera methods in order to avoid multiplicity effects. The crystal was so oriented that the unique axis and its reciprocal lattice counterpart are parallel to, and in the plane of, the film. This puts rows of constant (hk) in the plane of the film, and those satisfying ($h-k \neq 3n$) are sensitive to faulting. The effects of the faulting can be observed along the length of the row. Random faulting broadens points in these rows only along the row. Periodic faulting increases the number of spots within a given distance along the rows. Both of these effects may occur simultaneously. The structurally pure crystals show no broadening or polytypism in their patterns, within the limits of the experiment.

References

1. Dana, J. D., The System of Minerology, John Wiley, New York (1946).
2. Strock, L. W. and Brophy, V. A., Amer. Minerol. 40, 94 (1955).
3. Mueller, H., Neues Jb. Min. Geol. u Pal. 84, 43 (1952).
4. Allen and Crenshaw, Amer. J. Sci. 34, 41 (1912).

Abstract Number 61

INFRA-RED ABSORPTION OF N-TYPE (Zn,Cd)S

R. M. Potter

Lamp Development Department
General Electric Company
Cleveland, Ohio

Kroger et al[1] have shown that n-type CdS crystals with low resistivity can be prepared with relative ease. In contrast, n-type ZnS has not yet been reported. From the energetics of the problem, discussed by Kroger[1], it appears that one of the factors which makes it more difficult to prepare n-type ZnS is the greater band-gap of this material (3.7 e.v. compared to 2.4 e.v. for CdS)[2]. Since solid solutions of ZnS and CdS have band gaps intermediate between those of pure ZnS and CdS[2] one might expect that a certain range of compositions of (Zn,Cd)S might be made n-type. The objett of this work was to prepare (Zn,Cd)S containing various Zn:Cd ratios and to determine the range of compositions, if any, which could be made n-type.

Since only powdered samples of (Zn,Cd)S were immediately available, it was necessary to find a method of establishing the presence of extrinsic electrons other than the conventional electrical methods, which are reliably applicable only to single crystals. The method of free carrier absorption was suggested by results on n-type ZnO, for which the infra-red absorption coefficient varies as a positive power of wavelength[3]. Such absorption might be expected for n-type CdS, but has not been reported.

Single crystals of CdS:In were obtained from the Harshaw Chemical Co. and from the Eagle-Picher Co. The former were vapor-grown, were reportedly n-type and were strongly conducting as received (about 20 $ohms^{-1}$ cm^{-1}); the latter were melt-grown and insulating as received. After overnight annealing at 750°C in a sealed quartz tube containing cadmium, the melt-grown crystals became conducting (about 0.2 ohm^{-1} cm^{-1}). Thermoelectric measurements confirmed that they were n-type.

The transmission spectra of polished samples of CdS crystals about 2 mm thick were measured in the 2 to 15 micron region. In Fig. 1, the log of the absorption coefficient (α) is plotted against the log of the wavelength (λ) for samples of each of the two types of crystals. Both show absorption which obeys a λ^n law reasonably well, with an n of about 2.2 for the Harshaw (H) and 3.7 for the Eagle-Picher (E.P.) crystal. The absorption of the Harshaw crystal is about one to one and one half orders of magnitude greater than that of the Eagle-Picher

(a somewhat smaller difference than would be expected from the difference in conductivities). Firing of an Eagle-Picher crystal at 750°C in sulfur vapor destroyed both the conductivity and the infra-red absorption.

The correlation between conductivity and infra-red absorption having been established for single crystal CdS, further work was carried out on powdered samples, for which only absorption could be measured. Samples of $Zn_xCd_{1-x}S{:}10^{-4}$ Ga were prepared by dry mixing ZnS and CdS powders, adding Ga as a solution of the nitrate, drying, and sieving. The samples were then fired for about 1 hour, first in H_2S, then in sealed quartz tubes containing cadmium, both at 750° to 800°C. The relative diffuse reflectance was measured for the cadmium-fired samples, taking the reflectance of the corresponding samples fired in H_2S only as having 100% reflectance in the spectral region of interest. An approximate theory of the optics of powders[4] was used to estimate the absorption coefficient. Thus, for a given wavelength,

$$\frac{\alpha d}{r} \approx \frac{(1-R)^2}{R}$$

where α is the absorption coefficient in cm^{-1}, d the average particle diameter in cm, r the single particle reflectance, and R the measured diffuse reflectance. The values of d and r were taken as 2×10^{-4} cm and 0.15, respectively. The results for x = 0, 0.2, and 0.4 are shown in Fig. 1. The slopes are 2.8, 3.1, and 3.4 for x = 0, 0.2, and 0.4, respectively. The powdered CdS:Ga is presumed to be n-type because single crystals of CdS:Ga heated in Cd at a similar vapor pressure were shown by Kroger to be strongly n-type. The similarity between the absorption data for the $Zn_{.4}Cd_{.6}S$:Ga and the $Zn_{.2}Cd_{.8}S$:Ga and for the CdS:Ga is good evidence that the former two are also n-type. The values of α are about one order of magnitude greater than those for the Harshaw single crystal. This is presumably due to a lower doping concentration in the latter.

Diffuse reflectance spectra for $Zn_xCd_{1-x}S{:}10^{-4}$ Ga with x = 0.6 through 0.9 will be reported. For compositions between x = 0.6 to 0.85, the spectra show a structure which is tentatively ascribed to transitions of electrons from donor levels to excited levels or to the conduction band. For the composition x = 0.90, the absorption is negligible.

From the data obtained so far, it appears fairly certain that (Zn,Cd)S:Ga can be made n-type at least up to 0.4 mole fraction of ZnS, and possibly to about 0.85 ZnS. These compositions correspond to band gaps of about 2.9 e.v. (x = 0.4) and 3.5 e.v. (x = 0.85).

Preliminary electrical measurements on mosaic clusters of single crystals of $Zn_{.4}Cd_{.6}S$:Ga support the conclusion of high free electron density made on the basis of optical measurements on the powder. Conductivities of the order of 1 $ohm^{-1}cm^{-1}$ have been measured for these samples at room temperature.

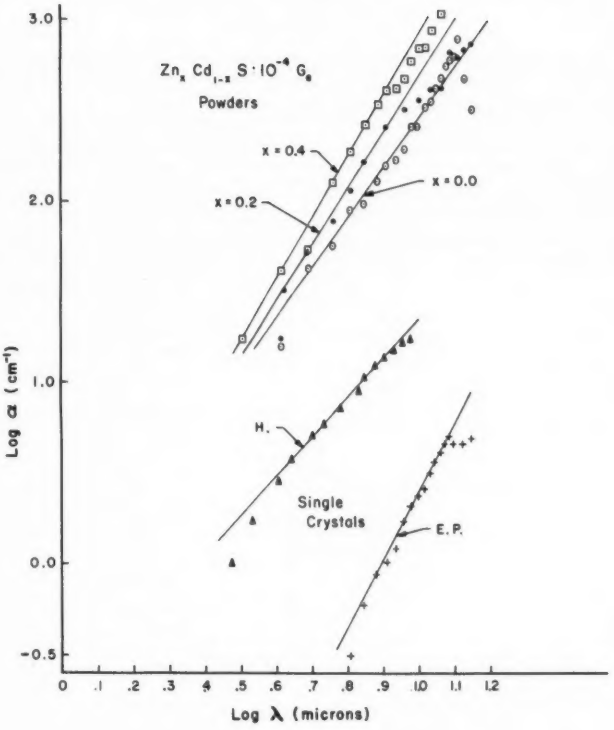

Fig. 1—Absorption of CdS:In single crystals and of (Zn,Cd)S:Ga powders. The data for x = 0.2 and 0.4 are each shifted upward by 0.15 log units for clarity.

References

1. F. A. Kroger, H. J. Vink, and J. van den Boomgaard, Z. Physik. Chem. 203, 1 (1954).

2. F. A. Kroger, "Luminescence in Solids Containing Manganese" p. 69, Jacob Van Campen, Amsterdam, 1940.

3. J. F. Hall, Jr. and W. F. C. Ferguson, J. Opt. Soc. Amer., 45, 714 (1955).

4. M. A. Weinstein, Personal Communication [See also Urbach et al, "Solid Luminescent Materials" (1946 Cornell U. Symposium) p. 285, John Wiley and Sons, Inc., New York, 1948.]

Abstract Number 62*

FORMATION OF PHOSPHOR FILMS BY EVAPORATION

L. R. Koller

Research Lab., General Electric Co.,
Schenectady, N. Y.

Thin luminescent films of zinc sulfide phosphors have been prepared by evaporation of powder phosphors in vacuo. The procedure consists in depositing the film on a heated substrate so that a crystalline rather than an amorphous film is formed. This is accomplished by carrying out the evaporation in a container with walls at the same temperature as the substrate. Cathodo-, photo-, and electroluminescent films have been made by this method. Other phosphors have been made by modifications of this procedure.

*Enlarged Abstract not Available.

Abstract Number 63*

CONTINUOUS FILMS OF II-VI PHOSPHORS AND PHOTOCONDUCTORS MADE BY VAPOR REACTION

D. A. Cusano

Research Lab., General Electric Co.
Schenectady, N. Y.

During the past several years a large number of continuous films of II-VI and other compounds have been made by improved vapor reaction techniques. Most of these have been zinc-cadmium sulfide phosphors and photoconductors, prepared with groups IB, IIIB, VB, VIIB, and manganese impurities. The salient luminescent, electrical, and electro-optical properties are discussed and, where possible, related to existing data on single crystals or granular material of similar chemical constitution. In addition, methods of fabrication and impurity introduction are described.

*Enlarged Abstract not Available.

Abstract Number 64

POWDER AND TRANSPARENT PHOSPHOR SCREENS UNDER HIGH AMBIENT ILLUMINATION

Austin E. Hardy

Radio Corporation of America
Lancaster, Pa.

At the present state of the art of making transparent phosphor screens, the best powder screens combined with a low-transmission faceplate will out-perform the best transparent screens in respect to contrast range at the same power input under high diffuse ambient illumination. This difference in performance is due to two factors:

1. the very low efficiency of transparent screens (5 to 10 per cent of that of the best powder screens), and
2. the finite specular reflectivity of the faceplate first surface plus the phosphor-faceplate interface and the phosphor-air (vacuum) interface.

An approximate expression for contrast range or contrast ratio of a powder screen is:

$$C.R. = \frac{Lt + ARg + A(R_S - R_g)t^2}{ARg + A(R_S - R_g)t^2} \qquad (1)$$

or

$$C.R. = \frac{L}{A}\,\frac{t}{R_g + (R_S - R_g)t^2} + 1 \qquad (2)$$

where

L = phosphor-screen luminance in footlamberts per square foot

$$\frac{\text{Footlamberts/watt x watt,}}{\text{ft}^2}$$

A = diffuse ambient illumination in footcandles,

t = transmission of faceplate,

R_g = front-surface reflectivity of the faceplate (Fresnel reflection),

R_S = diffuse reflectivity of the phosphor screen.

Because of the R_g term in equations (1) and (2), the contrast ratio will go through a maximum as a function of t. Differentiating (2) in respect to t and equating to 0 leads to an expression for t for a maximum contrast ratio. The contrast ratio is a maximum when $t = \sqrt{\frac{R_g}{R_S - R_g}}$. For $R_g = 0.04$ and $R_S = 1.0$, t = 0.20 or 20 per cent trans-

mission. Thus, it can be seen that the faceplate transmission for maximum contrast is determined only by the ratio of the front-surface reflectivity to the screen reflectivity, and does not involve the ambient illumination in any way.

If the t = 0.20 value is put back into equation (2), the contrast range is given by

$$C.R. = \frac{2.5L}{A} + 1 \tag{3}$$

For a transparent phosphor screen the contrast ratio is given approximately by

$$C.R. = \frac{L_C + AR_C}{AR_C} \tag{4}$$

or

$$C.R. = \frac{L_C}{AR_C} + 1 \tag{5}$$

where

L_C = luminance of the transparent phosphor screen in footlamberts per square foot,

A = diffuse ambient illumination in footcandles,

R_C = total direct reflectivity which is due to reflection at the air-glas interface, the glass-phosphor film interface, and the phosphor-air interface.

For Willemite (index = 1.7) on glass (index = 1.47), $R_C = 0.10$; for CsI (index = 1.8), $R_C = 0.12$; and for ZnS (index = 2.4), $R_C = 0.23$.

If the R_C value of 0.10 is used for Willemite, equation (5) becomes

$$C.R. = \frac{10L_C}{A} + 1 \tag{6}$$

For equal contrast, equation (3) equals equation (6), and $L_C = 0.25L$. As a result, a transparent phosphor screen would have to have 25 per cent of the luminance of a powder screen (without an absorbing faceplate) in order to have the same range contrast. If the luminance of the transparent screen is less than 25 per cent of that of the powder screen, then it will be inferior to the powder screen in respect to range contrast.

Substituting the value of R_C for CsI and ZnS in equation (6) and equating to equation (3) leads to luminance values of 32 and 57 per cent respectively, which the transparent screens must have in order to equal the range contrast of a powder screen with a 20 per cent transmission faceplate.

If it is assumed that transparent phosphor screens can be made with the required luminance-efficiency values calculated above, it can be shown that they will have a higher absolute luminance than the powder screen as viewed through the 20 per cent transmission faceplate. However, it is possible to calculate the faceplate transmission to be used

with the powder screen for equal luminance and equal range contrast.

The reflectivity of the powder screen with an absorbing faceplate is approximately

$$R = R_g + (R_s - R_g)t^2 \qquad \text{See equation (1)} \qquad (7)$$

For a transparent screen the reflectivity is

$$R = R_c \qquad \text{See equation (4)} \qquad (8)$$

For equal reflectivity equation (7) = equation (8):

$$R_g + (R_s - R_g)t^2 = R_c \qquad \text{and} \qquad t = \sqrt{\frac{R_c - R_g}{R_s - R_g}} \qquad (9)$$

The term t is not only the transmission of the faceplate, but is also the luminance efficiency that the transparent screen must have in respect to the powder screen in order to equal the powder screen in luminance and contrast. For Willemite, CsI, and ZnS, the values of t are 26, 30, and 45 per cent, respectively. Although the values of t calculated from equation (9) are not the ones for maximum contrast range, with a powder screen they do represent the conditions under which a powder screen with an absorbing faceplate and a transparent screen are equal.

The next consideration is what luminescent efficiencies can be obtained with transparent and powder phosphor screens. Table I summarizes some pertinent data. It is apparent from the data in Table I that all transparent phosphor screens yet reported in the literature have but a small fraction of the luminescent efficiency of good powder screens. Moreover, none of good powder screens. Moreover, none of the transparent phosphor screens approach the efficiencies calculated by equation (9) which are required to match the performance of powder screens with a low-transmission faceplate.

Table I

Phosphor Screen	Surface Brightness Footlamberts/ft²/watt*
Powder P20, aluminized (ZnCdS:Ag)	65[1]
Powder P4, aluminized (ZnS:Ag + ZnCdS:Ag)	36[1]
Powder P1, aluminized (Zn_2SiO_4:Mn)	30[1]
Transparent P1, not aluminized (Zn_2SiO_4:Mn)	1.6[1] 1.1[2]
Transparent P5, not aluminized ($CaWO_4$)	0.24[1] 0.18[2]
Transparent ZnS:Mn, not aluminized	0.3[1] 0.4[2]
Transparent ZnS:P:As, not aluminized	2.[3]
Semi-transparent CsI:Tl, not aluminized	8[1]

*At 15 to 20,000 volts and 1 $\mu A/in^2$

The final consideration is what efficiencies can be expected from transparent screens. Feldman[4] has calculated the light loss in transparent films by internal reflection based on the critical angle effect. His values are listed in Table II.

Table II

Material	Index of Refraction	Critical Angle	%Light Loss
ZnS	2.4	25°	95
$CaWO_4$	1.9	32°	92
$Zn_2S:O_4$	1.7	36°	90
CaF_2	1.4	46°	85

For Willemite (Zn_2SiO_4:Mn, P1), for which there is good data for the powder and transparent form, powder P1 aluminized has an efficiency of 30 footlamberts per square foot per watt. Unaluminized, this efficiency would be $\frac{30}{1.8} = 16.7$.

A value of 90 per cent of this figure leads to a figure of 1.5 footlamberts per square foot per watt as a possible goal for transparent Willemite. As can be seen from Table I, this value is in good agreement with measured values. If it is assumed that this agreement is not just fortuitous, one can surmise that the intrinsic efficiency of the luminescent process in powder and transparent screens can be equal, and that the low luminance of transparent screens is due principally to internal trapping of the generated light.

Studer and Cusano[3] report apparent light losses of only 50 per cent for transparent Willemite. If this is true, then the intrinsic efficiency of that particular transparent Willemite may have been only 1/2 the intrinsic efficiency of the powder form.

In conclusion, it appears that truly transparent phosphor screens will have to have efficiencies of 17 to 29 footlamberts per square foot per watt, depending on the index of the phosphor, in order to equal the luminance and contrast range of the best powder phosphor deposited on a low-transmission faceplate. As a result, transparent phosphors at the present level of their efficiency are inferior to powder screens for viewing under high diffuse ambient illumination.

However, transparent screens still retain their advantages of increased resolution, no halation, and low white noise.

References

1. RCA Lancaster measurements

2. J.O.S.A. 47 pages 790 (1957), Charles Feldman

3. J.O.S.A. 45 page 493 (1953), Studer et Al.

4. SMPTE Vol. 67 pages 455-460.

Abstract Number 65

MECHANISM OF DEPRECIATION OF ELECTROLUMINESCENT PHOSPHORS

I. L. Smith, R. M. Potter and M. Aven*

Lamp Development Department
General Electric Company
Cleveland, Ohio

It has been known for some time that zinc sulfide phosphors and pigments deteriorate in moist air, particularly if subjected to short wavelength radiation. The deterioration starts with slight greying of the exposed phosphor or pigment surface, and after passing through a series of increasingly darker shades of grey, terminates as a very dark grey or black. The blackening can be partly reversed by leaving the deteriorated phosphor in the dark for some time in moist air.

Soon after the discovery of electroluminescence in zinc sulfide, it was found that cells made with zinc sulfide phosphors exhibit blackening very similar to the above described deterioration. Often the deterioration occurs so slowly that the bleaching process is able to keep up with the blackening, and the cells do not appear grey or black. At the same time the electroluminescence brightness may have decreased to only a few percent of the initial.

Several theories have been proposed to account for this process. Thornton has attributed electroluminescence depreciation partly to migration of donors (e.g. chlorine) to the surface of the phosphor particles[1] and partly to diffusion of oxygen into the crystal lattice[2]. Roberts[3] has postulated that the migration of donors and acceptors (e.g. copper) to nearest neighbor sites with respect to each other with the resulting shift of the corresponding energy levels, is responsible for the brightness decay.

The experiments to be described in this paper indicate, however, that, while the above described mechanisms may well be operative in long term depreciation of electroluminescent phosphors, the process which leads to a decrease of electroluminescence brightness to one half of the initial value in times of the order of one year or less, is caused by chemical attack of zinc sulfide by water.

The proposed mechanism is based on the work by Gordon, Seitz and Quinlan[4] on the depreciation of zinc sulfide phosphors under ultraviolet

*Present address: General Electric Research Laboratory, Schenectady, New York.

excitation. According to these workers some zinc sulfide dissolves* in the water adsorbed on the surface of the phosphor particles, and dissociates into zinc and sulfur ions. Ultraviolet excitation produces free electrons in the conduction band and free holes in the valence band of zinc sulfide. Some of these free carriers are trapped in sites close to the zinc and sulfur ions in the adsorbed aqueous layer, and can react with these, producing elemental zinc and sulfur:

$$\begin{aligned} Zn^{++}\,(aq) + e^{-} &\rightarrow Zn^{+}\,(aq) \\ 2\,Zn^{+}\,(aq) &\rightarrow Zn^{++}\,(aq) + Zn\,(s) \\ S^{=}\,(aq) + e^{+} &\rightarrow S^{-}\,(aq) \\ 2\,S^{-}\,(aq) &\rightarrow S^{=}\,(aq) + S\,(s) \end{aligned} \qquad (1)$$

The elemental zinc is the product which causes the black appearance of depreciated zinc sulfide. The bleaching process involves reaction of zinc and sulfur to form zinc sulfate (in the presence of light), zinc hydroxide (in dark) and hydrogen. Omitting the intermediates, these reactions can be written as

$$\begin{aligned} Zn(s) + S(s) + 4H_2O\,(l) &\rightarrow ZnSO_4(s) + 4H_2(g) \\ Zn(s) + 2H_2O(l) &\rightarrow Zn(OH)_2\,(s) + 2H_2\,(g) \end{aligned} \qquad (2)$$

In the present study electroluminescent ZnS,ZnO:Cu,Cl was mixed with a wet dielectric (Monsanto Aroclor 1256 to which a small quantity of water and acetone was added), and operated at about 3×10^4 volts/cm and 60 cps until the electroluminescence brightness had decra sed to 20 percent of the initial. Copious evolution of an odorless gas, probably hydrogen, occurred during operation. Analytical identification of residual depreciation products confirmed the formation of elemental zinc and sulfur and zinc sulfate. Zinc hydroxide was not found.

It is thus seen that the depreciation products of zinc sulfide under electroluminescence excitation are, with the exception of zinc hydroxide, the same as those found under ultraviolet excitation. In view of this finding and the evidence for electrons in the conduction band and holes in the valence band with electroluminescence excitation[5] just as with ultraviolet excitation, it is very likely that the depreciation mechanisms in the two cases are similar in their gross features.

The details of the depreciation process for the two types of excitation, however, are different. Experiments have shown that the removal of the opaque depreciation products from the surface of electroluminescence depreciated phosphor particles almost completely restores

*Although Gordon et al. use the term "dissolves," it is felt that the process may be more accurately described as an effect of the adsorption of water on the surface of the zinc sulfide particles; this produces a weakening of the Zn-S bonds, in the outermost zinc sulfide layer, and effects some exchange of ions between the zinc sulfide and the water phase.

the response to ultraviolet excitation while the electroluminescence response is permanently impaired. Similar removal of ultraviolet depreciation products restores the phosphor response to both ultraviolet and electroluminescence excitation. These results have been interpreted to mean that under ultraviolet excitation the destruction of zinc sulfide is general, all parts of the crystallite surfaces being equally affected; in electroluminescence depreciation, on the other hand, the surface destruction is confined to small localized regions. The latter is not unexpected in view of the general belief that electroluminescence excitation takes place in small localized volumes where the electric field is higher than average. It has been assumed that these high field regions occur adjacent to occlusions of copper sulfide, due to geometrical field concentration or production of a depletion layer. Now, it is possible that the localized nature of electroluminescence depreciation is due to a larger free carrier concentration in the vicinity of the high field regions, and that otherwise the mechanism is exactly analogous to that proposed by Gordon et al for depreciation of zinc sulfide phosphors under ultraviolet excitation. It is also possible, however, that in the case of electroluminescence depreciation the first step (equation 1) is electrochemical rather than photochemical. This is easy to visualize if a depletion layer is assumed to be responsible for the creation of the high field regions. In the zinc sulfide phase the depletion layer will bear a positive space charge, while the copper sulfide will be negative. With an applied field more of the donors in the zinc sulfide phase will be depleted and the potential difference between the copper sulfide and zinc sulfide adjacent to it will increase. When this potential difference exceeds the electrochemical deposition potential for zinc and sulfur, zinc ions in the adsorbed water layer covering both the copper sulfide and the zinc sulfide phases will be reduced to free zinc at the negatively charged copper sulfide phase, and sulfur ions will be oxidized to free sulfur at the positively charged zinc sulfide phase. The process will then lead to attrition, and eventual annihilation of the high field region.

Which of these two mechanisms is predominant cannot be stated at this time. It is hoped that further experimentation will help clarify this problem.

References

1. W. A. Thornton, J. Appl. Phys., 28, 313 (1957).
2. W. A. Thornton, Electrochem. Soc., Enlarged Abstracts, Spring Meeting 1958, p. 26.
3. S. Roberts, J. Appl. Phys., 28, 262 (1957).
4. N. T. Gordon, F. Seitz and F. Quinlan, J. Chem. Phys., 7, 4 (1939).
5. P. Zalm, G. Diemer, and H. A. Klasens, Philips Res. Rep., 9, 81 (1954).

Abstract Number 66

ELECTROLUMINESCENCE MAINTENANCE*

W. A. Thornton

Research Dept., Westinghouse Electric Corporation
Bloomfield, N. J.

The maintenance of light emission during the operating life of an electroluminescent phosphor is vital to its practical application as a light source. The maintenance of phosphors of the ZnS:Cu,Cl type has been studied.

There have been three[1-3] previous papers on electroluminescence maintenance. The first[1] related the normal maintenance (brightness-time) curve to observations on photoluminescence, dark capacitance and conductance, photoconduction, waveform, and low-temperature maintenance data by assuming field-diffusion of traps or donors within the phosphor crystal. The second paper, by Roberts,[2] based in part on results obtained much earlier,[4] gives an empirical relation approximately describing typical brightness-time behavior, and also concludes that deterioration is due to physical processes within the phosphor crystal. In the third paper,[3] deep traps appearing in the phosphor crystal during deterioration are ascribed to incoming oxygen ions; the presence of the deep traps was indicated by thermoluminescence measurements and by the fact that brightness-voltage changes with deterioration could be reproduced by firing into the phosphor deep-trap-producing impurities[5] such as In,Cd and Ga, and could be temporarily removed simply by heating the deteriorated lamp. That oxygen is involved was indicated by similar thermoluminescence behavior of oxygen[5] in ZnS, by the fact that small amounts of ZnO fired into the phosphor led to the same brightness voltage changes as deterioration, and by the appearance of free zinc[6] on the phosphor crystals during deterioration.

The present paper deals with the maintenance of the phosphor alone, independent of the type of dielectric material (which has no effect if stable and dry) and includes the observations partially listed as follows. In ZnS:Cu,Cl phosphors the maintenance is best for roughly equal additions of copper and chlorine and improves, apparently without limit, with increase of the total addition. Maintenance improves roughly as visual color of the electroluminescence approaches the yellow region of the spectrum; highest brightness and maximum maintenance are generally consistent for a given color. Total light emitted over the lifetime of the

*Much of the work described in this paper was carried out under Contract AF33(616)-5811 from the Wright Air Development Center.

lamp is a maximum for the green region and falls off sharply in the blue and yellow-green; this is not due to luminosity but is a physical effect.

Lifetime (to half of initial brightness) is proportional to mean particular diameter, in blue and green ZnS:Cu,Cl and yellow-emitting ZnS:Cu,Mn,Cl, up to about twelve microns and becomes relatively constant for larger particle diameters. This effect, practically a factor of three of four due to particle diameter, is much smaller than that due to copper and chlorine additions (factor of 20 or 30).

At frequencies above 1000 c.p.s., a brightness equal to half of the initial brightness is reached after a certain number of cycles of operation (lifetime is inversely proportional to frequency) and at lower frequencies most phosphors show an appreciably longer lifetime in cycles. Lifetime depends only weakly on voltage or field-strength on the phosphor, varying by a factor of about two or less even though initial brightness of identical lamps differs by a factor of several hundred. Lifetime varies exponentially with temperature, with better maintenance at lower temperature. Lifetime is independent of relative humidity below about 40% but decreases rapidly as humidity becomes higher; for this reason all of the data in this paper were obtained under conditions of very low humidity. Moisture is apparently harmless so long as the voltage is not applied.

Two "lifetimes" may be realized from an electroluminescent lamp by operating it first at high-frequency and low-voltage and then at low-frequency and high-voltage. The same initial brightness can be used in both cases. In the second case (LFHV) the initial brightness is obtained at the same voltage and frequency necessary before the first deterioration (HFLV); that is, the first deterioration has no effect on the second, and under the latter (LFHV) conditions the lamp is still completely fresh. This effect is due to very marked localization of the ionization region at low voltage and/or high frequency.[3] Constant brightness operation (by increasing the applied voltage gradually as deterioration proceeds) leads to a lifetime several times longer than that of an identical lamp run at constant voltage, if the voltage and brightness of both lamps at the end of "life" are the same.

Because the impedance of a normal electroluminescent lamp increases during life, an artificial improvement in maintenance can be realized by including a fixed impedance in series with the lamp. The increase in voltage across the lamp (at constant applied voltage) counteracts the reduction in brightness due to deterioration. Improvements in lifetime of five to eight times result from series impedances equal in order of magnitude to the initial impedance of the lamp.

Pre-aging at voltages and frequencies other than those at which the lamp is to be operated leads to significant improvements in lifetime. For example, lifetime can be doubled at a reduction of twenty per cent of initial brightness by pre-aging at any one of a number of combinations of voltage and frequency one of which (12 Kcps and 300 volts) requires twenty minutes, for a certain lamp.

Electroluminescence maintenance depends on the relative concentration of phosphor powder and embedding medium; lifetime is about three times longer at low concentrations than at high, there being a rather sharp transition region near equal parts by weight of phosphor and plastic. Phosphor layer thickness affects maintenance, of course, only to the small extent characteristic of voltage or field dependence already described. Lifetime improves with thickness of "clear coat" or phosphor-free layer by a factor of about five (even in dry environment), partly because of the series impedance effect mentioned above and partly because of the (small) field dependence; however, the operating voltage for such lamps is relatively high.

The emission spectra of about ten ZnS:Cu,Cl phosphors were compared when fresh and after deterioration to a few per cent; no change was observed.

Recent improvements in maintenance of the same basic phosphors have been made possible by alterations in activation and by modified firing procedures, including only maintenance improvement of the phosphor itself aside from artificial improvements concerned with the complete lamp. Lifetimes have been improved by factors of ten to one hundred to a point where lifetimes of yellow and green emitting phosphors are between 3×10^9 and 10^{10} cycles (in dry environment). These phosphors are equivalent in brightness to the previous short-lived phosphors.

References

1. W. A. Thornton, Bull. Amer. Phys. Soc., II, 1, 301 (1956); J. Appl. Phys., 28, 313 (1957).
2. S. Roberts, J. Appl. Phys., 28, 262 (1957).
3. W. A. Thornton, Papers presented at Electrochemical Society Meeting, New York City, April 27 - May 1, 1958, and at International Symposium on Solid State Physics, Brussels, June 2-7, 1958 (Proceedings in press).
4. S. Roberts, G. E. Research Laboratory, Unpublished Work (1952).
5. W. Hoogenstraaten, J. Electrochem. Soc., 100, 356 (1953).
6. F. A. Kröger and J. A. M. Dikhoff, J. Electrochem. Soc., 99, 144 (1952).

EFFECTS OF INTERACTION AMONG PARTICLES IN ELECTROLUMINESCENT LAYERS

Arthur T. Halpin and Paul Goldberg

Sylvania Electric Products Inc.
Flushing, N. Y.

This report is directed to an understanding of optical and electrical behavior of electroluminescent layers in terms of the properties of the individual constituent phosphor particles. Of prime concern is how single particle behavior is modified by interaction with neighbors. Experimentally the single particle data required for this problem are the luminous flux and electrical dissipation, both as functions of applied field and phosphor volume fraction. With these quantities the performance of a cell made up of many particles may be compared with that predicted from the properties of isolated particles and the differences expressed in terms of interaction.

Interaction between grains is likely to be important for a number of reasons. Reports have already been published describing changes in the luminous flux from particles upon establishing contact with electrodes and with neighbors[1,2]. Also high fields, when applied to semiconducting particles in close proximity, can be expected to cause local breakdown with attendant high in-phase current which may dominate the overall electrical behavior of the cell.

The experimental approach in this work was to study the dependence of cell brightness (emittance) and electrical losses as functions of phosphor volume fraction and applied voltage. The resulting data, when put in appropriate form, can be extrapolated to infinite dilution. The extrapolated properties will be those of isolated noninteracting randomly oriented grains and will be used in interpreting cell data at practically useful values of volume fraction. Another variation in the physical system employed in exploration of the interaction problem is the use of a fluid dielectric to allow particle orientation and contact and the comparison with suspensions employing a mechanically rigid dielectric.

Dependence of Particle Brightness on Volume Fraction

The brightness (L) was obtained for electroluminescent layers over a wide range of phosphor volume fractions (v_1) including the extremely dilute region. A suitable representation of the relationship between phosphor emittance and concentration of particles in the mixture was afforded by plotting the ration L/v_1 against v_1. L is expected to vary

with v_1 since cells with more phosphor particles will emit more light. The quantity L/v_1, however, is proportional to the luminous flux per unit volume of phosphor, or to the flux per particle. Variations in L/v_1 with v_1 will show effects of interaction. Our studies reveal a strong dependence of L/v_1 on v_1 such, for example, that the flux per particle at the highest v_1 employed is at least twice that at the lowest v_1. This enhancement of L/v_1 with increased phosphor concentration was found to be characteristic of mixtures employing either fluid or rigid suspending dielectrics. Measurements on cells employing a rigid matrix reveal in the dependency of L/v_1 on v_1 three ranges of v_1 of differing character: (i) a rapid rise in L/v_1 from extremely low v_1 up to $v_1 \leqslant 0.03$, followed by (ii) a region of constant L/v_1 up to $v_1 \leqslant 0.1$ and finally (iii) a further climb in L/v_1 in the region $v_1 > 0.1$. In cells employing a fluid dielectric, a similar effect on luminous output per particle is observed with increasing v_1 although the three characteristic regions are not as well resolved.

This behavior may be explained in terms of interaction processes coming into play with higher v_1. In the mixture of crystallites, dispersed and oriented randomly, a certain fraction of particles will be in contact with one another or with an electrode. Higher v_1 increases this fraction. Interactions of this nature are known to enhance the brightness of the contacting particles[1,2]. Accordingly, the brightness dependence on v_1 of the rigid mixture suggests that (a) at very low volume fractions (i.e., $v_1 \leqslant 0.03$) the rapid gain in L/v_1 reflects a rise in the fraction of particles in contact; (b) in the next higher range of v_1 ($v_1 \geqslant 0.03$) almost all particles are in contact and L/v_1 is independent of v_1. At very high densities ($v_1 > 0.1$) the observed further increase in L/v_1 may tentatively be ascribed to the formation of extensive particle aggregation. A similar description is applicable for fluid mixtures except that the higher mobility of particles in a fluid medium allows a given number of contacts to occur at lower v_1 than in the rigid medium. Extrapolation of L/v_1 data to infinite dilution in rigid media, with voltage as a parameter, yields values which are proportional to the average brightness per particle for ideally isolated, non-interacting randomly oriented particles.

The flux per particle may also vary with v_1 owing to changes in a particle's internal field as its electrical environment is modified. Such variations with v_1, however, should be more gradual than those found experimentally.

Statistical calculations have been carried out to obtain the concentration of particles in contact as a function of v_1. For fixed voltage and frequency, we assume that a contacted and an uncontacted particle each has a definite luminous flux associated with it. Then, on the basis of these assumptions, the observed dependence of L/v_1 on v_1 can be calculated in the region of low v_1. The details of the statistical method will be discussed further.

Dielectric Behavior as a Function of Volume Fraction

An electroluminescent condenser is essentially a two-phase dielectric system[3]. In principle, formal methods are available for calculating the properties of one phase (i.e. the dielectric constant and electrical loss) from data on the pure suspending dielectric and on the two-phase mixture[3,4]. These formulas are derived under an assumption of zero interaction between particles. Owing to the experiments described above, the formulas were found to be invalid for electroluminescent layers except at the lowest values of v_1 where the extent of interaction becomes negligible. The complex dielectric constant of the phosphor phase, and the electric field distribution were computed at $v_1 = o$ based on extrapolated mixture data. These calculated values are assumed to be representative of the intrinsic electrical properties of isolated electroluminescent grains.

The dissipation factor for the mixture, $\tan \delta = \epsilon''/\epsilon'$, increases superlinearly with volume fraction at a rate determined by the applied field. These curves converge at $v_1 = 0$ to the measured $\tan \delta$ of a layer containing only the suspending dielectric. The dielectric conductivity of the mixtures, $\sigma = \omega\epsilon''$, were calculated[5] from the $\tan \delta$ values for each v_1. The ratio σ/v_1 (voltage as parameter), is somewhat similar in its dependence on v_1 to the quantity L/v_1. Here σ/v_1 values are obtained at $v_1 = o$ by extrapolation for each voltage and may be related to the conductivity of an ideally isolated grain. Efficiency values calculated from L and σ data show a rising trend with falling v_1. The voltage dependence of individual particle properties as modified by interparticle contact will be reviewed and models for the changes in electrical and optical properties of particles upon establishing contact will be discussed.

References

1. A. Kremheller, J. Electrochem. Soc. 107, 8 (1960).
2. D. Hahn and F. W. Seemann, Z. Physik 146, 644 (1956).
3. S. Roberts, J. Optical Soc. America 42, 850 (1952).
4. J. A. Reynolds and J. M. Hough, Proc. Physical Soc. B 70, 769 (1957).
5. A. H. Von Hippel, "Dielectrics and Waves" J. Wiley and Sons, Inc., New York, N. Y., p. 5 (1954).

Abstract Number 68

"ON THE PHYSICAL CHARACTERISTICS AND CHEMICAL COMPOSITION OF ELECTROLUMINESCENT PHOSPHORS"

Paul Goldberg and Sixdeniel Faria

Sylvania Research Labs.
Bayside, New York

The aim of this work is to examine the surface and volume of Cu-activated electroluminescent zinc sulfide phosphors to ascertain the degree of their physical and chemical homogeneity and to relate the results to concepts expressed in the literature concerning the source of electroluminescent excitation in such materials. The principal experimental approach was the step-by-step removal of the phosphor surface by chemical etching. At each successive etching stage the following properties were examined: electroluminescent brightness, electrical dissipation, surface appearance using the electron microscope, crystal structure and activator content.

The results show that the polycrystalline phosphors are nearly uniform in chemical, physical and electroluminescent properties as one passes from the surface and penetrates deeply into the crystallite bulk. An exception to this is the existence of a thin surface layer, much like that found in cathode ray phosphors, which appears inefficient in terms of its electroluminescent behavior. Following the removal of this layer the electroluminescent properties vary with the extent of etching in a fashion like that previously described for particle size reduction[1,2]. These results are at odds with the concept[3] that a surface chemical phase is responsible for the potential barrier and thus for the source of electroluminescence excitation since strong electroluminescence persists following the removal of substantial amounts of surface material. They imply that electroluminescence excitation is due to the microscopic distribution of impurities within the ZnS crystallites rather than to the presence of additional bulk surface phases. The following describes results of experiments which gave rise to these views.

Electroluminescent Properties of Etched Phosphors: The brightness (L) and electrical loss of a family of phosphors etched progressively more heavily with 6N HCl were measured as a function of voltage (V). Two effects are found: (i) after initial etching the brightness and efficiency are improved at all voltages. This may be attributed to the removal of the inefficient surface layer. (ii) Further etching gives increased slopes on plots of $\log L$ vs. $V^{-1/2}$ as would be expected for decreases in particle size[1,2]. Accompanying this change in slope is a further increase in efficiency and an increase in the voltage at which

maximum efficiency occurs. This also resembles changes attendant upon reduction in particle size[1]. This trend prevails to the limit of the reduction effected in these experiments; i.e. about 50% reduction in size or 90% reduction in phosphor mass. The data are used as a basis for reassessing Destriau's experiments with etched electroluminescent phosphors[4,5].

Chemical Analysis for Activator Inhomogeneity: Quantitative analyses for Cu content of the same phosphor family were performed spectrographically. Before analysis, the materials were washed with 1% KCN solution to remove any loosely bound Cu_2S which forms by precipitation on exposed surfaces subsequent to dissolution of the phosphor material. The following table indicates the uniformity of activator concentration throughout the particle volume.

Wt. % removed by etching	Fraction of initial size (calculated)[a]	% Cu found (+ a.d.)	No. of samples analyzed
0	1.00	0.065 ± .002	4
25	.91	.066 ± .002	3
33	.87	.065 ± .002	2
70	.67	.067 ± .003	3
89	.48	.069 ± .002	4

a-Calculated from weight loss assuming spherical geometry.

Crystal Structure: The structure of the family of phosphors which has undergone successive etching is, to a first approximation, uniform throughout the lattice. Subtle changes in structure and in photoluminescence are observed upon penetrating the bulk which may be explained in terms of a non-uniform cooling rate over the crystallite surface and volume during phosphor preparation.

Surface Appearance: Electron microscope examination of the phosphors reveal in unetched specimens a surface marred by many small craters and elevations. Initial etching with 6N HCl removes this rough exterior. The particles, in most cases, do not show marked preferential etching of special crystal faces. This is true even after etching away 90% of the phosphor mass at which point the particles show noticeable size reduction. The materials possess surface striations not shown by non-electroluminescent ZnS:Cu,Cl phosphors.

Special Etch Patterns: In selected specimens etch geometries were found which were not typical of the materials reported above. The results, however, may be of significance to the structural character of the phosphor grains.

In one cubic phosphor, etched with hydrochloric acid, (to 99% of its mass removed) a geometrical polarity was apparent: one end of each of the particles showed sharply pointed pyramids while the opposite end was fairly smooth. The effect may be a consequence of the absence in the sphalerite structure of a center of symmetry. Microscope observations of the light output from the grains show that the crystal axis thus revealed by etching is also of special significance for electroluminescence: the emission is far stronger with the field parallel to this axis than with field perpendicular to it. The consequences of these observations will be discussed.

References

1. W. Lehmann, J. Electrochem. Soc. 105, 585 (1958).
2. P. Goldberg, ibid. 106, 34 (1959).
3. P. Zalm, Philips Res. Rep. 11, 353, 417 (1956).
4. G. Destriau, Symposium at Brooklyn Polytech. Inst., Brooklyn, N. Y. Sept. 9, 1955.
5. G. Destriau and H. F. Ivey, Proc. IRE 43, 1911 (1955).

Abstract Number 68A

DETECTION OF IONIZATION OF Eu^{++} IN THE PHOSPHOR SrS-Eu,Sm BY THE PARAMAGNETIC RESONANCE ABSORPTION METHOD

V. V. Antonov-Romanovsky, V. G. Dubinin, A. M. Prokhorov, Z. S. Trapenznikova and M. V. Fock

P. N. Lebedev Physical Institute,
Academy of Sciences of the U.S.S.R.,
Moscow, U.S.S.R.

According to the modern theories, a luminescence centre in a phosphor is a complex formation, which includes the activator, the lattice ions and vacancies adjacent to the activator and apparently also some additional admixtures that are accidentally formed or artificially introduced during the phosphor preparation. Therefore change of the charge of luminescence centres under excitation (proved by a great number of experiments) does not mean that the charge of the activator is changing and not of any other component of the luminescence centre. The spectrum of phosphorescence is determined mainly by the activator, and therefore it is natural to assume that the charge of the activator is changing, however there exists another possibility of explaining luminescence of the activator under recombination[1].

Recombination may take place not on the activator, but near it in the luminescence centre. The energy released under recombination excites the activator which then emits. Thus the last stage of the recombination process leads only to fluorescence of the activator (a stage of a changed state of ionization of the activator is absent).

Thus, as a result of excitation the valency of the activator may either change by ± 1 due to trapping a hole or an electron, or be constant, i.e. when this change is equal to 0. The method of paramagnetic resonance absorption enables one to solve this question in some cases.

For this study we took the phosphor SrS-Eu,Sm. This phosphor was selected for two reasons: first, the activator Eu which is bivalent in non-excited phosphors reveals a paramagnetic resonance absorption even at room temperature[2] that considerably simplifies the process of investigation and, second, the phosphor is able to store large light sums under excitation due to Sm^3, which is also a rather essential fact.

It should be pointed out that in recent work[3] there has not been found any change of a paramagnetic absorption of Eu^{++} under excitation of this phosphor. The authors of the papers explain it either by the fact that the phosphor stores an insufficiently large light sum, or by other reasons. In spite of the negative result of the experiment, the authors do not come

to a conclusion concerning the constancy of the valency state of Eu^{++}. Thus the problem of the change of the valent state of the activator was not clarified.

We succeeded in finding a decrease of the amount of Eu^{++} under excitation of the phosphor.* Excitation was carried out by visible light in the absorption band ($\lambda \sim 440$ mμ) which depends on the Eu activator. At the moment of excitation the decrease of the paramagnetic absorption which we designated as ΔN, was about 15%, and in ~ 10 minutes after removing the excitation it was about 10%.

It was interesting to compare the above data with the decrease of ΔK, the coefficient of optical absorption which depends on Eu. In 10-20 minutes after removing the excitation ΔK is approximately 11%. Thus $\Delta K \sim \Delta N$. This fact shows that the additional absorption is associated with optical transitions in the Eu^{++} ion proper and not, for example, in some neighbouring ion disturbed by the presence of Eu^{++}.

Simultaneously, we also carried out measurements of the total number of quanta, S, emitted by the excited phosphor starting 10-20 minutes after removing the excitation. Measurements gave 6.5×10^{15} quanta. Calculation shows that not less than $\sim 4\%$ of Eu introduced are excited. Since in this case, according to a very rough estimate, the quantum yield of radiation under recombination $q \sim \frac{1}{2}$, we obtain that (at the moment t = 10 - 20 min.) about 8% of luminescence centres are ionized.

For the sake of convenience we present the data in the following table:

Table I

Decay time t per minute	0	10-20
ΔN	$\sim 15\%$	$\sim 10\%$
ΔK	-	$\sim 11\%$
$\frac{S}{q}$	-	$\sim 8\%$

Decrease of concentration of Eu^{++} when the phosphor is under excitation is possible for two reasons: 1) Either due to transition of Eu^{++} into Eu^{+} after trapping an electron ($Eu^{++} + e^{-} \rightarrow Eu^{+}$), or 2) due to an additional ionization of Eu^{++} ($Eu^{++} - e^{-} \rightarrow Eu^{+++}$). We believe and shall try to prove below that the second possibility is more probable.

*Preliminary results were reported at the Conference on physics of alkali-halide crystals (Tartu, June 30 - July 4, 1959). Similar results were obtained by Title (R. S. Title. Quantum Electronics-Resonance Phenomena. Symposium. Bloomingburg, N. Y. September 14-16, 1959).

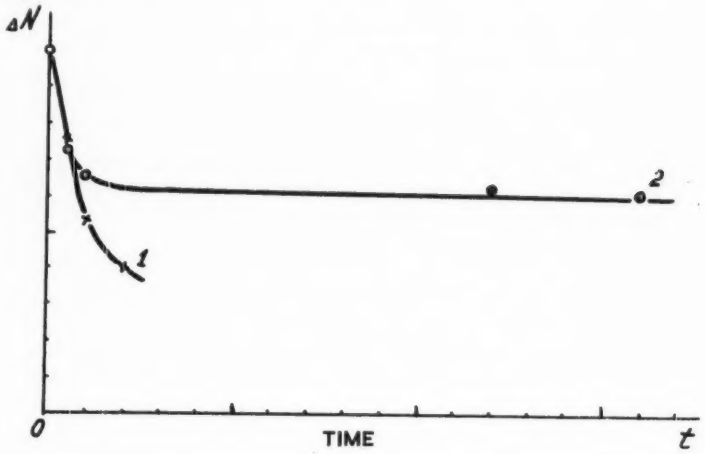

Figure 1

The phosphor SrS with a single activator Eu, in contrast to a phosphor having both Eu and Sm, stores negligible light sums[3]. It proves that a single Eu is unable to form deep electron traps. But in the phosphor SrS-Eu,Sm the activator Sm is in the trivalent state and therefore it is preferentially able to trap an electron than a bivalent Eu^{++}. That is why formation of a monovalent Eu^{+} is hardly probable under excitation, and therefore a decrease in the amount of Eu^{++} is undoubtedly associated mainly with transition of Eu^{++} ions into a trivalent state Eu^{+++}. Certainly, the most direct proof of the presence of Eu^{+++} in the excited phosphor would be Eu^{+++} lines detected in the luminescence spectrum (a bivalent Eu^{++} gives a wide band in a red region of the spectrum).

After removing the excitation the amount of Eu^{+++} must decrease on account of their recombination with the electrons released by heat from traps, and therefore the value ΔN must decrease in time. The corresponding data for two phosphors are presented in Fig. 1.

References

1. P. Pringsheim. Luminescent Materials, Symposium (1948), p. 443; F. A. Kröger. Luminescence in Solids Containing Manganese. Amsterdam (1940); V. L. Levshin. Izv. Acad. Nauk (USSR). (Ser. physical), 9, 356 (1945).
2. B. Blaney, W. Low. Proc. Phys. Soc. A., 68, 55 (1955); W. Low, Phys. Rev., 98, 426 (1955); A. A. Manenkov, A. M. Prokhorov, Z. A. Trapeznikova, N. V. Fock Opt. and Spektr. (USSR), 2, 470 (1957).
3. V. V. Antonov-Romanovskij, V. L. Levshin, Z. L. Morgenstern, Z. A. Trapeznikova. Izv. Acad. Nauk (USSR), (Ser. physical), 13, 75 (1949).

Abstract Number 69

COPPER-CHLORIDE RELATIONSHIPS IN PHOTOLUMINESCENT AND ELECTROLUMINESCENT ZINC SULFIDE PHOSPHORS

A. L. Solomon & P. Goldberg

Sylvania Research Laboratories
Bayside, N. Y.

Most electroluminescent ZnS phosphor preparations appear to depend upon arriving at a state where the copper activator appears in excess of the coactivator, which serves essentially as a solubility controlling agent for the activator. It is believed the copper in excess is essentially undissolved in the ZnS and creates a barrier region which is responsible for the electroluminescence excitation process[1-8]. Obtaining this state in ZnS:Cu, Cl is complicated since relatively large amounts of chloride are used as crystallizing agents. In some laboratories this state of excess copper has been obtained by introducing large amounts of copper or by reducing the chloride content by heat treatment[3-7]. Low coactivator concentrations in ZnS:Cu,Cl systems have also been prepared by introducing small amounts of chloride during crystallization in a controlled atmosphere[5]. This report seeks to separate the process of crystallization (and the accompanying appearance of photoluminescence) from the factors which govern the appearance of electroluminescence. In the present work ZnS is initially crystalized by heat treatment with copper and chloride. The chemical and photoluminescent properties are determined. Additional copper is then introduced into the system in another heat treatment to generate electroluminescence. The chemical and photoluminescent properties are then redetermined.

A series of ZnS:Cu,Cl phosphors were prepared from precipitated ZnS with copper concentrations ranging to 3.5×10^{-3} g.at./mole and 9% by weight of mixed chloride flux. The crystallization was carried out in covered quartz crucibles in air at 1200°C for several hours. Samples were then analyzed for Cu and Cl. Figure 1, a plot of Cu/Cl vs. Cu up to 9×10^{-4} g.at.Cu/mole, shows two distinct regions and the suggestion of a third, which may be explained in terms of copper and chloride solubility in ZnS.

1) At low copper concentrations, where $Cu/Cl < 1$, the chloride content has been found to be essentially that of a sample crystallized under equivalent conditions with no copper. The limit of copper incorporation in this region depends on the solubility of chloride alone in ZnS under the specified conditions of preparation.

2) The appearance of a plateau in the region of Cu/Cl≃1 indicates that a nearly one-to-one copper-chloride interaction is the solubility determining factor for both copper and chloride.

3) At higher copper concentrations, the solubility of copper-chloride "pairs" is exceeded and the curve rises with the appearance of undissolved copper. The copper concentration at which this region begins and the rate of rise of the curve has been found to differ among series of samples. The bulk of the undissolved copper, however, is removable by treatment with aqueous alkali cyanide solution. An analysis of the copper and chloride in samples so treated shows the Cu/Cl ratio which is found in the plateau region.

Though the plateau region has been found repeatedly for several series of samples, different series have shown plateaus at ratios below Cu/Cl = 1; a value of 0.7 is representative.

Following the suggestion of earlier workers[9-10], we find that the photoluminescence of these samples is related to the Cu/Cl ratios. In the low copper region (1), the familiar green emission with long afterglow is found. In the plateau (2) and higher copper regions (3), the emission is blue to green with increasing copper and with relatively short emission decays. When copper additions to the materials of regions (2) and (3) in a second thermal treatment are attempted, no change in photoluminescence is observed. When sufficient copper is added to region (1) materials to bring them to Cu/Cl≧1, abrupt photoluminscent changes appear, i.e., they change from green with long afterglow to blue with short decay. Accompanying the photoluminescent change, electroluminescence appears. An example (Figure 2) is given showing the coincidence of the two effects when Cu/Cl = 1. Further copper additions result in relatively little change of electroluminescence. The appearance of electroluminescence at the limit of activator/coactivator approximately equal to unity agrees with previous work on ZnS:Cu,Al[5]. If no copper addition is made to region (1) materials during a second heat treatment, no electroluminescence appears.

When the copper addition during a second thermal treatment of region (1) materials is carried out over the temperature range, 600°C to 1200°C, a distinct difference appears between the photoluminescent change and the appearance of electroluminescence. The photoluminescent change green to blue is found to occur at relatively low temperatures (Figure 3). The intensity of this photoluminescence is essentially constant up to the higher temperatures. In contrast, electroluminescence is much more temperature sensitive, showing a maximum near 800°C (Figure 3). When samples of weak electroluminescence from the 1100°C region are annealed for long periods at approximately 800°C, no gain in electroluminescence is found. If these 1100°C samples are subjected to additional copper during another heat treatment near 800°C, the electroluminescence is raised significantly. Furthermore, it has been noted that materials differing only in the temperature of the second thermal treatment show the same copper and chloride concentrations, within experimental error, but show one to two orders of mag-

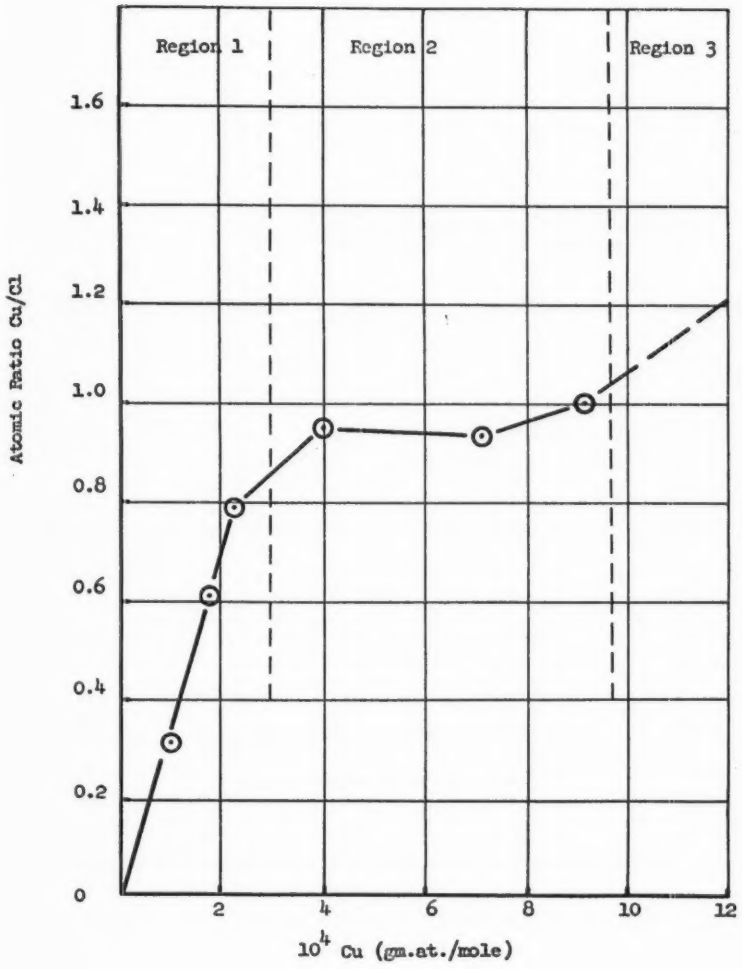

Fig. 1—Cu/Cl Rates vs. Cu Used in First Thermal Treatment.

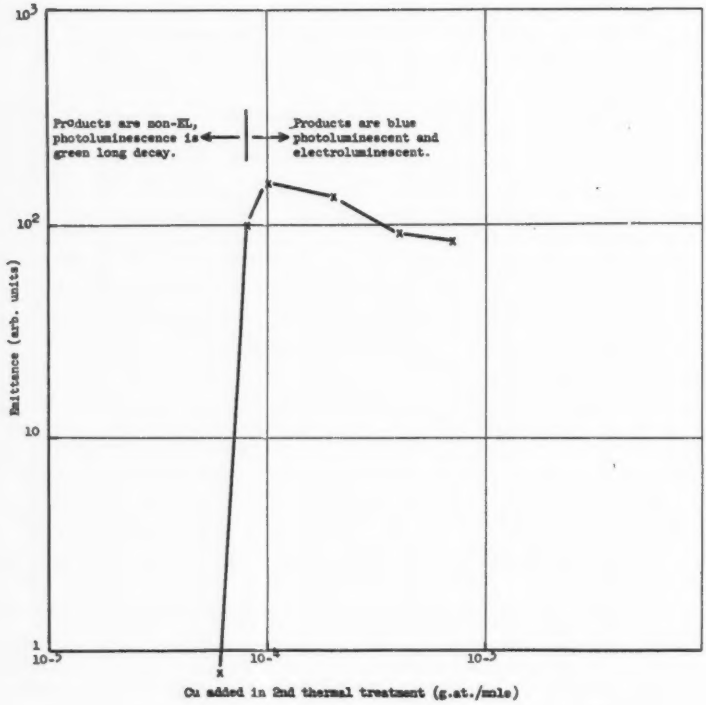

Fig. 2—Emittance vs. Cu Used in Second Thermal Treatment.

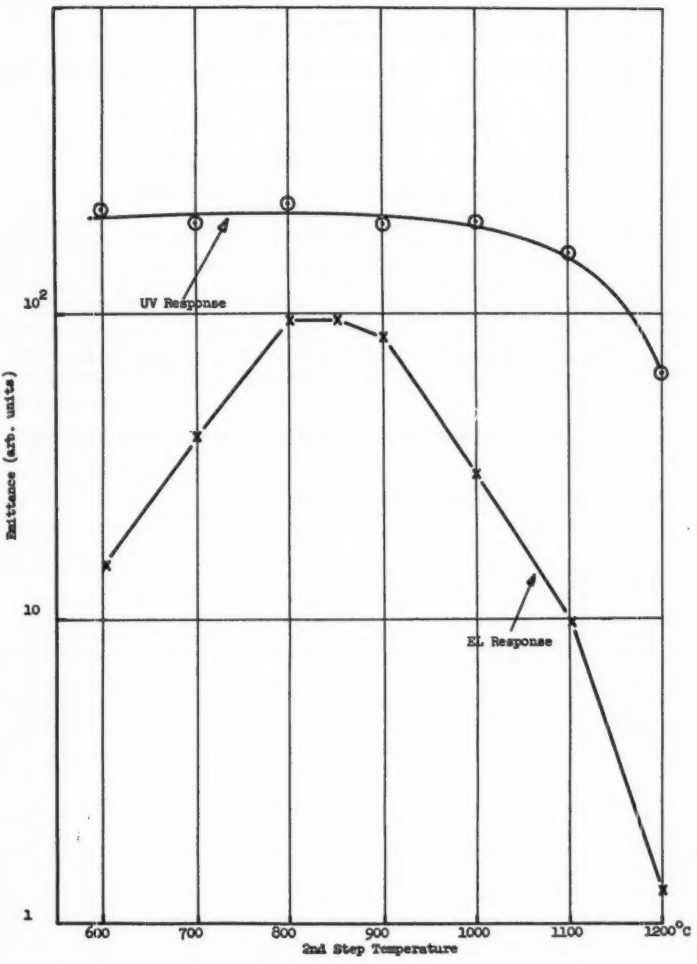

Fig. 3—Emittance vs. Temperature of Second Thermal Treatment.

nitude difference in electroluminescence. This suggests that the phosphor undergoes critical physical changes in experiencing a conversion from the non-electroluminescent to the electroluminescent condition.

References

1. H. H. Homer, R. M. Rulon, K. H. Butler, J. Electrochem. Soc. 100, 566 (1953).
2. K. H. Butler, Science 129, 544 (1959).
3. G. Destriau and H. F. Ivey, Proc. IRE 43, 1911 (1955).
4. H. C. Frohlich, J. Electrochem. Soc. 100, 496 (1953).
5. P. Zalm, Philips Res. Rep. 11, 353, 417 (1956).
6. T. B. Tomlinson, J. Phys. Rad. 17, 634 (1956).
7. A. H. McKeag and E. G. Steward, J. Electrochem. Soc. 104, 41 (1957).
8. S. Larach and R. E. Shrader, J. Phys. Chem. Solids 3, 141 (1957); H. J. Hegyi, S. Larach and R. E. Shrader, J. Electrochem. Soc. 104, 717 (1957).
9. F. A. Kroger, J. E. Hellingman and N. W. Smit, Physica 15, 990 (1949).
10. R. H. Bube, J. Chem. Phys. 19, 985 (1951).

Abstract Number 70

EFFECT OF CdS ON ELECTROLUMINESCENCE OF ZnS:Cu, HALIDE PHOSPHORS

Arthur Dreeben

RCA Laboratories
Princeton, N. J.

Although the electroluminescent properties of ZnS phosphors have been widely studied, little information has appeared in the literature on AC field excitation of ZnS-CdS solid solutions. There have been descriptions of electroenhancement effects in some (Zn, Cd)S compositions with (Mn,Cl); (Mn, Au, Cl); and (Ag, Mn) activator systems.[1] Zalm[2] has mentioned that CdS has a deleterious effect on the electroluminescent brightness of ZnS:Cu, but to the writer's knowledge, no systematic investigation of this effect has been published. This report represents some results of such a study.

The (Zn, Cd)S:Cu, halide materials were prepared by standard phosphor techniques. In the firing process, use was made of the "sulfur-effect",[3,4] by adding a quantity of purified sulfur to each of the raw mixes. (For comparison one series was prepared without this addition). Bromide and chloride coactivated samples were fired at 950°C and those with iodide at 700° or 1075°C. All products were washed with an alkaline NaCN solution to remove excess copper. Electroluminescent properties were examined in castor oil cells.

The spectral distribution of the low-temperature (700°C) ZnS:Cu,I phosphor has not been reported before. It shows a broader band with an apparent peak in the blue at a slightly longer wavelength than the high-temperature material.[5] All samples show a shift to longer wavelengths with increasing proportion of CdS. Brightnesses were found to be quite sensitive to the presence of CdS. In most materials a rapid decrease occurs when CdS is in excess of several mole %.

The proportion of cubic and hexagonal phases in representative samples from each series has been established by X-ray diffraction examination. Some factors affecting the formation of these phases will be indicated. Within each series there is a marked decrease in brightness as the proportion of hexagonal phase increases. The influence of crystal structure on traps in ZnS:Cu phosphors has been reported by others. Bube,[6] for example, found differences in trap densities between the cubic and hexagonal modifications. More recently, Ballentyne,[7] showed that a redistribution of trapping states occurs when electroluminescent zinc sulfides transform from the hexagonal to the cubic structure. The possibility of such differences between cubic and hexagonal (Zn, Cd)S solid solutions will be discussed.

Chemical analyses showed that in bromide, and particularly in chloride coactivated samples, the amount of retained copper varied with increasing proportions of CdS. In the case of the chloride materials, it was also found that as CdS was added the phosphorescence (after irradiation with 3650 Å UV) increased. This is contrary to the typical effect of an increase in either copper or cadmium sulfide.[8] To account for these results, the formation of a new, cyanide insoluble phase involving copper, cadmium and sulfur is postulated. Some factors which apparently effect the stability of this phase will be mentioned.

It appears that the electroluminescent properties are influenced by simultaneous and perhaps inter-related effects between crystal structure, trapping states, and phase relationships involving the segregation of copper. The relative importance of each of these separately cannot be decided at present.

References

1. G. Destriau, J. Mattler, M. Destriau, and H. E. Cumlich, J. Electrochem. Soc., 102, 682 (1955), G. Destriau, Compt. rend., 245, 1913 (1957). P. M. Jaffe, J. Electrochem. Soc., 106, 667 (1959).
2. P. Zalm, Philips Res. Rept., 11 353 (1956).
3. S. Larach and R. E. Shrader, Paper on "Electroluminescent Chalcogenide Phosphors", Brussels International Conf. on Solid State Physics, 1958.
4. A. Wachtel, U. S. Patent 2,874,128 (1959).
5. I. J. Hegyi, S. Larach and R. E. Shrader, J. Electrochem. Soc., 104, 717 (1957).
6. R. H. Bube, Phys. Rev., 80, 655 (1950).
7. D. W. G. Ballentyne, J. Phys. Chem. Solids, 10, 242 (1959).
8. G. R. Fonda, Trans. Electrochem. Soc., 87, 339 (1945).

Abstract Number 71

ZnS:Cu,Cl AND (Zn,Cd)S:Cu,Cl ELECTROLUMINESCENT PHOSPHORS

A. Wachtel

Research Dept., Westinghouse Electric Corp.,
Bloomfield, N. J.

Investigations on the preparation of blue and green emitting ZnS:Cu, Cl EL* phosphors were based on previous work by Lehmann[1] who noted a considerable improvement in brightness as a result of firing in an atmosphere containing elementary S. This necessarily implies that oxygen or oxides are detrimental and therefore constitutes a departure from the original procedure employed by Destriau[2] and subsequently generally accepted conclusions as summarized by Wendel[3].

Cu incorporated in the form of blue or green emitting centers[4,5] was assumed to be a function of incorporated Cl which in turn could be controlled by firing a mixture of ZnS with $Cu(C_2H_3O_2)_2 \cdot H_2O$, 5 wt. % S and Cl usually added as NH_4Cl in silica tubes closed at one end and capped by similar tubes of slightly larger diameter. The assembly is enclosed in a larger silica tube which can be flushed with N_2. If the volume enclosed is not too large, then the phosphor, on firing, is in contact with a saturated atmosphere of its own thermal decomposition products, i.e., S, NH_3,HCl. The Cl content of these gases is a function of Cl added before firing.

Experiments have indicated that the mechanism of Cl incorporation consists not of simple retention, but of preliminary evaporation of Cl into the surrounding atmosphere, followed by absorption on ZnS+Cu which takes place at a slower rate. It is strongly decreased by the presence of S, and also decreases if the sample size fired is increased such that equal blue/green ratio of emission color may be obtained if the Cl addition is adjusted according to

$$\%Cl = X(0.97 + 0.003 \text{ wt. (in gm) of ZnS}),$$

where X = amount of Cl added to a 10gm sample. Under these conditions, with 5 wt. % S and two firings of 90 minutes each at 950°C, about 45% of the added Cl appeared to be assimilated, provided that Cu is present in excess.

For oxygen-free phosphors, EL-excitation requires such an excess of Cu, presumably present as Cu_2S[6,7]. The optimum amount (prior to

---

*Electroluminescence or electroluminescent is hereafter abbreviated EL.

NaCN washing) was found to be in the neighborhood of 0.005 to 0.006 gm-atoms Cu/mole ZnS. Fig. 1 shows EL brightness at two frequencies of excitation as a function of activator addition to 10gm samples, made according to

$$\%Cu = 0.55 + 0.45\ (\%Cl).$$

It is very similar to the dependence of brightness on Al addition as reported by Froelich[8].

In the absence of elementary S, or in the presence of ZnO, the Cl addition must be lowered approximately by a factor of 10 so as to obtain the same emission colors. However, even then, the EL output of such phosphors is much poorer than that of S-fired phosphors. The use of Pb was tried for various compositions including ZnO and low Cu additions such as described in the patent literature. The use of Cl additions almost 10 times higher than presently described were required to obtain blue-green emission and presumably optimum activator incorporation. Although this resulted in some improvement, even the best Pb-containing EL phosphors gave brightness values which were several times lower than those normally obtained without the use of Pb.

Optimum Cl incorporation for 10,000 c.p.s. excitation was also noted to result from firing ZnS + $Cu(C_2H_3O_2)_2 \cdot H_2O$ in an open boat in a current of $N_2 + S_2Cl_2$. In this case, no S is added to the sample. The limited formation of green centers appears to be controlled in a manner similar to that effected by firing in mixtures of H_2S+HCl; however in the present case, the atmosphere is strongly oxidizing with respect to ZnS. Phosphors prepared by firing in S_2Cl_2 are characterized by a lighter (less-yellow-green) body color after NaCN washing and a stronger dependence of EL brightness on applied voltage.

The dependence of blue/green ratio on Cl addition as described holds true only for Cl added as HCl or its equivalent, i.e., $ZnCl_2$ NH_4Cl or $CuCl_2$. Cl added in the form of alkali chlorides[9] results in increasingly blue emission, more so with increasing atomic weight of the cation. In the case of KCl, only blue-emitting phosphors are obtained which are characterized by much better maintenance than normal blue-emitting ZnS:Cu,Cl phosphors. The effect goes further such that in the presence of KCl, very large additions of "available" Cl (i.e., $ZnCl_2$, etc.) are required to cause a shift to green emission. This results in a further improvement in maintenance, but poorer emittance.

Substitution of Zn by Cd[10] results in a rapid decrease in EL brightness, possibly due to introduction of deep traps[10,11]. However, at the same time, the following phenomena are noted:

1. Formation of hexagonal phase. According to Zalm[10], this too should result in decreased emittance.
2. A shift in EL-excited emission color to shorter wavelengths with respect to the ultraviolet-excited emission colors.
3. Formation of a dark-colored separate phase, insoluble in NaCN

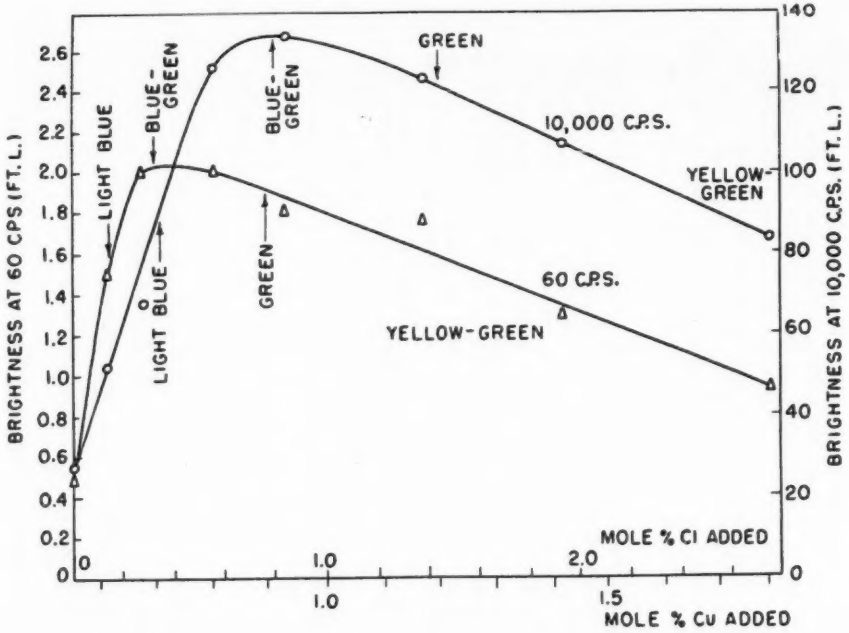

Fig. 1—Brightness of ZnS:Cu,Cl phosphors as a function of activator addition before firing. The Cl additions refer to 10 gm lots ZnS in 13.5ml tubes fired at 950°C 2 x 90 minutes, each time with 0.5 gm S added to the sample.

solution. When prepared in pure form, this material is black and shows a hexagonal x-ray diffraction pattern very similar to that of CdS. Chemical analysis shows 18.5% Cu. Its exact identity has not as yet been established, although it appears to be some type of (Cd,Cu)S.

Fig. 2 shows the effect of increasing substitution of Zn by Cd, either by excitation of the phosphor as is, or after mixing with copper filings (contact-EL[7]). In the latter case, the observed brightness is somewhat increased, and the normal shift in EL-excited emission color occurs. This means that at high Cd-concentration, a brighter orange contact-EL repres nts a much higher emittance than the dimmer green normally-excited EL. The results indicate that the phenomena associated with the presence of CdS interfere mainly with the EL-excitation mechanism. This view is also supported by the observation that cubic or hexagonal photoluminescent ZnS:Cu(0.01%),Cl are about equally efficient in contact-EL.

The interference caused by Cd could be partially avoided by preparing a normal green-emitting ZnS:Cu,Cl EL phosphor and refiring this with CdS at a lower temperature. The phosphor is washed in NaCN solution only after the firing with CdS. The refiring temperature was found to influence strongly the output of the phosphor, the optimum being in the neighborhood of 650°C. Experiments have indicated that this is a compromise between achieving sufficient incorporation of Cd, and avoiding the interfering phenomena. The maximum amount of Cd incorporated by this method, resulting in a cubic phosphor with green-yellow emission color, was 14 mole %. Despite its high luminosity (peak wavelength at 10,000 c.p.s. = 560mμ) the brightness is only about one-third that of a normal green-emitting phosphor. Etching in HCl causes a continuous shift in emission color to shorter wavelengths, so that this phosphor may be regarded as a non-homogeneous optically filtered system.

References

1. W. Lehmann, Canadian Pat. 579,685 (July 14, 1959).
2. G. Destriau, Phil. Mag. 38; 700, 774, 800, 885 (1947).
3. G. Wendel, Z. Phys. Chem., 206; 169 (1956).
4. F. A. Krōger, J. E. Heilingman, and N. W. Smit, Physica, 15; 990 (1949).
5. R. Bowers and N. T. Melamed, Phys. Rev., 99; 1781 (1955).
6. P. Zalm, J. Diemer, and H. A. Klasens, Philips Res. Rep., 9; 81 (1954).
7. W. Lehmann, J. Electrochem. Soc., 104; 45 (1957).
8. H. C. Froelich, J. Electrochem. Soc. 100; 496 (1953).
9. C. C. Beutler and J. S. Prener, U. S. Pat. 2,755,255 (July 17, 1956).

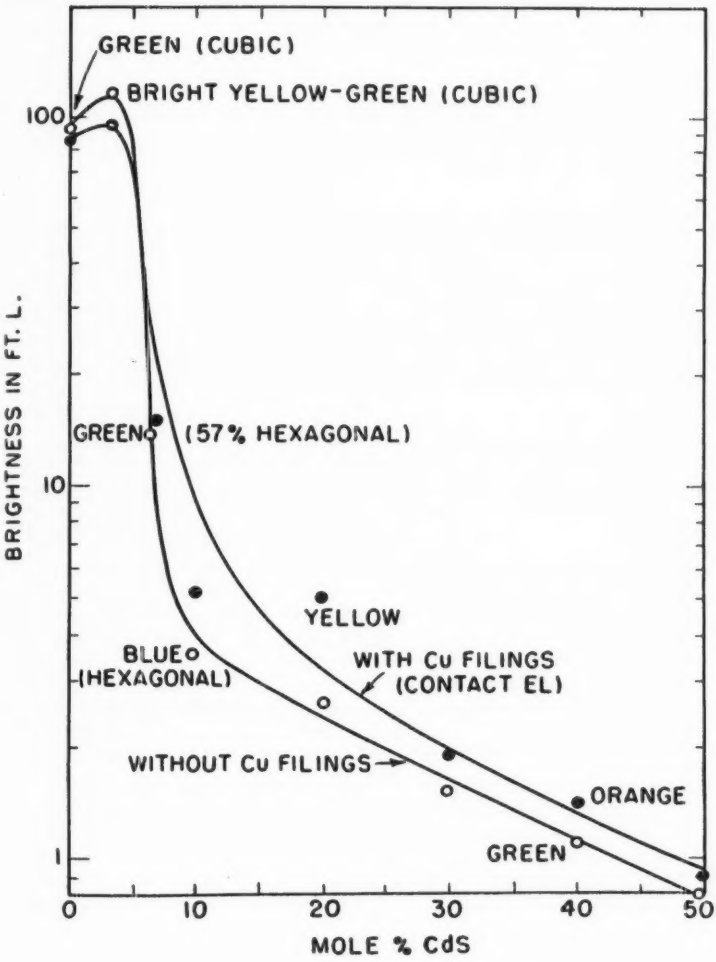

Fig. 2—Brightness at 10,000 cps excitation of (Zn,Cd)S:Cu,Cl phosphors as a function of Cd concentration.

10. P. Zalm, Philips Res. Rep. 11; 353 (1956).
11. C. H. Haake, J. Opt. Soc. Am. 47; 881 (1957).

(Zn,Hg)S AND (Zn,Cd,Hg)S ELECTROLUMINESCENT PHOSPHORS*

A. Wachtel

Research Dept., Westinghouse Electric Corp.,
Bloomfield, N. J.

The preparation of solid solutions of (Zn,Hg)S by hydrothermal synthesis was reported by Kremheller and Levine[1] and some of the photoluminescent properties of this system were recently described by Kremheller, Levine and Gashurov[2]. In the present study, the phosphor components are fired in sealed and evacuated silica tubes. In order to avoid excessive internal pressure during such firings, prefired ZnS:Cu phosphors and HgS prepared by reaction from the elements are employed. A small amount of elementary sulfur is also included, so as to ensure oxidizing conditions during this step.

Photoluminescent (Zn,Hg)S:Cu,Cl phosphors were prepared from ZnS:Cu (0.01 mole %):NaCl(5 mole %) by refiring with 0 to 80 mole % HgS. The emission spectra exhibit a continuous shift to longer wavelengths, the extent of which is about four times as great as caused by similar concentrations of CdS.

For the preparation of EL**-phosphors, the introduction of Hg lowers the optimum additions of Cu and Cl to about 0.2 mole % Cu and enough Cl so as to effect bright blue rather than green emission of the ZnS:Cu, Cl phosphors before refiring with HgS. Fig. 1 shows the emission spectra for 10,000 c.p.s. excitation of (Zn,Hg)S:Cu,Cl EL phosphors prepared from ZnS:Cu(0.2 mole %):Cl(0.075 mole %) refired with 0 to 25 mole % HgS. Although the final activator concentration decreased slightly due to dilution caused by HgS, a long wavelength emission band is seen to become pronounced at higher Hg concentrations.

On the other hand, replacement of Cl by Br+I, Ga, or In allowed the use of higher activator additions such as to produce predominantly green (long wavelength band) emission before refiring with HgS. Nevertheless, in contrast to ZnS, such red-emitting phosphors were also characterized by two emission bands whose relative height depends primarily on Hg content, although as in ZnS increasing coactivator

*This work was supported by Contract AF33(616)-5811 from the Wright Air Development Center.

**Electroluminescence or electroluminescent is hereafter abbreviated EL.

concentration was also noted to cause a shift in emission to longer wavelengths.

The emission color of a [(1-x)Zn,xHg]S:Cu phosphor may be duplicated by preparing a [(1-4n)Zn,4nCd]S:Cu phosphor and refiring this with (x-n)HgS. It was noted that the brightness generally increases with addition of Cd until the formation of the hexagonal phase becomes appreciable, irrespective of the actual concentration of Cd, which may be much higher in the presence of Hg. Similar results were also observed on phosphors coactivated with Br+I and with Ga. The effect is therefore primarily one of crystal structure. It supports the original contention of Zalm[3], according to which the cubic modification in ZnS is more suitable for EL.

Fig. 2 shows that phosphors prepared with increasing concentration of Hg or Cd+Hg and coactivated by a halogen exhibit a very sharp drop in output at low Hg concentration. This is noted on photoluminescence as well as EL. Thereafter, the brightness increases well beyond the point of maximum luminosity of emission. In the case of Ga coactivation, this initial decrease is absent inasmuch as ZnS:Cu,Ga is characterized by poor EL output, presumably due to the presence of deep traps[4,5] and the subsequent increase could be explained in terms of decreasing trap depth due to lowering of the conduction band, provided that one is dealing with a mechanism similar to that occurring with Cd-substitution[6]. This however, does not explain the very similar behavior of halogen-coactivated phosphors, as well as the fact that the EL behavior of the phosphors is reflected in similar differences of photoluminescence.

The frequency dependence of (Zn,Cd,Hg)S:Cu EL phosphors coactivated by Ga and In resulted in a decreased slope and early saturation of brightness which is probably an effect of trap depth.

Comparison of quantum efficiency with that of a standard green-emitting ZnS:Cu,Cl EL phosphor was made at 400 c.p.s., using red-emitting and deep-red emitting samples. Luminous efficiencies were determined as a function of voltage, and spectral distributions were corrected for energy ($dE/d\lambda$), luminosity ($dL/d\lambda$), and quanta ($dQ/d\lambda$). The quantum yields were calculated for the voltages at which maximum luminous efficiency was noted according to

$$K = \frac{B \times A}{6.5} \times \frac{Q}{L} \times 10^8 ,$$

where K = number of quanta emitted per second, A = area of the cell in cm^2, $Q = \int \lambda (dE/d\lambda) d\lambda$, $L = \int y (dE/d\lambda) d\lambda$, and B = observed brightness in foot-lamberts.

It was observed that the quantum efficiency K/W for the red-emitting phosphor is of the same order of magnitude as that of ZnS:Cu,Cl.

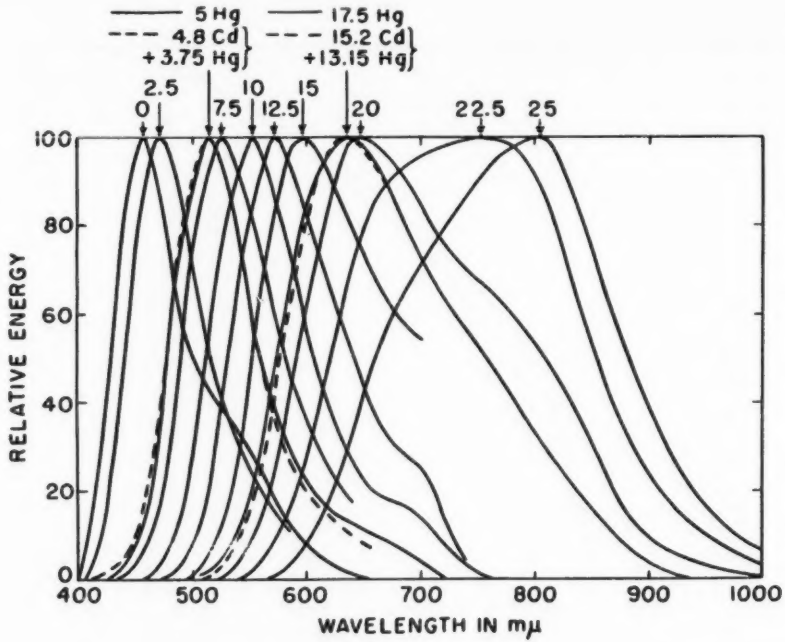

Fig. 1—Emission spectra of (Zn,Hg)S:Cu,Cl phosphors excited at 10,000 cps. Numbers denote mole % HgS.

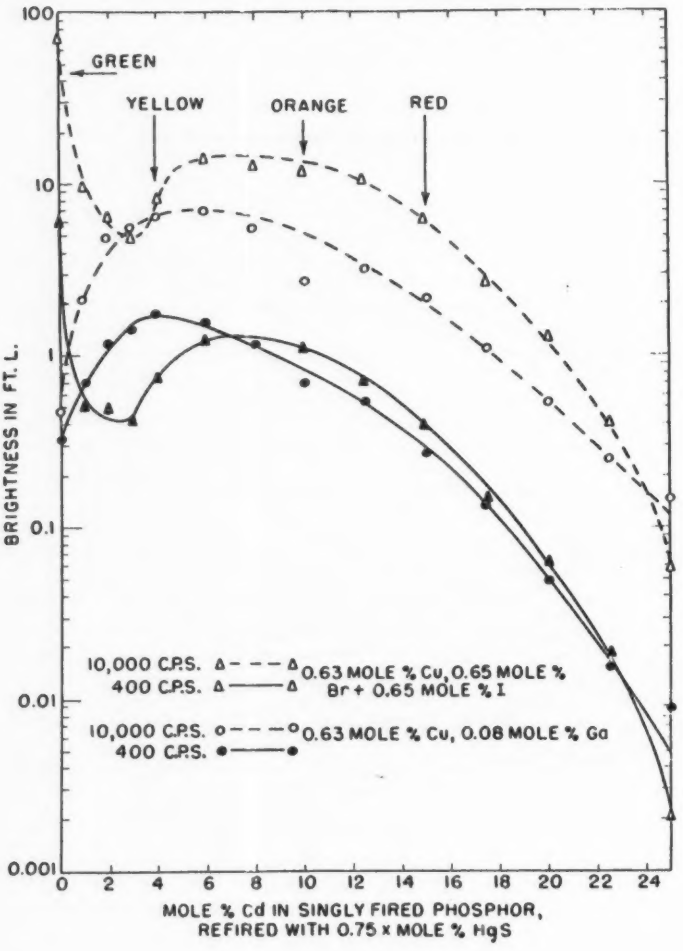
100
10
1
0.1
0.01
0.001
BRIGHTNESS IN FT. L.
GREEN
YELLOW
ORANGE
RED
10,000 C.P.S. Δ - - - Δ 0.63 MOLE % Cu, 0.65 MOLE %
400 C.P.S. Δ —— Δ Br + 0.65 MOLE % I
10,000 C.P.S. o - - - o 0.63 MOLE % Cu, 0.08 MOLE % Ga
400 C.P.S. ● ——●
0 2 4 6 8 10 12 14 16 18 20 22 24
MOLE % Cd IN SINGLY FIRED PHOSPHOR,
REFIRED WITH 0.75 x MOLE % HgS

Fig. 2—Brightness of (Zn,Cd,Hg)S:Cu,Br,I and of (Zn,Cd,Hg)S:Cu,Ga phosphors as a function of phosphor composition.

References

1. A. Kremheller and A. K. Levine, Sylvania Technologist, 10, No. 3 and Enlarged Abstract #59, ECS Spring Meeting, Philadelphia, 1959.
2. A. Kremheller, A. K. Levine and G. Gashurov, J. Electrochem. Soc. 107; 12 (1960).
3. P. Zalm, Philips Res. Rep., 11; 353 (1956).
4. W. Hoogenstraaten, J. Electrochem. Soc., 100; 356, (1953).
5. C. H. Haake, J. Opt. Soc. Am., 47; 881 (1957).
6. H. A. Klasens, J. Electrochem. Soc., 100; 72 (1953).

Abstract Number 73

THE INFLUENCE OF Mg AND Cd ON THE ELECTROLUMINESCENCE OF ZnS:Cu PHOSPHORS

P. M. Jaffe

Research Dept., Westinghouse Electric Corp.,
Bloomfield, N. J.

The influence of MgS on the cathodoluminescence of ZnS:Cu has been investigated by Smith[1]. The present investigation is concerned with the influence of MgS on the electroluminescence (EL) of ZnS:Cu phosphors prepared with additions of halogens (F,Cl,Br,I). The MgS content was varied up to 20 mole %*.

The phosphors were prepared by adding Cu (as the acetate) and the halide (as the respective ammonium salt) from stock solutions to ZnS. After drying, the required amount of MgS and $S^{2,3}$ were added. These latter operations were done in a dry atmosphere to avoid hydrolysis of the MgS. Crystallization was carried out in dry N_2 by firing at 950°C for 90 minutes. The fired samples were washed in NaCN+NaOH solution. The MgS was prepared by firing $Mg(NH_4)Cl_3 \cdot xH_2O$ first in dry HCl and then in dry H_2S.

The spectral characteristics and the brightness were examined in an EL cell with castor oil as the dielectric. Sinusoidal excitation was used. The results show that increasing amounts of MgS cause a decrease in the brightness and a shift in emission to shorter wavelengths. The changes are small up to 5.0 MgS but at 8.0 MgS they become abruptly large. X-ray diffraction shows that between 5.0 and 8.0 MgS there is a transition from cubic to hexagonal structure which causes the sudden changes. Unexpectedly, there is a lattice expansion with increasing MgS. In general, Cl, Br and I give similar results. Fluorine, however, does not appear to enter the lattice.

The influence of MgS on the system (Zn,Cd)S was also examined. Samples with the composition $0.9[(1-x)Zn \cdot xCd]S \cdot 0.1MgS:0.6Cu,0.3Cl$ were prepared (x=0.01, 0.03, 0.05, 0.1, 0.15 and 0.2 mole). Increasing Cd causes a progressive shift of emission to longer wavelengths and a decrease in brightness.

*All concentrations are in mole % unless specified otherwise.

References

1. A. L. Smith, J. Electrochem. Soc., 99, 155 (1952).
2. A. Wachtel, U. S. Pat. 2,874,128 (Feb. 17, 1959).
3. W. Lehmann, Canadian Pat. 579,685 (July 14, 1959).

Abstract Number 74

THE INFLUENCE OF HALOGEN-COACTIVATOR ON THE ELECTROLUMINESCENCE OF ZnS:Cu PHOSPHORS: PART I - GREEN EMISSION

P. M. Jaffe

Research Dept., Westinghouse Electric Corp.,
Bloomfield, N. J.

Rothschild[1] has shown that the use of Cl or Br as coactivator in photoluminescent ZnS:Cu phosphors has an effect on the spectral characteristics. More recently, Hegyi et al.[2] have investigated some of the effects of halide on the electroluminescence (EL) of ZnS:Cu. These latter workers find that I results in phosphors having only a blue emission while the emission from samples containing Cl and Br consists of blue and green bands of different relative intensity. The present investigation is concerned with the influence of halogen on the EL characteristics of ZnS:Cu. The effect of Cl and Br on the green emission will be considered in this paper.

Since the emission of Cl and Br coactivated ZnS:Cu can vary from blue to green, it was necessary for this work to prepare samples having similar spectral distributions, i.e., having the same ratio of blue to green centers. Samples were prepared with similar spectral distributions over the range of 60 to 4000 cps. Measurements were made in EL cells with castor oil as the dielectric; sinusoidal excitation was used. The following measurements have been made and the respective results obtained:

1. Brightness as a Function of Voltage. The brightness-voltage dependence was determined at 60,400 and 4000 cps. ZnS:Cu,Br was appreciably brighter than ZnS:Cu,Cl and has a slightly shallower slope. Both phosphors follow the relationship B exp $(V^{-\frac{1}{2}})$.

2. Brightness as a Function of Frequency. The brightness-frequency dependence was studied over the range of 60 to 10,000 cps and found to be similar up to 8000 cps. Above this frequency there was a deviation which is due to differences in the emission color.

3. Brightness Waveforms. The brightness waveforms of these phosphors consist of a primary and a secondary peak per half-cycle of the applied voltage. The primary brightness maximum occurs before the voltage maximum. The brightness maximum of ZnS:Cu,Cl at room temperature occurs a little earlier than that for ZnS:Cu,Br.

4. Glow Curves. Glow curves were obtained after 400 cps excita-

tion. Both phosphors show peaks at about - 135°C and +30 to 35°C. In addition ZnS:Cu,Br has a peak located around -20°C.

5. Maintenance. The maintenance (brightness as a function of operating time) was determined at 400 cps. The maintenance of ZnS:Cu,Br is slightly better than ZnS:Cu,Cl.

6. Temperature Dependences. The temperature dependence of the Cl and Br coactivated phosphor was measured at 60, 400 and 4000 cps. Differences in the structure and shape of the resultant curves were found and will be discussed.

7. Efficiency Measurements. Efficiency measurements were obtained at 50, 400 and 4000 cps. At 50 and at 4000 cps the maximum efficiency for both phosphor is about the same (1.5 l/w) while at 400 cps, ZnS:Cu,Cl is more efficient (3.1 vs. 2.2 l/w).

Conclusion. The substitution of Br for Cl as coactivator in ZnS:Cu phosphors results in a change in some of the El characteristics. These changes appear to be associated with the presence or absence of the electron trap at around -20°C. Whether these traps are directly associated with the presence of the Br (under the conditions of phosphor preparation reported on here) or are incidentally produced by the Br is not known.

References

1. S. Rothschild, Trans. Faraday Soc., 42, 629 (1946).

2. I. Hegyi, S. Larach and R. Shrader, J. Electrochem. Soc., 114, 717 (1957).

Abstract Number 75*

ELECTROLUMINESCENT TIME AVERAGE LIGHT OUTPUT OF A ZnS:Se PHOSPHOR

J. Mudar, S. Nudelman and K. Kamyszek
Willow Run Labs.,
University of Michigan
Ann Arbor, Michigan

The time average light output of an electroluminescent phosphor powder has been measured from 10 kcps to 18 mops. Fatigue increases with frequency so that at megacycle operation the output diminishes to 10-25% of initial values with a 30-min period. Mechanically shaking a phosphor-air EL cell after fatigue causes a partial restimulation of light output, with successive fatigue-shake cycles showing a decreasing effect. Electroluminescence and fatigue are temperature dependent.

*Enlarged Abstract not Available.

Abstract Number 76*

TEMPERATURE-INDUCED COLOR SHIFTS IN ELECTROLUMINESCENCE

L. W. Strock

Sylvania Lighting Products
60 Boston St., Salem, Mass.

The color of ZnS:Cu EL-phosphors is determined by the relative intensities of their separate blue and green band emission components for a given condition of excitation. The color of a finished phosphor may be varied over a wide range from blue to green by appropriate thermal treatment in air or other atmosphere. Regardless of Cu-content all phosphors reach their minimum blue/green color ratio at 260°C and, in general, are still green when heated to 400°C, but blue when heated to 150°C.

*Enlarged Abstract not Available.

Abstract Number 77

ON THE ROLE OF A STIMULATING ACTION OF EXCITING LIGHT IN THE LUMINESCENCE KINETICS OF THE CRYSTALLINE PHOSPHOR ZnS-Cu

L. A. Vinokurov, M. V. Fock

The P. N. Lebedev Physical Institute Academy of Sciences of the U.S.S.R. Moscow, U.S.S.R.

As is well known, stimulating action of the exciting light (SAEL) is due to the fact that the latter is absorbed by localized electrons and transfered to the conduction band.* The existence of this phenomenon had been proved long ago, but up to now only a small number of authors have taken it into account in their work. Meanwhile, the SAEL can be of a great importance, especially under strong excitation.

First of all, the SAEL slows down the increase of the stored light sum with growing excitation-intensity. At the limit the SAEL leads to constancy of the light sum at large intensities of excitation, although only a small portion of the traps are filled.

Further, if a crystalline phosphor has a system of electron traps with different depths, the SAEL leads to a sharp deviation of the electron distribution over traps from that characteristic of thermal equilibrium. During the period of afterglow when the exciting light is removed, the thermal distribution is gradually restored. This process has an essential influence on the luminescence decay.

Finally, the quantum yield of luminescence measured under large intensities of excitation appears to be lower than under small intensities on account of the fact that some portion of the quanta are absorbed by electrons in traps but not by luminescence centres[3].

We studied a powder and a single crystal of ZnS-Cu. The results obtained from those studies were similar.

A calculation shows that the stored light sum n depends on the excitation intensity E accorting to the formula

$$n = \sqrt{\frac{uE}{L + Q}} \tag{1}$$

where

$$L = \frac{\beta w_1 w_2}{\delta_1 w_2 + \delta_2 w_1} \quad \text{and} \quad Q = \frac{\beta_1 w}{\delta} \ . \tag{2}$$

*The exciting light may have also a quenching action.

The meaning of the symbols are clear from Fig. 1. Under the SAEL, probabilities of electron release from traps are equal to:

$$\left.\begin{aligned} w_1 &= w_{10} + D_1 E \\ w_2 &= w_{20} + D_2 E \end{aligned}\right\} \quad . \tag{3}$$

Hence it follows that at a small E the value $n \sim \sqrt{E}$, and at a large E the value n is constant. Fig. 2 shows the dependence $n = n(\sqrt{E})$ found experimentally for the powdered crystalline phosphor at different temperature. One can see that the deviation from porportionality takes place at comparatively small intensities of excitation. With increase of temperature this deflection becomes less sharp and takes place at large intensities of excitation. At the same time, the light sum is stored less at large intensities. This can be explained by the fact that with increase of temperature the probability of a thermal release of of electrons increases and, therefore, the probability of an optical release is to be compared with it at high intensities of excitation.

The electron distribution over the levels is given by the formulas:

$$\left.\begin{aligned} n_1 &= n\,\frac{\delta_1 w_2 + \delta_1 (L+Q)n}{\delta_1 w_2 + \delta_2 w_1 + (\delta_1 + \delta_2)Qn + \beta w_1 n} \\ n_2 &= n\,\frac{\delta_2 w_1 + \delta_2 (L+Q)n}{\delta_1 w_2 + \delta_2 w_1 + (\delta_1 + \delta_2)Qn + \beta w_2 n} \end{aligned}\right\} \quad . \tag{4}$$

Let $w_1 \gg w_2$, i.e., the level 2 is considerably deeper than level 1. Then it follows from formula (4) that in some intensity intervals the number of electrons stored on deep levels can decrease with increasing intensity of excitation.

As is well known, infrared light also releases electrons from traps, and this affects mainly the deep traps. Therefore in this case a flash must decrease under the action of infrared light. Fig. 3 shows the flash that takes place at the moment of applying infrared light under a constant excitation of the single crystal by light with different intensities. One can see that at small intensities of excitation the flash grows.

After removing the excitation, electrons pass from shallow traps to deep traps. This is displayed by the fact that the flash under application of infrared light during afterglow is the greater the longer the period of time that has passed between removing the exciting light and applying an infrared light. Only at the end of the decay does the flash start to decrease. One can see it clearly in Fig. 4.

Thus, due to a stimulating action of the exciting light the electron distribution over traps of different depths practically never is characteristic of thermal equilibrium, and therefore it must be taken into account when considerating both the stationary state and the decay of luminescence of crystalline phosphors.

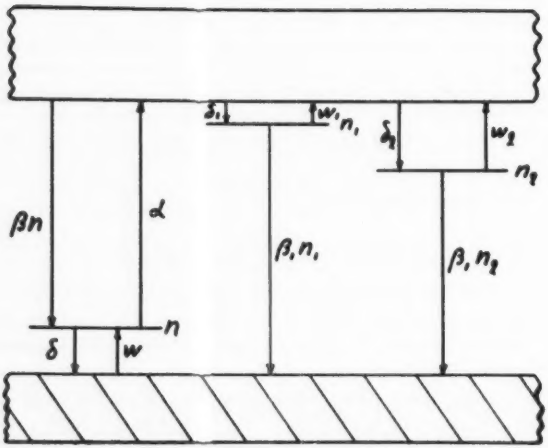

Fig. 1—A scheme of electron transitions in the crystalline phosphor with traps of different depths. The letters designate probabilities of the corresponding transitions.

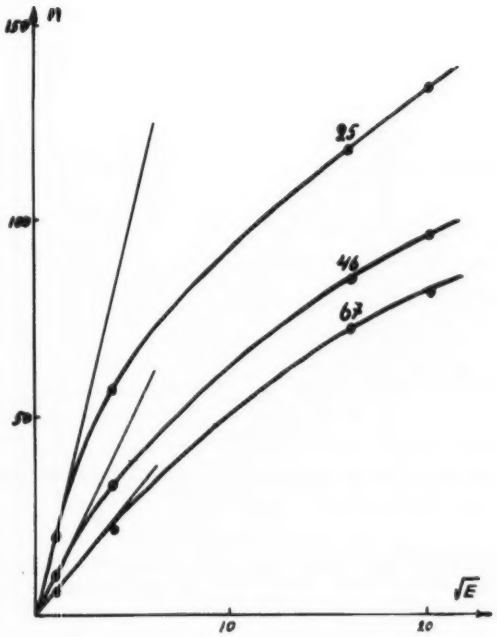

Fig. 2—Dependence of the stored light sum on a square root of the excitation intensity. Numerals designate temperature of the experiment (C°).

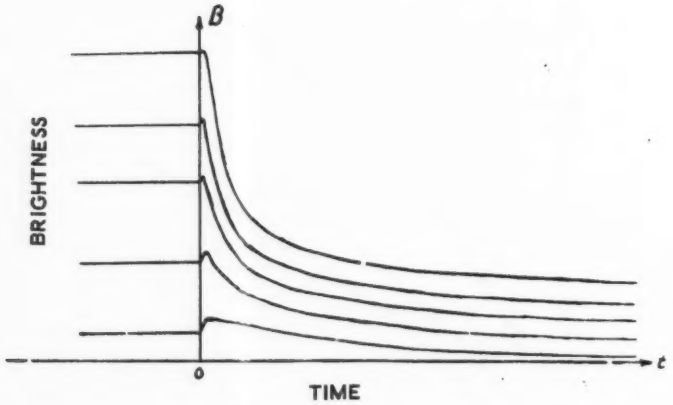

Fig. 3—Flashing and quenching actions of an infrared light under various intensities of excitation. A vertical line designates the moment of applying an infrared light.

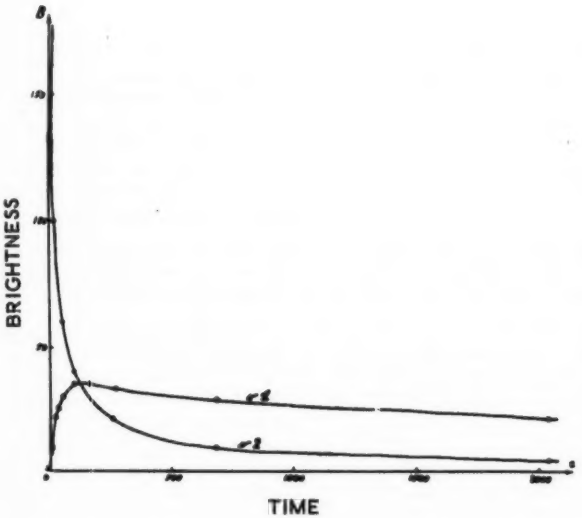

Fig. 4—Dependence of the value of the flash on the time of decay (curve 1) and a brightness of afterglow (curve 2) of the single crystal ZnS-Cu.

References

1. V. V. Antonov-Romanovskii, Izv. Acad. Nauk (USSR), (ser. fiz.), 13, 91 (1949).

2. V. V. Antonov-Romanovskii, Izv. Acad. Nauk (USSR), (ser. fiz), 15, 637 (1951).

3. L. I. Anikina, Dokl. Akad. Nauk (USSR), 88, 41 (1953).

Abstract Number 77A

ON THE VALENCY STATES OF MANGANESE IN PHOSPHOR SYSTEMS

V. V. Ossiko

The P. N. Lebedev Physical Institute
Academy of Sciences of the U.S.S.R.
Moscow, U.S.S.R.

F. A. Kröger[1] and some others assume that manganese can have different valency states in phosphors. In the phosphors with non-structural "bell-shape" spectra, manganese is bivalent. But in the case of phosphors with spectra in the red region and having a fine structure, manganese is tetravalent. Kröger[2] gives an experimental proof of the activating action of the tetravalent manganese. Williams proposed a theoretical explanation of the differences in the luminescence spectra of bivalent and tetravalent manganese.

The author determined contents of oxidized and total manganese in a large group of phosphors by means of chemical analysis.* The values of the average valency of manganese are $Bav = 2 + 54.93 \frac{g}{a}$. Here Bav = average valency of manganese in the system, g = the number of gram-equivalents of oxidized manganese per gram of the sample, a = total manganese (g/g). The values of Bav were compared with luminescence spectra of the corresponding phosphors. The phosphors under investigation are divided into three groups differing from each other in the correlation between the luminescent properties and the valency of manganese. The phosphors of group I do not contain oxidized manganese under usual conditions of preparation; all manganese is bivalent. Group II: Under usual conditions of preparation $Bav > 2$, but the luminescence spectra do not depend on Bav. After heating in a reducing atmosphere the luminescence spectra do not change even in the case when Bav becomes equal to two. Group III: $Bav > 2$ (but it does not reach four in any case). The luminescence spectra depend on the valency state of manganese: after heating in a reducing atmosphere and under sufficiently high temperature the luminescence either vanishes completely or changes its spectrum as the manganese is reduced to a bivalent state. (See tables)

When the data are compared it becomes clear that:

1. In all phosphors with green and yellow luminescence Bav = 2.

*Determination of the oxidized manganese contents was carried out by the method similar to that described by Kröger.

2. Among phosphors with orange-red and red luminescence there are phosphors with both Bav = 2 and Bav > 2.

3. There is no simple connection of Bav with crystallochemical characteristics of the phosphors: i.e. ionic radii, structure etc. Thus, for example, group III phosphors consist only of magnesium and lithium compounds, i.e. the compounds having cations with small radii. However the opposite supposition is not true: there are representatives of all three groups among magnesium phosphors.

In the work of Kröger[1] a thermodynamical consideration is given of equilibrium of Mn^{2+}, Mn^{3+}, and Mn^{4+} ions in a homogenious phase. Employing the formula obtained by an approximated integration of the Vant-Hoff equation

$$\ln \frac{C_{Mn^{3+}} \cdot Co_2^{\frac{1}{2}}}{C_{Mn^{2+}} \cdot Co_2^{\frac{1}{4}}} = \frac{\phi_1}{RT} + \text{const.}_1 \; ; \; \ln \frac{C_{Mn^{4+}} \cdot Co_2}{C_{Mn^{2+}} \cdot Co_2^{\frac{1}{2}}} = \frac{\phi_2}{RT} + \text{const.}_2$$

Kröger arrives at the conclusion that the valency of manganese in the phosphor (when equilibrium is reached) depends on T, oxygen pressure, and nature of the matrix (taken into account by the magnitude of thermal effect). It should be pointed out that in considering real solid solutions one must use the values of activities a (a = f·c) and not values of concentration c. This in turn should lead to dependence of concentration of the oxidized manganese not only on the above factors, but on the total concentration of manganese.

In order to elucidate the correlation of the manganese valency in the system with temperature, atmosphere of heating, and manganese concentration we studied the system ZnO-MnO-O_2 that by its physical-chemical characteristics can serve as a model of the other phosphors. Selection of that system can be explained by the relative ease by which it may be investigated with chemical and physical-chemical methods of analysis. Mixtures of zinc oxide and manganese dioxide with different molar ratios were heated at various temperatures in a stream of oxygen or nitrogen. The samples were analysed, as in the first part of this work. Fig. 1 shows curves of dependence of Bav. on composition of the samples for different temperatures and atmospheres of heating. Bav. depends on the relative content of manganese when other conditions are similar. The figure also shows that Bav = 2 up to a certain concentration of manganese, irrespective of the atmosphere of heating. It means that in this case the valency of manganese is determined solely by the crystallochemical structure of the matrix. Hence one can see that in the same phosphor under the same conditions of preparation, an average valency of manganese may be different depending on its concentration.

It should be also taken into account that change of the manganese valence state is accompanied, as a rule, by variation of a phase composition of the phosphor. By heating in oxygen, solid solutions of (Zn, Mn)O with high contents of manganese become two phase systems, together with the phase of (Zn,Mn)O (with smaller manganese content, there appears another oxide phase under a microscope.

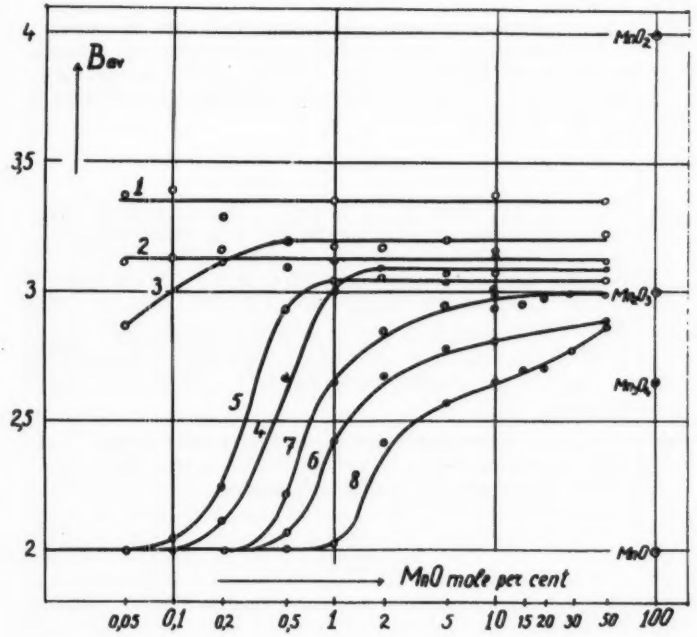

Fig. 1—Dependence of the average valency of manganese on its contents, temperature, and atmosphere of heating in the ZnO-MnO-O_2 system. Duration of heating is the same in all cases (30 min.)

1. 600°, O_2
2. 600°, N_2
3. 800°, O_2
4. 800°, N_2
5. 1000°, O_2
6. 1000°, N_2
7. 1200°, O_2
8. 1200°, N_2

Thus, the presence of oxidized manganese in a phosphor system does not permit one to draw the conclusion that luminescence is due just to oxidized manganese: it may be situated in the system as a separate phase and not take part in constructing the luminescence centres.

The connection between the manganese valency and the luminescence spectra is beyond doubt; however this connection has a complex character. Thus the red luminescence may be observed in the phosphors containing both a bivalent manganese and oxidized manganese; a structure in the spectra is observed not only with tetra-valent manganese, but, in some cases, with bivalent manganese, although this structure is different in the both cases.

TABLE I

Group I: $B_{av} = 2$, fluoresces in green, yellow, orange or red. (Mg; Mg, Be, Zn)F_2; (Mg; Mg, Ca; Mg, Sr; Mg, Zn)$_2$ PO_4F; (Mg; Sr)$_2$ P_2O_7; $MgO \cdot 2Li_2O \cdot WO_3$; $Zn_3(PO_4)_2$; Zn_2SiO_4; Zn_2GeO_4; (Zn, Sn; Zn, Cd, Sn; Zn, Ba) silicate; (ZnO; 3ZnO) B_2O_3; (Cd; Cd, NaF) phosphate; $CdSO_4$; $3CdO \cdot 3Li_2O \cdot 3SiO_2$; $5.5CdO \cdot 0.5Li_2O \cdot 3SiO_2$

Group II: $B_{av} > 2$ when fired in air; $B_{av} = 2$ when fired in NH_3. Fluoresces orange red and red. (2MgO; MgO; CaO; 0.25ZnO) SiO_2; (2/3 CdO; 1.5CdO, 4.5Li_2O) $3SiO_2$; Ba, Sr, Li silicate + Ce; $Mg_3(PO_4)_2$; SiO_2

Group III: $B_{av} > 2$ when fired in air; $B_{av} = 2$ when fired in NH_3. Fluoresces in narrow bands in red when fired in air. $MgO \cdot Li$; Mg_2TiO_4; $4MgO \cdot GeO_2$; Mg arsenate; Li_2TiO_3.

References

1. Kröger, F. A. Some Aspects of the Luminescence of Solids. Amsterdam, 1948.

2. Kröger, F. A. Luminescence of Solids Containing Manganese. Amsterdam, 1940.

Abstract Number 77B

PHYSICAL PROCESSES IN ALKALI HALIDE PHOSPHORS ACTIVATED BY MERCURY-LIKE IONS

Ch. B. Lushchik, I. W. Jaek, G. G. Liidja,
N. E. Lushchik and K. K. Schwarz

Physics and Astronomy Institute,
Academy of Sciences of the Estonian S.S.R.
Tartu, U.S.S.R.

In 1955-57 N. Lushchik synthesized indium-, gallium- and germanium- activated alkali halide phosphors. This made it possible to carry out a fairly complete investigation of NaCl, KCl, KBr, KI phosphors activated by the "mercury-like ions" Ga^{+}, Ge^{++}, In^{+}, Sn^{++}, Tl^{+}, Pb^{++}.

The present work contains a summary of some of the results of our investigation of diffusion precipitation, electronic-vibrational, electron-hole and exciton processes in these phosphors.

Diffusion and Precipitation

Phosphors were grown from melts in evacuated quartz tubes, and also synthesized by heating the alkali halide single crystals in the activator vapour at temperatures approaching their melting point. The diffusion of the mercury-like ions was investigated by measuring the activator absorption at various distances from the crystal surface. The ions Ga^{+}, In^{+}, Tl^{+} diffuse (possibly by means of vacancy mechanism) at rates close to the rate of self-diffusion. Diffusion coefficients of the ions Pb^{++} and Sn^{++} are several times greater than the self-diffusion coefficient. The mercury-like ions in alkali halide phosphors substitute for cations of the host crystal. For large activator concentrations and great numbers of host crystal imperfections, the activator ions are located in the lattice partly at normal substitutional sites and partly near the different lattice defects. This accounts for the different kinds of luminescence centers in mono-activated phosphors. Non-isomorphous impurities interact especially strongly with the point and line defects of the crystal. Ultramicroscopic investigation showed that in annealed unstable solid solutions (e.g. NaCl-Pb) activator ions are precipitated at dislocations. Activator Cottrell atmosphere near dislocations play an essential role in sensitized luminescence.

Electronic-Vibrational Processes in Luminescence Centers

Comparison of absorption, emission and excitation spectra of alkali halide phosphors and the spectral characteristics of free activator ions

has shown that the mercury-like ions Ga^+, Ge^{++}, In^+, Sn^{++}, Tl^+, Pb^{++} are the "kernels" of the luminescent centers. The mercury-like ions and the nearest ions of the host crystal form the quasimolecular luminescence centers. The principal activator absorption bands correspond to the electronic transitions $^1S_0 \rightarrow {}^3P_{0,1,2}$ and $^1S_0 \rightarrow {}^1P_1$ in the mercury-like ions. The emission bands correspond to the transitions $^3P_{0,1} \rightarrow {}^1S_0$.

The quantum efficiency of the luminescence of centers excited to a ^3P - state in the absence of thermal quenching is 0.8-0.9. The probability of radiationless transitions is well described by the following formula: $d = d_0 \exp(-Q/kT)$. The comparison of the optical and thermal (Q) characteristics of emission centers leads to the conclusion that a potential barrier overcome by radiationless transitions, conforms to Mott's model. We have not experimentally found any "tunnel radiationless transitions" (Kubo, Krivoglaz).

Within the bands of activator absorption the emission spectra and quantum efficiency of luminescence do not depend on the frequency of the exciting light (including the anti-Stokes' region). No optical quenching inside luminescence centers was detected (mechanism of Dexter-Klick).

There is rapid "thermostatization" of luminescence centers by the surrounding matrix material, so that the radiationless and optical transitions occur after the equilibrium distribution of centers with respect to vibrational energy is reached. Due to this fact the absorption and emission spectra are connected with each other in a relatively simple manner.

A detailed experimental examination leads to the conclusion that the simplified (one-oscillator, harmonical) quasimolecular model describes the luminescence centers only approximately. Some effects (e.g. the splitting of $^1P_1$ levels into three components) are connected with the interaction of mercury-like ions with non-radially symmetric local vibrations (the Jahn-Teller effect). In the centers with great Stokes' shifts anharmonic vibrations are important.

The Electron-Hole and Exciton Processes

Excitation spectra of KI, RbI and CsI phosphors show that the emission of the ions Ga^+, In^+, Tl^+ is excited not only in the activator absorption bands, but also in the exciton bands ($\lambda_m \approx 220$ mμ) and in bands corresponding to the optical "band to band" transitions ($\lambda_m \approx 185$ mμ).

The transfer of energy to the centers by means of an exciton mechanism (the excitation of the centers is probably due to "exciton impact") has a lower efficiency than the transfer of energy by means of an electron-hole mechanism. The latter is the principal mechanism when the phosphors are excited by short wavelength radiation.

Investigation of the changes of the absorption and excitation spectra after irradiation a in the exciton absorption bands shows that the excitons

interact not only with the ions Ga^+, In^+, Tl^+, but also with the host crystal defects, giving rise to electronic (F,M,R,F', etc.) and hole (V_2, V_1 etc) color centers. As a result of the dissociation of excitons on the bivalent mercury-like ions, the absorption of these ions decreases and activator color centers and V-centers are created.

Measurements of the "colour center production spectra" lead us to the conclusion that the F-centers and activator color centers are created by the excitation of phosphors in the absorption bands of the monovalent (not bivalent!) mercury-like ions, exciton and fundamental absorption bands.

After x-ray irradiation alkali halide phosphors activated by the ions Ga^+, In^+, Tl^+, exhibit a bright and prolonged phosphorescence and optical flash. Measurements of photostimulation and emission spectra show that emission of mercury-like ions (the transitions $^3P \rightarrow {}^1S_0$) arises after electrons have been released from F-, M-, N-, O- color centers of the host crystal. This is recombination luminescence.

Thermal bleaching of F-bands is a multistage process. Some stages of thermal bleaching are accompanied by the emission of the ions Ga^+, In^+, Tl^+. The efficiency of thermoluminescence is usually constant for the elementary stage of bleaching but it varies for different stages, and is considerably smaller for hole processes than for electron processes. The excitation spectra of the recombination luminescence have a stepped character. Within elementary bands of activator absorption the quantum efficiency does not depend on the frequency of the exciting light. The quantum efficiencies for different absorption bands differ considerably.

After the optical excitation of the luminescence centers there occurs the thermal ionization of centers (or some other process) and this leads to the recombination luminescence and the formation of electronic color centers.

Recombination luminescence is especially intensive after excitation of the phosphors by ultra-violet radiation in the region of the fundamental absorption bands, In the case of optical band to band transitions the quantum efficiency of recombination luminescence is tens of time greater than in the case of the excitation of phosphors within activator absorption bands. The sharp growth of effi iency that accompanies an increase in exciting frequency corresponds to the long wave edge of optical band to band transitions.

Details of the above results may be found in:

1. Transactions of the Physics and Astronomy Institute of the Academy of Sciences of the Estonian SSR, 1, 57 (1955); 3, 3, (1955); 4, 53, (1956); 6, 5, 63, 149, (1957); 7, 119, 134, 153, 193, 311, 340, (1958); 8, 3, 75, (1958); 10, 68, 122, 135, 166, 196, (1959); 11, 3, (1960).
2. "Proceedings of the 8th Conference on Luminescence" (Moscow, July, 1958), published in Tartu, 1959, pp. 27, 40, 101, 117, 153, 171.

Abstract Number 78

AN APPARATUS FOR THE PREPARATION OF SEMICONDUCTOR GRADE SILICON

Ray C. Ellis Jr.

Research Division, Raytheon Company
Waltham, Massachusetts

A film boiling technique has been used to thermally decompose silicon tetraiodide to produce semiconductor grade silicon. The apparatus consists of a reactor in which a graphite teardrop about 1 1/4" in diameter is submerged in silicon tetraiodide. The graphite is heated by induction to about 1800°C. There silicon is produced at a rate of about 120 g/hr. The molten silicon builds up on the graphite and then is continuously discharged by floatation from the reaction zone. The droplets of silicon burst forth from the surface of the molten silicon tetraiodide in a brilliant display and then solidify to polycrystalline pellets 1/8" to 3/8" in diameter. The average resistivity was found to be 5 - 10 Ω cm, p-type, from test crystals from each lot. Because carbon is soluble in molten silicon, the product was found to contain about 0.1% yellow, cubic silicon carbide which does not affect the resistivity, but does interfere with the growth of single crystals.

The iodine by-product is recycled. It is reacted with crude silicon to produce crude silicon tetraiodide which is subsequently purified by distillation.

TWIN GENERATION AND SEEDING MECHANISM IN DENDRITIC GROWTH

J. W. Faust, Jr. and H. F. John*

Westinghouse Research Laboratories
Pittsburgh, Pa.

Introduction

Billig,[1] Billig and Holmes,[2] and Bennett and Longini[3] have described the growth of dendritic germanium. These dendrites[4] have a lamellar twin structure parallel to the two flat $\{111\}$ faces. A procedure which is frequently used for producing a ribbon involves dipping a dendritic seed into an undercooled melt, allowing a small button to form on the end of the seed, and then withdrawing the seed and button under carefully controlled conditions.[3] New dendritic growth is seeded at some point where the twin structure intersects the surface of the button.

Bennett and Longini[3] have found that there are three preferred $<211>$ growth directions lying in the (111) plane, namely, the $[2\bar{1}\bar{1}]$, $[\bar{1}2\bar{1}]$ and $[\bar{1}\bar{1}2]$, as shown in Figure 1. They have shown experimentally that the presence of an odd number of twins gives a dendrite a "favorable" and "unfavorable" direction for propagation. If a dendrite seed is dipped vertically into the melt in the "favorable" direction, a preferred $<211>$ growth direction will point downward into melt, parallel to the axis of the seed, in the regions on both sides of the central lamellae. A ribbon can thus be pulled vertically from the melt. If the seed is rotated 180° into the "unfavorable" direction, two preferred $<211>$ growth directions point into the melt at 60° to the vertical. The growth of the ribbon will then proceed in a direction 60° to the axis of the seed. For an even number of twin planes, the region on one side of the central twin structure will be oriented in a "favorable" direction and the region on the other side will be oriented in an "unfavorable" direction. Whether the ribbon is propagated vertically or at 60° to the vertical in such a case appears to be a matter of chance.

In this communication the steps involved in the genesis and early stages of growth of a dendrite are examined.

Genesis of Primitive Dendrites

Primitive dendrites can be produced by dipping a randomly-oriented seed crystal without twins into a supercooled melt. Such random,

*This research was supported in part by the United States Air Force through Wright Air Development Center.

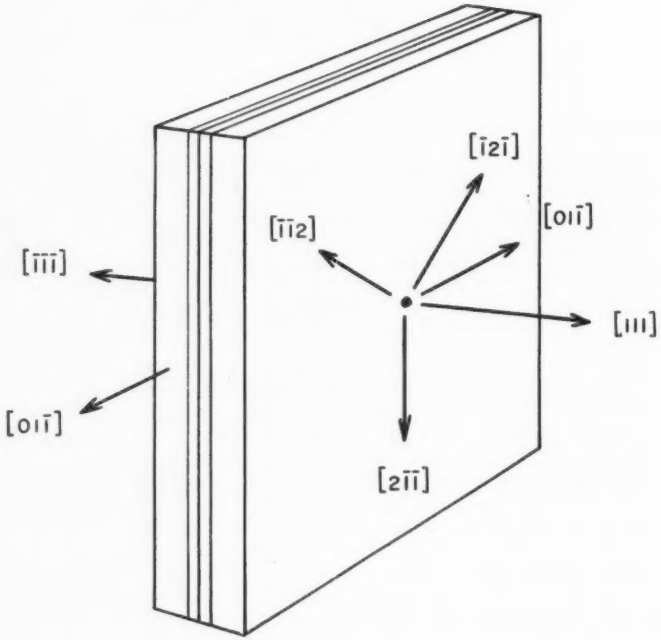

Fig. 1—Orientation relationships in a diamond-lattice dendrite with three twin planes.

primitive dendrites arise from favorably-situated twin lamellae which are generated at the rapidly advancing growth front, for example, by impurity segregation, thermal stresses, etc. Since the lamellae produced at the advancing front are generally surrounded by material of the same orientation as the parent growth mass, such lamellae must, of necessity, have an even number of twins. Only in cases where one twin of an even grouping is lost at a surface, by intersection with a grain boundary, or with a non-coplanar twin boundary, can a grouping with an odd number of twin planes be formed. Because of the growth situation produced by the presence of two or more closely-spaced twin planes, twin lamellae groupings which are suitably spaced and situated will grow out rapidly from the main growth mass. The propagation mechanism for dendrites is discussed by Seidensticker and Hamilton[5] in a later paper. These dendritic projections can be used as seed crystals for growing more dendritic material. Because of the relative infrequency of the loss of a twin from an even grouping, most primitive dendrites have an even number of twins.

Twin spacings in a considerable number of primitive dendrites have been examined by etching and fracturing techniques.[6] A large number of different spacings have been observed, with the peak of the distribution being around 5 microns between adjacent twin planes. The twin spacing present in a dendritic crystal will persist throughout all subsequent growth seeded from it.

Growth Button Studies

Considerable insight into the role of the twin plane in propagating dendritic growth can be obtained by examining the growth buttons formed when various seed crystals are dipped into a supercooled melt. In the case of a single crystal seed oriented in any $<211>$ direction, the equilibrium form is a faceted button with seven of the eight possible $\{111\}$ planes being present, as shown in Figure 2A.

When a $<211>$ seed crystal containing a single twin plane parallel to the axis of the seed is used, the shape of the button will depend on whether the seed is in the "favorable" or "unfavorable" growth direction, as discussed in the introduction. When the seed is in a "favorable" direction, a button forms which has the configuration shown in Figure 2B. When the seed is in the "unfavorable" direction, two preferred $<211>$ directions point into the melt at 60° to the axis of the seed. The resulting growth button is shown in Figure 2C.

It will be noted that the buttons formed are crystallographically bounded by $\{111\}$ planes. The buttons with single twins have a 219° ridge structure where the twin plane intersects the surface. Growth buttons containing three (or a higher odd number) twin planes will be macroscopically similar to a single twin growth button, with the very important difference that the intersection of the three twin planes with the surface provides a jogged region with alternate 219° ridges and 141° grooves separating the outer faceted portions of the buttons. The significance of this feature will be discussed in a subsequent paper by

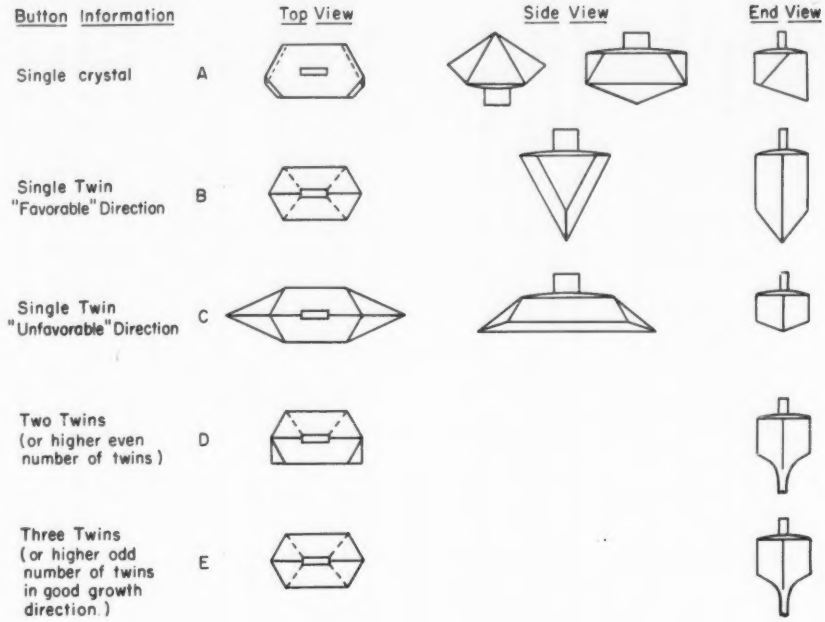

Fig. 2—Drawings of growth buttons.

Seidensticker and Hamilton,[5] who have developed a formal model for dendritic propagation which requires the presence of such a re-entrant structure. The button formed by a seed crystal containing two twin planes is shown in Figure 2D. It is obtained, in effect, by combining half an "unfavorable-direction," single-twin button with half a "favorable-direction" single-twin button. Any button with a higher even number of twins will have this same general morphology.

Seeding Studies

The structure of the button which forms on a dendrite seed is determined by the twin structure at the edges of the seed. For example, if a three-twin structure has degenerated to give a single-twin structure at the edge of the seed, as shown in Figure 3II, the button will be of the single twin form (Figure 2B or C). If a two-twin structure has degenerated to form an enclosed lamella, as shown in Figure 3IV, the growth button will be characteristic of that grown from a single crystal seed (Figure 2A), rather than a two-twin seed (Figure 2D). If the three-twin structure has degenerated to a single twin on one edge only (Figure 3III), then the growth button will be of the single-twin form on that side of the button, and a dendrite will grow only from the other side of the growth button.

It is possible, after a dendrite has been seeded and has started to grow, that the conditions will become such that the twin lamallae degenerate at the edges giving cross section II in Figure 3. The dendrite will continue to grow with this cross section because the growing tip is much narrower than the dendrite, as will be explained in Abstract #81. All that is necessary to ensure propagation is for the twin lamallae to be continuous across the growing tip.

When the buttons grown on seeds with cross sections II and IV, shown in Figure 3, are withdrawn from the melt, no dendrites are formed for reasons previously given; the buttons emerge with the shapes given in Figure 2. Buttons from cross section I or III, however, under the conditions most frequently used for seeding, grow long, projecting arms at the surface of the melt. These arms contain the twin structure which has been propagated from the seed through the growth button, and thus grow very rapidly under the correct conditions of supercooling. They are in reality [110] dendrites. Upon pulling, the thermal conditions change, causing the underside of the arms to narrow faster than they become thinner. It is such an area on one or both arms that is the starting point of [211] dendritic growth. A thermal steady state is quickly reached and the dendrite takes on its normal growth, being propagated longitudinally by mechanisms discussed in Abstract #80 and laterally by mechanisms discussed in Abstract #81.

Fig. 2—Drawings of growth buttons.

References

1. E. Billig, Proc. Roy. Soc. A229, 346 (1955). Acta Met. 5, 54 (1957).
2. E. Billig and P. J. Holmes, Acta Cryst. 8, 353 (1955). Acta Met. 5, 53 (1957).

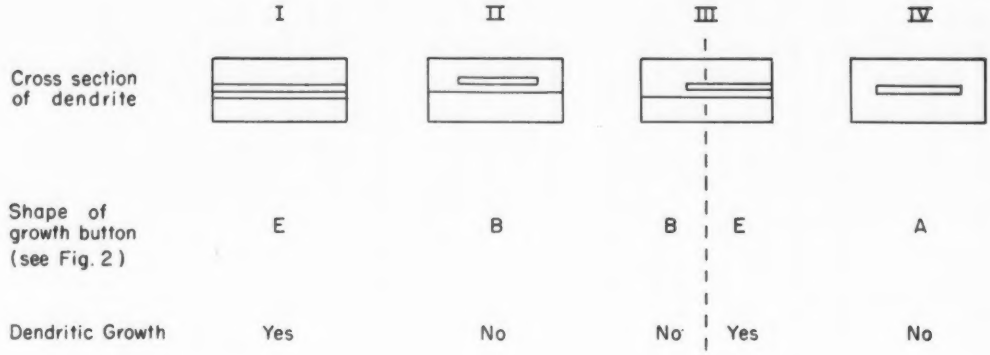

Fig. 3—Summary of twin lamellae continuity on growth button shape and dendrite growth. (Seed in the "favorable" direction.)

3. A. I. Bennett and R. L. Longini, Phys. Rev. 116, 53 (1959).

4. The reasons for referring to these ribbons as "dendrites" without further qualification will become apparent from Abstract #81.

5. R. G. Seidensticker and D. R. Hamilton, Abstract #80, manuscript submitted to J. Appl. Phys.

6. J. W. Faust, Jr. and H. F. John, "A Comparison of Etching and Fracturing Techniques for Studying Twin Structures in Ge, Si, and III-V Intermetallic compounds," submitted to the Journal of the Electrochemical Society.

Abstract Number 80

THE PROPAGATION OF GERMANIUM DENDRITES

R. G. Seidensticker and D. R. Hamilton*

Westinghouse Research Laboratories
Pittsburgh, Pa.

Billig,[1] and Bennett and Longini[2] have described the growth of relatively long dendritic crystals of germanium from undercooled melts. The lath-like crystals are bounded by two parallel $\{111\}$ side faces, and may possess sawtooth edges with faces that are usually curved but which sometimes approximate a $\{111\}$ habit. Other unusual features of these crystals are the apparently indefinite propagation of the structure in coplanar $<211>$ directions, and the invariable presence of a twinned structure.[2,3] These workers have attempted to describe the propagation mechanism on the basis of growth at a pair of screw dislocations or by consideration of the properties, on an atomic scale, of a single twin plane. Neither the screw dislocations required by the former, nor the dendrite with a single twin predicted by the latter have been observed. In the present work, we examine the behavior of crystals with a twinned structure from the viewpoint of corner nucleation. The essential argument involves the relative ease of nucleation in a re-entrant corner as opposed to nucleation on completed low index faces. It will be shown that two twin planes are a prerequisite for rapid, dendritic propagation of germanium crystals.

Figure 1 shows, in faint lines, a crystal of germanium containing a single twin plane and bounded by $\{111\}$ faces. It can be seen that the twin plane emerges from the solid in alternating ridges and re-entrant corners. The external angle between the adjacent faces in these two cases is 141° and 219° respectively. If the solid is placed in liquid germanium so supercooled that nucleation is allowed to take place only in the re-entrant corners, then the crystal has, initially at least, three directions in which growth is possible. These are $[2\bar{1}\bar{1}]$ $[\bar{1}\bar{1}2]$ $[\bar{1}2\bar{1}]$. As growth in the three re-entrant corners continues, the corners tend to "grow out." The reason for this is tht a given growth layer starting in the 141° re-entrant corner cannot extend beyond the $\{111\}$ planes that bound the adjacent ridge structures. If such growth were to take place, it would constitute nucleation on these planes contrary to the initial assumption. Thus the crystal with one twin has only transient initial growth. Once this growth is complete, the resulting solid is bounded

*This research was supported in part by the United States Air Force through Wright Air Development Center.

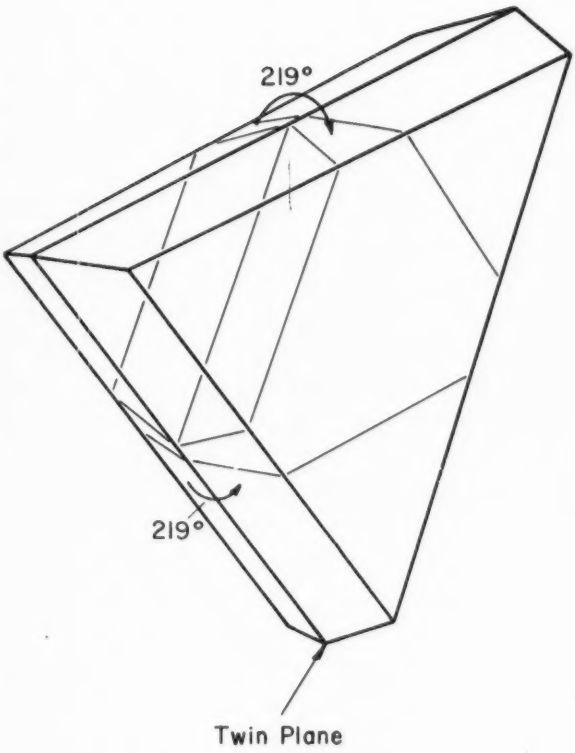

Figure 1

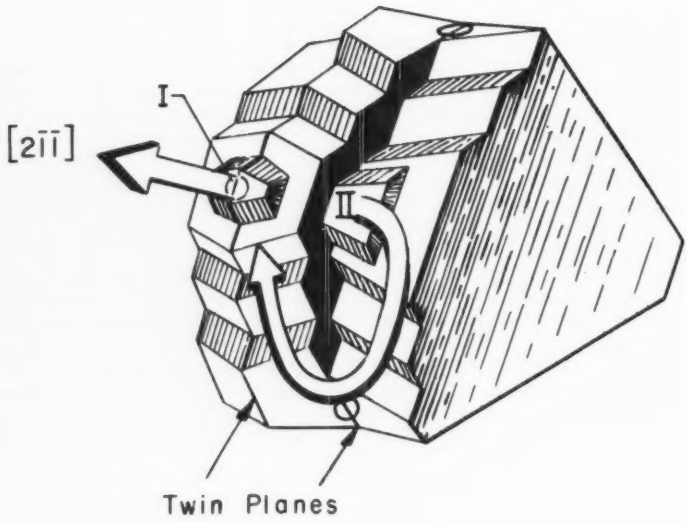

Figure 2

by the ridges and the side planes—regions where it has been assumed that nucleation will be difficult, Fig. 1 heavy lines.

If a second twin is added to the solid, a new situation occurs. A growth layer, starting at a re-entrant corner at the first twin plane, grows up to the second twin plane and there creates a new type of re-entrancy, one with an angle of 109-1/2°. The ridge structure that was previously present has been replaced by a corner which is favorable to nucleation. As a consequence, the requirement of nucleation about the adjacent ridge at the second twin plane has been removed. Thus the crystal with two twin planes possesses the important property that it cannot be entirely bounded by slow growing ridges. The crystal with two twin planes is capable of indefinite propagation in the <211> directions by corner nucleation. All six coplanar <211> directions are now equivalent because of the presence of thw two-fold symmetry axes which operate on the three original growth directions of the bicrystal.

Figure 2 is an attempt to show in a more realistic manner the actual nature of the growth at the very tip of the dendrite. Many steps are shown growing at once. Growth from one re-entrant corner supports nucleation in another, giving rise to an interesting sort of "spiral" flow of growth steps. The spiral does not arise from any single screw dislocation, or even from a single network of screws, but rather from the unusual geometry of the interface.

H. F. John and J. W. Faust, Jr., as reported in abstract 79 page 145, have observed that at least two twin planes have been present in all samples examined. Billig[3] also mentions this fact. Furthermore, germanium dendrites with two twin planes exhibit six-fold growth symmetry. Thus, the mechanism discussed above is in agreement with present experimental information. The presence of two twin planes in the germanium lattice is necessary to ensure indefinite easy propagation through corner nucleation.

References

1. Billig, E. Proc. Roy. Soc. A229, 346, 1955.
2. Bennett, A. I. and Longini, R. L., Phys. Rev. 116, 53, 1959.
3. Billig, E. and Holmes, P. J., Acta Met. 5, 53 (1957).

Abstract Number 81

SOME ASPECTS OF LATERAL GROWTH IN DENDRITES

H. F. John and J. W. Faust, Jr.*

Westinghouse Research Laboratories
Pittsburgh, Pa.

Growth processes in dendrites of diamond-lattice materials have been studied by means of metallographic techniques. Under certain conditions resistivity variations and structural differences give small variations in etching rate. By studying etched cross-sections and (111) faces of germanium dendrites, it has been possible to deduce, in a fairly straightforward way, the progress of growth during the formation of a dendritic ribbon. These studies have revealed that the formation of such ribbons is a more complex process than had been suspected by earlier investigators.[1,2,3] Some of the steps involved in the widening of a diamond-lattice dendrite bear a close resemblance to dendritic growth processes in metals, thus giving adequate justification for using the term, dendrite, when referring to ribbons of germanium as described by Billig[1] and Bennett and Longini.[3]

The processes involved in the formation of a dendrite will be discussed in relation to a series of photomicrographs. A summary is given below which groups the growth processes into four steps. However, it should be realized that these steps blend one into the other and the processes involved will be occurring simultaneously.

Step 1: Formation of the Core.

A region containing the twin planes is propagated rapidly ahead of other growth, by mechanisms described elsewhere.[4] When viewed in cross-section a short distance behind the advancing front, this central region has assumed a cruciform structure, with a well-defined growth region perpendicular to the twin planes. In the early stages, the extension of growth perpendicular to the twin planes may be greater than the extension of growth parallel to them. The core region may very soon reach an appreciable fraction of the final thickness of the dendrite while, at the same time, achieving only a small fraction of its final width.

Step 2: Formation of the I-Beam or Double I-Beam Structure.

When the growth perpendicular to the twin structure has reached an appreciable thickness, well-defined growth facets form along the outer

*This research was supported in part by the United States Air Force through Wright Air Development Center.

edges of the branches of the cruciform structure which are perpendicular to the twin structure. Lateral growth proceeds rapidly outward from these facets parallel to, but independent of, the central twin structure to form two arms on both sides of the central core. When viewed in cross-section, this structure has roughly an I-beam type of configuration. Under some circumstances the central region containing the twins may grow outward faster than the outside arms, to give a double I-beam configuration.

Step 3: Freezing Between the Arms.

During the extension of the dendrite to its final width, the outward growth of the central region containing the twins may, under certain circumstances, lag considerably behind the growth of the outside arms. In such a case, a very elongated I-beam structure is formed. The material between the arms solidifies by freezing inward from the arms. This particular feature is responsible for the degenerate twin structures frequently found when examining the cross-sections of dendrites. In cases when the central twinned region grew outward as fast or faster than the top arms, a region between each of the outside arms and the central region will be the last to freeze.

Step 4: Addition of Surface Layers.

The dendrite assumes its final form by the addition of thin growth layers onto the structure described above. These growth layers give the dendrite its characteristic flat faces. The growth of surface layers may proceed in several ways, one of which is described in a subsequent paper.[5]

Dislocations in dendritic ribbons usually occur in one or more of several general types of distributions. One of the most frequently encountered distributions is a stripe of dislocations down the center of one (or usually both) faces of the dendrite. The density of dislocations in this stripe will vary, ranging from essentially zero under ideal growth conditions to greater than 10^6 per cm^2. This central stripe consists of closely-spaced, highly-dislocated areas, from which arms of dislocations usually radiate. These arms consist of shallow dislocation loops. The highly-dislocated regions may extend to, but not across, the twin lamellae. Dislocations may also be present near one or both edges of one or both faces of the dendrite. The dislocations at the edges do not radiate from localized highly-dislocated centers, but have a more uniform distribution. Dislocations pockets, not visible on the outside, may be found near the central twin structure close to one or both edges of dendrite and running parallel to the flat (111) faces. It is shown that these dislocation distributions arise mostly from the stresses produced by the freezing of small liquid pockets trapped within the body of the dendrite. In the case of the central stripe, the opportunity for liquid entrapment arises from the way in which the corner growth progresses from the facets at the outer edges of the core (Step 2, above).

References

1. Billig, E., Proc. Roy. Soc. A229, 346 (1955). Acts. Met. 5, 54 (1957).
2. Billig, E., and Holmes, P. J., Acta Cryst. 8, 353 (1955). Acta Met. 5, 53 (1957).
3. Bennett, A. I. and Longini, R. L. Phys. Rev. 116, 53 (1959).
4. Seidensticker, R. and Hamilton, D., "The Propagation of Germanium Dendrites" Abstract No. 80, manuscript submitted to J. Appl. Phys.
5. Bennett, A. I., Longini, R. L., and Smith, W. J., "Growth of Atomically Flat Surfaces on Germanium Dendrites," Abstract No. 83.

Article Number 82

DENDRITIC GROWTH STUDIES BY PULSE PLATING TECHNIQUES

R. C. Smith*

Westinghouse Research Laboratories
Pittsburgh, Pa.

The technique of pulse electroplating, which is used to reveal resistivity differences in semiconductors,[1,2] has been applied to germanium dendrites. When a sample is plated using this technique, it is immersed in a plating cell containing a metallic salt solution, such as copper sulfate, and pulses of current are applied by charging a capacitor and discharging it across the cell. Variations in resistivity in the sample appear as corresponding variations in the plate—the lower the resistivity, the thicker the plate. The resistivity of the plating solution is usually adjusted to be somewhat higher than that of the sample. If the resistivity of the solution is allowed to be significantly lower than that of the sample, however, much better resolution can be obtained in the region plated in the meniscus of the plating solution. Thus better resolution has brought about a greater understanding of some aspects of dendritic growth in germanium.

When resistivity variations are revealed by this modification of the pulse plating method, they appear as lines or boundaries between the areas of differing resistivity. Three types of lines can be identified, each of which is related to the structure of the dendrite in some manner. One type of line meets the edge at the indentations of the serrations. These lines are essentially straight and easily resolved from the edge to the central portion of the dendrite. Another type of line meets the edge at the peaks of the serrations. As one follows such a line toward the center of the dendrite, it is found that these lines branch a number of times before the center is reached. Whenever a peak line branches, another line similar to the lines going to indentations is contained within the branches. The third type line crosses the other two types of lines changing direction when one of the other type lines is met, i.e., zigzaging lengthwise along the dendrite. It is also noteworthy that the central portion of the dendrite has no clearly discernible resistivity boundary lines.

Since any such resistivity variations must occur as a result of the growth processes, a study of these variations should disclose information

*This research was suppot ed in part by the United States Air Force through Wright Air Development Center.

about the growth of a dendrite. It appears that at least two growth processes, one longitudinal and the other lateral, are active when a dendrite is formed. During longitudinal growth a sort of rod is formed that has approximately equal width and thickness being nearly that of the final dendrite. Lateral growth then occurs and widens this rod. This central rod apparently has small serrations on its edge; and some of these serrations grow preferentially in comparison to others, resulting in a tendency for the serrations to merge and form larger ones as lateral growth proceeds.

The resistivity boundaries or lines are significant since they trace the paths of growth of the serrations during lateral growth. This is shown in Figure 1, which is an idealized drawing that represents the growth of a segment of one side of a dendrite from an initial edge, represented by the solid, jagged line, E_o, to a final edge, represented by the solid, jagged line, E_f. Two types of lines are shown: lines P_1, P_2, P_3, etc. to peaks of the serrations and lines V_1, V_2, V_3, etc. to the valleys. Following the peak lines from E_o toward E_f, one sees that they merge with neighboring peak lines to form new ones. Each time this happens a valley line is terminated. The merging of the lines, of course, represents the merging of peaks during the growth of an actual dendrite. The shading lines in Figure 1 show the regions of heavier plate.

The presence of at least two growth processes receives support from two sources, a simple comparison of longitudinal and lateral growth rates and the visual observation of the growth of a number of dendrites. It is shown that, for a dendrite two millimeters wide, being pulled at a rate of 150 mm. per minute with the tip 10 mm. below the surface of the melt, the rate of growth in the longitudinal direction is more than seven times the rate in the lateral directions. The visual support was obtained while watching crystals grow on the surface of a melt that had been supercooled to a degree that growth could take place spontaneously. Such growth is usually dendritic, proceeding from a nucleation point on the walls of the crucible. Most of the dendrites observed grew in two clearly discernible steps, first by the rapid formation of a sort of rod and second by the gradual widening of that rod to the dendrite shape.

Other suppositions concerning dendritic growth, are important. For example, it is felt that little thickening of the dendrite occurs during lateral growth because the resistivity variations can be resolved about as well near the center of each face as near the edge. In addition, the lines to the indentations of the serrations are thought to result from different growth conditions occurring at the upper and lower sides of each serration. Another point is that this mode of growth helps explain the wide variance in edge structure observed on germanium dendrites. Lastly, it should be emphasized that there is no way of knowing from the plating itself how far below the surface the resistivity variations extend.

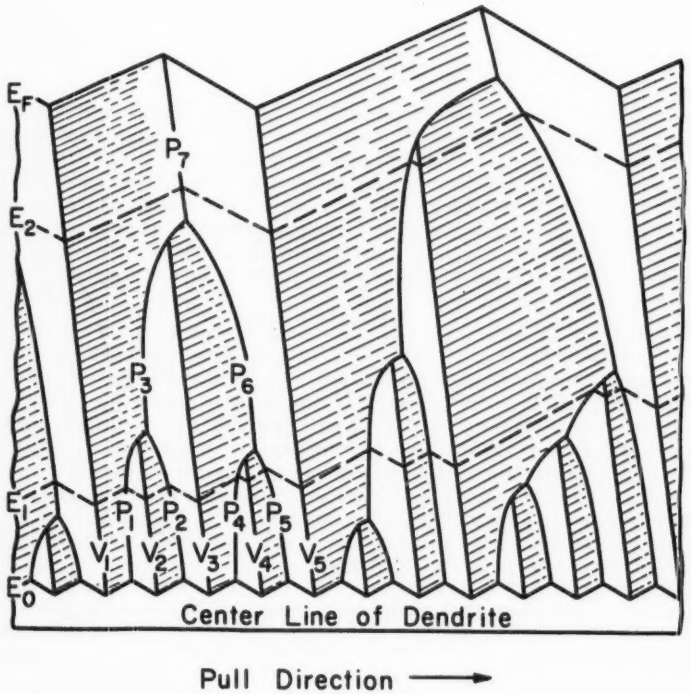
E_F
E_2
E_1
E_0
P_7
P_3
P_6
P_1
P_2
P_4
P_5
V_1
V_2
V_3
V_4
V_5
Center Line of Dendrite
Pull Direction

Figure 1

References

1. P. R. Camp, J. Appl. Phys. 25, No. 4, 549 (1954).
2. Gurion Meltzer, Recent News Paper, Fall, 1959, Meeting of the Electrochemical Society, Columbus, Ohio.

Abstract Number 83

GROWTH OF ATOMICALLY FLAT SURFACES ON GERMANIUM DENDRITES

A. I. Bennett, R. L. Longini and W. J. Smith*

Westinghouse Research Laboratories
Pittsburgh, Pa.

This paper presents a theory of the formation of flat surfaces during the growth of germanium dendrites. The theory assumes that the liquid-solid interface of the growing dendrite consists of two regions: (a) a planar extension, below the melt surface, of the flat faces of the dendrite strip, and below this, (b) a curved region extending to the top of the dendrite. Region (a) is supercooled, and growth in this region is limited by the rate of nucleation of new layers. Region (b) is at or very near the melting point, and growth there is limited by the dissipation of the latent heat of fusion.

During the growth process, new layers will occasionally be nucleated on the flat supercooled region. Such a layer, once nucleated, will spread rapidly over the entire supercooled region. When this layer grows to the surface of the melt it must of course terminate, and in so doing it forms a step, or corner, on the solid. Because there is a line energy associated with this corner, this step does not immediately rise from the liquid as the growing dendrite is pulled upward; instead, it is energetically more economical for the meniscus to remain attached to the step, rising with it until the increased vertical component of surface tension is sufficient to pull the meniscus free. During this sticking interval, additional planes will be nucleated, and will grow to the surface, thus creating a step several atomic layers in height. When the meniscus finally tears free of the step, it will return to its original position, perhaps overshooting as well, and the step formation process is repeated.

The velocity of propagation of a nucleated layer is limited by the rate at which the latent heat can be dissipated. An analysis of the thermal conditions at the edge of the advancing layer shows that the thermal limit to the velocity of propagation is roughly $v = 2 \times 10^3 \Delta T$ where v is in cm. sec^{-1} and ΔT is the local supercooling in degrees centigrade at the interface prior to passage of the edge. Experimentally it appears that ΔT may be of the order of 5°C; for this condition, $v = 10^4$ cm. sec^{-1}.

*This research was supported in part by the United States Air Force through Wright Air Development Center.

Two mechanisms are considered whereby the propagation of successive layers might interact thermally. The first mechanism depends on the fact that as a layer propagates, the evolved heat is assumed to reduce the local supercooling to zero. A subsequent layer cannot be nucleated until sufficient supercooling has been reestablished; then a certain minimum time will be required between nucleation of adjacent layers. This time τ is estimated at roughly $0.05/\Delta T^2$ μ sec. For ΔT = 5°C, $\tau = 2 \times 10^{-9}$ sec. A second possibility of thermal interaction is that if the edge of an advancing layer should be followed by the more rapidly advancing edge of the succeeding layer, the latent heat evolved by the first layer edge will decrease the velocity of the following edge when the distance between the two edges becomes sufficiently small. This interaction distance c is estimated as $10^{-4}/\Delta T$ cm, and for ΔT = 5°C, c = 0.2 microns. From experimental observations of the rate of thickening of germanium dendrites it appears that the average time between nucleation of successive layers exceeds 10^{-3} sec, so that the limits suggested by the preceding two mechanisms are not in fact approached.

From considerations of the surface energy at the intersection of the liquid surface and the dendrite face, an elementary calculation is made of the cosine of the contact angle of the meniscus. In spite of the crude nature of these estimates, the calculated cosine is not only of order unity but equals the observed value within the accuracy of observation, about a factor of two.

Abstract Number 84

DENDRITIC GROWTH OF INDIUM ANTIMONIDE

J. W. Faust, Jr., H. Nicholson and R. Moss*

Westinghouse Research Laboratories, and
Westinghouse Materials Engineering Department
Pittsburgh, Pa.

It has been shown in the preceeding papers (#79, 80, and 81) that the continuous growth of semiconductor dendrites requires the presence of at least two twin planes. The III-V intermetallic semiconducting compounds crystallizes in the diamond type lattice, which has a (111) twin composition plane. Since for elemental semiconductors, all eight {111} planes are equivalent, the twinning operation can be regarded either as a reflection of the material on one side of the twin plane to the other side or as a 180° rotation about the twin axis of one half of the bicrystal. For binary semiconductors, however, the {111} planes are not all equivalent,[1] thus it is necessary to regard the twinning operation as a 180° rotation about the normal to the twin plane. Thus, no matter how many twin planes a dendrite of a III-V intermetallic compound contains, one face will always contain group III atoms and the opposite face group V.

InSb dendrites were obtained by dipping a single crystal seed into a supercooled melt and pulling it rapidly from the melt. These primitive dendrites were then used to grow more dendritic material. Most of the primitive dendrites contained an even number of twins; the explanation of this has already been given.[2] The dendrites were examined unetched to study their morphology; by fracturing and by etching polished cross sections to study their twin structure; and by etching to study their crystal perfection.

Studies of the serration edges of the dendrites showed them to be faceted by {111} planes. Both types of {111} planes (i.e., planes that contain indium atoms and planes that contain antimony atoms) were present; there was no indication that one type grew more favorably than the other. Thus, for dendritic growth the polar axis does not appear to affect the growth of different {111} planes as it does in the Czochralski method.

The use of the fracture technique devised by the authors[3] for studying twin structures is complicated in InSb by the fact that primary

*This research was supported in part by the United States Air Force through Wright Air Development Center.

cleavage planes of the III-V intermetallic compounds are {110} planes. This results in many more cleavage marks on the surface, but does not affect interpretation of the twin structure. Twin structures can be revealed by the etching of mechanically polished cross sections. The interpretation of these results is straightforward; one does not find the apparent etching anomaly on $(\bar{2}11)$ and $(2\bar{1}\bar{1})$ planes that is found in germanium.[4]

Although the polar axis does not appear to interfer with the growth of InSb dendrites, it does affect the action of etches.[1] As a result of this, it is possible to determine which face of the dendrite contains indium atoms and which face contains antimony atoms. Most etches that reveal dislocations in InSb reveal them only on the face containing the indium atoms. From the similarity of the distribution of dislocations on InSb and Ge dendrites, it is felt that the etch is revealing all of the dislocations. This means that either only α or only β dislocations are present or that the etch is revealing both with equal ease.

There are three main groupings of dislocations: 1) a stripe of closely-spaced, highly-dislocated areas running down the center of the face, 2) random dislocations along one or both edges of the face, and 3) pockets of dislocations running parallel to the twin lamella near both edges. The latter grouping is revealed by etching the fractured cross sections. The similarity of the dislocation distribution to that found in germanium and silicon dendrites suggests that dislocations are introduced into InSb dendrites by the same mechanism given for germanium and silicon dendrites.[4] Comparison of the morphology, twin structure, and dislocation distribution of InSb dendrites with germanium and silicon dendrites strongly suggests that the mechanism of growth of these materials is the same.

References

1. J. W. Faust, Jr. and A. Sagar, J. Appl. Phys. 31, Jan. 1960.
2. J. W. Faust, Jr., and H. F. John. This meeting Abstract #79.
3. J. W. Faust, Jr., and H. F. John, submitted to J. Electrochem. Soc.
4. H. F. John, and J. W. Faust, Jr. This meeting Abstract #81.

PREPARATION OF HIGHLY ARSENIC-DOPED GERMANIUM*

Paul L. Moody and Alan J. Strauss

Lincoln Laboratory, Massachusetts Institute of Technology
Lexington 73, Massachusetts

Germanium containing impurity concentrations exceeding 10^{19} cm^{-3} is required for the fabrication of p-n junctions which exhibit the quantum-mechanical tunneling effect utilized in the Esaki diode.[1] Arsenic is a suitable donor impurity, since its maximum solubility in germanium is 1.8×10^{20} cm^{-3}.[2] However, crystals containing sufficient arsenic must be grown from melts which contain arsenic concentrations of the order of 1 - 10 atomic percent and consequently have high arsenic vapor pressures. To prevent evaporation of arsenic from the melts, such crystals haveb een prepared in sealed systems with heated walls, in the same manner as GaAs and InAs. Both a syringe-type Czochralski puller and a three-zone horizontal furnace have been used.

The syringe-type puller, which is shown schematically in Fig. 1, is a simplified version of a puller designed earlier for the growth of GaAs and InAs crystals.[3] A precision ground quartz tube is sealed near its lower end by means of a flat quartz plate upon which are placed a quartz crucible which contains the melt and a graphite susceptor. The upper end of the tube is sealed by means of a brass flange and a water-cooled brass plate containing an O-ring. A stainless steel pull rod passes through a Wilson seal in the brass plate and is threaded into a graphite fixture consisting of an accurately machined piston and a seed holder. A resistance furnace is used to heat the upper part of the quartz tube to prevent arsenic condensation, while induction heating is used to melt the germanium-arsenic charge.

The crystal growing procedure is essentially the same as that used with a conventional puller, except that the resistance furnace is heated to 580°C before the charge is heated and is maintained at that temperature throughout the run. The crystals are grown in an argon atmosphere at an extraction rate of 0.1 - 0.5"/hr. and a rotation rate of 10 RPM. In recent experiments, the initial arsenic concentration in the charge has been 9% by weight. Single crystal or large grain regions

*The work reported in this paper was performed by Lincoln Laboratory, a center for research operated by Massachusetts Institute of Technology with the joint support of the U. S. Army, Navy, and Air Force.

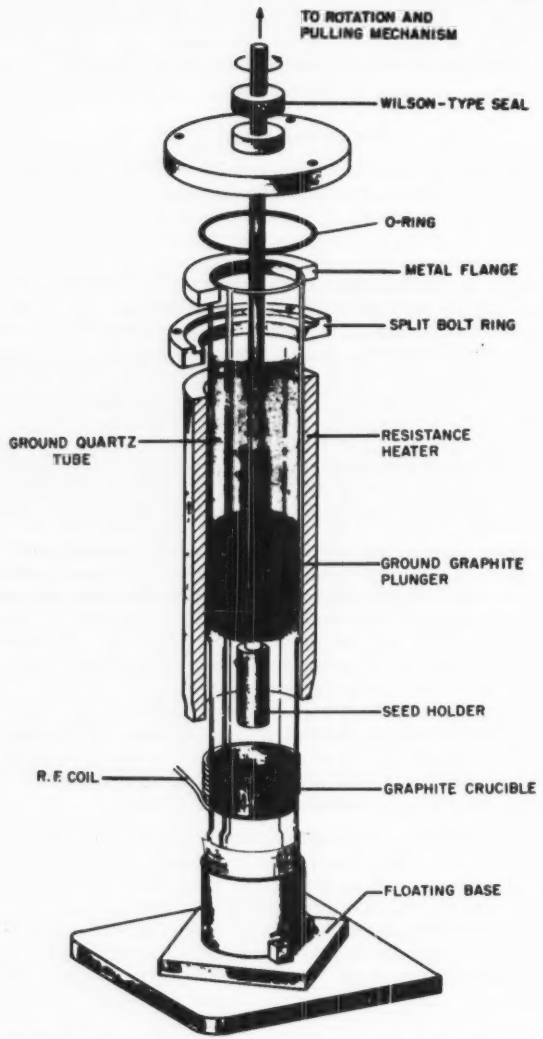

Fig. 1—Syringe-type crystal puller for arsenic-doped germanium

are generally obtained at the upper ends of the pulled ingots, but polycrystalline and eventually porous two-phase regions are found at the lower ends. The free electron concentrations in the single-phase regions are usually 3-3.7 x 10^{19} cm^{-3}. The latter value is the maximum which has been attained with the crystal puller.

The three-zone horizontal furnace was originally built and is regularly used for the preparation and zone refining of InAs. It has the usual features of furnaces designed for zone refining decomposing compounds.[4] All three zones are resistance heated. The procedure used for growing doped germanium crystals is similar to the one used for InAs. A quartz boat containing a single crystal germanium seed, polycrystalline germanium, and arsenic is placed in a quartz tube which is evacuated and sealed off. The quartz tube is placed in the furnace at the position required for fusing the seed to the polycrystalline material. The outer furnaces are first heated, the center furnace is then heated sufficiently to melt the germanium-arsenic alloy and part of the seed, and finally the quartz tube is pulled through the furnace by means of a quartz rod sealed to it at the end nearest the seed.

Only a few experiments with the horizontal furnace have been performed so far. In each case, a short region of single crystal material was obtained adjacent to the seed, then polycrystalline and finally two-phase porous material, as in the crystal puller. The maximum carrier concentration which has been attained is 4.5 x 10^{19} cm^{-3}.

The resistivity and Hall coefficient have been measured at room temperature and in some cases at liquid nitrogen temperature for over 40 rectangular samples (approximately 12 mm x 5 mm x 2 mm) cut from the grown crystals. Conventional DC potentiometric technique was used to measure resistivity, but this technique is unsuitable for Hall coefficient measurements on highly doped samples, since the Hall voltages are only a few microvolts, while the IR drop resulting from misalignment of the Hall probes is frequently several times greater than the Hall voltage. Therefore, the Hall voltage is amplified with a DC amplifier whose output is measured with a recording potentiometer; a sensitivity of 4 cm/μV is obtained on the recorder chart. The Hall coefficients measured in this manner should be accurate to within 10%.

Fig. 2 shows the room temperature resistivity of arsenic-doped germanium as a function of concentration calculated from the Hall coefficient data. According to these data, the Hall mobility decreases from 930 cm^2/volt-sec at 10^{18} cm^{-3} to 200 cm^2/volt-sec at 5 x 10^{19} cm^{-3}. Those measurements which have been made at liquid nitrogen temperature show that the Hall coefficient remains constant but that the Hall mobility increases by 10-20% above the room temperature value for samples containing more than 10^{19} cm^{-3} free electrons.

References

1. L. Esaki, Phys. Rev. 109, 603 (1958).

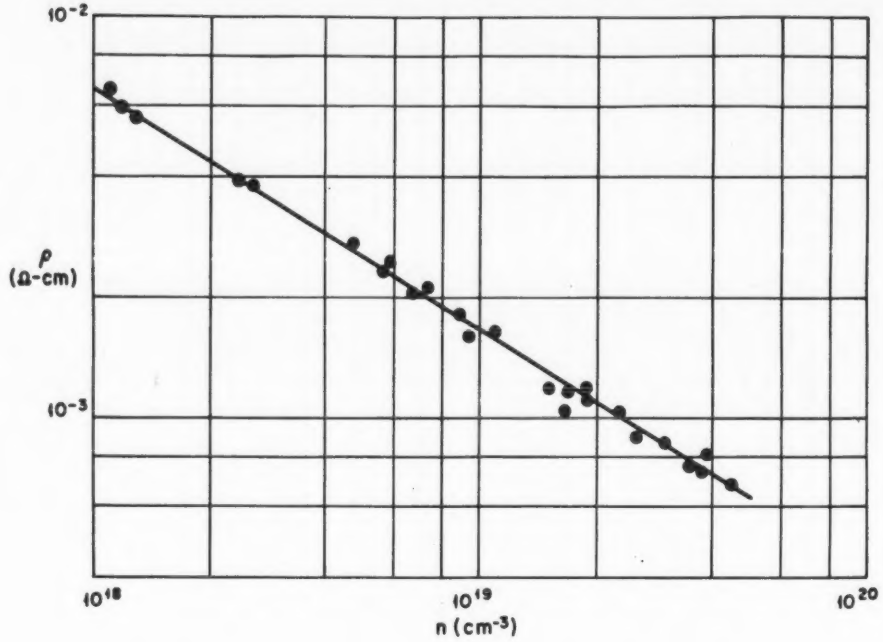

Fig. 2—Resistivity of arsenic-doped germanium at room temperature

2. F. A. Trumbore, Semiconductor Symposium of The Electrochemical Society, May 1959 (unpublished).

3. P. L. Moody and C. Kolm, Rev. Sci. Instr. 29, 1144 (1958).

4. J. van den Boomgaard, F. A. Kroger, and H. J. Vink, J. Electronics 1, 212 (1955).

Fig. 2—Resistivity of arsenic-doped germanium

Abstract Number 86

CRYSTAL MODEL STUDIES OF GROWTH PHENOMENA IN III-V COMPOUNDS

R. C. Sangster

Central Research Laboratories
Texas Instruments Incorporated
Dallas, Texas

Crystal growth phenomena for III-V semiconducting compounds have been studied by use of a versatile model of the zinc blende lattice. A series of color photographs will be presented to demonstrate the methods and results of this study.

The basic postulate used in this work is that the growth behavior of crystal surfaces may be analyzed in terms of the nature of the bonding, the type, and the packing density of the atoms present in the surface layers. In general, crystal growth will be favored when the growing surfaces closely approximate single stoichiometric planes, when the surfaces have an atom packing density and bonding closely similar to that of the liquid, and when the barriers to initiation or nucleation of growth of successive layers are either very small or nonexistent.

The following key results from a brief paper now being prepared for publication by the author and G. R. Pruett, also of these laboratories, will be used as background for this presentation:

(1) The $<113>$ or closely allied crystallographic axes represent the naturally preferred directions of growth for both indium antimonide and gallium arsenide, when growth is constrained to a single direction.
(2) Most existing crystal growth theories are inadequate and inappropriate when applied to conditions of constrained growth, such as those existing in the Teal-Little or zone-refining processes.
(3) Growth on all possible crystal surfaces in the zinc blende lattice may be analyzed in terms of growth on three fundamental surfaces: $\{100\}$, $\{110\}$, and $\{111\}$. All other surfaces may be represented as stepped structures built up from basic units of these three surfaces.

The following criteria have been used to define the concept "crystal surface" or "crystal surface layer" on an atomic scale:

(1) The "crystal surface layer" must be capable of generating the whole crystal volume, by simple translation or stacking operations.
(2) It must be stoichiometric.
(3) It must include all atoms directly involved in the "stepped" structures referred to above.
(4) It must contain all atoms which have abnormal or unsatisfied bonds due to their proximity to the surface of the crystal.

Since all of the higher indices surfaces may be described in terms of the three basic surfaces– {100}, {110}, and {111}, once the behavior of these basic surfaces has been elucidated, the growth behavior of the complex surfaces can be predicted without detailed reconsideration of the fundamental factors involved.

Arbitrarily, the study has dealt with low order growth directions only ($h + k + l \leqslant 7$). As a check to be reasonably sure that no highly significant growth directions were overlooked, the Miller indices and lengths were computed for all of the vectors connecting a given atom with the other atoms in the lattice within a cube, four unit cell edges on a side, centered on the given atom (see Table I). The first seven nearest neighbor directions were found to fall in the group of directions

Table I. Direction type and minimum distances between atoms for all of the vectors connecting a given atom with any other lattice site within a cube, four unit cell edges on a side, centered on the given atom and square with the conventional axes. Distances are in terms of unit cell edges. The underlined directions were studied during the work being reported.

Vector	Distance	Vector	Distance	Vector	Distance
111	.43	117	1.79	233	2.34
110	.71	155	1.79	177	2.49
113	.83	123	1.87	557	2.49
100	1.0000	137	1.92	134	2.55
133	1.09	355	1.92	377	2.58
112	1.22	337	2.05	577	2.77
115	1.30	114	2.12	334	2.92
135	1.48	157	2.16	122	3.00
130	1.58	120	2.24		
335	1.64	357	2.28	(140	4.12)

selected for study. Furthermore, as the work progressed it became apparent that all of the simple, naturally occurring planes of atoms in the zinc blende lattice were indeed being considered.

The results obtained can be summarized briefly as follows:

Growth on {100} surfaces is favored by the absence of any significant barrier to the deposition of new layers. Atoms can add anywhere on the surface with no net change in the nature or the number of chemical bonds present at the surface, except for peripheral or strictly second-order

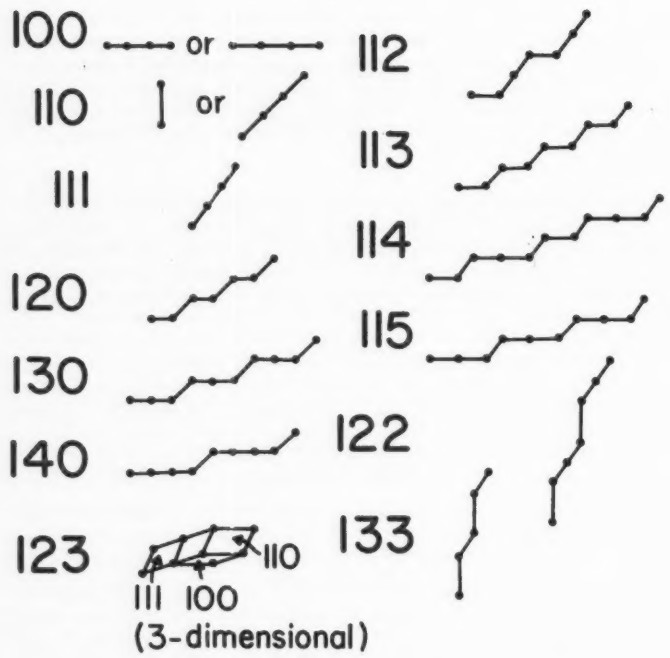

Fig. 1—Relative structures of the surfaces considered in this study. For all except {123}, perpendicular cross sections are shown. The dots represent linear rows of atoms of a given type (either III or V), the lines represent {100}, {110}, or {111} planes connecting these rows. The vertical distance shown for {110} is one unit cell edge, and the other distances are to the same scale. The angles are correct.

effects. However, growth is inhibited by the lack of clear-cut surface stoichiometry and by a low packing density.

Growth on {110} surfaces possesses a favorable surface stoichiometry but unfavorable nucleation and packing factors. Growth of a surface layer proceeds by individual, zig-zag, stoichiometric chains of atoms. Each chain must be nucleated by one or more atoms, each making a single bond to the completed surface layer, leaving three "unsatisfied" or liquid-solid bonds; or by the equivalent circumstance of one or more III-V diatomic "dumbbells" attaching themselves with two bonds each to the completed layer, leaving four bonds each unsatisfied. The completed surface layer is ideally planar and stoichiometric, but half of the atoms that would be required for uniform packing are missing.

Growth on {111} surfaces possesses favorable packing and surface stoichiometry, but exceedingly unfavorable nucleation characteristics. Formation of the initial nucleus for a new layer requires deposition of a three atom chain, making only two bonds to the surface, or the simultaneous but independent deposition of two singly bonded atoms of a specific type (either III or V, depending upon the orientation of the surface layer) as near but unbonded neighbors. Thereafter, growth occurs on three triangular edges of the completed seed layer as for {110} growth —by nucleation and growth of zig-zag chains, each completed chain advancing the growth front by one step.

Growth on "stepped" surfaces will be highly favored over that of the three basic planes when the steps are built up from {100} and {111} faces, a situation that will not exist for any other pair of the basic planes. One to one combinations of the {100} and {111} planes are probably favored over combinations in other ratios, since cancellation of the various unfavorable factors should be most nearly complete for this case. The {113} surfaces correspond to "stair-step" structures consisting of alternating {100} "treads" and diagonal {111} "risers." Thus, on the theory presented here, they would be expected to be the easiest growing surfaces in the zinc blende (sphalerite) lattice, in agreement with the experimental observations.

The stepped structures observed for all of the surfaces studied are shown in Fig. 1. Details of these surfaces and of their growth behavior will be presented. Other observations—such as the electrochemical polarity of surfaces like the {111} and the existence of favored growth directions within a given surface layer—will be discussed.

Abstract Number 87

ORIENTATION DEPENDENT DISTRIBUTION COEFFICIENTS OF TELLURIUM IN INDIUM ANTIMONIDE CRYSTALS

J. B. Mullin

Royal Radar Establishment
Malvern, England

Hulme and Mullin have previously reported[1] that tellurium has a different distribution coefficient on and off a {111} facet. They deduced that at pull rates of ~2 cm/hr. and rotation rates of ~100 r.p.m. that the distribution coefficient for tellurium on a {111} crystallographic plane differed by a factor of ~6 from the distribution coefficient just off the {111} plane; the values being ~3 and ~0.5 on and off the plane respectively. The present paper presents a more detailed study of this so called "facet effect." Only the results for tellurium are presented although[2] selenium and sulphur appear to show the "facet effect" whereas zinc and germanium do not.

The effect of the orientation of the growing interface on the distribution of tellurium in the indium antimonide was determined by growing crystals from melts doped with radioactive tellurium using suitably orientated seeds. A Czochralski technique was used to grow the crystals and pull rates of 1.5 cm/hr. and rotation rates of 100 r.p.m. were employed. Autoradiographs were taken of slices of the crystals that had been out perpendicularly to the growth direction. The autoradiographs represented a map of the tellurium concentrations in these slices. Suitable sections from these areas were cut out and their tellurium contents were measured using a radiochemical counting technique. The variation in the distribution coefficient over the growing interface throughout the history of the crystal growth was thus determined.

A region of enhanced tellurium concentration in Te-doped crystals pulled within 12° of the <111> direction have previously been correlated with the presence of {111} planar crystallographic facets on the solid at the interface. Crystals grown in a <111> direction generally show a central facet on a convex interface, but under conditions where the interface is known to be concave slices from such regions of growth produce a uniform density on an autoradiograph. It is concluded that no facets were present. Four small facets can sometimes be seen symmetrically situated about the edges of a convex interface produced by pulling a <100> crystal rapidly from the melt. Autoradiographs of slices of these crystals have a uniform central density with four small regions of high density corresponding to the traces of {111} and $\{\bar{1}\bar{1}\bar{1}\}$ planes on the growing interface. <110> crystals under similar

circumstances have two symmetrically opposite facets one a (111) and one a $(\bar{1}\bar{1}\bar{1})$ on the interface. But in no crystal yet pulled either from <110> or <100> seeds has conclusive evidence been found for {110} or {100} facets producing regions of enhanced tellurium concentration. Further, concave interfaces using either <100> or <110> seeds produce uniform tellurium concentrations in the pulled crystals, with no evidence of {111} facet formation on these interfaces. It is interesting that the presence of {111} and $\{\bar{1}\bar{1}\bar{1}\}$ facets is recorded by equal densities on autoradiographs, indicating that tellurium has a similar k on these faces. The effective distribution coefficient for tellurium across interfaces grown from various seeds were as follows - <111> seed k = 3.5 - 4.1 <100> seed k = 0.49; <110> seed k = 0.56; <311> seed k = 0.55. Direct measurements of k using $<\bar{1}\bar{1}\bar{1}>$ seeds have so far been frustrated due to twinning on that orientation.

The present results confirm the difference of k on and off a {111} facet. That this effect is due to a genuine difference in k on and off a {111} facet and not to a stirring effect is discussed fully elsewhere.[2]

The explanation of the variation of k with interface orientation must therefore reside in the variation in the exchange rates of solute atoms between solid and liquid on and off a {111} facet. The existence of 111 facets suggested that growth on a {111} plane is slow and involves the lateral movement of steps which are created by two dimensional nucleation or by virtue of the presence of a screw dislocation. If the interface just off the {111} is considered to consist of closely spaced steps their sideways velocity will be less than on a {111} facet. This would provide a mechanism for trapping an absorbed layer of Te atoms on a {111} surface resulting in a change in k. A more detailed knowledge of the nature of the solid liquid interface will probably be needed before an exact atomic description of the "facet effect" can be made.

References

1. K. F. Hulme and J. B. Mullin, 1959, Phil. Mag. 4, 1286.

2. J. B. Mullin and K. F. Hulme, submitted to Phys. & Chem. of Solids.

Abstract Number 88

ANISOTROPIC SEGREGATION IN InSb*

W. P. Allred and R. K. Willardson

Battelle Memorial Institute
Columbus, Ohio

Several investigators have studied the segregation of impurities in InSb[1,2,3,4]. The reported results vary widely. A large variation in segregation coefficients with respect to crystal orientation has been observed. Crystals pulled on the [111] axis show high concentrations of Se and Te in the center of the ingot. This effect is thought to be caused by a segregation coefficient of Se and Te greater than unity on the (111) facet and less than unity in other orientations. It has been reported that the segregation coefficient of Te in InSb can vary from 0.5[3] to 3.0[4] depending on the orientation of the crystal. Detailed measurements on pulled single crystals confirm this report and add emphasis to the need for a better understanding of segregation.

Figure 1 shows a single crystal grown by the Czochralski technique. The crystal was pulled from a quartz crucible. The crucible and seed were rotated in opposite directions, each at a rate of 6 rpm, giving a net rotational rate of 12 rpm of the seed with respect to the melt. After a small portion of the crystal was grown, 1.1 milligrams of Sb_2Se_3 was added as a doping agent. The crystal was pulled at a rate of 1 inch per hour and weighed 345 grams. The mobility and carrier concentration as determined by Hall and resistivity measurements are also plotted. The Hall and resistivity measurements were made on dumbbell-type samples cut from slices of the crystal.

The concentration of Se atoms added to the melt was calculated to be about 1×10^{17} cm^{-3}. The residual Te density was estimated to be about 3×10^{16} cm^{-3}. This calculation was based on Hall and resistivity measurements made on the undoped top section of the crystal.

The expected carrier concentration from Se ($k = 0.2$) impurity is plotted at the bottom of the graph. The expected carrier concentration of the combination of Se and Te is also plotted by using 0.5 as the segregation coefficient of Te.

It might be expected that the carrier concentration along the crystal would follow the calculated theoretical curve, using a segregation

*This research was supported by the Electronic Components Laboratory, Wright Air Development Center and in part by the Air Force Office of Scientific Research.

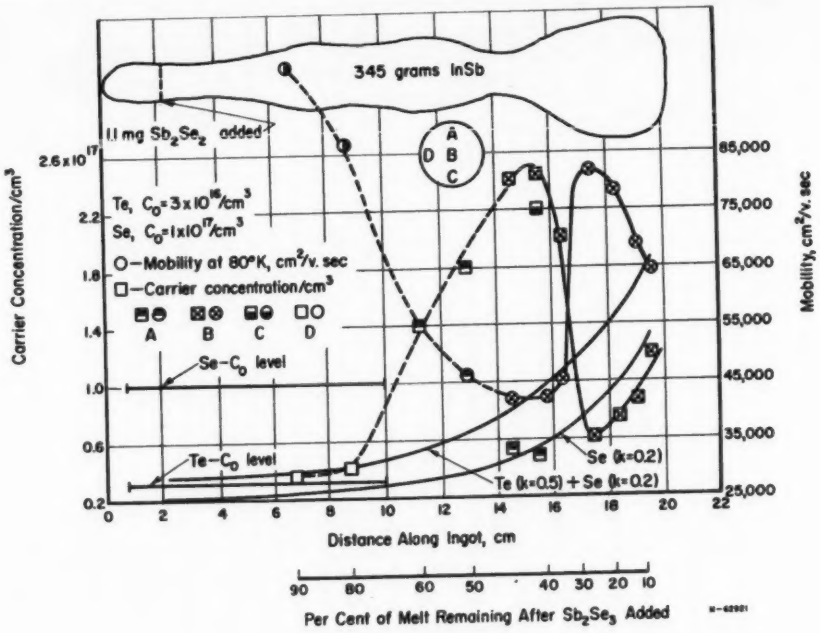

Fig. 1—Segregation in a crystal of InSb pulled in the [III] direction

coefficient of 0.5 for Te and 0.2 for Se. However, the carrier concentration, as observed from measurements on the Hall samples taken from the center of the ingot, varied from a factor of 3 higher to a factor of 2 less than the predicted values and seemed to depend more on the shape and orientation of the crystal than on the expected segregation of impurities. A large radial variation of impurity content was also observed. Samples cut from the same location in the ingot but from different radial positions (labeled A, B, and C in Figure 2) show a variation of impurity content ranging from 5×10^{16} cm^{-3} on the edge to 2.4×10^{17} cm^{-3} in the center of the pulled crystal. The extreme variation in impurity content is probably caused by the fact that the crystal-melt interface is nonplanar. Some of the solid-melt interface is therefore growing on other orientations than the (111), thus changing the segregation coefficient. The segregation coefficient of Se on the (111) facet is greater than 1 whereas that grown a few degrees from the [111] direction is near the reported value of 0.2.

Figure 2 illustrates the conduction type along the length of a second ingot. This ingot was pulled under the same conditions as the first ingot except that it was doped with Zn after about one inch of the crystal was pulled. The slices shown below the ingot were probed with a point contact at liquid-nitrogen temperatures, and the n and p areas were determined by the sign of the rectification pattern. The solid areas correspond to n-type regions and the shaded sections correspond to p-type regions. The clear areas showed no rectification and therefore were not identified as to conduction type.

The crystal twinned below Slice 3 and new crystals on the [110] direction began to appear. Figure 3 is the same ingot as shown in Figure 2. The conductivity type at 80°K was determined by a thermoelectric probe. The results are quite similar to those obtained by the rectification technique with n-type material down the center as long as the crystal is oriented in the [111] direction. The p-type in the center near Slice 8 could possibly be accounted for by the fact that the crystal had twinned and was growing near the [100] and [110] directions. This would put the (111) facets out to the edge and it would be expected that there would be a low concentration of Te and Se near the center and a high concentration near the edge. This diagram again shows that a crystal grown along the [111] direction has a different concentration of impurity in those areas where the crystal growth actually takes place in a direction perpendicular to the (111) facet than at other growth positions on the crystal.

Absolute values can be ascribed to the segregation coefficients in InSb only when the crystallographic orientation of the growth interface is specified. Unless special precautions are taken to control the growth interface, single crystals of InSb will be nonhomogeneous because of anisotropic segregation. Zone refining of polycrystalline InSb is undoubtedly complicated by this effect, since as the crystals change orientation the direction of segregation also changes. Since a wide variation is observed in the segregation coefficient in InSb, with respect to crystal orientation, it is likely that this effect will be observed in other compounds of the III-V group.

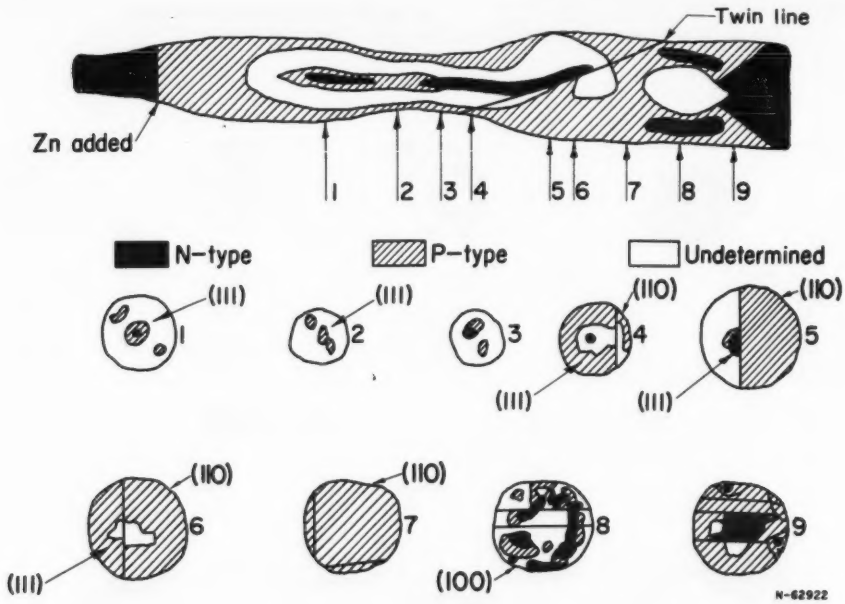

Fig. 2—Cross section of InSb crystal showing N-Type coring by point contact rectification at 80° K

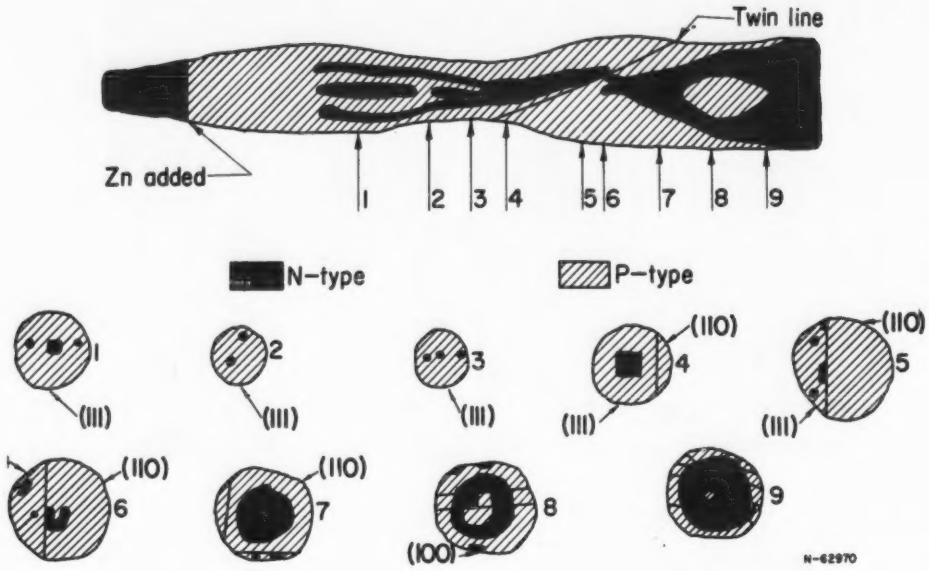

Fig. 3--Cross section of InSb crystal showing N-Type coring by thermo-electric prove at 80° K

References

1. T. C. Harman, J. Electrochem. Soc. 103, 128 (1956).
2. J. B. Mulling, J. Electronics and Control 4, 358 (1958).
3. A. J. Strauss, J. Appl. Phys. 30, 559 (1958).
4. J. B. Mullin and K. F. Hulme, "Facets and Anomalous Distribution Coefficients in InSb" (Late News Paper given at the Electrochemical Society Meeting, October 20, 1959). Details to be published.

Abstract Number 89

STUDY OF COPPER PRECIPITATION IN SILICON SINGLE CRYSTALS

G. H. Schwuttke

Sylvania Research Laboratories
Bayside, New York

This paper is concerned with the study of imperfections in silicon single crystals by copper precipitation. Copper precipitation in silicon has been used by Dash[1] with great success to make dislocation structures visible. His investigation showed this technique to be a very effective method for revealing different types of dislocations.

We have used this method to study imperfections in single-crystal silicon of different dislocation densities and different impurity concentrations, and have found that imperfections may react quite differently to their development by decoration. In crystals of high dislocation density (approximately $10^4/cm^2$ - $10^6/cm^2$) copper precipitates only along dislocation lines. In crystals of low dislocation density (less than $10^3/cm^2$) random precipitation takes place in addition to precipitation along dislocation lines.

Different kinds of decorated dislocations have been observed which are related to differences in Cottrell clouds surrounding dislocations. Random precipitation was also found to depend strongly on the impurity content of the crystal. In silicon crystals containing oxygen the copper precipitates prefer the region of high oxygen concentrations, thus delineating those areas having a high density of oxygen clusters.

The shape of the precipitate is found to depend upon the degree of super-saturation. The shape of the precipitate is not approximately spherical as usually assumed. At low copper concentrations ($\sim 10^{17}/cm^3$) the precipitates are in the form of needles, while at high concentrations ($\sim 10^{18}/cm^3$) the precipitates are more in the shape of plates.

The copper precipitates in silicon as nucleated by point imperfections have definite preferred orientations with respect to the crystal lattice. The particles prefer to segregate in (100) planes. The needles grow here in <110> directions while the plates prefer the <100> direction. Composite structures built up of needles and plates have been observed for precipitation from 1300°C. These structures when observed in (100) planes appear as crosses. If the plane of observation is the (111) plane, their projection appears as a star pattern. The needles always bisect the angle between the plates.

The influence of oxygen on the reliability of copper decoration of dislocations was also investigated. X-ray extention contrast

micrographs taken from the samples before copper decoration were used for comparison.

The experimental setup employed to observe copper precipitation in silicon consists of a microscope connected to a closed-circuit TV system.

Acknowledgments

I would like to thank Dr. P. H. Keck for many enlightening discussions and Dr. K. M. Arnold who grew most of the crystals used for these experiments.

The research reported in this paper was sponsored by the Electronics Research Directorate of the Air Force Cambridge Research Center, Air Research and Development Command, under contract No. AF 19-(604)-3482.

References

1. W. C. Dash; Phys. Rev. 98, 1536 (A) (1955); J. Appl. Phys. 27, 1193, (1956), Phys. Rev. Letters 1, 400 (1958).

Abstract Number 90*

REACTIONS OF OXYGEN IN Ge

C. S. Fuller, C. D. Thurmond and W. Kaiser

Bell Telephone Labs., Inc.,
Murray Hill, N. J.

Oxygen in solid solution in Ge undergoes aggregative reactions leading to the formation of donors and ultimately to more complex aggregates. The donor forming reaction is reversible and equilibria are established depending upon temperature and oxygen concentration. Solid solutions containing 0.9 to 6.0 x 10^{17} cm^{-3} oxygen have been investigated over the temperature range 325 to 527°C. By assuming that four oxygen atoms react successively at a Ge atom to form the singly-ionized donor structure, GeO_4, it is possible to fit the experimental curves with a single constant derived from mass action expressions and the charge and mass balance conditions.

*Enlarged Abstracts not available.

PREPARATION AND PROPERTIES OF THE PSEUDO-BINARY SYSTEM GaAs-AlAs*

E. P. Stambaugh, J. I. Genco and R. C. Himes

Battelle Memorial Institute
Columbus, Ohio

Several means of preparation of homogeneous alloys (and terminal compositions) in the pseudo-binary system GaAs-AlAs have been investigated with emphasis on the gallium-rich region. These methods are referred to as the (1) progressive casting or normal freeze technique, (2) zone leveling technique, and (3) thermal gradient technique. Induction heating was used in progressive casting and zone leveling; while resistance heating was used in the thermal-gradient crystal growth.

Basically, the alloys were prepared by direct combination of the elements at the melting point ($<1310°C$) and under an arsenic pressure slightly in excess of the dissociation pressure of the alloy (methods 1 and 2). The thermal gradient technique, which appears quite promising, differed from the progressive casting and zone leveling techniques in that the alloy was prepared at temperatures well below the melting point of the alloy and at a progressively increasing arsenic pressure.

Visual observation of the melt during preparation of several of the $A^{III}B^{V}$ compounds and alloys by zone leveling and crystal pulling has been severely hampered by deposition of an opaque film on the walls of the reactor in the vicinity of the ingot or melt. The difficulty has been eliminated by (1) maintaining the walls of the reactor tube (in the vicinity of the ingot) at temperatures greater than 900°C, and (2) elimination of volatile oxides from the system prior to the preparation.

The composition and degree of homogeneity of the alloys prepared by these techniques were determined by X-ray diffraction, metallographic examination, microhardness, and chemical analyses. Single phase, solid solutions of the GaAs-AlAs alloy containing varying proportions of AlAs have been prepared. Existence of solid solutions was verified by X-ray diffraction studies and metallographic examination.

The Knoop hardness of the GaAs-AlAs alloy varied depending on the composition from 481 kg/mm^2 (GaAs Knoop hardness) to 614 kg/mm^2 (AlAs Knoop hardness).

*This research has been supported by Bureau of Ships, Department of the Navy.

Lattice constants for GaAs and AlAs were determined to be 5.6533Å ± 0.0003 Å and 5.6585 Å ± 0.0009 Å, respectively. Lattice constant of an alloy specimen containing 10.37 mole per cent AlAs was determined to be 5.6537 Å ± 0.0003 Å, which (assuming Vegard's Law to apply) is in rather good agreement with chemical analysis. However, it is seen that, with the uncertainty involved, cell size cannot be employed as an accurate analytical tool in this system.

GaAs-AlAs alloy specimens of both n- and p-type conductivities have been prepared. Resistivities range from 10^{-2} ohm-cm to 10^{3} ohm-cm and thermoelectric powers as high as 540 μv/°C have been obtained. For p-type material in which the carrier concentration was 4.5×10^{17} cm^{-3}, Hall mobilities in the range of 160 cm^{2} $volt^{-1}$ sec^{-1} were obtained.

Abstract Number 92

PREPARATION AND PROPERTIES OF THE PSEUDO-BINARY SYSTEM GaSb-AlSb

J. F. Miller, H. L. Goering and R. C. Himes

Battelle Memorial Institute
Columbus, Ohio

Ingots of the pseudo-binary GaSb-AlSb alloy prepared by progressive casting and zone casting at various rates of crystallization. Results of X-ray diffraction studies, metallographic studies, hardness determinations, and chemical analyses indicate that, with the possible exception of a narrow composition range between 10 and 30 mole per cent AlSb, solid solution prevails in the system. Liquidus data are presented for the system.

Bulk specimens of single phase, solid solution alloy were obtained by use of low linear rates of crystallization (0.05 inch per hour), while at higher rates of crystallization (1/4 to 1-1/4 inch per hour) two intermingled solid phases were characteristically obtained. Progress was made toward preparation of sizeable homogeneous solid solution alloy specimens of uniform composition by use of the zone-casting technique in which material of a given composition (corresponding to some point on the solidus of the system) was used as the main charge, and material of the corresponding liquidus composition was used as a charge in the first zone length.

Physico-chemical properties of specimens so prepared were studied. Vegard's Law was found to be at least roughly applicable; with lattice constants for the alloys ranging between values of 6.0963 Å for pure GaSb and 6.1361 Å for pure AlSb. Optical energy gaps determined for alloy specimens increased regularly with cell size from a value of 0.68 ev for GaSb to a value of 1.74 ev for AlSb. Values of electrical resistivity and hole mobility for the relatively impure alloy specimens were also intermediate between those for the compounds in a like state of purity.

For purpose of illustration, data on a representative, zone-cast ingot are presented in Table 1. The observed relationship between lattice constant and optical energy gap in the alloy system is illustrated in Figure 1.

TABLE 1. ANALYSIS OF ZONE CAST INGOT, ZG2*

		Chemical	X-ray		Optical	Electrical			
Sample	Progression Along Ingot	Mole Per Cent GaSb	Lattice Constant, a_o (A)	Mole Per Cent GaSb (by Vegard's Law)	Energy Gap, ΔE (electron volt)	Hall Coefficient, R_H (cm^3/coulomb)	Resistivity, ρ (ohm-cm)	Hall Mobility μ (cm^2/volt-sec)	Density of Carriers, n_p (cm^{-3})
ZC2-1	9%	26 ± 4	6.1237 ±0.0003	31 ± 1	1.46	+58	0.22	220	1.3×10^{17}
ZC2-2	33%	38 ± 2	6.1200 ±0.0006	40 ± 2	1.43	+29	0.11	220	2.6×10^{17}
ZC2-3	54%	45 ± 3	6.1201 ±0.0003	40 ± 1	1.38	+20	0.075	223	3.7×10^{17}
ZC2-4	75%	96 ± 3	6.1007 ±0.0006	89 ± 2	0.74	+ 5	0.014	300	1.5×10^{18}

*Casting rate, 1/4 inch per hour; charge, 75 mole per cent GaSb - 25 mole per cent AlSb in first zone, 50 mole per cent GaSb - 50 mole per cent AlSb in remainder.

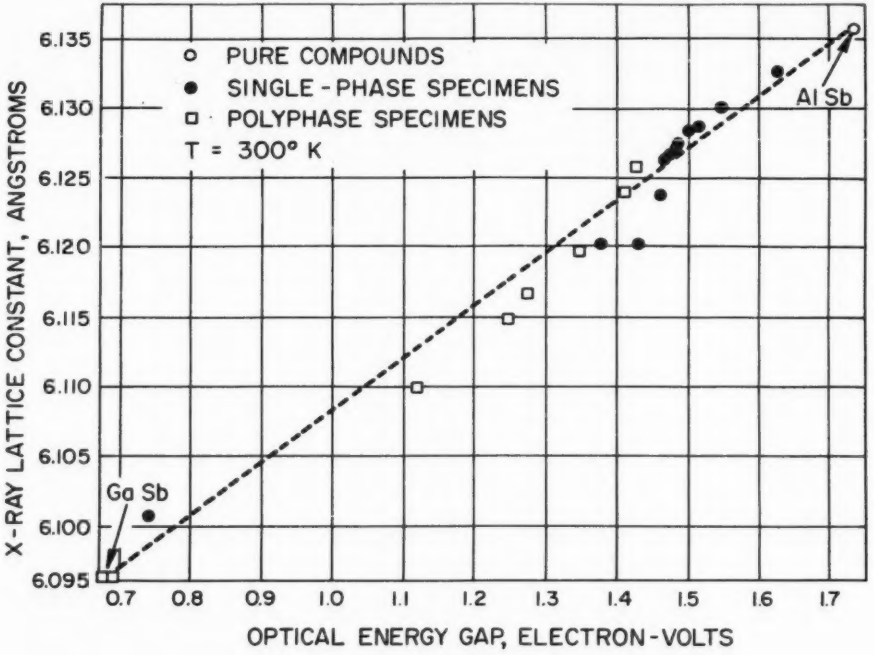

Fig. 1—Energy Gap Versus Cell Size for Solid Solutions of GaSb-AlSb.

Abstract Number 93

THE PHASE DIAGRAM FOR THE BINARY SYSTEM CADMIUM-TELLURIUM*

Donald R. Mason and B. M. Kulwicki

Department of Chemical and Metallurgical Engineering
University of Michigan
Ann Arbor, Michigan

Introduction

Samples of cadmium telluride have been prepared in our laboratory in conjunction with studies on ternary semiconductor compounds in the binary system CdTe-In_2Te_3.[1] In the original work on this system, Kobayashi[2] found that CdTe is the only compound formed between these elements, and indicated that its melting point would be in the range of 1041°C to 1050°C.

More recently, Lawson, Nielsen, Putley and Young[3] have reported a value of 1106°C. without describing the details of their measuring technique. D. deNobel[4] has published values for several additional points on the liquidus line in the cadmium-tellurium system, and represents the melting point of CdTe to be 1090°C. Visual observations of the first-to-freeze temperatures were made at each composition reported. Thomassen and Mason[1] observed a melting point for CdTe of 1098 ± 3°C.

In view of these discrepancies, the phase diagram for the cadmium-tellurium system has been redetermined. A series of samples was prepared in which the cadmium-tellurium compositions were varied over the range from 1 mol% Te to 98.7 mol % Te, using the purest available elements for their preparation. The latent heat transitions in each sample were determined by using the method of differential thermal analysis.

Experimental

The experimental operations comprising the sample preparation, the differential thermal analysis equipment and procedures, and the preliminary interpretation of the data have been discussed previously.[1]

*Contribution No. 2 from the Semiconductor Materials Research Laboratory, College of Engineering, University of Michigan, Ann Arbor, Michigan. This work was supported in part by grant NSF-G4127 from the National Science Foundation, and in part by Project MICHIGAN, under Department of the Army contract (DA-36-039-SC-78801) administered by the U. S. Army Signal Corps.

Thermodynamic Theory of Solid-Liquid Equilibrium

From thermodynamic analysis of the data, it is possible to estimate the latent heat of fusion of cadmium telluride, to establish the form of the liquidus lines on a theoretical basis, to predict the eutectic compositions, and to gain some insight as to the nature of the liquid regions. For purposes of calculation, the diagram can be considered to comprise two separate binaries, (I) the system Cd-CdTe, and (II) the system CdTe-Te.

The liquidus curve for a binary system which exhibits ideal solution behavior may be represented by the Schroeder-vanLaar equation.[5]

$$\ln x = \frac{\Delta H_f}{R} \left(\frac{1}{T_f} - \frac{1}{T}\right) \qquad (1)$$

where

x = mol fraction of component A in solution at T°K

T_f = melting point of component A, °

R = gas constant, 1,987 cal/gm mol °K

ΔH_f = latent heat of fusion of component A, cal/gm mol

In non-ideal solutions the departures from ideality are characterized by an activity coefficient, γ. By analyzing the liquidus data for a large number of binary systems containing germanium and silicon, Thurmond and Kowalchik[6] have postulated a new class of solutions, called elementary solutions, wherein the relative partial molar excess entropy and the relative partial molar enthalpy of mixing exhibit a particular dependence on concentration, but are not direct functions of temperature. The relationship between the activity coefficients and the excess thermodynamic functions can be represented by an equation in the form

$$\alpha = \frac{RT \ln\gamma}{(1-x)^2} = \frac{\overline{\Delta H}}{(1-x)^2} - \frac{T\,\overline{\Delta S}^E}{(1-x)^2} = a - bT \qquad (2)$$

where

$$a = \frac{\overline{\Delta H}}{(1-x)^2} = \text{constant}$$

$$b = \frac{\overline{\Delta S}^E}{(1-x)^2} = \text{constant}$$

$\overline{\Delta H} = a\,(1-x)^2$ = partial molar excess enthalpy of mixing of component A in elementary solutions

$\overline{\Delta S}^E = b\,(1-x)^2$ = partial molar excess entropy of mixing of component A in elementary solutions

γ = activity coefficient at composition x

Since the activity coefficients in the ideal solutions are equal to unity, the partial molar excess enthalpy and entropy are zero.

Calculation of the Latent Heat of Fusion

Using the liquidus data points from each DTA run an estimate for the latent heat of fusion of cadmium telluride at each data point was made using equation (1). The compound CdTe was chosen as component A. Cadmium was taken as component B in the system I, and tellurium was taken as component B in system II. On the tellurium-rich half of the system, the values of $\Delta H_f/R$ appear to be substantially independent of composition, and ideal solution behavior seems to be indicated.

On the cadmium-rich half of the diagram, the derived values of $\Delta H_f/R$ are not independent of composition, and the solution is non-ideal. At the composition CdTe the two segments of the curve apparently intersect at approximately the point where $\Delta H_f/R$ equals 5400, or ΔH_f = 10,700 cal/gm mol.

Theoretical Forms of the Liquidus Lines

By using the value of ΔH_f estimated above, a quantitive measure of the non-ideality of both binary systems can be obtained by calculating the activity coefficients and the functions defined in equation (2). From these calculations it again appears that the system (II) CdTe-Te is an ideal solution. The liquidus curve can be approximated by the expression

$$T = \frac{\Delta H_f}{\Delta S_f - R \ln x} = \frac{10,700}{7.80 - 1.987 \ln x} \qquad (3)$$

where x = mol fraction CdTe in Te = 2 (1-y)
y = atom fraction Te in Cd
$\Delta S_f = \Delta H_f/T_f$ = entropy of fusion, cal/gm.mol.°K.

It is also apparent that the system (I) Cd-CdTe forms an elementary solution, with

$$\alpha = 16,000 - 10.85\ T$$

i.e. $\overline{\Delta H} = 16,000\ (1-x)^2$ cal/gm mol

and $\overline{\Delta S^E} = 10.85\ (1-x)^2$ cal/gm mol°K

The liquidus curve in this region can be approximated by the expression

$$T = \frac{\Delta H_f + a\ (1-x)^2}{\Delta S_f + b(1-x)^2 - R \ln x} = \frac{10,700 + 16,000\ (1-x)^2}{7.80 + 10.85\ (1-x)^2 - 1.987 \ln x} \qquad (4)$$

where x = 2y mol fraction CdTe in Cd.

3.3 Calculation of Eutectic Compositions

The experimental melting point of CdTe (1371°K), the experimentally measured eutectic temperature on the tellurium side (723°K) and the derived latent heat of fusion (10,700 cal/mol) were used in equation (I) to predict the eutectic composition in the system (II) CdTe-Te. The predicted value of 0.986 atom fraction tellurium in cadmium indicates

that the eutectic should be distinguishable from pure tellurium. The same relationship can also be used to calculate the eutectic composition from the properties of pure tellurium. From its melting point (727°K) and latent heat of fusion (3230 cal/gm mol)[7] the eutectic composition is calculated to be x = .014, hence y = .993. We conclude that the eutectic lies at approximately 0.99 atom fraction Te.

In order to calculate the eutectic composition on the cadmium side from equation (4) the mol fraction of CdTe at the eutectic can be approximated as zero in all the terms except the logarithmic factor. Since the experimental eutectic temperature is known (595°K), the eutectic composition is calculated to be 10^{-6} atom fraction Te in Cd, which is experimentally indistinguishable from pure cadmium. However, our data would seem to indicate that the solidus transition temperature (322°C) is higher than the melting point of cadmium (321°C) and a peritectic pattern may be present. The liquidus curves and eutectic points derived above are plotted on Figure 1 along with all the experimental data, including that of deNobel[4] and Kobayashi.[2]

Slope and Curvature of the Liquidus Lines

The abrupt change in slope and curvature of the liquidus lines at the melting point of CdTe is also of interest. For system (II) CdTe-Te, the slope is obtained by differentiating equation (3). For the system (I) Cd-CdTe, the slope is obtained by differentiating equation (4). Evaluation of these derivatives indicates that the slope of the liquidus curve is discontinuous at the composition CdTe but symmetrical on either side as x approaches unity. The curvature of the liquidus curve is given by the second derivative of the T vs. x expressions. For the ideal solution system (II) CdTe-Te a moderately large negative value of the second derivative indicates that the liquidus curve should be convex upwards as x approaches unity (pure CdTe) from the tellurium side as shown on the right half of the diagram; i.e., as x increases the slope is decreasing.

In contrast, however, for the elementary solution system (I) Cd-CdTe we find the second derivative of the solution curve is positive at the melting point of CdTe. Hence this slope is positive and increasing, thus giving the observed curvature to the liquidus curve as x approaches unity from the cadmium side.

Acknowledgment

We are indebted to Dr. C. D. Thurmond for providing us with a preprint of his paper. A. M. G. D.

References

1. Thomassen, L., and Mason, D. R., "Phase Diagram for the Binary System CdTe-In_2Te_3," Abstract in J. Electrochem., 106, 206c (1959) Electrochemical Society, Fall Meeting, Columbus, Ohio, Oct. 21, 1959.

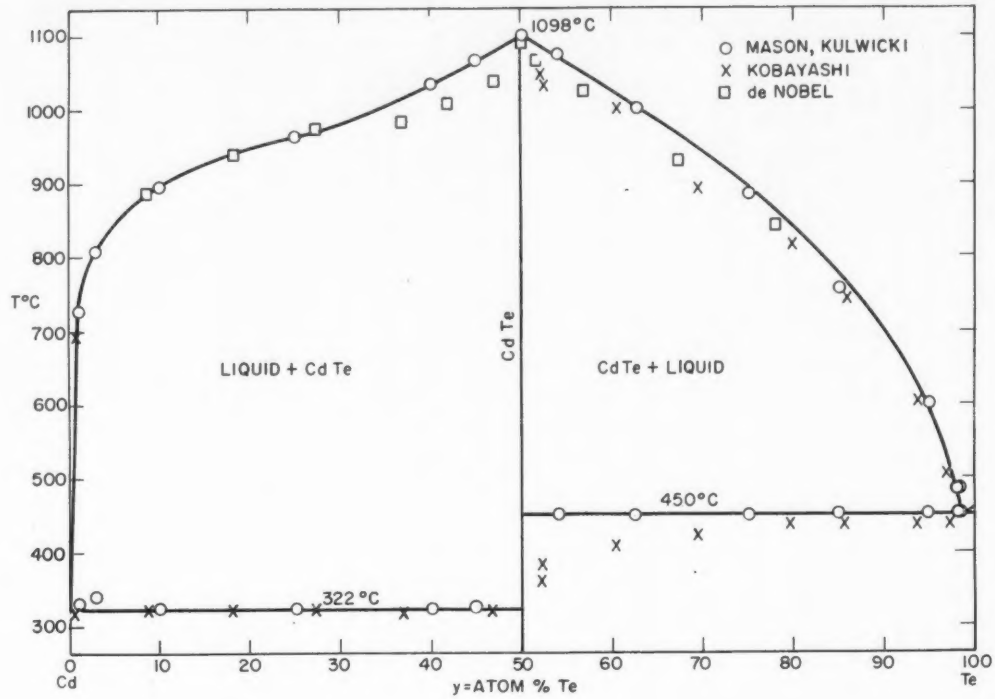
1098°C
MASON, KULWICKI
KOBAYASHI
de NOBEL
T°C
LIQUID + Cd Te
Cd Te
Cd Te + LIQUID
450°C
322 °C
y=ATOM % Te
Cd
Te

Figure 1

2. Kobayashi, M., "Uber die Legierundendes des Tellurs mit Cadmium und Zinn." Zeits. anorg. chem. 69, 1-9 (1910).

3. Lawson, W. P., Nielsen, S., Putley, E. H., and Young, A. S., "Preparation and Properties of HgTe and Mixed Crystals of HgTe-CdTe." J. Phys. Chem. Solids, 9, 325-329 (1959).

4. deNobel, D., "Phase Equilibria and Semiconducting Properties of Cadmium Telluride." Phillips Res. Repts. 14, 361-399 (1959).

5. Prigogine, I., and Defay, R., Chemical Thermodynamics p. 358, Longmans, Green & Company, New York. (1954)

6. Thurmond, C. D., and Kowalchik, M., "Germanium and Silicon Liquidus Curves." Bell System Technical Journal, in press, January 1960.

7. Perry, J. H., "Chemical Engineers Handbook." 3rd Edition, p. 212, McGraw-Hill, New York, (1950).

Figure 1

Abstract Number 94

EFFECT OF INHOMOGENEITIES ON THE HALL COEFFICIENT IN InSb*

R. T. Bate

Battelle Memorial Institute
Columbus, Ohio

Hall measurements have become a standard technique for the determination of carrier concentrations in semiconductors. Their use is based upon interpretation of the Hall coefficient by means of the relation

$$R = r/ne \tag{1}$$

for an extrinsic n-type semiconductor, where e is the electronic charge, n is the number of electrons per cm^3, and r is the "Hall coefficient factor," which is determined by the band structure and scattering mechanisms.[1] In weak magnetic fields, r may differ appreciably from unity but it is quite well established theoretically that r approaches unity for strong magnetic fields.[2] The dividing line between weak and strong fields is defined by the condition

$$10^{-8}\mu H = 1 \tag{2}$$

where μ is the carrier mobility in $cm^2/v\text{-}sec$ and H is the magnetic field intensity in gauss. Since the electron mobility in high purity InSb at 77°K is in the neighborhood of 5×10^5 $cm^2/v\text{-}sec$, magnetic fields strong enough to satisfy the strong field condition at this temperature are easily obtained. Thus, one would expect the strong field Hall coefficient to give an unambiguous value of the electron concentrations in this material.

This expectation is borne out in part by curve A of Figure 1, which shows a plot of the Hall coefficient of a sample of high purity n-type InSb at 77°K as a function of magnetic field. This sample was cut from a crystal whose growth axis was about 10° away from a <111> direction. The magnetic field was parallel to the growth axis. Note the saturation at strong fields and the increase with decreasing field to a weak field limit. Within experimental error, this behavior is the same as that predicted by a simple band model and the combination of two scattering mechanisms.[3] The excellent agreement of the shape of the curve with theory leaves little doubt that $r \to 1$ in strong fields for this sample.

*This work was supported by the U. S. Air Force through the Air Force Office of Scientific Research of the Air Research and Development Command.

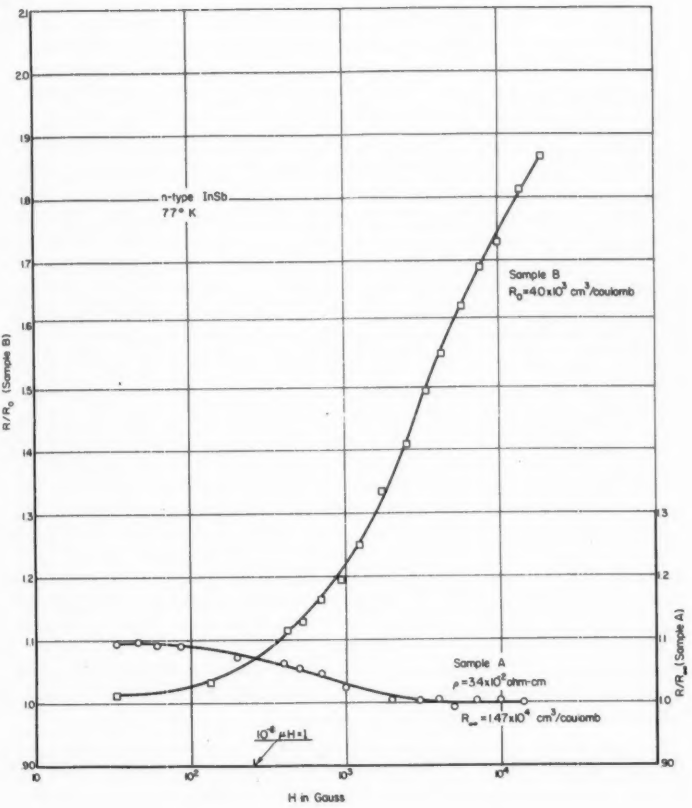

Fig. 1—Magnetic field dependence of the Hall coefficients of two samples of n-type InSb.

It should be emphasized, however, that the theoretically predicted saturation of the strong field Hall coefficient at unity depends on the assumption that the impurities in an extrinsic semiconductor are uniformly distributed. There are many reasons why a crystal grown from the melt may not be homogeneous. If the melt is well stirred, the difference in solubility of the impurity in the liquid and the solid will lead to segregation of the impurities along the direction of growth. If the melt is stirred by rotation, insufficient mixing at the center of the melt coupled with a rapid growth rate may produce radial impurity gradients in the crystal. In material which has been previously zone refined, however, one would not have expected these mechanisms to lead to strong impurity gradients, because the residual impurities left after zone refining should have distribution coefficients close to unity.

Recent studies of the segregation of donor impurities in InSb have disclosed, however, that the distribution coefficient of selenium, tellurium, and the residual donor, which is thought to be tellurium, in InSb are highly anisotropic.[4] This anisotropy, in combination with the formation of facets at the solid-liquid interface,[4] leads to the formation of "cores" of donor impurities in crystal grown in certain crystallographic directions. These cores are regions of high donor concentration which have relatively sharp boundaries. The concentration of donors in these regions can easily be a factor of ten larger than that outside.

Curve B of Figure 1 is a plot for a sample very similar to sample A, except that it was cut from a crystal grown along the <111> direction. The large change from weak to strong fields makes it impossible to estimate the carrier concentration or mobility from Hall measurements on such samples. It is believed that the striking difference between the two curves may result from the situations illustrated in Figure 2. Independent investigations[5] have shown that a slight misorientation of the seed crystal causes the donor (tellurium) core to be displaced to the side of the crystal as shown on the left in Figure 2, but that the core is usually near the center of the crystal as shown on the right when the growth axis is in the <111> direction. Thus, if sample A were cut out as shown, it would be fairly homogeneous, but sample B would contain two regions of very different donor concentration. It is hypothesized that this inhomogeneity is responsible for the peculiar behavior of the Hall coefficient in sample B.

Although the exact calculation of the Hall coefficient in an inhomogeneous sample requires the solution of a difficult boundary value problem, a semi-quantitative understanding of the observed effect can be gained from consideration of the special case illustrated in Figure 3. We consider a sample made up of two regions characterized by resistivities ρ_1 and ρ_2 and by Hall coefficients R_1 and R_2 respectively. Current flows along the x direction and the sample is situated in a magnetic field perpendicular to the plane of the figure. The Hall voltage V_H, is measured between points C and D which are situated at the intersections of the boundary between the two regions with the edges of the sample. If J_{x1}, J_{y1}, E_{x1}, and E_{y1} are the components of current density

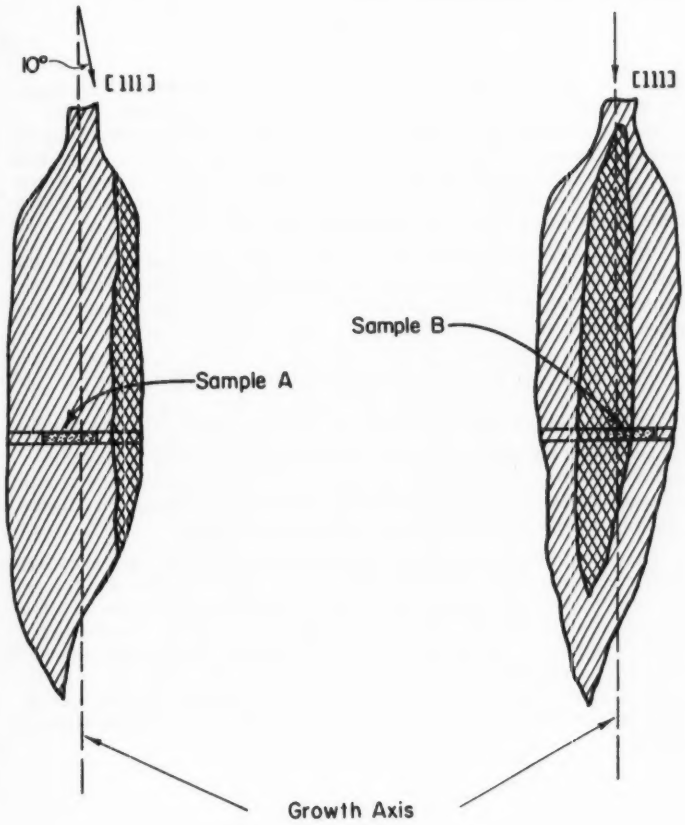

Fig. 2—Probable crystal configurations from which samples were cut.

and electric field at the boundary CD in region 1, and J_{x_2}, J_{y_2}, E_{x_2}, and E_{y_2} are the corresponding values at the boundary in region 2, then the problem can be solved approximately by assuming $J_{x_1} = J_{x_2}$, $J_{y_1} = -J_{y_2}$ and using the fact that $E_{y_1} = E_{y_2}$. With these assumptions, the measured Hall coefficient is simply

$$R' = \frac{\rho_1 R_2 + \rho_2 R_1}{\rho_1 + \rho_2} \tag{3}$$

Thus, the measured Hall coefficient is a function not only of the Hall coefficients in the two regions, but also of the resistivities. Since these resistivities are magnetic field dependent, they introduce an extraneous magnetic field dependence into the measured Hall coefficient R'. The equation predicts that R' is constant in weak magnetic fields and increases or decreases in strong fields depending on the magnetic field dependences of R_1, R_2, ρ_1 and ρ_2.

The necessary criterion for the observation of a characteristic like that of sample B in Figure 1 can be determined by differentiating the expression for R' with respect to H. Ignoring the magnetic field dependences of R_1 and R_2 we obtain

$$\frac{1}{R'}\frac{\partial R'}{\partial H} = \frac{\rho_1 \rho_2}{\rho_1 + \rho_2}\,\frac{R_2 - R_1}{R_2\rho_1 + R_1\rho_2}\left(\frac{1}{\rho_1}\frac{\partial \rho_1}{\partial H} - \frac{1}{\rho_2}\frac{\partial \rho_2}{\partial H}\right) \tag{4}$$

In order to observe characteristic B, we must have $\frac{1}{R'}\frac{\partial R'}{\partial H} > 0$, which requires that the region with the larger Hall coefficient (in absolute value) have the smaller magnetoresistance. If the two regions are uncompensated n-type, the requirement reduces to a magnetoresistance which increases with increasing donor concentration.

Thus, to predict the magnetic field dependence of the observed Hall coefficient in an inhomogeneous sample one has to know in detail how the intermediate and strong-field magnetoresistances behave as a function of impurity concentration in homogeneous samples. Magnetoresistance data[3] on high purity n-type InSb indicate that the dependence on impurity concentration at 77°K is in the proper direction and of the right magnitude for the model of Figure 2b to predict the behavior of sample B in Figure 1 if the proper ratio of impurity concentrations is assumed.

References

1. A. C. Beer, J. Phys. Chem. Solids 8, 507 (1959).
2. J. A. Swanson, Phys. Rev. 99, 1799 (1955).
3. R. T. Bate, R. K. Willardson, and A. C. Beer, J. Phys. Chem. Solids 9, 119 (1959).
4. See abstracts by J. B. Mullin and by W. P. Allred and R. K. Willardson in this issue.

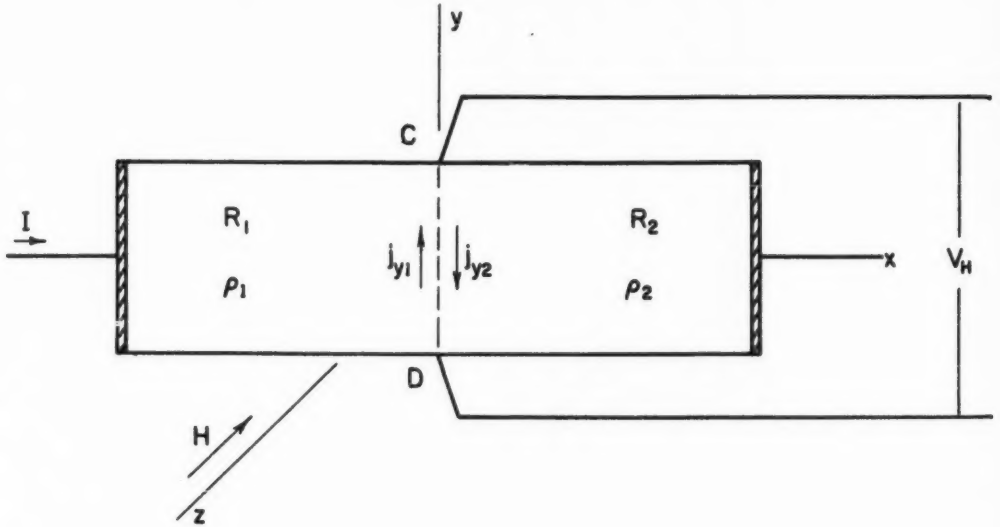

Fig. 3—Simplified model of Hall sample from which Hall coefficient is calculated.

5. W. Bardsley (Private communication). Some of these results were presented in a "recent news" paper entitled "Facets and Anomalous Distribution Coefficients in InSb" by J. B. Mullin and K. F. Hulme at the September 1959 meeting of the Electrochemical Society.

Abstract No. 95

PROPERTIES OF P-TYPE GaAs PREPARED BY COPPER DIFFUSION

F. D. Rosi, D. K. Meyerhofer and R. V. Jensen

RCA Labs., Radio Corporation of America
Princeton, N. J.

Purification of arsenic by hydrogen sublimation and gallium by vacuum annealing resulted in the preparation of high resistivity (10^6 ohm-cm), n-type GaAs crystals by the horizontal Bridgman technique. Conversion of this material to p-type was accomplished by the inward diffusion of copper from the crystal surface. Measurements of Hall mobility as a function of hole concentration in the range, 2×10^{16} cm^{-3} to 3×10^{17} cm^{-3}, at room temperature showed a dependence which is consistent with theory. The analysis suggests a lattice mobility for holes of 450 $cm^2 V^{-1}$ at 300°K. The mobility varied approximately as $T^{-2.3}$ in the range 76° - 300°K. At the low temperatures the number of ionized impurities ranged from 2×10^{15} cm^{-3} to 1×10^{16} cm^{-3}. The energy levels associated with copper in GaAs are 0.023 ev and 0.15 ev above the valence band.

Abstract Number 96

PREPARATION AND PROPERTIES OF ZnSb*

R. C. Bourke, R. Simon, and E. H. Lougher

Battelle Memorial Institute

Because of the existence of a peritectic in the Zn-Sb system, precautions must be taken in the preparation of ZnSb. A normal, slow, directional freeze would, of course, result in extensive segregation and a resultant inhomogeneous specimen. The compound was, therefore, prepared by two different methods; a modified hot-pressing technique and a more common quench-and-anneal process. Hot-pressed specimens were found to be more homogeneous than those prepared by quenching and annealing. However, the electrical properties of the two materials are similar, although the mobility of the hot-pressed material is slightly higher. A specimen of stoichiometric, hot-pressed ZnSb had a room-temperature resistivity of 0.6 ohm-cm, thermoelectric power of +700 $\mu V/^{\circ}K$ and Hall mobility of 220 cm^2/volt-sec, values higher than have been reported previously for ZnSb. Lead doping, even to the point of saturation, failed to substantially affect the Hall coefficient of the compound. Tin, however, was found to be an effective p-type doping agent.

The electrical resistivity and Hall coefficient data as functions of temperature in the range of 77°K to 450°K indicate the onset of intrinsic behavior for the higher resistivity specimens at about room temperature. Analysis of the data yields a band gap of 0.32 ev at 0°K. Preliminary optical data at room temperature and 77°K, however, show the principal absorption edge to be at about 0.6 ev, with a negative temperature coefficient. The difference between the electrical and optical data is being investigated further, with special consideration being given to implications of a complicated band structure.

Preparation

High-purity zinc (99.999 per cent) and antimony (99.9999 per cent) were used in preparing the compound. All specimens were prepared by reacting stoichiometric amounts of the elements (at 580°C) in previously cleaned, evacuated, quartz ampoules. The ampoules were sealed at a pressure of 1×10^{-6} mm of Hg or lower.

*Supported by the Thermoelectric Cooling Research Group.

The hot-pressed specimens were prepared in the following manner. To prevent extensive segregation, the molten material was quenched to room temperature by quick immersion of the ampoule in an oil bath. The resultant specimen was then ground to a fine powder with an Alundum mortar and pestle in an argon-filled dry box. The powder was placed in a 1/2-inch pre-outgassed graphite die which was then quickly transferred to the hot press system shown in Figure 1. The system was alternately evacuated and filled with dry argon several times. An atmosphere pressure of argon was then maintained during the hot pressing. The die was heated inductively to 530°C under a pressure of 5000 psi for 15 to 20 hours. Satisfactory specimens were obtained by this method and, thus, no extensive effort was made to determine the optimum hot-pressing conditions. All stoichiometric ingots were single-phase, compact material having a density of better than 99 per cent of that calculated from X-ray data, 6.363 g/cm^3. However, the average grain size was found to be fairly small, 40 to 50 microns.

Several methods of preparation of the quench-and-anneal material were tried. However, the most homogeneous, solid specimens were obtained by quenching the molten material at a temperature (~540°C) just below the fusion range, to prevent extensive segregation of the peritectic phases, and then programming the temperature of the ingot down at approximately 10 degrees per hour to an annealing temperature of 480°C. The ingot was annealed at this temperature for 24 hours and then was cooled to room temperature at the same rate. The slow cooling was employed to prevent cracking of the ingot as observed in quenched ingots.

The effects of Sn and Pb additions on hot-pressed and quenched-and-annealed material were studied. The doping agents were added directly to the material prior to reaction.

Contrary to the results of the work by Deviatkova,[1] Pb-doping, even to the point of saturation, failed to substantially affect the resistivity of the compound. Tin, in contrast to lead, apparently is a suitable p-type doping agent. Table 1 illustrates the effects of the two doping agents on the room-temperature resistivity of ZnSb. All the quenched-and-annealed specimens contained small amounts of Zn-rich and Sb-rich phases, while the hot-pressed ingots were all single-phase ZnSb, except for those specimens in which the solubility of the doping agent was exceeded (2 per cent Pb and 1 per cent Sn).

ELECTRICAL AND OPTICAL MEASUREMENTS

Measurements were made of the electrical resistivity, Hall coefficient, and thermoelectric power of the stoichiometric hot-pressed, the 0.5 mole per cent ZnPb hot pressed, the stoichiometric quenched and annealed, the 1 mole per cent ZnSn quenched and annealed, and the 2 mole per cent ZnSn quenched and annealed specimens (specimen Numbers 1, 5, 9, 10, 12, of Table 1, respectively) in the temperature range of 77°K to 475°K.

The Hall coefficients for Specimens 1, 5, and 9 are not quite constant in the extrinsic range, but decrease gradually as the temperature is increased above 77°K until the onset of intrinsic conduction at about room temperature. The Hall coefficients for specimens 10 and 12 are essentially constant over the entire temperature range. The carrier concentrations at about 77°K are 3.5, 4.6, and $12.2 \times 10^{16}/cm^3$ for Specimens 9, 1, and 5, respectively, and those of Specimens 10 and 12 are 1.2 and $1.6 \times 10^{19}/cm^3$, respectively.

The Hall mobilities for Specimens 1, 5, and 9 show about a $T^{-1.1}$ dependence with temperature over the entire extrinsic range. The Hall mobility of the heavily-doped specimen 10 has a $T^{-0.5}$ dependence, whereas that of the other heavily-doped specimen (12) does not have a simple exponential temperature dependence. The curve of log (R_H/ϱ) as a function of log T for specimen 10 has a slope of about -0.5 at the low temperature and a slope of about -1 at the high temperature end. The corresponding curve for specimen 12 has a slope that varies from about 0 to about -1 from the low to the high ends of the temperature range, respectively. The somewhat weaker temperature dependence of mobility than the standard $T^{-1.5}$ for scattering on thermal lattice vibrations might be accounted for by some amount of impurity scattering for specimens 1, 5, and 9. An appreciable contribution of ionicity to the lattice binding would also tend to give the observed effect. Large contributions from impurity scattering probably account for the observed mobility behaviors of the Sn doped specimens.

From the known concentration of acceptors and known variation of the mobility of the holes with temperature extrapolated into the intrinsic region, the concentrations of both carriers, n_e and n_h, as functions of temperature in the intrinsic region can be computed from the Hall coefficient and resistivity data. The plot of log $n_e n_h/T^3$ as a function of T^{-1} for the stoichiometric specimens is a straight line. The energy gap between the bottom of the conduction band and the top of the valence band at 0°K computed from the slope of this line is 0.32 ± 0.02 ev. The square root of the product of the effective masses of the holes and of the electrons is computed to be 0.2 times the mass of the free electron, essentially independent of temperature from room temperature up to about 150°C, under the assumption that the energy gap has a negligible temperature dependence.

Preliminary optical measurements at 77°K and room temperature show an absorption edge at about 0.6 ev with a negative temperature coefficient. This value is just about double the energy of thermal excitation of electrons into the conduction band. Investigations are in progress to interpret the optical data in terms of direct and indirect transitions, and to ascertain whether the apparent difference between the thermal and the optical values for band separation can be explained in terms of specialized band structure.

The thermoelectric powers for Specimens 1, 5, and 9 vary from approximately 700μV/deg C at room temperature to about 400μV/deg C at 77°K. The thermoelectric powers for Specimens 10 to 12 vary from about 200μV/deg C down to about 100μV/deg C over this temperature

TABLE 1. EFFECTS OF Sn AND Pb ON ROOM-TEMPERATURE RESISTIVITY OF ZnSb.

Specimen Number	Composition[a]	Room Temperature Resistivity, ohm-cm	Method of[b] Preparation
1	Stoichiometric	0.65	HP
2	0.1 at % Pb	0.65	HP
3	0.5 at % Pb	0.64	HP
4	0.1 mole % ZnPb	0.50	HP
5	0.5 mole % ZnPb	0.26	HP
6	2.0 mole % ZnPb	0.10	HP
7	1.0 mole % ZnPb	0.14	QA
8	2.0 mole % ZnPb	0.06	QA
9	Stoichiometric	0.63	QA
10	1.0 mole % ZnSn	4.3×10^{-3}	QA
11	1.0 mole % ZnSn	3.6×10^{-3}	HP
12	2.0 mole % ZnSn	5.2×10^{-3}	QA

(a) The notations ZnPb and ZnSn imply only that the Pb or Sn was added as a substitute for the Sb, and not that such compounds actually exist.

(b) HP = hot pressed; QA = quenched and annealed.

range. Analysis of the thermoelectric power data by standard techniques yields a value of the effective mass of the holes in the valence band that ranges from 0.2 free electron masses at 77°K, to 0.4 electron masses at about 200°K and up to 0.5 electron masses at 250°K.

Since the temperature dependence of the mobility is approximately constant over the above temperature interval, it does not appear that the nature of the charge carrier scattering mechanism has changed significantly in going from 77° to 250°K. Therefore, the apparent variation of m_h with temperature may be another indication of complex band structure.

The thermal conductivity of Specimen 10 is measured to be 0.018 watts/deg K-cm at room temperature, resulting in a thermoelectric figure of merit of 0.6×10^{-3}/deg K. Since the electrical resistivity is known, the phonon contribution to the thermal conductivity can be estimated. This enables an approximate analysis to be made of the figure of merit to be expected for various degrees of doping of ZnSb. The result is that the doping represented by Specimen 10 is not far from optimum.

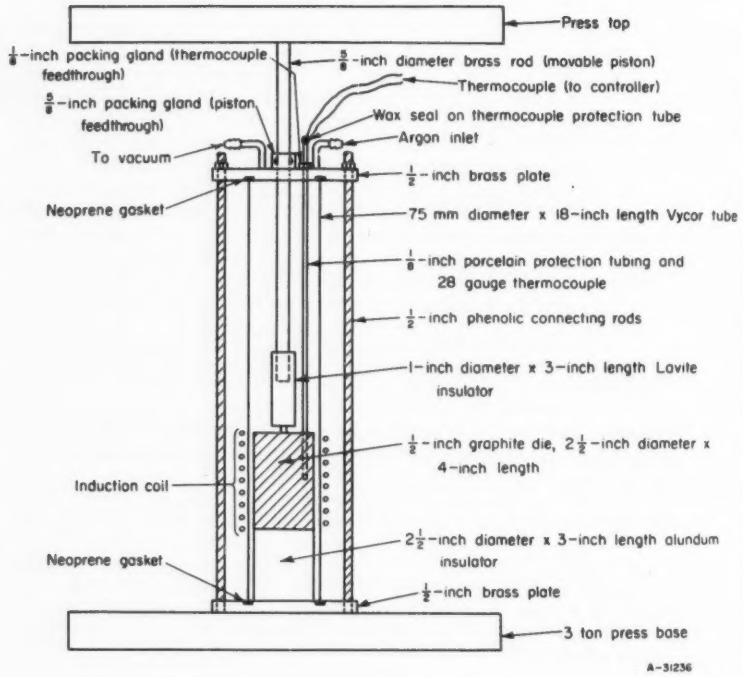
Press top
1/8-inch packing gland (thermocouple feedthrough)
5/8-inch diameter brass rod (movable piston)
Thermocouple (to controller)
5/8-inch packing gland (piston feedthrough)
Wax seal on thermocouple protection tube
Argon inlet
To vacuum
1/2-inch brass plate
Neoprene gasket
75 mm diameter x 18-inch length Vycor tube
1/8-inch porcelain protection tubing and 28 gauge thermocouple
1/2-inch phenolic connecting rods
1-inch diameter x 3-inch length Lavite insulator
1/2-inch graphite die, 2 1/2-inch diameter x 4-inch length
Induction coil
2 1/2-inch diameter x 3-inch length alundum insulator
Neoprene gasket
1/2-inch brass plate
3 ton press base
A-31236

Fig. 1—Hot-Press System

References

1. Deviatkova, E. D., Maslakovets, In. P., and Stilbans, L. S., Zh. Tekh. Fiz., 22 (1), 129-42 (1952).

Abstract No. 97

THE PREPARATION AND PROPERTIES OF GALLIUM PHOSPHIDE*

C. J. Frosch, M. Gershenzon and D. F. Gibbs**

Bell Telephone Laboratories, Incorporated
Murray Hill, New Jersey

The high decomposition pressure of phosphorus at the melting point of gallium phosphide requires the development of modified techniques[1,2] for producing large single crystals under controlled conditions. This talk will describe (1) a pressure chamber for producing large multicrystalline ingots of gallium phosphide at high phosphorus pressures, (2) the present status of an investigation of the floating zone technique for growing single crystals of gallium phosphide at high phosphorus pressures from these ingots and (3) some of the properties of these materials.

The pressure chamber consists essentially of a heavy wall steel cylinder with suitable end closures for pressurizing with argon. A controlled furnace on each side of a high frequency heating coil provides the minimum temperature zones for regulating the phosphorus pressure. An externally controlled drive shaft provides the movement for the reaction vessel. Windows at the center of the pressure chamber permit observations and temperature measurements during the processing. The pressure assembly is mounted on a swivel to allow either horizontal or vertical operation.

The ingot reaction vessel consists of an evacuated quartz tube containing a 40-50 gram charge of gallium in a quartz, graphited quartz or graphite boat. It also contains a weight of phosphorus which is in excess of that required to react with all of the gallium and to maintain the desired phosphorus pressure calculated as P_4. An argon pressure of 10 atmospheres above the phosphorus pressure in the reaction vessel is maintained throughout the run.

In making an ingot the minimum temperature furnaces are brought to control before one end of the gallium sample boat is raised to the reaction temperature. Then the reaction vessel is moved slowly through the high frequency heating coil. The boat temperature is lowered to about 900°C before returning the vessel to the starting position for additional passes.

---

*Some of this material was presented at a symposium on III-V compounds at Battelle Memorial Institute on November 4, 1959.

**Now at H. H. Wills Physics Laboratory, Bristol, England.

Large solid ingots generally cannot be produced in quartz or graphited quartz boats. The boats and ingots usually crack during the first pass due to sticking and expansion of the gallium phosphide during solidification. The cracking of the boat does not permit a second pass which seems necessary for the consistent production of solid ingots. Large gallium phosphide ingots now are produced consistently in graphite boats at temperatures of about 1500°C or higher, phosphorus pressures from 6 to 30 atmospheres with feed rates of .50 mm/min or less for the first pass and .75 mm/min or less for the second pass. The ingots produced in graphite boats usually are transparent with a light yellow to dark amber color. These often contain fairly large single crystals.

Small bars cut from the multicrystalline ingots are employed in the investigation of the floating zone technique for growing controlled single crystals of gallium phosphide. These are enclosed in an evacuated quartz envelope with suitable quartz supports for centering. The envelope also contains a sufficient quantity of free phosphorus to provide the required pressure calculated as P_4. The phosphorus pressure is controlled by either a minimum temperature as in the case of the ingot preparations or an exact weight of phosphorus based on the internal void volume of the quartz envelope.

In the initial floating zone experiments a film having the approximate composition of gallium phosphide began to deposit on the envelope walls before a molten zone could be initiated in the bar. This effect, referred to as fogging, greatly reduced the visibility of the bar especially with increasing time and temperature. Direct observation of the bar and hence control of the molten zone became increasingly more difficult even during a single floating zone pass. These runs usually were lost either because of failure to produce a molten zone or separation of the bars by collapse of the molten zone. Fogging is greatly reduced or eliminated by heating the envelope walls to about 950°C or higher during the floating zone operation. This is accomplished by bringing two high temperature furnaces very close to the high frequency coil. Under these conditions excellent visibility of the bar is retained even after several floating zone passes.

Up to five floating zone passes have been made in gallium phosphide bars at phosphorus pressures from 6 to 22 atmospheres. These bars generally were quite non-uniform in cross-section after processing. However, more uniform bars are gradually being obtained with experience and modifications in the high frequency coils. Bars processed at phosphorus pressures of about 10 atmospheres or lower generally contain opaque regions with tiny bubbles just beneath their surface. The bubbles often contain free gallium which also is present on the surface of these bars. Bars processed at 10 to 22 atmospheres phosphorus pressure are transparent with no free gallium except in the last molten zones which were frozen very rapidly. This indicates that the equilibrium phosphorus pressure for a stoichiometric melt may be above 22 atmospheres. While single crystals have not yet been produced by the floating zone method, enhancement of the crystal size is

evident and seeding seems feasible. The current status of this development will be described.

The molten zone is visible for control because of a lower emissivity than the immediately adjacent solid bar. The apparent temperature difference is about 40°C. At 22 atmospheres phosphorus pressure a temperature of 1430°C has been measured immediately adjacent to a narrow molten zone. A probable emissivity correction and the previously mentioned non-stoichiometric composition places the maximum melting point above this figure.

The most recent electrical measurements on gallium phosphide ingots and floating zone purified bars will be presented. A very appreciable purification is shown to result during the floating zone processing.

References

1. J. van den Boomgaard and K. Schol, Philips Res. Rep., 12, 127 (1957).

2. J. M. Whelan and G. H. Wheatley, Phys. and Chem. of Solids, 6, 169 (1958).

PREPARATION AND CHARACTERISTICS OF p-n JUNCTIONS IN GALLIUM PHOSPHIDE

M. Gershenzon and R. M. Mikulyak

Bell Telephone Laboratories, Inc.
Murray Hill, New Jersey

Both diffused and alloyed diodes have been prepared from single crystals of 0.01 to 10 ohm-cm GaP grown at temperatures and pressures close to their equilibrium melting point values.[1] Diffusion at 800°C., where the decomposition rate of GaP is slow although its vapor pressure is ~10mm Hg, has been successfully used to prepare junctions. The maximum operating temperature of such structures is limited by the mobility of the diffusant. For example, zinc, with a diffusion constant of 10^{-7} -10^{-6} cm^2 sec^{-1} at 700-800°C., becomes sufficiently mobile at 500° to degrade the junctions. Alloyed diodes prepared by using Ag-1% Zn alloys or Ag-1% Te mixtures produce rectifying contacts to n and p type material respectively, and exhibit regrowth layers ~1 micron thich then fabricated at 800-900°C. in a hydrogen atmosphere. In all cases ohmic contact was established by alloying.

The diode properties classify the junctions into three groups: diffused diodes, slowly alloyed diodes (1-5 minute alloying cycle), and rapidly alloyed diodes (molten alloys quenched after ~5 seconds). The diffused diodes exhibit breakdowns to 35 volts. Forward currents and reverse currents beyond breakdown become limited by a series ohmic junction resistance of ~ 1 mho/cm^2 . Room temperature rectification ratios up to 3×10^6 are observed, the reverse current increasing tenfold for a 200° temperature increment while the forward current increases much more slowly. The rapidly alloyed diodes break down at 5-10 volts, show no series resistance, exhibit rectification ratios of 10-10^3, and lose their rectifying properties between 300 and 500°C. The slowly alloyed diodes are intermediate in behavior between the two other types, presumably due to an inevitable small amount of diffusion. Alloyed diodes, prepared with 10^3 ohm-cm GaP whiskers grown from the vapor phase, were characterized by breakdown potentials as high as 135 volts. From the voltage dependence of the capacity in the reverse direction it is deduced that all the junctions are abrupt.

Several types of deviations from ideal junction behavior are apparent, and are most pronounced in the rapidly alloyed units. The forward currents depend exponentially upon bias. However, the exponents are up to a factor of 10 lower than that expected for an ideal diode. Reverse currents do not saturate, but increase with potential and temperature as follows. $I = kV^n \exp(-\theta/T)$ k, n and θ are constants with n

lying in the range 1 to 3, the higher values being appropriate for the diffused diodes. This current is accompanied by light emission covering the entire visible spectrum. It cannot be attributed to surface conduction. As the reverse bias is increased the depletion layer capacity becomes dominated by a rapidly rising temperature and frequency dependent component. Finally, abrupt changes in the steady-state operating parameters lead to recovery times up to about one minute.

The series junction conductance, which occurs only in the vicinity of the junctions prepared by diffusion increases linearly with the area of the junction and has never been noted unless the diffusion results in an inversion of the majority carrier type. It is attributed to the formation of a compensated layer at the junction because the diffusions are performed at temperatures where GaP is extrinsic and consequently the solubilities of electrically-active impurities are governed by the initial concentration of donors and acceptors. The temperature dependence of this resistance primarily reflects the ionization of a built-in donor state previously reported.[1]

The remaining anomalies are presumed due to the existence of recombination-generation centers within the transition region. The presence of such centers has been deduced from Hall Effect measurements, photoluminescence, electroluminescence, and photoconductivity. These sites permit recombination within the transition layer at forward bias, thereby decreasing the dependence of current upon voltage. Carrier generation at these centers leads to the non-saturating reverse current and to the excess capacity at reverse bias. The transient effects reflect the life-times of the traps since they are due to the repopulation of the levels as the bias and consequently the quasi-Fermi levels are abruptly altered.

The breakdown fields, determined by extrapolating the normal depletion layer capacities through the region of anomalous behavior, lie in the range 10^5 to 10^6 volts/cm. Breakdown in the diffused diodes occurs by an avalanche mechanism via microplasmas. Broad band light emission, including photon energies considerably greater than the band gap, is directly proportional to the number of observed microamps. Current noise at breakdown is caused by the discrete appearance of these microplasmas as the bias is increased. The reverse breakdown of these microplasmas as the bias is increased. The reverse breakdown characteristic of the rapidly alloyed diodes is much softer than that corresponding to the diffused structures. A similar light emission spectrum is observed originating from spots, but these are frequently of macroscopic size. In this case the light intensity from each spot is a function of the bias and the total light intensity is no longer simply related to the number of luminescent areas. Tunneling through local inhomogeneities in the space charge field is proposed to account for this type of behavior.

Reference

1. C. J. Frosch, M. Gershenzon and D. F. Gibbs - Symposium on "Preparation of Single Crystals of the III-V Compounds" - Battelle Memorial Institute, Columbus (1959).

Abstract Number 99

PREPARATION AND PROPERTIES OF GROWN P-N JUNCTIONS OF InSb*

H. C. Gorton, A. R. Zacaroli, and F. J. Reid

Battelle Memorial Institute
Columbus, Ohio

Grown p-n junctions of InSb have been prepared by adding zinc to high purity melts. The crystals were pulled in an atmosphere of hydrogen (purified by diffusion through palladium) from zone-refined InSb which was vacuum heat-treated at about 530°C prior to pulling. P-type impurities were removed by evaporation during the heat treatment. In producing a junction, a portion of the n-type melt was pulled and the crystal was removed from the melt to allow for the addition of a small quantity of InSb containing about 10^{19} zinc atoms/cm^3. Time was allowed for the zinc to become evenly distributed through the melt, after which the pulling was resumed. Several crystals containing grown junctions were prepared by this method. Bridge-type Hall samples were cut from the crystal about 2 millimeters from either side of the junction. These samples were used to obtain the electrical characteristics of the bulk n- and p-type materials. Material on the n-type side of the junctions had electron mobilities greater than 350,000 cm^2/volt-sec at 77°K and carrier concentrations in the 10^{14}/cm^3 range. Carrier concentrations of material on the p-type side of the junctions were varied from 10^{14} to 10^{18}/cm^3.

The p-n junction regions of the crystals were diced, and electrical contacts to the p- and n-type sides of the diodes were formed by alloying electrodeposited films of gold to the InSb. Specific contact resistances achieved were on the order of 0.035 ohm cm^2 at 77°K.

Current-voltage characteristics were obtained at selected temperatures between that of pumped-on nitrogen and the intrinsic temperature of the material. The reverse characteristic at 70°K was ohmic, indicative of the predominance of leakage currents. Peak inverse voltages were near 5 volts. The exponential portion of the forward characteristic at 70°K between 0.1 and 0.18 volts extended from 10^{-5} to 10^{-2} amp, with a slope of q/1.7 KT. The reverse current at a constant voltage was obtained as a function of temperature between 55°K and 170°K. The temperature dependence of the reverse current was exponential with a

*This research was supported by the Electronics Components Laboratory, Wright Air Development Center.

slope of 0.025/KT below 120°K and 0.2/KT above 120°K. The small value of the slope of the curve below 120°K is attributed to the predominance of leakage current in the reverse direction.

The lifetime of minority carriers in the junction region was determined at liquid nitrogen temperature by the open circuit voltage decay method, and values near 25 millimicroseconds were obtained.

Abstract Number 100

THE INFLUENCE OF CRYSTAL SIZE ON THE SPECTRAL RESPONSE LIMIT OF EVAPORATED PbTe AND PbSe PHOTOCONDUCTIVE CELLS

W. D. Lawson, F. A. Smith* and A. S. Young

Royal Radar Establishment, Malvern

The sensitive layer in photoconductive layer cells is usually prepared by an evaporation or chemical deposition process followed by some sensitising process, e.g. a heat treatment in oxygen and/or vacuo. The sensitivity and spectral response of such layers depend markedly on the preparation and sensitising treatment, and although some very sensitive cells have been prepared the processes employed are mainly empirical[1] and the precise effect of each stage in the treatment is not always clear. This paper shows that the long wavelength limit of spectral response of PbTe and PbSe cells is related to the size of the crystals in the layer and can be controlled by controlling crystallite size. If the deposition process gives a layer with small crystals the spectral response is initially restricted to shorter wavelengths; subsequent heat treatment promotes growth of the crystals with a corresponding extension of response to longer wavelengths.

A series of lead telluride cells were prepared by an evaporation process[2]. During deposition the glass substrates on which the layers were formed were held at different temperatures, from 90°K to 720°K, in order to produce layers with different mean crystallite sizes. Each layer was about a micron thick. Spectral responses were measured using a Leiss double monochromator[3] fitted with rock salt prisms. The output beam, chopped at two independent frequencies, 5 c.p.s. and 800 c.p.s., was split into two halves, one of which was fed to a thermocouple in a servosystem to control the aperture of the input slit and maintain constant energy output from the monochromator over the wavelength range 1 to 7 microns. The thermocouple responded to the 5 c.p.s. chopping frequency. The other half of the beam was deflected to the cell under test and the 800 c.p.s. signal developed was amplified[4] and fed to a pen recorder.

After the spectral responses were measured, the structure of the layers was examined by X-ray diffraction and electron microscopy. Preshadowed aluminum replicas were used for the E.M. study since

*A.E.R.E. Harwell.

the layers themselves were too thick for electrons to penetrate. The size of crystals in the layers could be observed directly from the electron micrographs and were confirmed by the broadening of the lines in X-ray Laue photographs.

It was found that layers formed on the colder substrates had smaller crystallite sizes as expected, and their spectral responses did not extend over the full wavelength range possible for PbTe (5.8/u) but terminated at shorter wavelengths. The spectral response showed a progressive extension to longer wavelengths with increase in crystal size and the results indicate that the full wavelength response to 5.8/u is only achieved when the crystals are greater than a critical size—between a quarter and half a micron. One cell, H14, formed at 90°K showed small crystals and a short wavelength response only, but after subsequent heat treatment its response extended to 5.8/u and X-ray and E.M. photographs showed that the crystal size had increased.

Similar results have been obtained with PbSe layers prepared in the same way, and in particular the response of cells prepared at 90°C has been extended to progressively longer wavelengths up to the limit of about $7/u^5$ by subsequent heat treatment at increasing temperatures.

References

1. T. S. Moss. Proc. I.R.E. 43, 1869, 1955.
2. A. S. Young. J. Sci. Instr. 32, 142, 1955.
3. V. Roberts. J. Sci. Instr. 29, 134, 1952.
4. D. A. H. Brown. J. Sci. Instr. 29, 292, 1952.
5. A. F. Gibson, W. D. Lawson, T. S. Moss. Proc. Phys. Soc. A 64, 1054, 1951.

Abstract Number 101

ON THE MECHANISM OF CHEMICALLY ETCHING GERMANIUM AND SILICON

Dennis R. Turner

Bell Telephone Laboratories, Incorporated
Murray Hill, New Jersey

Chemical etching of metals and semiconductors is really electrochemical in its action, i.e., there are local anode and cathode areas on the surface with a current flowing between them. The magnitude of this current determines the etch rate. The corrosion current density on silicon, for example, as determined from etch rate data of Robbins and Schwartz,[1] can be as high as 190 amperes per cm^2. Yet when n-type silicon is made the anode in an electrolytic cell, the surface etches very slowly since the maximum current density is just a few $\mu A/cm^2$. Brattain and Garrett[2] showed that holes were required to carry out the anodic dissolution of semiconductors and the limiting current density was due to hole depletion at the surface. This suggests that there must be a large source of holes at the surface of the semiconductor during chemical etching.

The mechanism of chemical etching was studied by means of single electrode potential measurements on n- and p-type Ge and Si in both etching and nonetching solutions. In nonetching solutions, the electrode potentials of Ge and Si do not vary with conductivity type or resistivity, but in etching solutions they do vary. The relation between the electrode potential of Ge dipping in HNO_3-HF acid mixtures and the equilibrium hole density is shown in Figure 1. The electrode potential is a logarithmic function of the equilibrium hole density up to about 10^{16} holes per cm^3. With strongly p-type Ge, $p_0 > 10^{16}$ holes/cm^3, the potential varies only slightly with hole density. Similar results are obtained for p-type silicon. N-type Si, however, differs from n-type Ge in that the electrode potential does not vary with resistivity. The reason for this behavior is as yet unknown. The rate of etching and the physical condition of the surface are also factors which influence the measured electrode potentials of Ge and Si.

The potential changes that occur at Ge and Si electrodes in etching solutions are similar to those obtained when Ge and Si electrodes dipping in nonetching electrolytes are illuminated with light. Light produces hole-electron pairs in the surface region of the semiconductor and the electrode potential changes observed are readily explained by the changes that occur in the concentration of the minority charge carriers in the surface region.[2] Since chemical etching produces similar potential changes, it is assumed that excess holes and electrons are

produced at the surface during etching. Other observations tend to support this interpretation: (1) the photovoltaic effect on Ge and Si electrodes disappears even at moderate rates of etching, (2) the rectifying characteristic of a broad-area pn junction is completely eliminated if either side of the junction is exposed to a chemical etching solution, and (3) the saturation current density of n-type Ge or Si made anodic in an etching solution increases in proportion to the rate of chemical etching. These effects can be explained satisfactorily only by assuming that large numbers of holes and electrons are produced at the surface of semiconductors during chemical etching.

The mechanism of chemically etching Ge and Si must include a source of excess holes and electrons. Silicon dissolution takes place at local anode sites while the oxidizing agent is reduced at local cathode sites. The anodic reaction on silicon, for example, in HNO_3-HF acid mixtures is as follows:

$$\mathrm{Si} + 2\mathrm{H_2O} + n\mathrm{e}^+ \rightarrow \mathrm{SiO_2} + 4\mathrm{H}^+ + (4-n)\mathrm{e}^- \xrightarrow{6\ \mathrm{HF}} \mathrm{H_2SiF_6} + 2\mathrm{H_2O}, \tag{1}$$

where e^+ represents a hole and n is the average number of holes required to dissolve one silicon atom; n may range from 2 to 4 depending on the current multiplication factor.[2]

The main function of the oxidizing agent in the chemical etching solution is not ot oxidize the semiconductor as is sometimes proposed[1] (Ge and Si are readily oxidized in most oxygen-containing systems), but to provide an easily reduced material for the cathode reaction. The electron transfer process in the reduction of an oxidizing agent on Ge or Si involves the transfer of an electron from the valence band to the ion being reduced which is equivalent to hole injection. This concept was formulated independently by Gerischer and Beck[3] and Dewald.[4]

The reduction of nitric acid is a complicated reaction involving many steps. The over-all reaction of the reduction of nitric acid at cathodic sites on Ge or Si during chemical etching in HNO_3-HF acid mixtures can be written as follows:

$$\mathrm{HNO_3} + \mathrm{H}^+ \rightarrow \mathrm{NO_2} + \mathrm{H_2O} + \mathrm{e}^+ \tag{2}$$

The holes required for the anode reaction, therefore, are supplied by the cathode reaction.

The over-all reaction for chemically etching silicon in HNO_3-HF mixtures obtained by combining the reactions at local anodes and cathodes (Equation 1 plus 4 times equation 2—to maintain charge balance) is

$$\mathrm{Si} + 4\mathrm{HNO_3} + 6\mathrm{HF} \rightarrow \mathrm{H_2SiF_6} + 4\mathrm{NO_2} + 4\mathrm{H_2O} + n\mathrm{e}^+ + n\mathrm{e}^- \tag{3}$$

A similar set of equations can be written for etching Ge in the same solution. In the course of dissolving one Si atom in HNO_3-HF mixtures, 4 molecules of HNO_3 and 6 of HF are used up. This ratio of HNO_3 to HF is the solution composition that gives the maximum etching rate on silicon.

With more HNO_3 and less HF, the rate of etching is controlled by the diffusion and convection of HF to the silicon. The arrival of HNO_3 at the surface becomes rate determining when less HNO_3 and more HF than the 4 to 6 ratio is present in the solution bulk.

The number of excess holes and electrons produced in chemically etching silicon and germanium depends on the rate of etching and the current multiplication factor ($\alpha = \frac{4}{n}$) in the anode reaction. If n is 2, then $\alpha = 2$; but if 4 holes are consumed in dissolving a Si or Ge atom, then $\alpha = 1$ and no excess holes and electrons are produced. Potential measurements on Ge and Si electrodes indicate that $\alpha > 1$, since the potential is a function of the conductivity type and resistivity.

References

1. H. Robbins and B. Schwartz, J. Electrochem. Soc., 106, 505 (1959).
2. W. H. Brattain and C. G. B. Garrett, Bell System Tech. J., 34, 129 (1955).
3. H. Gerischer and F. Beck, Z. Phys. Chem., 13, 389 (1957).
4. J. F. Dewald, "Semiconductors," Chapter 17, Reinhold Publishing Corporation (1959).

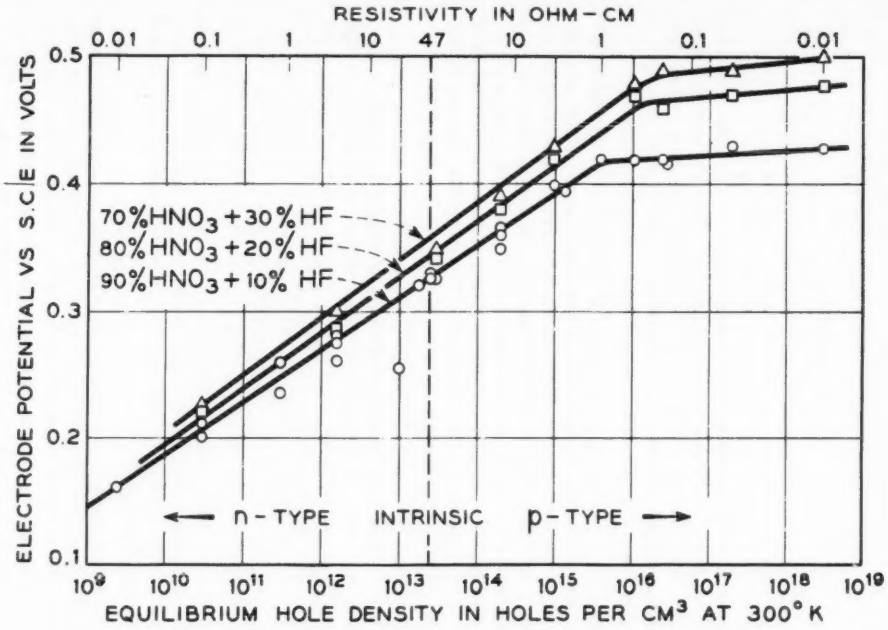

Fig. 1—Electrode potentials of Ge in HNO_3-HF mixtures vs. resistivity and equilibrium hole density.

Abstract Number 102

EXPERIMENTAL MICRO-ETCH TECHNIQUES ON MILLIMETER WAVELENGTH DIODES

D. G. Langlais

Philco Corporation, Philadelphia, Pa.

Transistor micro-etch techniques were applied to improve sensitivity of a germanium mixer diode operating at 70 KMC. In order to show the relation between the sensitivity (crystal noise figure) of the diode and the physical properties of the germanium and whisker point contact, it is necessary to consider simple mixer diode theory.

The crystal noise figure is the product of the conversion loss and the noise temperature. A reduction of conversion loss brings about the desired improvement. The R_sC_b product (R_s, spreading resistance; C_b, barrier capacitance), being proportional to the conversion loss is also proportional to $a/N^{\frac{1}{2}}b$ (a, whisker contact radius; N, majority carrier density; b, majority carrier mobility). In recent years doping of germanium was optimized. Reduction of a had almost reached its limit when Messenger advanced the micro-etch theory as a possible way of further reducing the R_sC_b product.

Micro-etch theory states that by using a crystal with a very thin membrane, it is possible to reduce the R_s without increasing the C_b. While the C_b is proportional to a^2 in both conventional and micro-etch structures, only in the former is the R_s dependent on a. In the micro-etch structure R_s is proportional to W/a^2 where W is the base width. By combining the C_b and R_s relationships, the R_sC_b product is found to be proportional to W, all other crystal parameters being optimized.

The goal outlined by micro-etch theory is making the base width an order of magnitude less than the minimum stable a (4×10^{-4} cm). A base width of approximately 0.02 mil and a conversion loss of 3.5 ratio was the aim of this work.

Micro-etching (jet electrolytic etching) consists of an electrochemical system in which etching action is confined to a specific region of a crystal blank which is made negative to the jet. The resultant surface of the etch pit must be electropolished, i.e., non-preferentially etched. The base width is controlled by an infra-red detection system. The signal actuates an electromechanical system which terminates the etching at the proper thickness. This system is standard in the manufacture of Philco SBT, MAT and MADT devices.

At the beginning of this study, it was understood that in order to achieve a thin window area (the flat bottom region of the etch pit) into which a whisker point could be placed while contained in a micro-wave package, it would be necessary for the window area to be as large as

possible. Very close tolerances required of diode components when using a small window area were not practicable.

Standard jet-etching techniques can yield a large etch pit, however, the thin region of the etched blank is not flat and the resulting window area is very small. On the other hand, the standard techniques are sensitive enough to produce a base thickness of about 0.02.

A standard technique tried included the use of a 14 mil diameter jet at a current of about 12 milliamperes with a solution containing small amounts of sulfuric acid, sodium fluoride, manganese sulfate, and ferrous ammonium sulfate. The above conditions yielded a blank with a base width of 0.02 mil but a window area diameter of less than 1 mil. Under similar conditions while using a 12 mil jet and a 6 1/2 ma. current, it was possible to achieve a flat window area diameter to about 2 mils; but, the base width increased to 0.05 to 0.08 mil. Larger window area diameters (to 7 mil) were achieved but only at the cost of an increase in base width (.1 mil).

In the current range stated above only single ring generation is produced. By using currents in the 60-70 ma. range it is possible to generate a second ring. This permits etching with large jets and results in a steep wall after the second ring generation and an etch pit bottom which just slightly slopes toward a flat window area which is 6 to 7 mils in diameter and has a base thickness of about 0.1 mil.

Carrying the study further was necessary to approach the base width goal of 0.02 mil. Test diodes were fabricated periodically as a method of detecting any decrease in R_s. Results were compared with Philco 1N2792 70 KMC mixer diodes and showed no improvements.

Up to this point only slight variations in standard micro-etching techniques had been tried. The use of light for the generation of holes was thought important in achieving steeper etch pit walls and, thus, larger pit bottoms. However, the hole life-time was shown to be extremely short in highly-doped material and removal of lights did not affect the geometry of the etch pit, but rather improved the sensitivity of the thickness control system by elimination of noise caused by the lights in the detection system.

Germanium material was cut as close as possible to either <110> or <111> orientation (depending on which type material was used). It was found that only minimum care was required in cutting wafers to give the same geometry of etch pit. Also use of either <110> or <111> oriented material made no change in etch pit geometry.

By using an etching current high enough for second ring generation with a solution double in strength to that mentioned below in standard techniques, a significant improvement in etch pit geometry is seen. The flat window area is about 6 mils in diameter. A refinement in cut-off control has made a base width of 0.05 mil quite reproducible. A thyratron circuit cuts off the etching action by sensing the magnitude of the signal.

A plated back-contact previously micro-alloyed was depth alloyed in an attempt to reduce the "effective" base width. Non-uniform alloying produced erratic results. However, even with only a micro-alloyed back-contact improvement was seen in a number of cases.

The 0.05 mil base width has shown a reduction in average R_s from 14 ohms (Philco 1N2792 diode) to 8 ohms. A similar reduction in conversion loss resulted and an improvement of 2 db. in sensitivity was noted in the crystal noise figure when comparing the best micro-etch diode with the best 1N2792. The best diode fabricated had an R_s of 9 ohms, a conversion loss of 3.02 ratio and a very good crystal noise figure of 5.95 db.

The desired base width was not attained by the use of micro-etch techniques partially due to the weakness of the crystal membrane and the etching equipment sensitivity. Mechanical problems developed in the processing of crystal blanks with window areas 6 mils in diameter and only 0.05 mils thick seem to be difficult to solve. However, some improvement in sensitivity was seen.

Abstract Number 103

NON-DIFFUSION OF BORON THROUGH SOLID QUARTZ

Frank Keywell and Marshall Nechtow

Hughes Semiconductor Products
Newport Beach, California

Silicon dioxide films are penetrated by boron when the system B-Si-O is at high enough temperature to form a boro-silicate liquid phase. In this case, there may be oxide mask failure due to the advance of the liquid phase to the underlying silicon. The principal object of the present study was to observe the system boron-silicon dioxide at suitably low temperature where the system remains solid hence any advance of boron through the quartz would proceed by diffusion through a solid. This presents a true diffusion process, thus it appeared possible to measure the diffusion coefficient of boron through quartz by application of an initial thin borosilicate phase, frozen in by quenching from a high temperature, followed by a long diffusion at low temperature where the system remained solid. A measurable diffusion coefficient, however, was not observed because the boron appears "fixed" in solid quartz at low temperature.

It has been reported previously that the distribution of boron in an SiO_2 mask has a sharp front characteristic of a two phase system.[1] The transition from liquid to solid phase takes place in less than 700 Å, as determined by concentration of boron in silicon under a graduated series of thin oxide masks. The presence of two sharply defined phases affords a method for studying the diffusion characteristics of boron in SiO_2 at reduced temperature. A liquid phase of known thickness is formed in an oxide at elevated temperature, then quenched in by rapid cooling to form an oxide with its upper portion loaded with boron while the lower portion adjacent to the silicon has no boron. The sample is next heated at reduced temperature in order to remain solid and penetration of the SiO_2 is recorded by conversion of n-type silicon under the oxide. In order to freeze in a known thickness of liquid phase, a group of oxide samples, 2000A thick on high resistivity silicon, were exposed to a B_2O_3 source at 1100°C for 15 minutes. Reference oxides 700Å and 1000Å were used to place the penetration of boron between these limits since the 700Å oxide was penetrated by boron (conversion under the oxide) and the 1000Å oxide film was not penetrated. The samples were quenched to freeze in the borosilicate layer, then they were placed in an oven at 950°C to test for the length of time required for penetration of the remaining c.a. 1150Å of oxide. It was found that oxides could remain at 950°C for ten weeks without penetration of boron through the

1150Å film. If a sample was re-heated at 1300°C for an hour it would show conversion under the oxide. Since the boron did not penetrate 1150Å of quartz in ten weeks, the diffusion coefficient of boron through solid quartz must be less than 3.11×10^{19} cm²/sec. The diffusion coefficient of boron through solid quartz is hence less than the corresponding coefficient in silicon by a minimum factor of 20,000.[2] The non-diffusion of boron in solid quartz is attributed to chemical binding of boron atoms in the Si-O lattice.

References

1. F. Keywell, Meeting of the Electrochemical Society, Phila., May, 1959.
2. C. S. Fuller and J. A. P. Ditzenberger, Vol 27, No. 5, May 1956, p. 544.

OXIDATION-INDUCED DIFFUSION IN SILICON

H. W. Cooper, E. I. Doucette, and R. A. Mehnert

Bell Telephone Laboratories
Murray Hill, New Jersey

The formation of thermal oxide layers on silicon causes a redistribution of bulk impurities[1] which may either be gettered at the oxide-bulk interface or be rejected into the bulk crystal. For silicon, whose oxide grows at a parabolic rate, a rigorous solution for the variation of impurity concentration with time and position in the crystal has been obtained, subject to the assumption of concentration-independent diffusion constants.

The equation to be solved is:

$$\frac{\partial N(y,\,t)}{\partial t} = \frac{D\partial^2 N(y,\,t)}{\partial y^2} \qquad (y > \delta(t))$$

where y is the distance from the original crystal surface before oxidation and $\delta(t)$ is the thickness of silicon which has been oxidized. Designating the initial background impurity concentration as N_B, the impurity concentration in the oxide as N_O, and the assumed* time-independent crystal surface concentration as N_s, the boundary conditions are:

$$N(\infty,\,t) = N_B,$$
$$N(\delta,\,t) = N_s,$$

$$\text{and } (N_s - N_O)\frac{d\delta}{dt} = -D\frac{(\partial N)}{(\partial y)_\delta}$$

The solution was then shown to be

$$N(y,\,t) = \frac{(N_s - N_B)\ \text{erfc}\ (y/2\sqrt{Dt})}{\text{erfc}\ (\delta/2\sqrt{Dt})} + N_B$$

for the case of pile-up (rejection into the crystal) or for the case of depletion (gettering at the oxide-bulk interface). Defining a segregation coefficient $S = \frac{N_O}{N_s}$ and a pile-up parameter $P = \delta/2\sqrt{Dt}$, the surface pile-up or depletion ratio was shown to be:

*We initially assume that N_s is a constant and then show that this can be true only when a parabolic oxidation rate is observed.

$$\frac{N_B}{N_S} = 1 - \sqrt{\pi}\ (1\text{-}S)\ Pe^{P^2}\ \text{erfc}\ P$$

To facilitate application of the above solutions to particular cases, graphs were developed depicting the pile-up parameter, P, vs. temperature for the common impurities in silicon. Graphs were also developed presenting the surface pile-up or depletion ratio vs P. With the aid of these charts, impurity concentration variations with position and time at the surface and in the interior of an oxidized silicon crystal are completely defined when the initial background impurity concentration, the time and temperature of oxidation are known.

An application of oxidation-induced diffusion is in the creation of one or more p-n junctions by using two or more compensating impurities which have different diffusion constants and/or segregation coefficients. For the case of two compensating impurities, p-n junctions will occur wherever

$$N_d - N_a = 0$$

Equating the above solutions for N(y, t) allows the solution for the precise position and motion of the junction.

Experimental verification of the effects described above was attempted using a crystal doped to 8×10^{16} a/cc of aluminum and 6×10^{16} a/cc of antimony. For oxidation at 1100°C, values of the constants N_B, N_S, P and D were calculated, and the results for each impurity applied to the rigorous solution.

Since aluminum depletes rapidly with oxide growth at 1100°, while antimony piles up slowly, the junction depth will occur close to that depth where aluminum concentration equals antimony background concentration. This approximation results in an equation for the junction depth (in microns) equal to:

$$X_j = 2.115 \times 10^{-2}\ \sqrt{t},$$

where t is given in seconds. The approximation is valid to within 1 part in 10^{20}.

Experimentally, slices of the selected crystal were oxidized at 1100°C for various times. Junctions resulted in each case, and over an interval of 1×10^4 to 3.16×10^4 seconds of oxidation, the increase in junction depth with time corresponded exactly with theory. The agreement between experiment and prediction was fortuitously close, considering the uncertainties involved. Junction depths were observed corresponding to the equation

$$X_j = 1.61 \times 10^{-2}\ \sqrt{t}$$

Several methods have been employed[1] to characterize the impurity distribution and junction formation due to oxidation-induced diffusion. An experiment was designed to measure the segregation coefficient of an impurity during oxidation-induced diffusion to correlate estimates and experiment.

Chemical analytical techniques are of insufficient sensitivity to determine the segregation coefficient. The most accurate analysis for boron in silicon, capable of detecting 1 part in 10^6 of boron, would require 10^{23} a/cc of boron in the crystal for an accurate analysis of the boron in the oxide layer.

Radiotracer analysis was suggested by the nature of the problem, and for ease in handling and counting radio-indium[114] was selected. P-type silicon doped to $\sim 4 \times 10^{15}$ a/cc with indium was irradiated for 1 week at Brookhaven. Two slices of the irradiated material were oxidized for 10^4 seconds in dry oxygen at 1100°C. One slice was dissolved entirely and used as a reference standard. A fourth ($control_0$ slice was successively etched without oxidation in the same manner and with the same acid as the oxidized slices.

The radioactivity of the control slice gave the background impurity density for all slices and the semi-logarithmic plot of its radioactivity with time gave the identity of the major and minor impurities. The control slices' etch rate, assuming uniform background impurity concentration, gave the amount of radioactive material which should have been found in a slice for given etching time and solution, if the slice hadn't been oxidized (diffused). The ratio of the radioactivity of the etchant employed on the oxidized slices, compared with the control slice, permitted calculation of the segregation coefficient of indium.

The experimental results were obtained using three counting systems at 2 locations. The counting efficiencies of each of the 3 systems were standardized and related. Experimentally, the segregation coefficient obtained was close to unity, in contrast to the value of $>10^3$ estimated[3] by consideration of the equilibrium properties of indium in the $Si\text{-}SiO_2$ system. The value of the segregation coefficient experimentally obtained is good evidence that the segregation of indium during the oxidation of silicon is not an equilibrium process under these conditions.

The phenomenon of oxidation-induced diffusion presents interesting device implications. With suitably compensated crystals, precisely controlled diffusions may be accomplished allowing wide choices of surface densities by control of oxidation temperature. Predeposition or paint-on are unnecessary. Surface cleanliness and crystalline perfection are much less important. Large-area junctions required in solar cells and large integrated devices may be prepared by this technique. In addition, two or more junctions may be prepared in a two impurity crystal by oxidizing the crystal at two or more successive temperatures.

A number of fundamental side effects can now be attributed to oxidation-induced diffusion. Even the slightest oxidation of a semiconductor surface results in a redistribution of impurities. In some cases, thin skins of inverted material may result which will afford contact problems. This is particularly prominent in the case of oxide-masking on silicon.

References

1. M. M. Atalla and E. Tannenbaum, Electrochemical Society Meeting (Columbus, October 1959).

2. C. D. Thurmond, to be published.

Abstract Number 105

GASEOUS DIFFUSION OF ARSENIC IN GERMANIUM

Carl Pihl and Kurt Lehovec

Sprague Electric Co.
North Adams, Mass.

Previous studies of the gaseous diffusion of phosphorous in germanium have been extended to include vapor diffusion of arsenic in germanium. Data will be presented on surface concentration of arsenic in germanium as a function of arsenic pressure in the gas phase. At sufficiently high arsenic concentrations a liquid phase of germanium arsenide forms and this phase has been identified by electron diffraction. Evidence will be presented that this liquid phase suppresses thermal conversion.

*Enlarged Abstract not Available

Abstract Number 106

OPEN TUBE DIFFUSION OF ANTIMONY INTO GERMANIUM

A. E. Blakeslee

Bell Telephone Laboratories
Allentown, Pa.

Very shallow (≈1 micron) n-type layers were formed in germanium by diffusion of antimony. In order to produce layers with high average resistivity but reasonably high impurity gradients at the junctions, a two-step diffusion process was used. The desposition step was carried out in a conventional two-furnace open tube system with hydrogen as the carrier gas, metallic antimony at temperature T_S as the diffusant source, and polished germanium bars at temperature T_W in the "work" furnace. The out-diffusion step (so-called even though it also necessarily involves some further in-diffusion) was carried out in a separate furnace at temperature T_{od} in a hydrogen stream containing no antimony. The main object of this work was to determine the dependence of the measurable parameters sheet resistivity (ρ_{dep} or ρ_{od}) and junction depth (x_j) upon the pertinent temperatures and times of the two-step process.

The sheet resistivity data for the constant times, t_{dep} = hr. and t_{od} = 4 hr., were found to fit the expressions

$$\rho_{dep} = 1.117 \times 10^{-8} \exp \left[\frac{3778}{T_S} + \frac{16,900}{T_W} \right]$$

and $$\rho_{dep} = 4.159 \times 10^{-8} \exp \left[\frac{3971}{T_S} + \frac{18,480}{T_W} - \frac{2519}{T_{od}} \right]$$

with temperatures expressed in °K, for the temperature ranges: T_S 400-535 C; T_W, 625-700°C; T_{od}, 600-675°C. The constancy of the slope of log ρ_{dep} vs. $1/T_S$ for all T_W indicates that the surface concentration is directly proportional to the vapor pressure of antimony at T_S. After taking into account the variation of electron mobility with temperature and the tetrameric nature of the antimony vapor at experimental temperatures, this slope leads to a value of 45.9 kcal. for the heat of sublimation of antimony at 500°C, in excellent agreement with the 46.1 kcal. listed by Stull and Sinke[1].

Linear relationships were found between ρ_{dep} and $t_{dep}^{-\frac{1}{2}}$ and between ρ_{od} and $t_{od}^{\frac{1}{2}}$, experimental scatter from the straight lines being considerably greater in the second case. It was difficult to measure the very small junction depths precisely with the copper plating technique, but where valid x_j data were available for the deposition step, a proportionality between x_j and $t_{dep}^{\frac{1}{2}}$ was observed. The final junction depth is more strongly dependent on T_{od} than on T_S or T_W.

The diffused antimony distribution resulting after deposition can be represented quite closely by a simple complementary error function. The distribution after out-diffusion is the difference of two erfc terms, the first representing in-diffusion and the second out-diffusion. No significant surface rate limitation was encountered, such as reported by Miller and Smits[2] for out-diffusion of antimony from uniformly-doped germanium. Verification of the simple complementary error function distributions is afforded by: (1) the linearity of $1/\rho_{dep}$ vs. $t_{dep}^{\frac{1}{2}}$, a relationship which follows if the distribution is erfc; (2) the agreement between measured sheet resistivity and that calculated assuming erfc to apply; and (3) evidence that a constant surface concentration in dynamic equilibrium with the antimony vapor is rapidly achieved.

Surface concentrations (C_o) and diffusion constants (D) for antimony were calculated from the experimental data, with the aid of Veloric and Greig's[3] graphical solutions of the concentration-mobility product integral. Surface concentrations in the range 10^{18} - 10^{19} cm^{-3} were found. These values of C_o are close to the saturated solid solubility data reported by Thurmond et al[4]. Diffusion constants obtained at 650°C and 700°C are lower by a factor of 5-10 than published values, e.g. those of Bösenberg[5]. No satisfactory explanation has yet been found for this discrepancy in D. The explanation may lie in the somewhat different experimental conditions employed in this work with respect to those of previous authors.

References

1. D. R. Stull and G. C. Sinke, "Thermodynamic Properties of the Elements", American Chemical Society, Washington, D. C. (1956), p. 41.
2. R. C. Miller and F. M. Smits, Phys. Rev. 107, 65 (1957).
3. H. S. Veloric and W. J. Greig, RCA Review, to be published.
4. C. D. Thurmond, F. A. Trumbore, and M. Kowalchik, J. Chem. Phys. 25, 799 (1956).
5. W. Bösenberg, Z. Naturforsch. 10a, 285 (1955).

Abstract Number 107*

SURFACE CONCENTRATION OF INDIUM IN GERMANIUM FROM GASEOUS DIFFUSION II

Karl Busen and Earl Meeks

Sprague Electric Co.
North Adams, Mass.

Previous investigations on the indiffusion of indium from the vapor phase into germanium at 837°C are now extended to diffusion temperatures of 775° and 900°C. The experiments are carried out again in a specially designed closed system and values for the surface concentration of indium in the germanium for different indium vapor pressures are presented. Diffusion coefficients of indium in germanium derived from our experiments are compared with published values.

*Enlarged Abstract not Available

Abstract Number 108

A DIFFUSION MASK FOR GERMANIUM

E. L. Jordan and D. J. Donahue

Radio Corporation of America
Semiconductor and Materials Division
Somerville, New Jersey

Silicon can be oxidized to form a surface coating of silicon dioxide which can be used as a diffusion mask to prevent the diffusion of specific impurities[1]. The silicon dioxide mask plus photoengraving techniques make it possible to prepare devices completely by diffusion. Such techniques permit the precise control of the area of diffusion, junction depth, and level of doping.

While it is easy to form the oxide layer on silicon by heating the material in an oxidizing atmosphere, the same technique cannot be used on germanium. When germanium is heated to diffusion temperatures in an oxidizing atmosphere, its surface is rapidly attacked and pitted.

A technique has been developed for forming a silicon dioxide film on germanium. The film is formed by the thermal decomposition of an organic-oxy-silane in an inert atmosphere at temperatures approaching those used in diffusion. The thickness of the film can be varied from under 2000 Å to over 20,000 Å. By proper selection of doping level and film thickness the coating functions as a diffusion mask.

The film has been successfully used to prepare an npn double diffused germanium transistor where complete masking has been obtained against arsenic surface concentrations as high as 10^{20} atoms per cubic centimeter[2]. Masking against p-type materials has also been investigated but with limited success. In this case masking can be achieved; however, the physical characteristics of the film limits its use to low and medium concentration of p-type dopes such as gallium.

The thermal decomposition of the organic-oxy-silane is carried out in a 30 mm O. D. Vycor tube 3 feet long placed in a split tube furnace. Rubber stoppers with appropriate inlet and outlet connection are used at either end of the tube, and the material to be coated is placed in the center of the heat zone. Argon is used to purge the furnace, and as the carrier gas for the silane. After the furnace has been thoroughly purged, the argon is allowed to bubble through a trap containing the silane, and the argon-silane mixture is passed through the furnace. The temperature of the furnace is then raised to 750°C where it is maintained during the decomposition. The furnace is then purged with argon again and allowed to cool to room temperature.

The thickness of the film can be controlled by the time of deposition as shown below.

Furnace Temp. °C	Silane Temp. °C	Time - Min.	Film Thickness Å
750	50	5	1500
750	50	10	2000
750	50	20	6000

The thickness of the coating to be deposited on a wafer is determined by the device processing techniques and practical considerations based on the difference in thermal expansion coefficients of the film and the germanium. Also, when the coating is to be used in conjunction with photo-resist techniques, a further limitation is placed on the thickness. Too thick a coating will require etching times so long that the photo-resist mask will fail.

The effectiveness of the coating as a mask against arsenic and antimony diffusions has been proven by over one hundred successful diffusion runs. The coating has prevented arsenic diffusions under conditions that produce surface concentrations ranging from 10^{17} to 10^{20} atoms per cubic centimeter.

The diffusion powders were germanium arsenic alloys ranging from a fraction of a percent arsenic up to 5% arsenic (by weight). Diffusions at temperatures up to 900°C can be made with complete masking when powders yielding surface concentrations of 10^{18} and 10^{19} atoms per cubic centimeter are used.

When the mask is used against p-type impurities (gallium and aluminum) a much thicker film is required for masking. While masking has been obtained at 2×10^{19} the film thickness required for masking at this concentrations causes excessive damage to the germanium surface. The damage becomes manifest in the form of a badly cracked surface.

References

1. C. J. Frosch and L. Derick "Surface Protection and Selective Masking During Diffusion in Silicon" - J. Electrochem. Soc., V 104, pp. 547-552, Sept. 1957.

2. H. S. Veloric, D. Rauscher, E. L. Jordan, "Diffusion Masking in Germanium and Double-Diffused Germanium Transistors" - Semiconductor Device Research Conference, Ithaca, New York, June 17, 1959.

Abstract Number 109*

THE DIFFUSION OF PHOSPHORUS IN SILICON

I. M. Mackintosh

Bell Telephone Labs., Inc.
Murray Hill, N. J.

A process is described for producing N-type, phosphorus-diffused layers in silicon. The diffusions are carried out in a closed system, using as the diffusion source a glass consisting of P_2O_5 and CaO.

Surface concentrations between 10^{21} and 10^{15} cm^{-3} can be obtained with reproducibilities between 2% and 20%, junction depths from about 0.02 mil upwards with reproducibilities between 2% and 5%. The process is compatible with the oxide masking of layers with surface concentrations as high as 10^{21} cm^{-3}.

Data are presented for the diffusion coefficient, and the value of the activation energy for this process is discussed.

*Enlarged Abstract not Available

Abstract Number 110

EXPERIMENTAL EVIDENCE OF SURFACE DAMAGE AND PRECIPITATION IN DIFFUSED SILICON

L. Gerlach and R. R. Haberecht

Corporate Research & Development
P. R. Mallory & Co., Inc.

The results of an investigation to determine the cause of certain bulk defects which have an adverse effect on the electrical characteristics of silicon will be discussed.

One type of defect commonly encountered is called "surface damage", a term which will be defined in reference to photomicrographs of cross-sectioned silicon material. Since it can be shown—(and which has been previously reported)—that "surface damage" can extend several mils into the bulk of the silicon, this damage obviously occurs during the surface preparation, the diffusion process, or a combination of the two. The effects of slicing, lapping, cleaning, and etching of the silicon prior to diffusion were investigated with regard to the surface condition. An apparent strain, resulting from the mechanical operations (slicing and lapping), was observed; however, after a low temperature heat treatment, the strain was no longer visible.

A similar type of strain was observed on slices from which at least ten mils had been removed by etching. Therefore, it was concluded that the strain or surface damage occurs in the diffusion process itself. It may not be, necessarily, the propagation of strain during an elevated temperature heat treatment, but the effect of impurity atoms already present or introduced into the silicon during diffusion. This effect could not be observed after the generation of a controlled adherent complex surface layer on the silicon.

Under certain conditions, the generation of this surface layer results in a precipitation in the diffused region rather than the strain or "surface damage" that can be seen in photomicrographs. This precipitation indicates that there are at least one or more impurity elements present which have reacted to give a product insoluble in silicon.

Also seen in the photomicrographs is an abnormal concentration gradient which has been verified by electrical measurements. Fluctuation in this gradient and the junction depth can be produced at temperatures and/or times that are not consistent with the diffusion coefficient of any known impurities. These fluctuations seem to be the result of the mechanism associated with the heat treating effects attributed to oxygen and its complexes. Since these effects have been observed with

both Czochralski and floating zone type crystals, it is assumed that it is the oxygen from the B_2O_3 (source of diffusant) that has diffused into the silicon from the surface which contributes to the observed effects. The possibility of complexes forming in silicon has been reported by several investigators (Tweet, Fuller, Pell, etc.); however, the mechanism is still undetermined.

Abstract Number 111*

PRECISION LAPPING, DAMAGE AND DIFFUSION

C. J. Spector and T. E. McGahan

Bell Telephone Labs.
Murray Hill, N. J.

Silicon slices have been experimentally lapped and polished to less than 0.003 in. with opposing faces optically plane and parallel to within 0.00002 in. Modified planetary lapping techniques have been used so that the strains usually induced by "one side at a time" processes are absent. Data are presented to correlate rate of lapping, depth of damage (measured by x-ray "rocking angle" techniques), and impurity diffusion parameters with abrasive particle size.

*Enlarged Abstract not Available

*Abstract Number 112

A NEW SOLUTION TO NEW DIFFUSION AND A NEW APPLICATION OF ANALOG SOLUTIONS

R. Moore and J. Colburn

General Electric Co.
Syracuse, N. Y.

An analytical expression for the diffusion profile obtained during the two-step diffusion process for the germanium mesa transistor has been developed by two independent analyses. The form of this equation makes numerical solutions difficult; however, some curves obtained by digital means are presented. A more direct approach is the use of a passive electrical analog. The analogy is shown together with some of the curves obtained and these are shown to be equivalent to the analytical results.

*Enlarged Abstract not Available

Abstract Number 113

LOCALIZED BREAKDOWN IN DIFFUSED SILICON JUNCTIONS

B. David James and Philip S. Flint

Fairchild Semiconductor Corporation
Palo Alto, California

Regions of low breakdown from avalanche multiplication in diffused p^+n and n^+p silicon junctions have been studied. The breakdown plasmas are made visible by the emission of light as reported by Chynoweth and McKay[1]. As well as the breakdown plasmas existing below the surface at the junction interface and visible when the junction depth is not more than about 2 microns, there exist breakdown regions at the surface, indicating the emergence of a "pipe" through the diffused layer, of the same type of doping as the bulk material. Thus in a p^+n junction, a cylindrical n region connects the surface with the base. These pipes can reduce the breakdown of a diode from 140 volts to 10 - 40 volts, indicating that they are very highly doped regions. This has been verified by placing a fine prove in the center of a pipe and obtaining an estimate of its resistivity, which is about 10^{-2} as large as that of the bulk material.

Since there occur many more pipes in p^+n diodes than in n^+p diodes, most attention has been focused on the former.

The physical structure of the pipes, which are about 2 - 20 microns in diameter, can be examined by surface staining, etching and examination of their surface profile by the Foucault knife edge test. Sectioning and staining reveal their structure below the surface. The pipes are usually fairly accurately circular in shape and light emission takes place at the junction, as revealed by staining.

Etching the surface with a variant of the well known Dash etch revealed an interesting structure to the pipes. A deep pitting occurs inside the pipe which sometimes takes the form of short line pits oriented along the $\langle 110 \rangle$ directions. In other pipes, etching gives one deep pits in the center of the pipe, or a group of pits which do not show any orientation.

It may be thought that the single pits correspond to line dislocations, while the lines are dislocation loops. However, matching the single etch pits inside pipes with pits on the reverse surface of the silicon wafers was quite unsuccessful, indicating that they did not reveal dislocations. Copper decoration of dislocations has also shown that there is no correlation between the dislocations and pipes. Moreover, wafers in which dislocations were artificially introduced had no more pipes

than dislocation-free wafers. It is inferred from this that the line etch pits do not reveal the presence of dislocation loops as has sometimes b been thought. The assumption involved is that the same phenomena are responsible for the pipes in both cases. It is suggested that the pits reveal vacancy clusters.

Since vacancies are acceptors, these clusters would provide centers for segregation of donor impurities merely by their coulomb attraction. This would account for the much more frequent occurrence of n^+ pipes through the diffused p-type layer than of p^+ pipes through a diffused n-type layer. Indeed in the case on n^+p junctions, pipes are thought to be due to alloying, mentioned below.

Three other relations exist that complete the phenomenology on which the model for pipes is based. There are more pipes through p^+n junctions for low bulk resistivity n-type material than for high resistivity material. The incidence of pipes is increased by about a factor of 20 if the silicon surface is oxidized prior to diffusion. The occurrence of pipes depends only on the type of dopant, and does not depend on which element of a given type is used for doping.

It does not seem likely that oxidation increases the number of pipes by virtue of oxygen entering into the lattice and acting as donors in aggregates such as SiO_4. Fuller and Logan[2] and Kaiser, et al,[3] have shown that donor states are formed by aggregates of less than five bound oxygen atoms, but that these donor states disappear on heating to temperatures above 500°C. Oxidation and diffusion were carried out above 1100°C, at which temperature oxygen donor states do not appear. Moreover, the dependence of the occurrence of pipes on the bulk resistivity of the silicon would not be expected were oxygen the cause.

The interpretation that has been made of the observed phenomena is that on heating, the n-type dopant of the bulk silicon tends to segregate around vacancy clusters by virtue of their electrostatic attraction. These vacancy clusters are formed in considerable numbers during the oxidation as demonstrated by their presence only to a depth of 15 - 20 below the water surface. The formation of superficial vacancy clusters may be the only role of oxidation in pipe formation, although it may also cause a significant enhancement of the surface concentration of n-type dopant which is left behind after the surface silicon is removed as the dioxide. This surface enhancement of concentration has been used by Atalla[4] to make p-n junctions in silicon doped with gallium and antimony. The gallium is not masked by the oxide, while the antimony is, leading to an inversion of type at the surface.

Alloyed pipes may be formed by dust on the surface of the wafer which alloys with the silicon. On regrowth, these may result in an n^+ region surrounding the dust which could be due either to the preferential segregation of bulk dopant into the silicon, or to the fact that the dust itself may be n-type. It is therefore of the first importance to observe meticulous cleanliness at all stages to avoid a high percentage of low breakdown junctions.

References

1. A. S. Chynoweth and K. S. McKay, Phys. Rev. 102, 369 (1956).
2. C. S. Fuller and R. A. Logan, Journ. Appl. Physics, 28, 1427 (1957).
3. W. Kaiser, H. L. Frisch and H. Reiss, Phys. Rev., 112, 5, 1546 (1958).
4. M. M. Atalla, Meeting of the A.I.M.E., Aug. 31 to Sept. 1, 1959, Boston, Mass.
5. K. S. McKay, 94, 877 (1954).

Abstract Number 115

PRODUCTION OF A GERMANIUM PNPN SWITCHING TRANSISTOR BY POST-ALLOY DIFFUSION

Fred Barson and John Gow

International Business Machines Corporation
Poughkeepsie, New York

A process has been developed for fabricating a three-terminal germanium PNPN switching transistor similar to that described by Klein and Kordalewski[1]. In order to discuss the fabrication process, it is convenient to review briefly a few basic design considerations mentioned by these authors. First, this device was designed to be normally "on," that is, to show a low impedance between emitter and collector when no bias is applied to the base. Referring to Figure 1a, for example, this device can be held off by a negative bias applied to the base. When this bias is removed, as by superposing a positive pulse to bring the base to zero bias, the device switches on and current flows through the load R_L in series with the transistor. Once the device turns on, the base loses control and the external circuitry controls the current flow. To turn the device off, the collector circuit must be opened mechanically or the current otherwise limited to a very small value.

Figure 1b shows the two transistor analogy which is useful in the analysis of the PNPN transistor. Here the device is thought of as being two transistors, a PNP and an NPN, with a common collector junction. It is seen that there is no base contact to the PNP transistor section. Hence, the saturation current of the reverse-biased collector junction is increased due to the gain (α_{PNP}) of this transistor, and the avalanche breakdown of this junction is also lowered from its inherent value.[2] To minimize these effects it is desirable to keep the current gain of the PNP transistor low, perhaps 0.3 or less. At the same time, in order for the device as a whole to be a normally "on" switch, the sum $\alpha_{PNP} + \alpha_{NPN}$ must be greater than unity. For this reason, and so as to keep relatively small the base current required to bias the device "off", it is necessary that the current gain α_{NPN} be at least 0.7 or 0.8.

In figure 2 is shown the structure used in the present process of fabricating this device. The large collector area relative to the emitter is favorable for heat transfer to the case as well as for achieving an α_{NPN} of about 0.85. The base ring, emitter dot, and collector dot, with compositions indicated on the drawing, are all alloyed to the germanium in a single firing. The alloying time is about 45 minutes at 760°C. This allows for diffusion from both emitter and collector dots, giving graded junctions with high breakdown voltages. The composition of the collector

dot is such that it recrystallizes net P-type germanium on cooling, however, producing the PN "hook" collector. This is the so-called "post-alloy diffusion" process described earlier by Schwartz and Slade[3] in making PNP transistors. In the present case, however, the gallium and antimony concentrations are such that the recrystallized region of the collector (the emitter of the PNP transistor) is highly conpensated. In fact, the PNPα is kept low by compensating this region sufficiently that the emitter efficiency is very poor. It is estimated from indirect measurements that the PNPα of devices made in this way is about 0.2-0.4. This can be varied by varying the ratio of antimony to gallium in the dot. The composition of this collector dot is critical for controlling the process. However, once the proper starting materials are obtained, the process is very simple and inherently results in high yields. By employing this post-alloy diffusion technique, no pre-diffusion of the germanium is required. All junctions are formed during the alloying, and alloying depths are not critical.

Processing of the units subsequent to the alloying is novel enough to warrant further description. Immediately after alloying, the unit is bonded to the gold-plated copper stud indicated in Figure 2. The unit and stud are then handled as a sub-assembly through etching and through an in-process electrical test, before the stud is mounted in the case or leads attached. The units can be completely etched electrolytically through the collector alone. Electrical contact is made through the copper studs simply by placing the studs in a gold-plated mesh basket which is made anodic relative to a sodium hydroxide solution electrolyte. Following etching, the junction characteristics and trigger points are measured. Contact to the base and emitter is made by means of small probes, while the copper stud serves as the collector contact. Poor units can be discarded at this point or recycled through etching. In this way, relatively few poor units pass on to the more expensive operations of committing them to headers, attaching leads, and final-testing.

Some typical room temperature characteristics of PNPN transistors made by the process described are listed in Table 1. The symbols represent the breakdown voltages of the emitter junction (BV_{ebo}) and of the collector junction (BV_{cbo}). The base current I_{beo}* is that which flows when the device is biased "off"; and $I_{b\ trig}$ is the base current flowing at the point just prior to the device switching on. Positive $I_{b\ trig}$ indicates a unit which is not normally "on" but requires a slight amount of positive current to switch it on. Such units are acceptable, in many cases, if the current required is only very slight. V_{ce} indicates the voltage drop across the transistor in the "on" state. It is reported at a current level of 200 ma, which is approximately the current handling capacity of the device in the absence of any external heat sink.

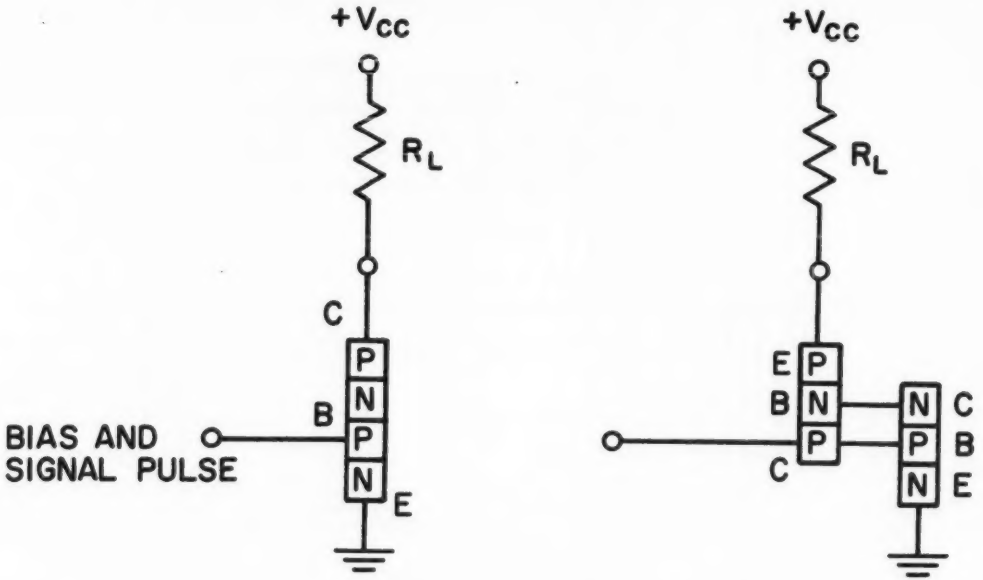

Fig. 1—A. Simple Schematic Circuit
B. Two-Transistor Analogy

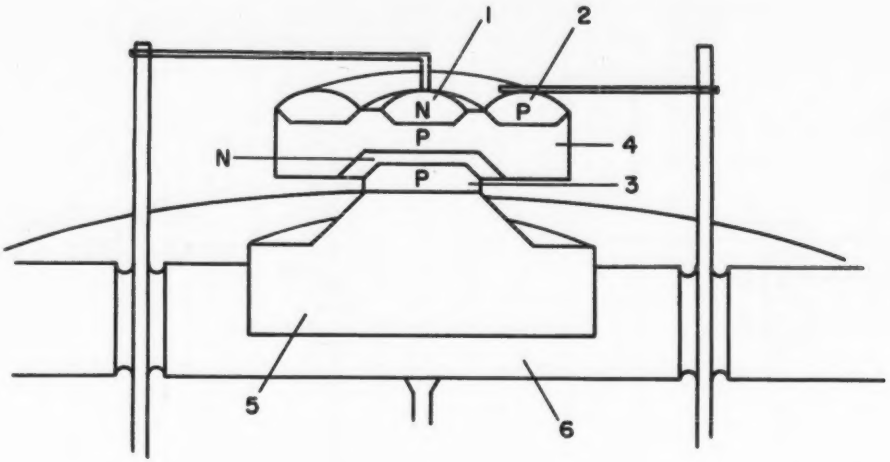

1-EMITTER (90% PB-10% SB)
2-BASE RING (98% PB-2% IN)
3-COLLECTOR (PB-1% SB-0.005% GA)
4-GERMANIUM (P-TYPE, 7-10 OHM-CM)
5-STUD (GOLD-PLATED COPPER)
6-HEADER

Fig. 2—Geometry of Unit (Not to Scale)

Table 1. Typical Device Parameters

BV_{ebo}	>40 volts
BV_{cbo}	>100 volts
I_{beo}*	10-30 μ amps
$I_{b\ trig}$	-20 - +10 μ amps
V_{ce}	0.5 - 0.6 volts

References

1. M. Klein and A. P. Kordalewski, IBM Journal Research Develop., 3, 377 (1959)
2. S. L. Miller and J. J. Ebers, Bell System Tech. Journal, 34, 883 (1955)
3. R. S. Schwartz and B. N. Slade, "A High Speed PNP Alloy-Diffused Drift Transistor for Switching Applications," Presented at the 3rd Annual Electron Devices Meeting, Washington, D. C. October 31, 1957.

Abstract Number 116

"A HIGH FREQUENCY PNP DIFFUSED SILICON TRANSISTOR PRODUCED BY THE OXIDE MASKING TECHNIQUE"

O. Stavik

Northern Electric Company
Montreal, Quebec

Introduction

A high frequency pnp diffused silicon transistor has been made using the oxide masking technique. The electrical characteristics of this transistor are similar to those of the npn diffused silicon mesa transistor. It has been used in complementary symmetry with a 2N560 in various types of circuits with good results. The manufacturing technique can readily be adapted for producing pnp power transistors.

Silicon slices of resistivity 0.5 - 0.7 ohm. cm. are first diffused with arsenic to a depth of 5×10^{-4} cm. During this first diffusion, an oxide layer is formed which is sufficiently thick to mask against the second diffusant, namely boron. Oxide is removed from the silicon surface in the form of stripes or rectangles, and boron diffused through these areas to a depth of $3.5 - 4 \times 10^{-4}$ cm. to produce emitter junctions, thus giving a base layer of $1.0 - 1.5 \times 10^{-4}$ cm. The desirable dimensions of the collector junction are established by mesa etching.

Preparation of Material

P-type silicon of bulk resistivity 0.7 ohm. cm. is cut into slices and lapped by standard methods to a thickness of 0.012 in. These are further hand-lapped on a glass plate with 305 abrasive and finally polished mechanically on a bowl polisher. The surface finish obtained by this method is superior to results achieved by chemical etching. The polished surface is flat to within 0.001 in. over a 1.0 in. diameter slice. A high degree of flatness is important for the photographic technique used to produce the stripe or rectangular emitter pattern in the oxide film.

Diffusion

The arsenic diffusion is carried out in an open tube furnace. Arsenic is predeposited on the silicon slide at 1100°C for 15 minutes, using As as a source heated to 230°C. The As vapour is transported by a flow of dry nitrogen gas. The actual diffusion cycle is programmed to increase the temperature from 1100°C - 1270°C at a rate of 500°C per

hour. The plateau duration is five hours, and the cooling rate 500°C per hour. With an atmosphere of wet nitrogen gas, a silicon dioxide layer of 5000 Angstrom units thickness is grown on the surface of the slice. Thus the collector diffusion and oxidation is combined into one operation. After diffusion, a 5 bevel is lapped (and polished) at one end of the slice and copper-plated to reveal the junction. The depth of the junction is determined by counting interference fringes produced by sodium light. The depth of diffusion can readily be controlled to 5×10^{-4} cm. $\pm$ 3×10^{-5} cm. The sheet resistivity after arsenic diffusion is of the order of 70 - 100 ohms per square.

Oxide is removed from the slice in striped or rectangular pattern (both patterns will give equally good results) using the well known photoresist technique and etching in ammonium bifluoride.

The boron diffusion is carried out in an open tube furnace using boric acid as a source and dry nitrogen gas as carrier. The boric acid contained in a porcelain crucible, is placed in the hot zone of the furnace at 1050°C and left for 30 minutes before the silicon slice is introduced. The diffusion cycle is programmed to increase the heat from 1050°C to 1170°C at a rate of 500°C per hour. The plateau duration is from 25 - 30 minutes and the cooling rate 500°C per hour. The depth of diffusion can readily be controlled to withint $\pm 3 \times 10^{-5}$ cm. The sheet resistivity after boron diffusion is of the order of 2 - 5 ohms per square. To obtain uniform diffusion depth, and to avoid undesirable deposits on the surface, it is essential to use a very low flow of nitrogen gas.

Assembly

Rectangular metal contacts are evaporated onto the base and emitter areas and alloyed. The dimensions of the contacts are 0.002×0.005 in. spaced 0.002 in. apart. A study has been made of the resistance between two such contacts on different resistivity n- and p-type silicon. The lowest base to emitter forward resistance would be obtained by using silver on the base and gold on the emitter. It is, however, rather inconvenient to use two different metals and, since pure gold forms relatively good ohmic contact both on the base and the emitter surface, this is being used. Both contacts are evaporated simultaneously and then alloyed at 550°C. The base to emitter forward voltage using gold contacts is approximately one volt at 15 Ma. Gallium doped gold is evaporated onto the reverse side of the slice and alloyed to facilitate bonding of the wafers to the header. Mesas are prepared by spraying wax through a mask with rectangular holes of dimensions 0.008×0.009 in. and etching the slice in a solution containing five parts nitric acid, three parts glacial acetic acid and three parts hydrofluoric acid. The final dimension of the mesas is 0.007×0.008 in. with slightly rounded corners. A silicon slice one inch square will yield one thousand wafers. This figure can be almost doubled without much difficulty. The wafer is assembled on a standard three lead header using 0.001 in. gold wire for base and emitter connections. The gold wire is compression bonded to the metal contact areas.

Electrical Characteristics

The pnp transistor reported on here was designed to work in complementary symmetry with an npn transistor of the 2N560 type in high frequency amplifier circuits. Several units have been tried in development circuits with very satisfactory results. In Table 1 are listed performance data for the parameters which were of particular interest in the design of this transistor. The average values were taken from a batch of one hundred transistors. The maximum or minimum figures represent the best performance data recorded on units from this batch. As mentioned before, the base to emitter forward resistance can be improved, if desired, by choosing more suitable metal contacts. Common emitter current gain as high as 200 has been measured and frequency cut-off of 200 mcs can be obtained by this design. However, 120 mcs is a more realistic aim.

TABLE 1

ELECTRICAL PERFORMANCE DATA FOR
PNP DIFFUSED SILICON TRANSISTOR

	Average	Maximum	Minimum
Collector breakdown (BVces) I_c = 10μAdc, Vbe = 0	50 volts		
Emitter forward (Veb) I_c = 0, I_e = -15 mAdc	1.0 volts		0.80 volts
Saturation or "on" voltage I_c = 10 mAdc, I_b = 0.4 mAdc	2.0 volts		1.5 volts
Current gain, common emitter I_c = -10 mAdc, V_{cb} = 5 Vdc	40	200	
Cut-off frequency α- cut-off	120 mcs	200 mcs	

Abstract Number 118

PHYSICAL METALLURGY IN SEMICONDUCTOR DEVICE FABRICATION

I. GOLD ELECTRODE ATTACHMENTS TO SILICON AND GERMANIUM

L. Bernstein, W. B. Warren, and B. G. Bender

Hughes Products
Newport Beach, California

In the process of device fabrication; a parent semiconductor die is usually bonded to a suitable material which must be both electrically and thermally conductive. For optimum device properties, a bond so formed should be ohmic in nature (or at least as closely non-rectifying as possible) and as low in resistance as is possible. Ohmic contacts can generally be achieved by providing proper "doping" impurities in a low resistance bond. Low resistance bonds are formed by maximum wetting and alloying, broad area contact, and of course, crack-free connection. It is not the purpose of this investigation to study the doping level effects of various systems but rather the problems concerned with producing these low resistance bonds.

In device processing, corrosive acids are used to etch junctions and improve electrical properties. Materials with good corrosion resistance are therefore not only desirable, but at times necessary. Gold meets this requirement quite well. The melting points of gold eutectics with germanium and silicon (356 and 370°C, respectively) are high enough for adequate device stability, yet low enough to provide ease of fabrication. In addition, they contain sufficient quantities of gold (88 and 94 wt %, respectively) to confer good etch resistance. For these reasons, investigations of gold alloys and materials were emphasized.

Successful electrode attachment and/or alloying depend on surface-energy relations between the liquid metal and the solid substrate, cleanliness of the system, thermodynamics of the system, solubilities in the systems involved, and spreading of the liquid metal. The factors influencing some of these conditions are discussed.

Electrode attachments were divided into two groups—those in which contacts were relatively small in area compared to the die surface, and those in which the die was mounted to a tab larger in area than the die surface. The former are referred to as small area contacts; the latter as large area. Experiments were run, making both small and large area bonds under three types of atmospheric conditions: (1) low moisture content ambients permitting no manual manipulation of parts; (2) high moisture ambient with hand manipulation; and (3) medium moisture

content ambient in a conventional conveyor type furnace. Binary gold alloys containing Pb, Bi, Sn, Be, Sb, and Si, were used in small area contacts. In some cases ternary alloys were studied to determine their effect on limiting fusion penetration, improving wetting properties, and eliminating fusion cracking. Thermal expansion curves of Si, Ge, Au-Sn and Au-Sn with In additions are presented as a means of interpreting results.

Large area contacts were studied using nickel, nickel-iron and molybdenum backing materials, which were either gold or gold alloy clad or plated. In some cases there was an additional tin or antimony plate before alloying.

Thirteen photomicrographs are presented showing typical attachments.

Abstract Number 119

PHYSICAL METALLURGY IN SEMICONDUCTOR DEVICE FABRICATION

II. STUDIES OF GOLD-ALUMINUM AND GOLD-TIN IN ELECTRODE ATTACHMENT

L. Bernstein, W. B. Warren, and B. G. Bender

Hughes Products
Newport Beach, California

Semiconductor devices are often fabricated by alloying aluminum on to silicon surfaces to produce either a P-N junction of a P+ ohmic contact, depending upon the original doping of the silicon. Subsequent processing to produce a practical device may include attachment of a gold, or gold-alloy, electrode to the aluminum-silicon eutectic material which is the result of the first step. This paper reports the results of studies of the causes of mechanical and electrical failures of devices which were traced directly to effects which can occur during such electrode attachments.

All cases of failure studied are shown to occur at the alloy-eutectic interface where the presence of a brittle, porous, purple phase, identified as $AuAl_2$, was detected in relatively large amounts. An additional new phase, identified as Au_2Al is also shown to appear which, so far as could be determined, is not critical to device stability.

The first phase of the report covers a study of electrode attachment to aluminum-silicon eutectic using pure gold, as well as a variety of gold alloys. It is found that good metallurgical bonds can be made with pure gold at temperatures as low as 425°C. $AuAl_2$ is always detectable, but in such minor degree as to be without effect upon the bond, in spite of the fact that $AuAl_2$ is not formed in the binary Au-Al system at temperatures below 625°C. Device failure can occur, however, through rapid formation of large volumes of this material at elevated temperatures or through build-up of like volumes over extended periods of time at lower temperatures. The existance of this multiphased, time-temperature sensitive system indicates that equilibrium conditions are not achieved in normal electrode attachment processes of this type and the importance of tight process detail control is made evident.

Of the gold alloys studied, only the Au-Sn eutectic bonds well to the Al-Si eutectic without agitation and/or flux. With this four-component system excellent bonds can be made at temperatures as low as 375°C with insignificant formation of $AuAl_2$, but the time-temperature relationships noted above apply.

When the Au-Sn, Al-Si system is further complicated by addition of a metallic lead-wire, surface energy relationships appear which direct the wetting away from the aluminum-rich surface and toward the wire, in some cases. Compatibility in this solid-liquid-solid system was improved by addition of small amounts of indium.

To aid in the explanation of some of the mechanical phenomena which are described, thermal expansion curves were run on samples of $AuAl_2$, Au_2Al, Au-Sn eutectic, Al-Si eutectic, and Si. Some mechanisms are postulated and the thermal expansion data are presented.

Abstract Number 120

EFFECTS OF HIGH ALUMINUM CONCENTRATION IN EMITTERS OF GERMANIUM ALLOYED POWER TRANSISTORS

H. K. Becherer and Ernest Paskell

General Motors Co.
Kokomo, Indiana

The investigations leading to this paper were started in an attempt to achieve reasonable d.c.-current gain with an emitter current density of 100 to 250 amp/cm². In general, the paper by L. D. Armstrong, C. L. Carlson and M. Bentivegna, published in "Transistors I: P-N-P Transistors using high-emitter-efficiency alloy materials," has been very helpful in making the first attempts. No further studying work with pure indium has been made as almost all types of transistors contain a certain amount of gallium in the emitter-indium. Therefore, all investigations and comparisons reported here are related to indium-gallium-alloys on one hand and indium-aluminum-alloys on the other hand.

With the addition of silver and gold as carrier agents, the content of gallium in indium can be considerably increased and still maintain a usable alloy. But the situation with a higher percentage of aluminum in indium is completely different. Two main reasons are the cause for the different behavior.

The first reason: Aluminum tends to form aluminum-oxide very easily and, therefore, to effect local penetration due to delayed wetting on some parts of the area causing a non-uniform base width. The second reason, is the ability of the aluminum to increase excessively the dissolving capacity of the indium in respect to germanium. Therefore, if we are able to eliminate the formation of an oxide of the aluminum, the increased dissolving capacity should be shown in a reduction of the number of unwetted areas. One slide will show a normal regrown p-type germanium region containing a certain percentage of gallium after the removal of the indium, and the other slide will show a regrown p-type germanium region found under the emitter-indium with an aluminum content higher than two per cent. Until now more than 200 elements have been investigated by cross-sectioning and not a single unwetted area found.

Another slide made from a regrown region shows clearly the formation of an aluminum-germanium-eutectic. This eutectic is also shown on a cross-section after polishing. While the normal n- and p-type germanium has a bright reflection of light in the microscope, the germanium-aluminum-eutectic has a gold reflection of the light. It is shown, also, that the eutectic does not reach the junction. At the present time, it is still not known how high the aluminum content is in the

p-germanium region. However, it is not very difficult to ascertain that the aluminum-content in this region is considerably higher than in a similar region alloyed with indium containing less than 2% aluminum.

Another slide shows that during the etching of the cross-section to make the junction visible, the aluminum-bearing p-type-emitter region is attacked considerably faster than the collector region. Therefore, a proper etch to make a collector-junction visible will cause an emitter-regrown-germanium to be too heavily etched resulting a darker color in the reflecting light. Also, it is easy to established that the shape of the junction edge has been changed. A soft curve, like is shown on the collector-junction is converted to an obtuse angle or a series of obtuse angles giving the appearance the edge is sharply curved. This shape of the edges of the junction is particularly prominent when the content of the aluminum exceeds a certain percentage.

The presence of a higher percentage of aluminum in the p-type-germanium changes the electrical behavior as well as the material properties. This paper will bring a complete comparison between two types of transistor. Both are now being mass-produced and have essentially the same dimensions including E- and C- areas, wafer-size, and base-width between junctions. The only difference being: One type of transistor contains the normal percentage of gallium and silver in the emitter-indium, while the other type contains more than 2% aluminum in the emitter-indium. Also, the surface treatment is basically the same. It was necessary to make minor changes in the sequence of the surface treatment because of the different behavior and a certain dissolving action of aluminum in the liquids of the washing cycle, but the final surface treatment is exactly the same, so that the surface recombination velocity between both types is identical.

The emitter containing the aluminum-indium-alloy does not affect the collector-diode or the open-base-voltage. Only the reverse characteristic of the emitter diode is somewhat changed from the normal unit. While the normal emitter-reverse-characteristic has a more or less good saturation with a soft or sharp breakdown between 80 and 120 volts, the aluminum-emitter-reverse-characteristic has only a short saturation up to 20 volts followed by an ohmic slope out to the comparable breakdown of the normal unit. The d.c.-gain is considerably higher at higher emitter current density level.

	E-diode at 8 ma	C-diode at 8 ma	Open-base at 300 ma	Base-volt. at 5 amp.	Base-volt. at 25 amp.
Al-type	40-60	80-120	50-75	.65 volt	1.4
Normal	80-120	80-120	50-75	.65 volt	1.6

	Gain at 5 A/cm^2	Gain at 20 A/cm^2	Gain at 100 A/cm^2	Gain at 250 A/cm^2
Al-type	48	35	26	15
Normal	48	27	9	-

In addition to these data, the paper will present data about the aging-effect, behavior at different temperatures (between -30 and +70°C), and life-test data.

All records given here are based on more than 1000 units.

A short comparison between the results given in the above mentioned paper by L. D. Armstrong, C. L. Carlson and M. Bentivegna and the data in this paper will be made.

It is not the purpose of this paper to give any details about production-procedures, but it might be mentioned that the accumulated yield-figure is almost as high as for the normal produced transistor-type.